# Controlled hybridization of helical electroactive foldamers for the design of homo – and heteroduplexes

Soussana Azar

COLLEGE DOCTORAL PAYS DE LA LOIRE
ED MATIERE, MOLECULES MATERIAUX ET GEOSCIENCES

université angers

# THESE DE DOCTORAT

DE
L'UNIVERSITÉ D'ANGERS
SOUS LE SCEAU DE
LA COMUE ANGERS – LE MANS

ECOLE DOCTORALE N° 596
*Matière, Molécules, Matériaux et Géosciences*

Spécialité : Chimie organique et supramoléculaire

**Soussana AZAR**

## Hybridation contrôlée de foldamères hélicoïdaux électroactifs pour la conception d'homo– et d'hétéroduplexes

**Thèse présentée et soutenue à Angers, le 1er Décembre 2023**

**Unité de recherche : Laboratoire MOLTECH–Anjou, UMR CNRS 6200**

**Composition du Jury :**

**Rapporteurs**

| | | |
|---|---|---|
| **Dr Amparo Ruiz Carretero** | Chargée de Recherche CNRS | Institut Charles Sadron, Strasbourg |
| **Dr Victor Maurizot** | Chargé de Recherche CNRS | Université de Bordeaux |

**Examinateurs**

| | | |
|---|---|---|
| **Dr Christelle Gautier** | Chargée de Recherche CNRS | Université d'Angers |
| **Dr Sébastien Ulrich** | Directeur de Recherche CNRS | Université de Montpellier |
| **Pr Marc Sallé** | Professeur des Universités | Université d'Angers |

**Directeur de thèse**

| | | |
|---|---|---|
| **Pr David Canevet** | Professeur des Universités | Université d'Angers |

# Acknowledgements

First, I would like to thank my supervisor, Prof David Canevet, for his years of guidance, patience and continuous support. I am deeply thankful for the invaluable advice, fruitful discussions, and extensive knowledge he has imparted to me throughout this journey.

Thanks to Dr Amparo Ruiz Carretero and Dr Victor Maurizot for taking the time to read and judge my work and together with Dr Sébastien Ulrich, Dr Christelle Gautier and Prof Marc Sallé for being part of my jury thesis. I am deeply grateful for the insightful discussions we shared during my defense. Thank you for your appreciation of my work.

I would like to thank Dr Philippe Blanchard for welcoming me into the MOLTECH-Anjou Laboratory.

I would like to thank Emilie Blanchard and Véronique Verkruysse for their administrative tasks in the lab, and to Virginie Jonnin Hrouch regarding the administrative tasks for LUMOMAT grant. Thanks to Yohann Morille for his role as the computer coordinator of the lab.

Thank to Dr Claire Fave and Dr Mathieu Raynal for being part of my thesis committee. I recognise the valuable discussions and scientific insights they provided during these years.

I would like to thank all the members of $S_2$OMaF team, thanks to Dr Sébastien Goeb, for his strong leadership both scientifically and socially, and thanks to Prof Marc Sallé, Prof Piétrick Hudhomme and Dr Antoine Goujon. I appreciate all the valuable scientific discussions, insightful advice and the good moments.

I would like to thank Prof Nazario Martìn's group for welcoming me during a one-month research stay at their laboratory at the Complutense University of Madrid. Though it was a short period, I gained invaluable knowledge and thoroughly enjoyed my time there. Thank you Prof Nazario Martìn and Prof Maria Àngeles for the discussions and your supervision during the stay. I would like to thank Juan for sharing the bench with me and for his help in the lab. Thank you Jenny for her help and advice in preparing the azide-$C_{60}$. It was a pleasure to meet each one of you: Juan, Arturo, Jenny, Manu, Gema, Sergio, Jesus, Jaime, Patricia, Francesco, Valeria and Dr Jesus. I appreciate all the wonderful moments and memories we shared.

Thanks to Dr Christelle Gautier and Dr Eric Levillain for their help with the spectroelectrochemical measurements and the analysis of the experiments.

I wish to extend my appreciation to the entire SFR Matrix team for their invaluable assistance in analysing the products. I am deeply grateful to Dr Magali Allain for providing us with all the wonderful crystallographic structures, to Dr Ingrid Freuze for mass spectrometry, and to Benjamin Siegler for the NMR experiments.

Throughout this journey, I had the opportunity to teach classes at the University of Angers. I would like to thank Dr Maitena Oçafrain for her confidence in assigning me this role and thanks to Emmanuel Cadeau and Nadège Blon for their help during the practical works.

I would like to express my gratitude to the ‘non-permanent’ colleagues with whom I have spent these three years, sharing countless unforgettable moments through both the good and bad times.

First, I am grateful that I had the chance to work with colleagues on the same thematic. I would like to thank first Dr Youssef Aidibi for his support and help since my first day in Angers, even before we became colleagues working on foldamers. Thank you for the countless scientific discussions and all the knowledge you transferred to me. Many thanks also to Marie Voltz. Thanks to Louis Hardoin for his support and all the good conversations. Special thanks for the ‘blender figures’ you’ve created. I wish you every success and hope for excellent results. Finally, it is true that we became colleagues at the end of my PhD, but I want also to thank Emilien Husson for his support and I wish you the best of luck. Then, I want to thank also Romain Guechaichia and Jennifer Bou Zeid, who share the lab K106 with us. Thank you for creating the best working environment in the lab (and in the office). I deeply thank Romain for his support, especially during the printing of my manuscript.

To my favorite trio, partners in laugher, adventure and everything in between - Aline Makhloutah, Elie Bou Rahhal and Tatiana Ghanem - thank you for everything. I am truly blessed to have such wonderful friends by my side, supporting me through thick and thin.

Special thanks to my dearest and kindest friend - Dr Adèle Gapin – for her support, advice and our little conversations.

There are also plenty of friends and colleagues to whom I would express my gratitude during this journey: Dr Arthur David, Rana Abdel Samad, Dario Puchan Sanchez, Axel Houssin, Féderica Solano, Dr Nataliya Plyuta, Dr Talia Bseibess, Dr Ali Yassin, Dr Pierre Josse, Dr Maxime Roger, Khaled Youssef, Jihad Abdo, Dr Yohan Cheret, Dr Augustin Ayoub, Dr Julien Billon, Dr Théo Travers, Dr Clément Drou, Dr Maurizio Mastropasqua, Dr Maria Saadeh, Dr Simon Séjourné, and Dr Mélissa Merheb.

Very special thanks goes to my best friend Mariem for her support, and encouragement. I am very grateful to have you.

Special thanks to Fadi and Rania El Kara for the wonderful ‘pot libanais’ and most importantly, for being my second family while I am away from home.

Finally, I would like to thank my family for their support and unconditional love. Thank you for attending my defense and being there for me. Dad, my angel, your unwavering support and prayers, have brought me to where I am today. Thank you for always believing in me.

*To my double B!*

## Table of contents

# List of abbreviations

| | |
|---|---|
| ***A*** | Acceptor |
| ***ACN*** | Acetonitrile |
| ***β–CD*** | β–Cyclodextrine |
| ***BIPY*** | Bipyridinium |
| ***Boc*** | *tert*–Butoxycarbonyle |
| ***BuLi*** | *n*–Butyllithium |
| ***CBPQT$^{4+}$*** | Cyclobis(paraquat–p–phénylène) |
| ***CD*** | Circular dichroism |
| ***COSY*** | Homonuclear correlation spectroscopy |
| ***$C_t$*** | Total concentration |
| ***CT*** | Charge transfer |
| ***CV*** | Cyclic voltammetry |
| ***d*** | distance |
| ***D*** | Donor |
| ***DBU*** | 1,8–Diazabicyclo[5.4.0]undec–7–ene |
| ***DCM*** | Dichloromethane |
| ***DCC*** | Dicyclohexylcarbodiimide |
| ***DAN*** | Dialkoxynaphthalene |
| ***DIPEA*** | N,N–Diisopropylethylamine |
| ***DMAP*** | 4–(Dimethylamino)pyridine |
| ***DMF*** | N,N–Dimethylformamide |
| ***DMSO*** | Dimethylsulfoxide |
| ***DNA*** | Deoxyribonucleic acid |
| ***DOSY*** | Diffusion ordered spectroscopy |
| ***e.g.*** | exempli gratia/for example |
| ***$Et_2O$*** | Ethyl ether |
| ***EtOAc*** | Ethyl acetate |
| ***$Et_3N$*** | Triethylamine |
| ***exTTF*** | Extended tetrathiafulvalene |
| ***HIV*** | Human Immunodeficiency Virus |
| ***HOMO*** | Highest Occupied Molecular Orbital |
| ***$K_{dim}$*** | Dimerization constant |
| ***LDA*** | Lithium diisopropylamide |
| ***LUMO*** | Lowest Unoccupied Molecular Orbital |
| ***M*** | Monomer |
| ***MeOH*** | Methanol |
| ***NDI*** | Naphthalene diimide |
| ***NMR*** | Nuclear magnetic resonance |
| ***NOESY*** | Nuclear Overhauser effect spectroscopy |

| | |
|---|---|
| ***OiBu*** | Isobutoxy |
| ***PDI*** | Perylene diimide |
| ***PE*** | Petroleum ether |
| ***PNAs*** | Peptidic nucleic acids |
| ***Py*** | Pyrene |
| ***SCE*** | Standard calomel electrode |
| ***SOMO*** | Singly Occupied Molecular Orbital |
| ***TCNQ*** | Tetracyanoquinodimethane |
| ***TFA*** | Trifluoroacetic acid |
| ***TMTSF*** | Tetramethyltetraselenafulvalene |
| ***THF*** | Tetrahydrofuran |
| ***TTF*** | Tetrathiafulvalene |
| ***UV*** | Ultraviolet |
| $V^{2+}$ | Viologen |

# General introduction

Over the past few decades, chemists have paid a particular attention to the rich supramolecular chemistry of foldamers. The latter constitute a new family of oligomers that adopt well –defined compact architectures stabilized by non –covalent interactions. The development of these edifices is mainly inspired by the complexity and the amazing variety of functions accomplished by biomacromolecules included proteins and DNA. These structures have already found numerous applications related to catalysis, molecular recognition and responsive materials. Indeed, the imagination of chemists for the construction of foldamers, leads to a wide diversity of building blocks, encompassing not just natural ones but also synthetic monomers.

Some of these structures fold into helical form and hybridize to form double and multiple helices with unique physicochemical properties. Understanding the parameters that govern the equilibrium between single and hybridized species has emerged as a new challenge in this field, and constitutes a subject for further investigations. Thus, achieving reversible control over the hybridization equilibrium between single and double helices have not yet been deeply explored.

In this context, this PhD work focuses on the analysis of helical oligopyridine dicarboxamide foldamers endowed with electroactive chromophores that display redox and donor –acceptor properties. These architectures were designed to allow for controlling the hybridization phenomenon in a reversible manner in both cases: to create homoduplexes through redox stimulations in the first case, and heteroduplexes through donor –acceptor interactions in the second one. On this ground, the thesis manuscript is structured as follows:

The *first chapter* serves as a general introduction to foldamers. It will explain their origins, and the different types of structures that lead to the formation of a wide diversity of natural and non –natural foldamers. A particular attention will be devoted to the chemistry of helical oligopyridine dicarboxamide foldamers and their behaviour in solution and in the solid state. Furthermore, the hybridization process and the parameters that govern the equilibrium will be investigated. The last part will focus on the efforts conducted by the researchers to elaborate foldamers that respond to redox stimulations and heteroduplexes by donor –acceptor interactions.

The *second chapter* focuses on the efforts made in the synthesis of oligopyridine dicarboxamide foldamer functionalized with a redox unit, tetrathiafulvalene (TTF). Analyses

were performed in both the neutral and oxidized states in solution to enable the reversible control of the hybridization equilibrium, and explore the parameters influencing it. In particular, this study investigates the impact of the radical cation dimerization on the hybridization process. Note that a particular attention is dedicated to the organization of the helices in the solid state.

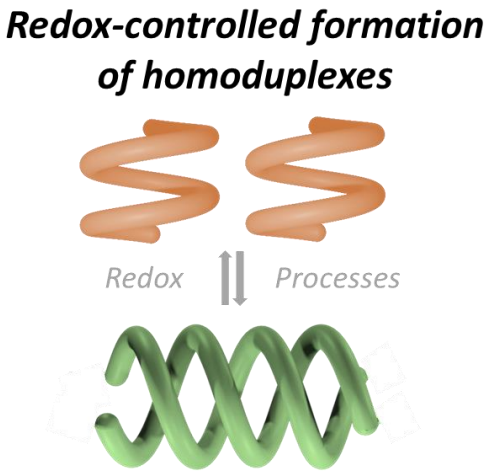


The *third chapter* details the design of a series of foldamers endowed with donor and acceptor chromophores. The aim of this chapter is to elaborate heteroduplexes in a selective manner by taking advantage from donor –acceptor properties. The choice of the chromophores as well as their behavior in solution will be detailed. Furthermore, the impact of the donor – acceptor interactions on the hybridization properties is described, and particularly their supramolecular arrangement in solution.

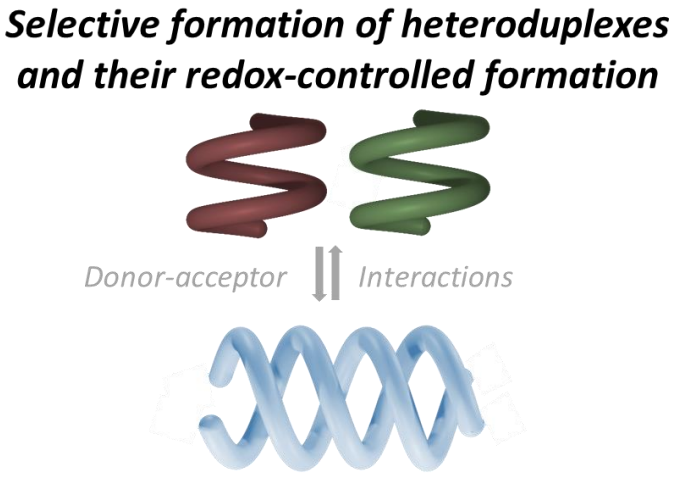

# Chapter 1

# Helical foldamers: Structures, Supramolecular chemistry and Applications

# I. Origin and definition

## A. From biomacromolecules to foldamers

One of the most impressive challenge for Mankind consists in understanding Nature, particularly when it comes to explore the essentials of life, starting from molecules at the cellular level, to an entire human being at a macroscopic point of view. In the human body, small building blocks assemble to give rise to complex systems, such as nucleic acids, proteins and polysaccharides. These crucial biomacromolecules, which play an important role in living systems, are characterized by four distinct structural levels: secondary, tertiary, and for some, quaternary structures that emerge from simple linear sequences (Figure I–1). The latter consist of repeating covalently linked monomers (nucleotides, α–amino acids and carbohydrates) leading up to primary structures. The overall inter– or intramolecular interactions induce the folding of the linear sequence and result in the adoption of the so–called secondary structures. Typical secondary structures of proteins include α–helices, β–sheets and turns,[1] while nucleic acids adopt double helical arrangements for instance, as in the case of DNA.[2,3] When these secondary structures interact through weak intramolecular forces, tertiary structures are formed. Alternatively, such interactions occurring in an intermolecular manner lead to the formation of quaternary structures.

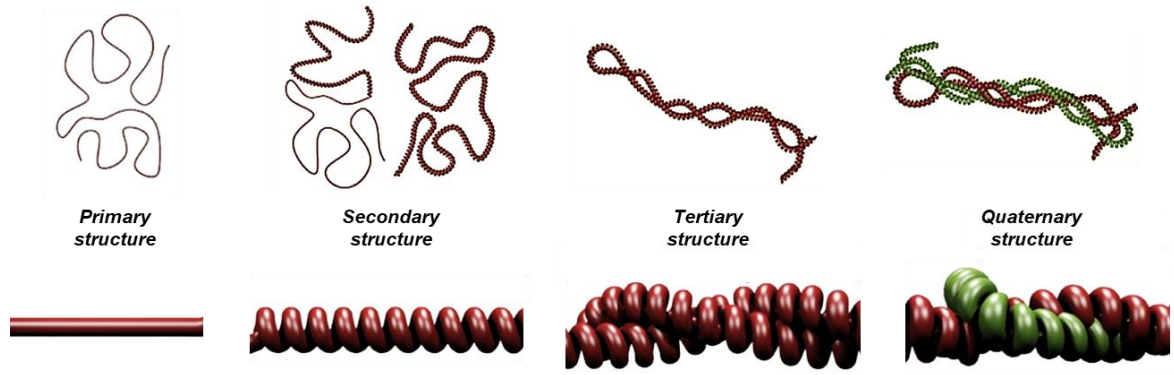


*Figure I–1. Primary, secondary, tertiary and quaternary structure levels in linear polysaccharides.*[4]

These sophisticated biopolymers govern fundamental biological processes. Indeed, in the absence of these structures, transmission and translation of genetic information, enzyme catalysis, storage, molecular recognition and numerous other functions could not be achieved. This is why understanding the relationship between biomacromolecular structures and their functions remains a challenge that needs to be tackled.

In particular, helical biomacromolecules are ubiquitous and have a prominent role in biological processes. This explains why chemists have shown a tremendous interest in designing and developing diverse arrays of helical polymers. The history of these polymers dates back to 1955 when Natta *et al.* discovered the single helical structure of an isotactic polypropylene (Scheme I–1) in the solid state,[5] concomitantly with the discovery of the double helical structures of DNA.[3] Since then, significant progress has been done in the advancement of synthetic polymers leading to the development of the field of foldamers, which emerged along the 90ies.

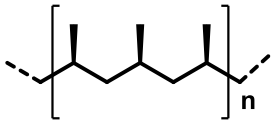


*Scheme I–1. Representative scheme of an isotactic polypropylene.*[5]

Foldamers were first described by Gellman in 1998 as '*any polymer with a strong tendency to adopt a specific, compact conformation*'.[6] Moore proposed a more specific definition in 2001, by considering that '*any oligomer that folds into a conformationally ordered state, which is stabilized by a collection of non–covalent interactions in solution*' is a foldamer.[7] Thus, the "folding" process appears as a requirement, and this explains why all oligomers that possess a helical conformation, such as helicenes, cannot be classified as foldamers.

The primary structure of a foldamer consists of repetitive monomers included in a backbone. The folding of the chain through a collection of non–covalent interactions between non–adjacent and neighbouring motifs gives rise to the secondary structures. The fascinating secondary structures of the foldamers developed to date reflects the progress in this field.[8] For example, α–helices,[9–11] β–sheets[12–14] and turns,[15–17] double and multiple helices[18,19] have been reported (Figure I–2).

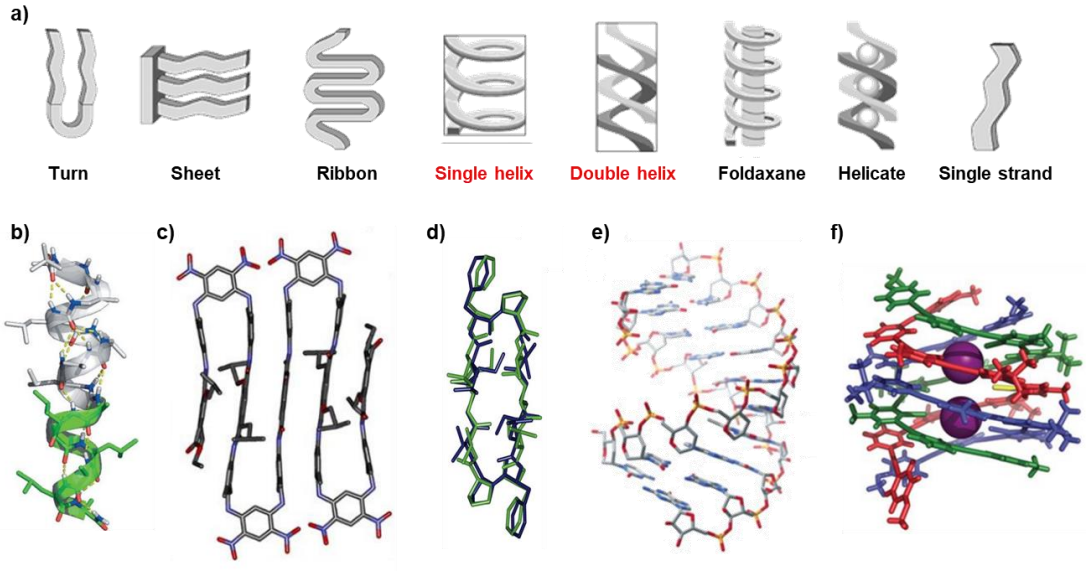


*Figure I–2. a) Schematic representation of different types of foldamer–based secondary structures,[7] b) helical structure,[11] c) β–sheet,[20] d) turn,[15] e) double helix[21] and f) triple helix.[22]*

Among them, the helical structure constitutes the most reported structural arrangement adopted by foldamers, most likely for reasons of stability and solubility. Their chirality also gives them a potential in catalysis[23] and chiroptics,[24,25] which explains why the scientific community developed so many structures. Helices are indeed chiral: for a given structure built from achiral motifs, a pair of left– and right–handed (*M* and *P*) conformations is obtained, leading to a racemic mixture (Figure I–3–a). On the contrary, diastereoisomeric conformations are derived from enantiomerically pure chiral monomers depending on the capacity of these monomers to induce a preferential chirality (Figure I–3–b).

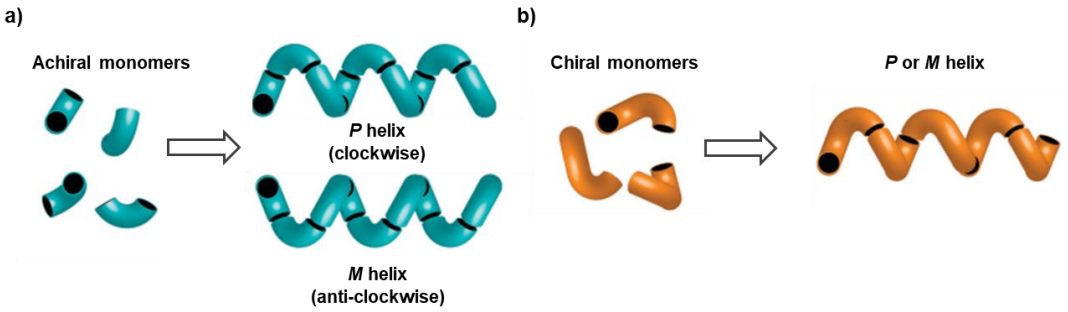


*Figure I–3. a) Schematic representation of helices built from achiral monomers adopting M and P handednesses. b) A helix built from chiral monomers adopts a preferential helical structure (M or P) since M and P helices are diastereoisomers in this case.[26]*

## B. Internal and external parameters driving foldamers

Distinct backbones have been shown to adopt helical conformations under specific conditions, which illustrates that folding process may be affected by several internal and external parameters. Internal factors are associated to the structure of the foldamer, including:

1) the characteristics of the building blocks (size, shape, rigidity and rotational restrictions), 2) the bridging spacer employed to connect the latter components, and 3) the non–covalent attractive or repulsive intramolecular interactions. Typically, hydrogen bonds and/or π–π stacking play an important role in stabilizing the folding process by a collection of intramolecular interactions taking place between the adjacent and non–adjacent monomers. In addition, the rigidity associated to aromatic backbones interferes to minimize the entropic cost associated with the formation of an organized structure from flexible building blocks.

External parameters also significantly affect the conformational structure of foldamers. These include temperature,[27] concentration,[27,28] pH[29] and nature of the solvent.[30,31] In addition, depending on the functional group, application of a chemical potential[32] and irradiation by light[33–37] can also be considered as examples of external stimulation.

## C. Towards tertiary and quaternary structures

In biomacromolecules, a variety of functions arises only from tertiary and quaternary structures. This is the reason why, chemists have aimed at elaborating such complex structures. This definitely constitutes a challenging task, which explains why tertiary and quaternary structures remain scarcely reported in the literature.

Recently, Huc *et al.* successfully predicted the formation of a tertiary structure by computational modelling, which was verified by X–ray diffraction analyses (Figure I–4–a).[38] This team also described a pseudo–quaternary structure composed of eight helices (Figure I–4–b).[39] These structures are constituted through intermolecular hydrogen bonds between donor and acceptor sites bridging water molecules. Additionally, the Gellman group also reported a quaternary structure (Figure I–4–c), which is composed of α–β–peptides (Scheme I–2).[40] The progress in synthesizing these structures is still modest because the prediction of these structures remains complicated. Indeed, their design demands developing approaches that merge different expertise and know–how, including molecular modelling, the designing of the oligomer sequence and the selective control of handednesses.

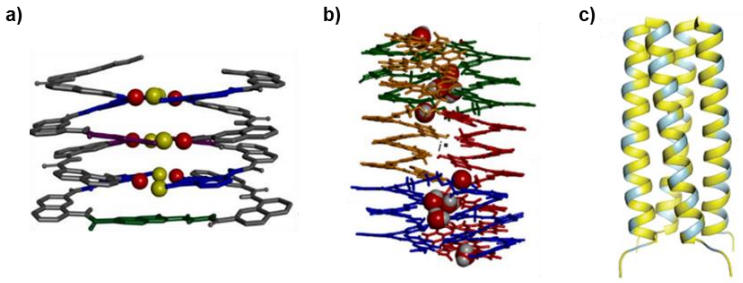


*Figure I–4. a) Tertiary,[38] and b) pseudo–quaternary structures of foldamers reported by Huc and coworkers,[39] c) quaternary structure of a foldamer described by Gellman and coworkers.[40]*

# II. Types of foldamers

Nature has established an approach of folding and assembly of biomacromolecules in order to settle and to direct their sizes, shapes and functionalities by using 20 α–amino acids for proteins and 5 nucleobases for nucleic acids. The development of discrete non–natural oligomers with predictable and interesting conformational tendencies similar to biopolymers is necessary to create foldamer–based backbones. Since the folding is established by a series of non–covalent interactions, synthetic foldamer backbones should comprise complementary sites to create non–covalent interactions (*e.g.* H–bond donors and acceptors). In this context, a wide range of backbones that are able to fold into secondary structures has been reported to date.[41] These can be classified into two main categories according to the nature of the constituting monomers: 'biotic' and 'abiotic' foldamers.[7,42]

Before the term "foldamer" became prevalent, several biopolymers analogues were efficiently designed and synthesized. The most prominent examples include peptide nucleic acids (PNAs),[43] peptoids,[44,45] oligoureas,[46] and β–, γ– and δ–peptides,[47,48] which were first described by Gellman and Seebach (Scheme I–2). The corresponding building blocks are derived from naturally occurring monomers, which explains why they are named 'biotic' or 'bio–inspired' foldamers.

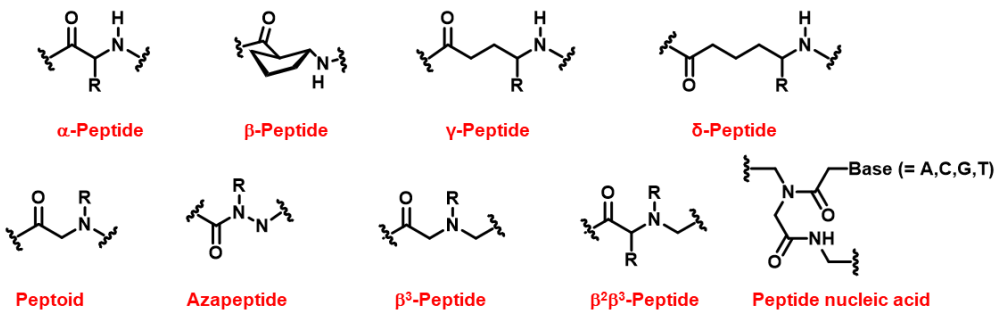


*Scheme I–2. Monomers employed within biotic foldamers.[7]*

On the contrary, 'abiotic' foldamers are built from artificial backbones (*e.g.* aromatic units), which means that the monomers are synthetic (Scheme I–3). Since Hamilton and his team reported the first family of abiotic foldamers in 1996,[49] the growth of this class of foldamers largely expanded. This presumably results from their unique features, including a high stability, solubility in organic solvents, and the production of highly predictable folded structures. Thereby, plenty of synthetic abiotic foldamers have been reported to date by Huc,[50] Lehn,[27] Moore,[51] Li,[52] Gong,[53] Yamaguchi,[54] and Yashima[55] and others. Given the scope of the present manuscript, the following paragraphs will focus on abiotic foldamers.

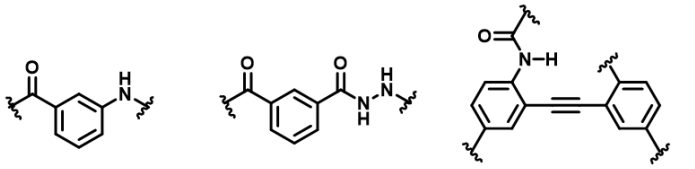


*Scheme I–3. Monomers employed within abiotic/aromatic foldamers.*[56]

# III. Aromatic foldamers

## A. Principle types of structures

Since 2000, much effort has been devoted to the rich chemistry of foldamers, and specifically, aromatic ones. Changing the alkyl monomer to an aromatic one offers a wide structural diversity and a variety of folding modes, by allowing additional non–covalent interactions, such as π–π stacking. Additionally, aromatic components offer the advantage of being functionalizable at various positions, which is a singular and positive aspect in comparison to peptides monomers. The design of such structures follows a "bottom–up" approach, involving the preparation of individual monomers and their consecutive assembly to create sophisticated foldamers. For example, Chen *et al.* reported the design of a helical polymer consisting of pyridine and oxadiazole aromatic monomers **I–0** (Figure I–5), which acts as a nanochannel.[57,58] The latter shows appealing properties to promote the transport of cations through a lipid bilayer membrane in a highly selective manner. In addition, it was shown that the length of these nanotubes can be adjusted and reach sizes as large as 2.7 nm.

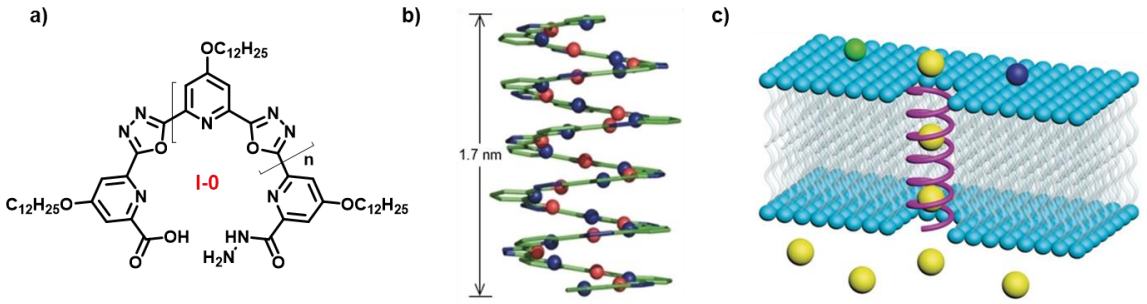


*Figure I–5. a) Chemical structure of an oligo(pyridine–oxazole) foldamer developed by Chen et al., b) Optimized geometry of the heptadecamer calculated at the ωB97X/6–31G* level, c) Schematic representation of the foldamer included in bilayer membrane and promoting ion transport.*[58]

In this context, the progress in the field of aromatic foldamers has led to the development of miscellaneous families of abiotic foldamers, such as oligoarylamides, oligoethynylhelicenes, *m*–terphenyl–based foldamers, oligoresorcinols, oligo(ethynylpyridines), *m*–phenylacetylene,[59] and others (Scheme I–4). Noticeably, these aromatic foldamers have found diverse applications in the fields of HIV (Human Immunodeficiency Virus) treatment,[60] catalysis,[23] photo–controlled folding,[34,61] or selective guest encapsulation.[62]

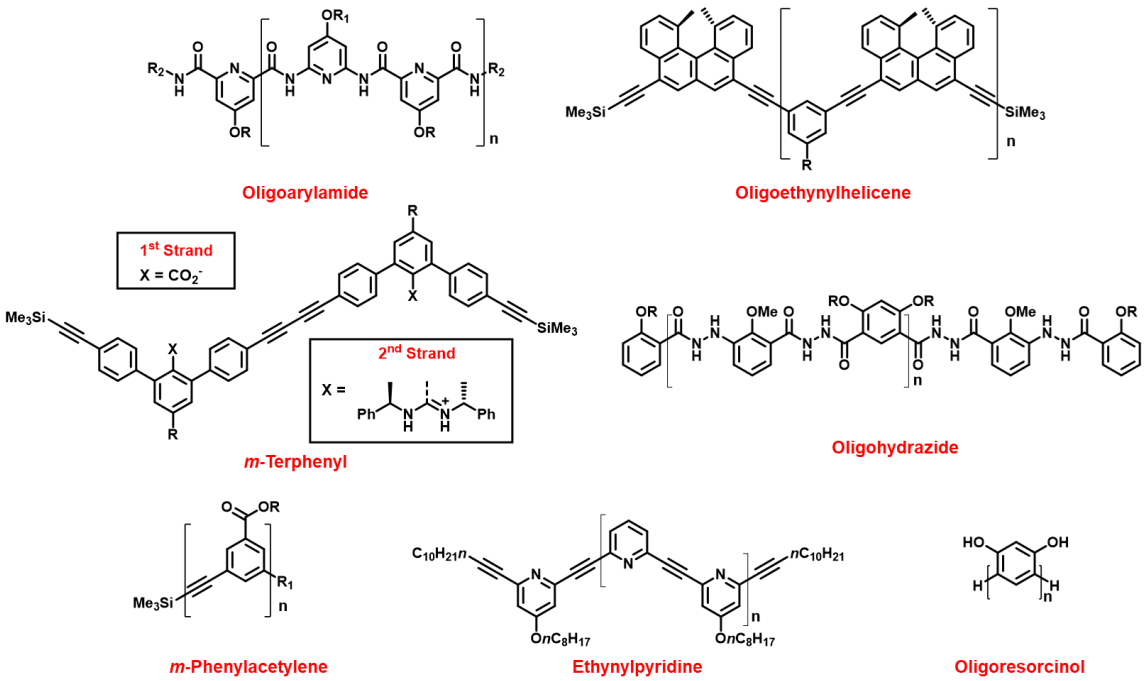


*Scheme I–4. Chemical structures of aromatic foldamers.*[41]

The majority of these aromatic foldamers are random coil structures in their single form, and display helical conformations as dimers (dimerization–induced folding). Nevertheless, oligoarylamide foldamers exhibit a helical structure, which is essentially maintained by a network of hydrogen bonds, which makes them part of the rare foldamers capable of adopting helical structure in a unimer state.

# B. Oligoarylamide foldamers

## B.1. Generalities and folding properties

The aromatic oligoamide foldamers described so far highlight promising capacities for mimicking secondary structures of biomacromolecules.[50,63] Indeed, they exhibit a combination of notable properties: 1) the stability of their folded secondary structures even in the presence of competitive solvents; 2) the predictability of their folding; 3) a good propensity to crystallise; 4) a rather straightforward synthesis that involves coupling reactions between activated carboxylic acids and amines and which can be used to elaborate long sequences.

The amide function in aromatic foldamers differs from those of proteins. Regarding the latter, the amide is connected to a $sp^3$ carbon atom, while it is attached to aromatic rings for oligoamide foldamers. Thus, the conjugation between the amide functions and the aromatic units leads to restricted rotations about NHCO–aryl and CONH–aryl bonds (Scheme I–5). These bonds may have two preferential *syn* and *anti* conformations, which induce a partial coplanarity between aryl and amide units.[64] These conformations are also affected by a series of repulsive and attractive interactions that take place between amide functions and substituents of the aryl rings specifically on the *ortho*–position. In the following scheme, all the conformations are presented. [50,63]

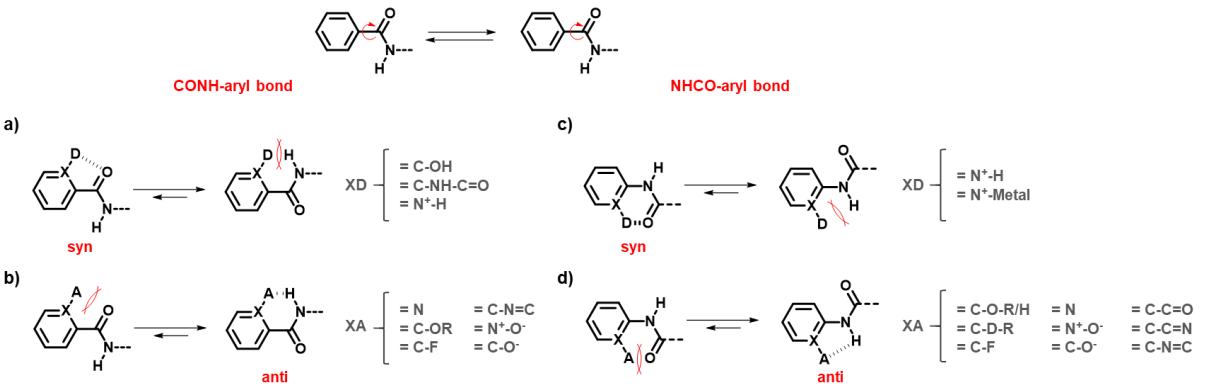


*Scheme I–5. Conformational preferences of an aryl amide sequence through attractive and repulsive interactions of various CONH–aryl and NHCO–aryl linkages.[50]*

The orientation of the amide function, the shape and the size of the building blocks, as well as the endo– or pericyclic character of the hydrogen bonds network, govern the obtaining of the adopted conformation. These parameters result in varying angles, leading to either high or moderate curvature, which in turn leads to different cavity diameters. Consequently, different numbers of units per turn can be generated as shown in the following Scheme I–6.[50]

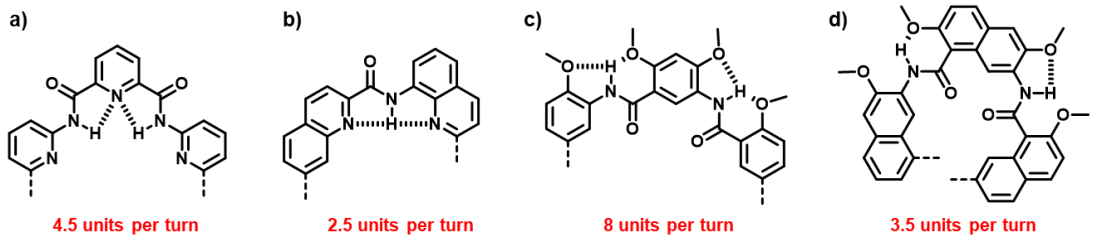


*Scheme I–6. Bending of oligoarylamide foldamers depending on intramolecular hydrogen bonds: a) and b) endocyclic, c) and d) pericyclic intramolecular hydrogen bond.*[50]

In 1994, Hamilton and coworkers described the first examples of oligoamide foldamer constructed from pyridine–2,6–dicarboxamide and anthranilamide monomers.[65] When the oligomer is exclusively formed from anthranilamide monomers (**I–1**), the intramolecular hydrogen bonds induce the adoption of a sheet conformation (Figure I–6–*Left*). Alternatively, introducing pyridine–2,6–dicarboxamide monomers within the same oligomer generates a helical compact structure **I–2** (Figure I–6–*Right*).[49] Therefore, these examples show how modifying a simple structural detail can trigger the alteration of the overall conformation and behavior in solution.

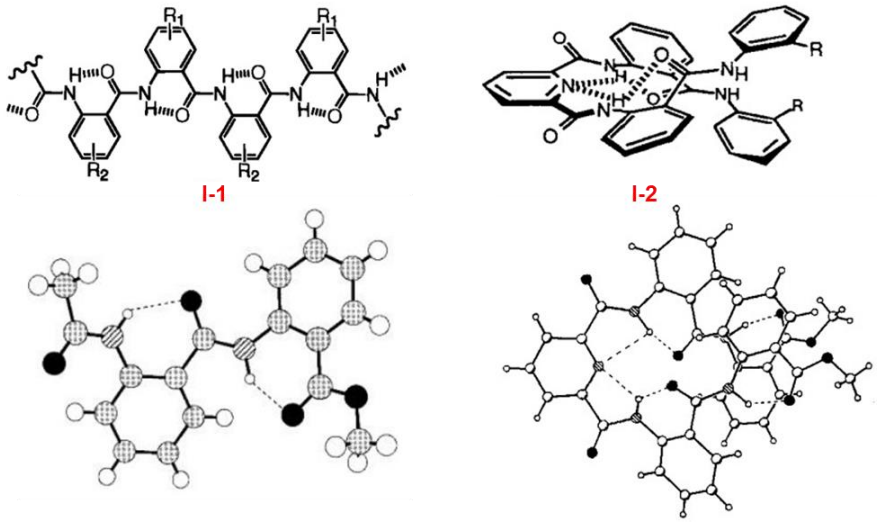


*Figure I–6. Left. First aromatic foldamers described by Hamilton: oligoanthranilamide **I–1** and its corresponding crystallographic sheet structure.*[49] *Right. Oligo(anthranilamide–pyridine–2,6–dicarboxamide) **I–2** and its corresponding crystallographic helical structure.*[66]

Later on, Lehn, Huc and coworkers enlarged this family of foldamers and reported an oligoarylamide skeleton endowed with alternating pyridine–2,6–dicarboxamide and 2,6–diaminopyridine (Figure I–7–a). In this case, the folding is stabilized by π–π stacking, interstrand hydrogen bonds N···H–N, and electrostatic repulsions between the nitrogen atom of pyridyl rings and oxygen atom of the carbonyl functions. The X–ray crystal structure of foldamer **I–3** shows the strong effect of hydrogen bonds on the radius of curvature of the

oligomer; the latter, which is defined by 6 and 6' carbon atom bonds, is as small as 39°, while one could expect a 60° value (Figure I–7–b–c).

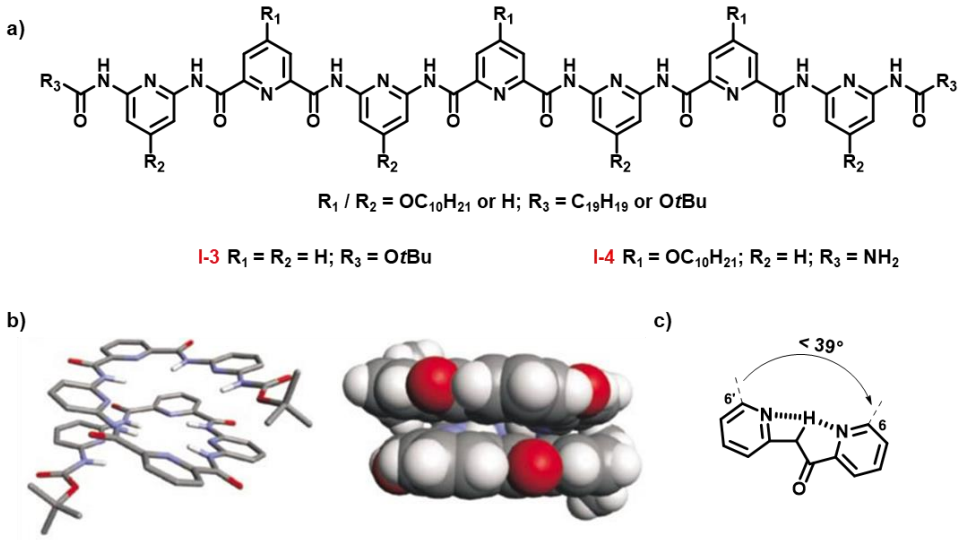


*Figure I–7. a) Chemical structure of an oligopyridine dicarboxamide foldamer, b) Crystallographic structure of foldamer **I–3** in its single helical form, c) folding mode.*[27]

As far as this skeleton is concerned, it appears also important to underline the contribution of Huc and collaborators, who took advantage from the acid–base properties of pyridine units to control the folding and unfolding processes of helical structures (Figure I–8). Upon addition of excess TFA, diaminopyridine rings can be protonated in a selective manner, which induces the unfolding of oligomer **I–4** leading to a linear sequence in solution (Figure I–8–b). Subsequently, the helical character can be regenerated by applying two different strategies: 1) by adding stronger triflic acid, which induces the protonation of all pyridine rings and lead to strong electrostatic repulsions between neighbouring pyridine rings, and 2) by introducing an excess of base such as triethylamine.[29,67] In this case, the base deprotonates the pyridinium ion, which regenerates the helical conformation promoted through intramolecular hydrogen bonds.

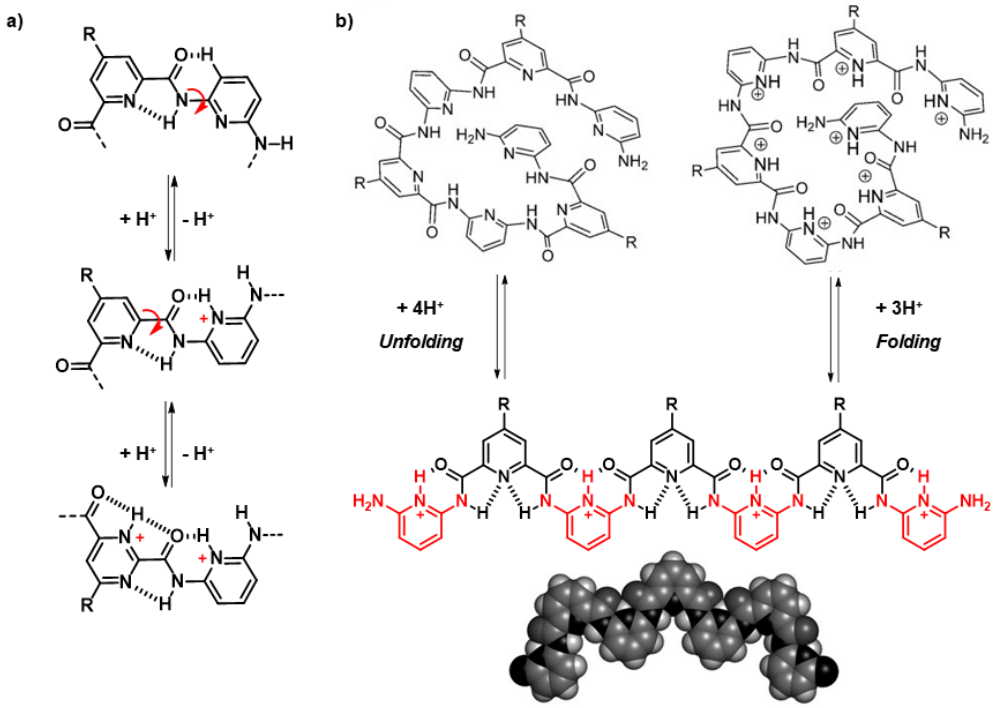


*Figure I–8. a) Rotation around the aryl–amide bonds due to consecutive protonations in the presence of an acid source, b) Acid induced conformational switching of foldamer **I–4**, and the obtained crystallographic structure of the linear conformation.*[29,67]

## B.2. Towards host–guest chemistry and molecular recognition

Molecular recognition relies on the complementarity between the binding sites of the host and the guest. Indeed, one should note that the folding process of oligomers into helical structures promotes the appearance of a cavity, which may serve as a recognition site. On the other hand, foldamers may also display superficial binding pockets, just as some proteins do.

In this context, investigating the possibility to tune the size, shape and chemical nature of the guest–binding site encouraged scientists to explore the molecular recognition properties of oligoarylamide foldamers. Depending on the foldamer skeleton, two categories of molecular recognition based on such foldamers can be defined. The first one relies on the internal cavity formed upon folding of a linear sequence, while the second one corresponds to binding processes that occur at the surface and involves the side chains.

### B.2.a. Molecular recognition within the cavity

The families of foldamer receptors reported so far have allowed for considerable improvements in the design of the shape and the cavity size of helical oligomers. This notably allowed for developing systems that bind anions, cations and neutral guests, with particularly high binding constants and selectivities.[68,69] For instance, Huc and coworkers described the

ability of oligopyridine dicarboxamide to catch water molecules. This fact was captured in the solid state by X–ray structures,[70] and in solution by developing the concept of 'molecular apple peal' (Figure I–9).[71] The analysis in solution by $^{1}$H NMR spectroscopy at low temperature showed the presence of two peaks for water molecules, which are in slow exchange at the $^{1}$H NMR timescale. These ones correspond to the encapsulated and free water molecules, as confirmed by NOESY spectroscopy, which evidenced contacts between the confined water molecule and some of the amide protons within the cavity.

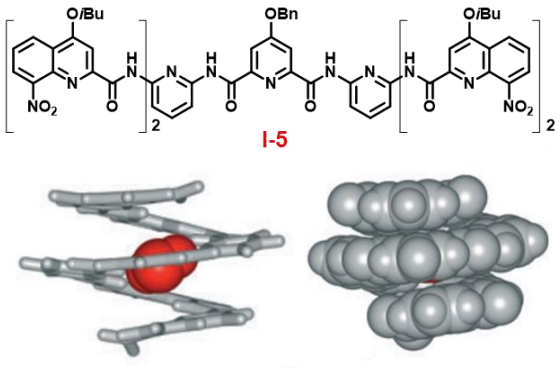


*Figure I–9. Chemical structure of foldamer **I–5** and its corresponding crystallographic structure in a single helical form capturing one water molecule.*[67]

Elongating the foldamer skeleton resulted in the encapsulation of two water molecules by **I–7** and introducing larger building blocks (**I–8)**, such as quinoline and/or anthracene units, constituted a relevant manner to increase the helix diameter,[72,73] and encapsulate larger guests, like 4–amino–1–butanol (Figure I–10).[74]

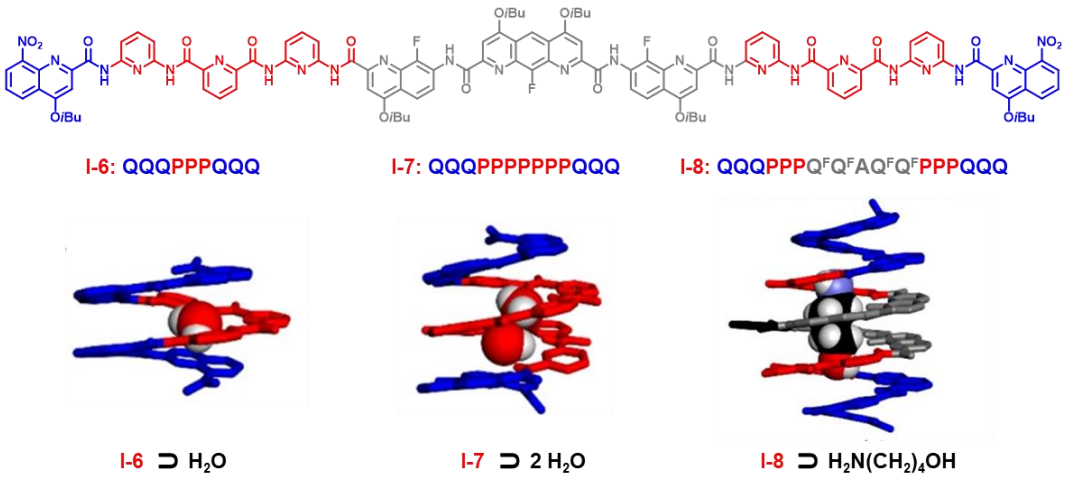


*Figure I–10. Representative chemical structure of oligopyridine dicarboxamide foldamers containing three different monomers: pyridine, quinoline and anthracene. Crystallographic structures of foldamers **I–6** encapsulating one water molecule, **I–7** encapsulating two water molecules, and **I–8** encapsulating 4–amino–1–butanol.*[72,74]

### B.2.b. Molecular recognition at the surface

The recognition phenomenon may also occur on the surface of helical oligomers. In this situation, the bound guest is generally larger than the foldamer backbone itself. This type of recognition is most often encountered for proteins and DNA for biological applications.[75] However, numerous examples were reported on this subject for abiotic foldamers.[76–79] Most of these examples involve the construction of tweezer receptors with short oligomers.[80] As an illustrative example, helical foldamer **I–9** was selected because it constitutes quite a sophisticated system and displays an interesting behavior (Scheme I–7).[77]

It is functionalized by six electron–donor zinc porphyrin rings at the side chain of its skeleton. The folded conformation in $CDCl_3$ was confirmed by $^1H$ NMR spectroscopy with amide protons appearing in the downfield region. $^1H$ NMR and UV–visible absorption spectroscopy showed that the foldamer forms a 1:6 complex in the presence of $C_{60}$–ligand **I–10** with a high binding constant ($3.6 \times 10^4$, $CDCl_3$, 25°C). A combination of non–covalent interactions guarantees the matching: the nitrogen atom coordinates the Zinc porphyrin and the π–π stacking between $C_{60}$ and porphyrin core. In addition, the appearance of CD signals upon titration with **I–10** indicates a chiral induction from the guest to the host.

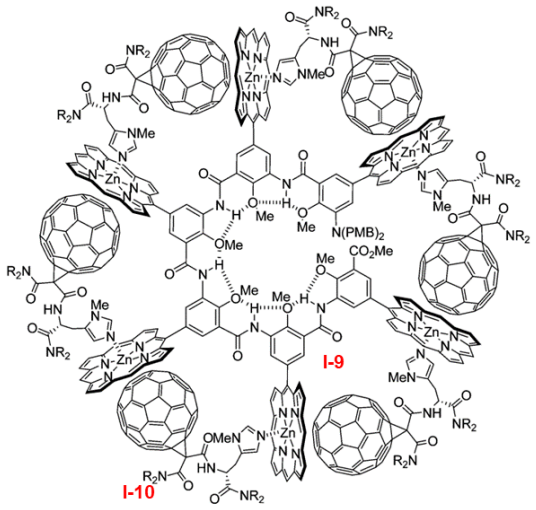


*Scheme I–7. Chemical structure of complex 1:6 formed between helical foldamer **I–9** and chiral $C_{60}$–ligand **I–10**.*[77]

## B.3. Towards hybridization and self–recognition

It is not rare that oligoarylamide foldamers exhibit a remarkable behavior in solution at high concentrations: some actually tend to dimerize to adopt a double helical arrangement and exhibit self–recognition.

Contrary to helicates, these double helices are obtained in the absence of metal ions, which constituted a significant leap in the field of supramolecular chemistry in the early 2000s.[81–84] This result established a novel route to design and elaborate duplexes, notably to explore their physico–chemical properties. The following paragraph illustrates the progresses made in developing foldamers able to hybridize into double and multiple helices.

# IV. Hybridization of helical foldamers

As mentioned above, nature gave the most relevant examples of hybridization through the double helices of DNA and collagen[85] and multiple helices of gramicidin.[86] The fundamental role accomplished by these multiple helices is key, notably regarding the genetic information storage by DNA. When foldamers form multiple helices, the hybridization of two identical strands leads to homoduplexes, which are very common in the literature, while heteroduplexes are obtained when different strands associate. The hybridization phenomenon involves a series of non–covalent interactions within two or more intertwined strands to form double or multiple helices. Diverse categories of double helical structures have been designed so far, built from ion pairing, hydrogen bonding, aromatic stacking and/or solvophobic interactions.

## A. Hybridization into homoduplexes

### A.1. Oligoarylamides

A very interesting family of double helical foldamers is derived from aromatic oligoarylamide. These oligomers fold into a single helical conformation stabilized by a series of intramolecular hydrogen bonds.[28] This single helix is able to extend like springs and dimerize to form double helical strands. This phenomenon results in an expansion of the surface area between the aromatic rings (Figure I–11). Indeed, intramolecular aromatic stacking is substituted by intermolecular π–π interactions between pyridine units layered on top of each other, which stabilize the edifice. As a result, this stabilization is primarily driven by an enthalpic effect that compensates for the entropic cost.[87–89]

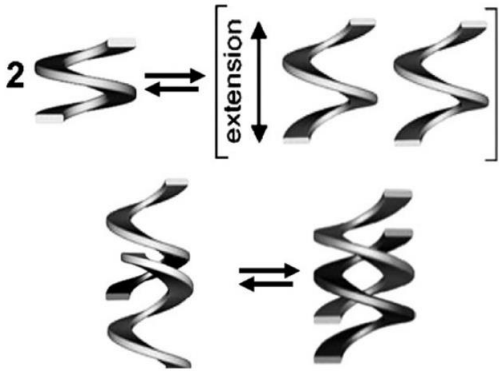


*Figure I–11. Representation of the extension/compression of two single helical strands and eddy–like slippage of one single helical strand inside the other to create a double helical structure.*[87–89]

The dynamics of these foldamers in solution is readily followed by $^{1}$H NMR spectroscopy. The NMR signals can be assigned to single and double helices upon varying the concentration or the temperature: double helices are favored upon increasing the concentration or lowering the temperature. This equilibrium is most often slow at the NMR timescale, which explains the progressive disappearance of the signals assigned to the double helix to the benefit of the single helix ones along dilution experiments. When the equilibrium state is reached, the measured proportions of single and double helices permit the evaluation of the dimerization constant using a non–linear regression analyses.[27,89] This equilibrium is influenced by the solvent composition:[27] the dimerization constant $K_{dim}$ tends to increase in solvents featuring moderate polarities, such as chloroform, and to decrease in polar and competitive solvents to hydrogen bonds, such as DMSO and pyridine.

On the other hand, the hybridization equilibrium of these oligomers is affected by different internal parameters. It was evidenced by $^{1}$H NMR spectroscopy that increasing the length of oligomers leads to a significant enhancement in the hybridization propensity to form double helices ($K_{dim}$ (**I–12**) = $10^4$, while $K_{dim}$ (**I–15**) > $10^6$) Figure I–12).[90] This result highlights the role of π–π stacking in stabilizing the duplex structure. However, expanding the length of oligomers lowers in a significant way the kinetics of association and dissociation between single and double helices from minutes for heptamer to weeks for tridecamer.

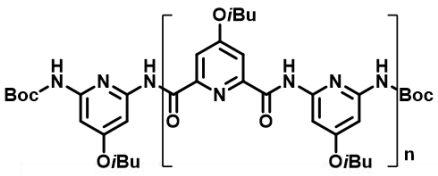


| | I-11 (n = 2) | I-12 (n = 3) | I-13 (n = 4) | I-14 (n = 5) | I-15 (n = 6) |
|---|---|---|---|---|---|
| $CDCl_3$ | - | 31000 | $5.10^5$ | $>10^6$ | $>10^6$ |
| Pyridine-$d_5$ | - | 10 | 19 | 42 | 307 |

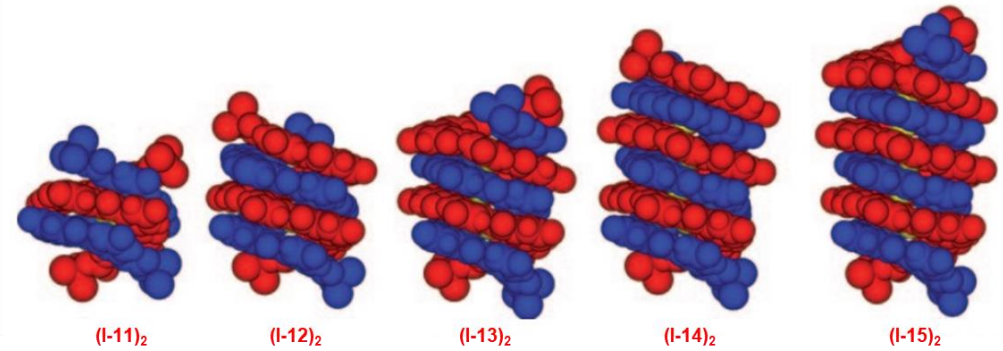


*Figure I–12. Structures of foldamers **I–11** to **I–15**, the crystallographic structures and the association constants of the corresponding homoduplexes.*[90]

The enlargement of the helix diameter by introducing bigger monomers generates a pronounced stabilization of the double helical structure, with dimerization constants exceeding $10^7$ in numerous organic solvents.[91] Increasing the surface engaged in intermolecular π–π stacking and lowering the enthalpic cost by increasing the helix diameter are responsible for the improved hybridization ability (Figure I–13).

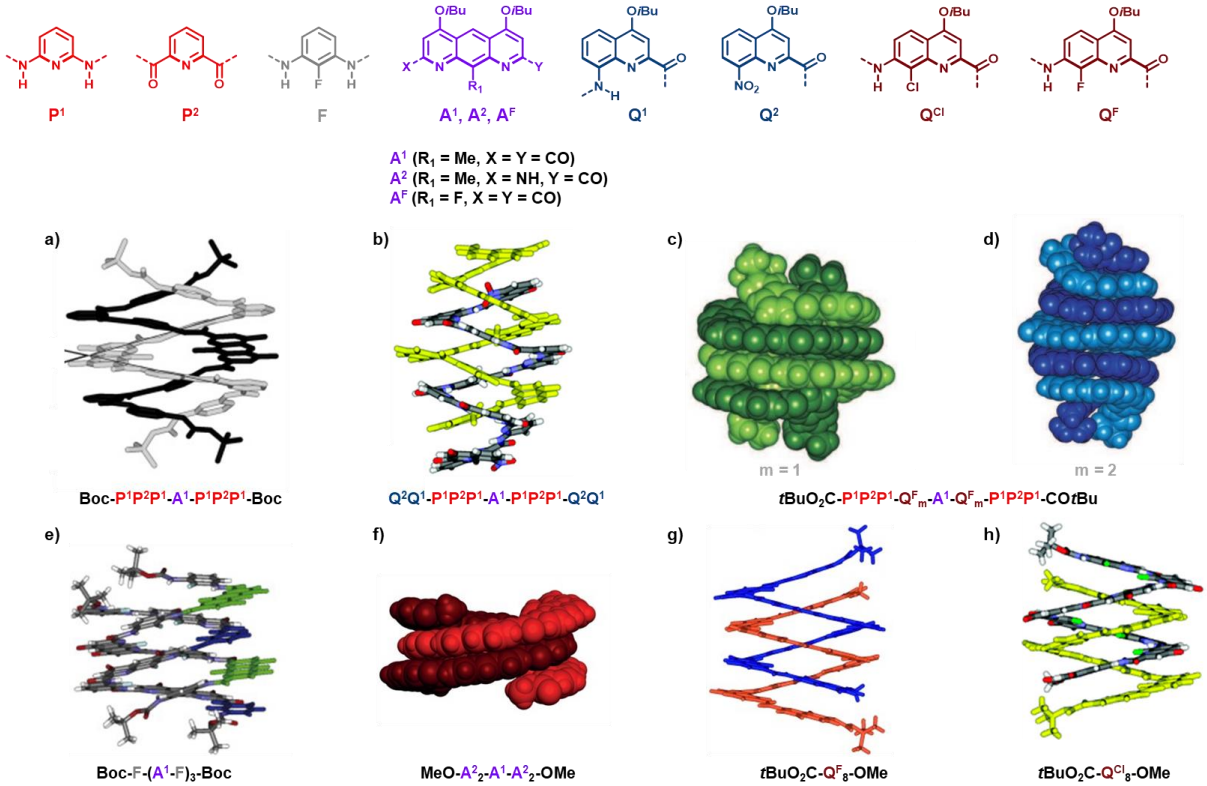


*Figure I–13. Representative structural formulas of monomers with color–coding*[41] *and the crystallographic structures of the corresponding homoduplexes $a_2$,*[92] *$b_2$,*[93] *$c_2$,*[94] *$d_2$,*[94] *$e_2$,*[95] *$f_2$,*[96] *$g_2$*[18]*, and $h_2$.*[97]

The important role of side–chain/side–chain interactions in stabilizing the folded structures of proteins is known for decades.[98–101] In this context, foldamer skeletons have been functionalized with various side chains, generally through the position 4 of pyridyl rings (Figure I–14–a). The studies conducted by $^1$H NMR spectroscopy demonstrated that introducing decyloxy chains on each pyridyl moiety of foldamer **I–18** leads to a significant enhancement of the dimerization constant ($K_{dim}$ = 6.5 × $10^4$ in $CDCl_3$) in comparison to foldamer **I–16** ($K_{dim}$ = 30 in $CDCl_3$), which lacks side chains. Here, the electron donor character of decyloxy chains as well as an interdigitation of the alkyl chains are responsible for the stabilisation of the duplex, by increasing the π–π interactions between aromatic rings.[31,102]

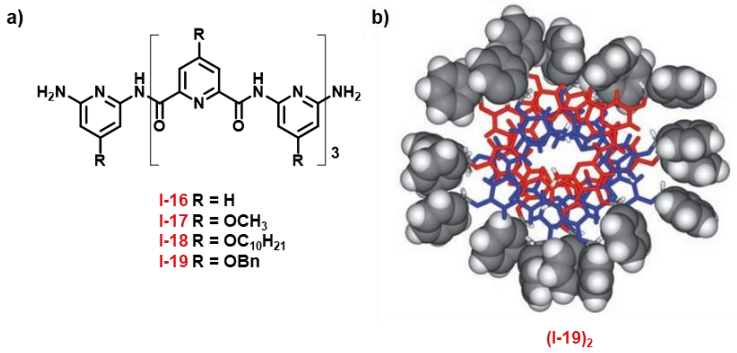


*Figure I–14. a) Structures of foldamers **I–16** to **I–19** with their corresponding side chains,[31,102] b) Crystallographic structure of foldamer **I–19** in its double helical form.[103]*

Switching from alkyl to aromatic chains also proves to affect the hybridization equilibrium. The dimerization constant ($K_{dim}$ = 5.3 × $10^5$ in $CDCl_3$) of foldamer **I–19** exhibits a tenfold increase in comparison to **I–17** ($K_{dim}$ = 8.2 × $10^4$ in $CDCl_3$) and **I–18**.[103,104] The high stability of the duplex is attributed to the interstrand interactions between the aromatic rings of the side chains, which was confirmed through a crystallographic structure (Figure I–14–b). These side chain interactions appear powerful, since this foldamer hybridized in a solvent competitive to hydrogen bonds, such as DMSO.[105]

## A.2. Helicene–based foldamers

As mentioned before, other types of building blocks dimerize to form duplexes based on aromatic interactions. Ethynylhelicene oligomers are considered part of these families, as the formation of duplexes is guaranteed when the backbone includes a minimum of six monomer units.[54] The stabilization of these duplexes depends on the hard or soft character of the side chains (**I–20** to **I–24**). Considering that the helicene monomer presents a soft character,

the organization of soft–hard (helicene–side chain) monomers was found as optimal to form stable double helices, compared to soft–soft organization (Figure I–15).[106]

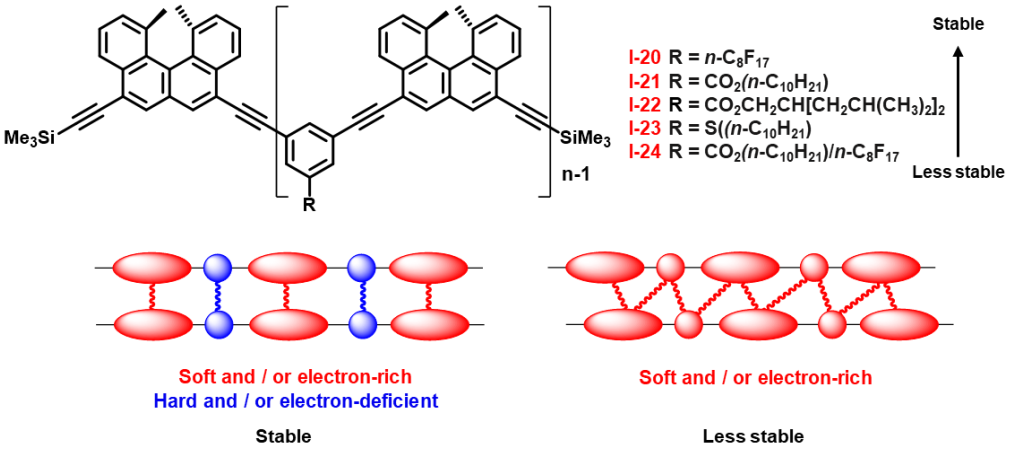


*Figure I–15. Structures of foldamers **I–20** to **I–24** with their corresponding side chains and illustration of the stable and less stable duplexes depending on the organization between soft and hard monomers.*[106]

The substitution of alkyne linkers by other functional groups such as amide (**I–25**, **I–26**),[107,108] aminomethylene (**I–27**)[109–111] or sulfonamide (**I–28**)[112,113] may allow additional types of non–covalent interactions to take place, such as hydrogen bonds, which improve the stability of the duplexes (Scheme I–8). Moreover, Yamaguchi *et al.* showed that these duplexes are solvent[54] and temperature responsive.[54,110,114] They dissociate in the presence of soft aromatic solvents and at high temperature, while they are stabilized in hard aromatic solvents and at room temperature (25°C).

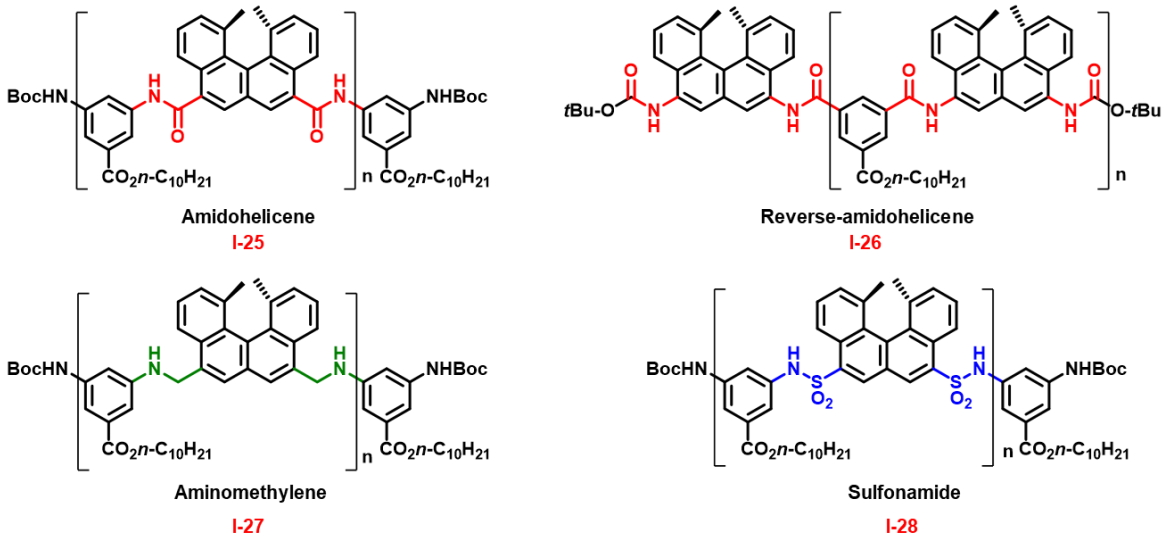


*Scheme I–8. Representative scheme of various linkers used for the construction of helicene–based oligomers: amide **I–25** and **I–26**,[107,108] aminomethylene **I–27**,[109] and sulfonamide **I–28**.*[112]

## A.3. Other backbones forming homoduplexes

The examples described in paragraph §IV.A.1 and §IV.A.2 highlighted the ability of foldamers to dimerize in organic solvents. As reported by Yashima and coworkers, this can also be successfully achieved in water with oligoresorcinols (Figure I–16–a). Indeed, synergetic solvophobic interactions allow for the formation of such species in aqueous environments, while this foldamer remains in a random coil structure in most organic solvents (*e.g.* methanol).[115] Single and double helices of the short oligomer **I–29** were obtained depending on the composition of solvent (Figure I–16–b). Considering the longer oligomer **I–30**, it was shown that upon the addition of β–cyclodextrin, double helices were dissociated because a [3]pseudorotaxane composed of one strand of **I–30** and two β–CD macrocycles was formed. Interestingly, the incorporation of adamantane derivative led to the formation of inclusion complexes and hence, to the consequent release of the single strand and regeneration of the double helices **(I–30)$_2$** (Figure I–16–c).[116] This constitutes an original example of a reversibly controlled double helix formation by adding additional components to the medium.

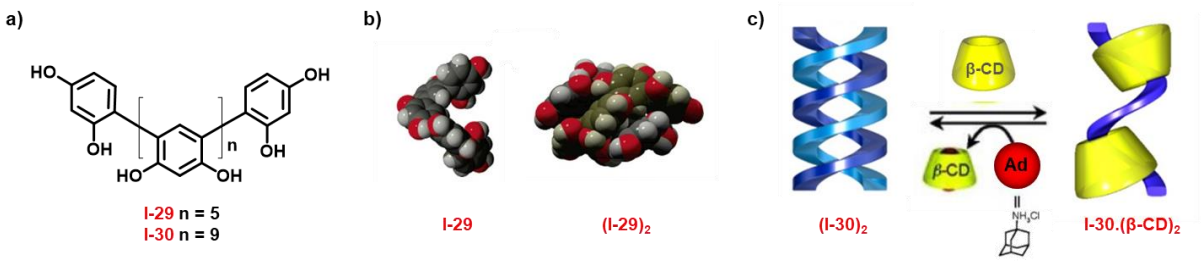


*Figure I–16. a) Structures of oligoresorcinols foldamers **I–29** and **I–30**, b) X–ray structures of foldamer **I–29** as single helix (crystallized from $CHCl_3/CH_3CN$) and double helix (crystallized from water), c) Schematic representation of the reversible hybridization of **I–30** upon adding β–CD and adamantane derivative.*[115,116]

Eventually, while most duplexes are stabilized by π–π stacking, Wisner and coworkers designed a family of foldamers constituted by alternative pyridine and thiazine dioxide (*e.g.* **I–31**), which dimerize to form double helical structures stabilized mainly by hydrogen bonds.[117] The interstrand hydrogen bonds were evidenced by $^1$H NMR spectroscopy, the NH hydrogen donor of thiazine dioxide shifted downfield upon increasing the concentrations (Figure I–17).

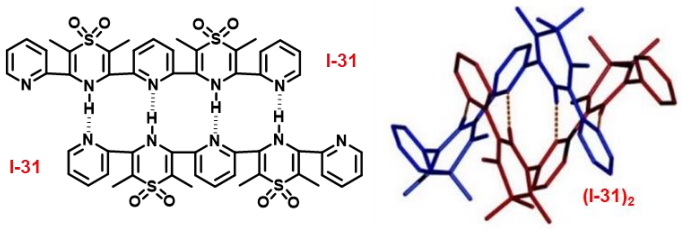


*Figure I–17. Structure of foldamer **I–31** and its corresponding double helical crystallographic structure.*[117]

# B. Hybridization of helical foldamers into heteroduplexes

## B.1. Cross–hybridization of foldamers displaying similar skeletons

The hybridization of two non–identical strands into duplexes requires an additional and complementary driving force in order to synthesize heteroduplexes selectively. This probably explains why heteroduplexes remain rare scarce in the literature.

*m*–Terphenyl–based foldamers, mainly developed by Yashima, hybridize to form duplexes based on specific complementarity between both strands bearing carboxylic acid and amidine functions, as illustrated with **I–32** and **I–33** (Figure I–18). As both strands are constructed from different and complementary building blocks, this family of oligomers dimerize to form hetero–double helices. These duplexes display a high stability, even in polar solvents, due to partially charged structure of amidinium–carboxylate salt bridge, and their dimerization constant is predicted to be higher than $10^6$ at 25°C in moderately polar solvents like $CHCl_3$.[55]

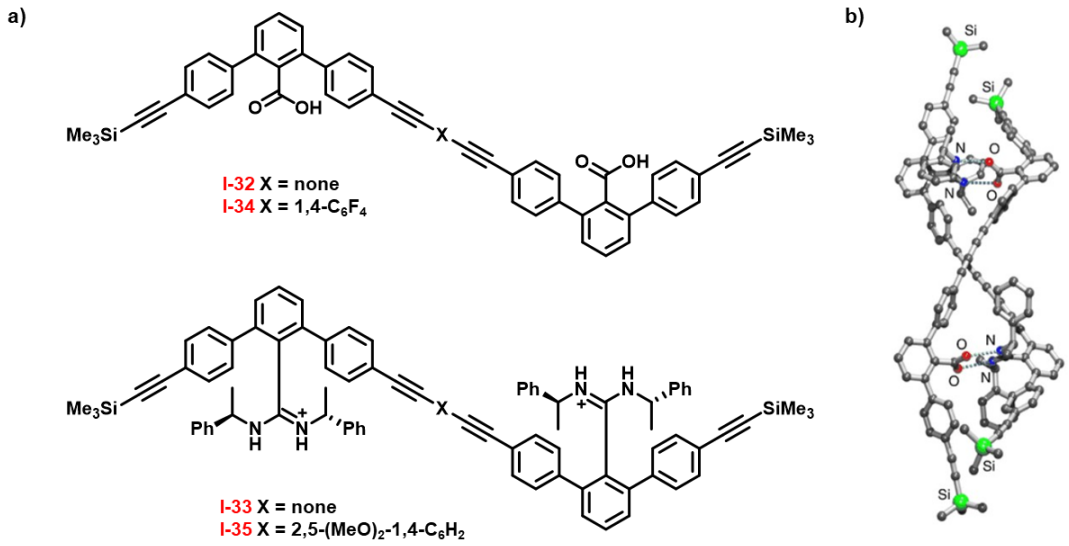


*Figure I–18. a) Structures of foldamers **I–32** to **I–35** bearing amidinium and carboxylate functions. No linker separating monomers for **I–32** and **I–33**, **I–34** contains an electron–deficient linker and **I–35** contains an electron–donor linker, b) Crystallographic structure of heteroduplex **I–32** and **I–33**.*[118,119]

Various structural parameters can influence the strength of the interaction between both strands. For instance, Yashima and coworkers showed that introducing a methylene bridge between the phenyl ring on one hand, and the carboxylic acid function or the amidine one, leads to a weaker ion pairing phenomenon.[118] Alternatively, an additional driving force can be set up to enhance the stability of the duplex: by introducing the 2,3,5,6–tetrafluorophenyl unit (**I–34)** and the 2,5–dimethoxyphenyl one (**I–35**) on the *p*–phenylene connectors, a significant increase

of the dimerization constant was evidenced (Figure I–18). This effect was rationalized by the authors in terms of aromatic interactions between electron–poor and electron–rich moieties.[119]

Taking advantage from the chirality of some foldamers, Yamaguchi and coworkers have recently described the formation of heteroduplexes **I–36•I–37** using a new methodology based on pseudoenantiomeric ethynylhelicene oligomers. The latter consists of (*M*) and (*P*) helicenes bearing different side chains. Through CD spectroscopy measurements, it was found that mixing different helicities leads to the formation of heteroduplexes, which proved to be more stable than the corresponding homoduplexes (Scheme I–9).[120]

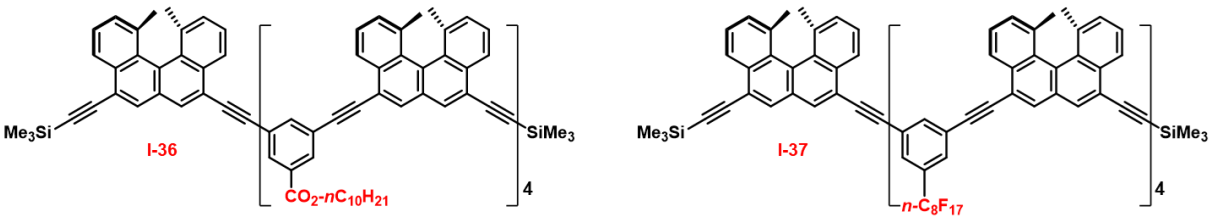


*Scheme I–9. Structures of ethynylhelicene foldamers **I–36** and **I–37** bearing different side chains.*[120]

Regarding the family of oligoamide foldamers, Huc and coworkers reported the cross–hybridization between pyridine dicarboxamide oligomer **I–38** and its oxidized derivative **I–39** (Figure I–19–a). In solution, both oligomers dimerize into homo–double helices with moderate dimerization constant: $K_{dim}$ (**I–38**) = 30 and $K_{dim}$ (**I–39**) = 125 in $CDCl_3$ at 25°C. On the contrary, heteroduplex formation between both oligomers was found to be more favorable in the same conditions with a significantly higher dimerization constant ($K_{dim}$ (**I–38•I–39**) = 1140). This particular stability apparently results from electrostatic repulsions, as suggested by theoretical calculations.[121] Eventually, it was found that oligoamide foldamers made from quinoline building blocks bearing fluorine (**I–40**) and chlorine (**I–41**) atoms undergo cross–hybridization because of their steric complementarity, as demonstrated by $^1$H NMR spectroscopy and mass spectrometry (ESI MS) (Figure I–19–b).[97] In a similar way, foldamers built from the same skeleton but bearing different side chains in an equimolar ratio mainly afforded heteroduplex **I–42•I–43** and to a lesser extent, homoduplexes **(I–42)$_2$** and **(I–43)$_2$** (Figure I–19–c).[91]

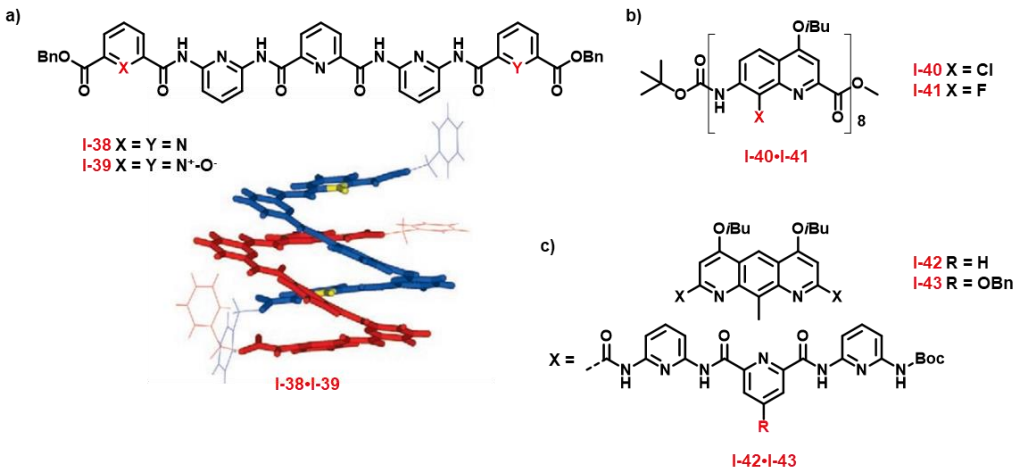


*Figure I–19. Structures of oligopyridine dicarboxamide foldamers and their heteroduplexes.*

## B.2. Cross–hybridization of foldamers displaying different skeletons

The examples discussed so far mentioned cross–hybridization processes between similar skeletons. Noteworthily, this phenomenon is sometimes observed between very different strands. For instance, Huc and coworkers demonstrated the ability of a short oligomer (**I–44**), which strongly tends to hybridize ($K_{dim} > 10^7$), to partially dissociate and undergo cross–hybridization with oligomer **I–45** ($K_{dim} > 10^5$). As evidenced in the solid state (Figure I–20),[96] introducing a quinoline monomer was found to enlarge the helix diameter and thus, improved their capability to hybridize into double helices.

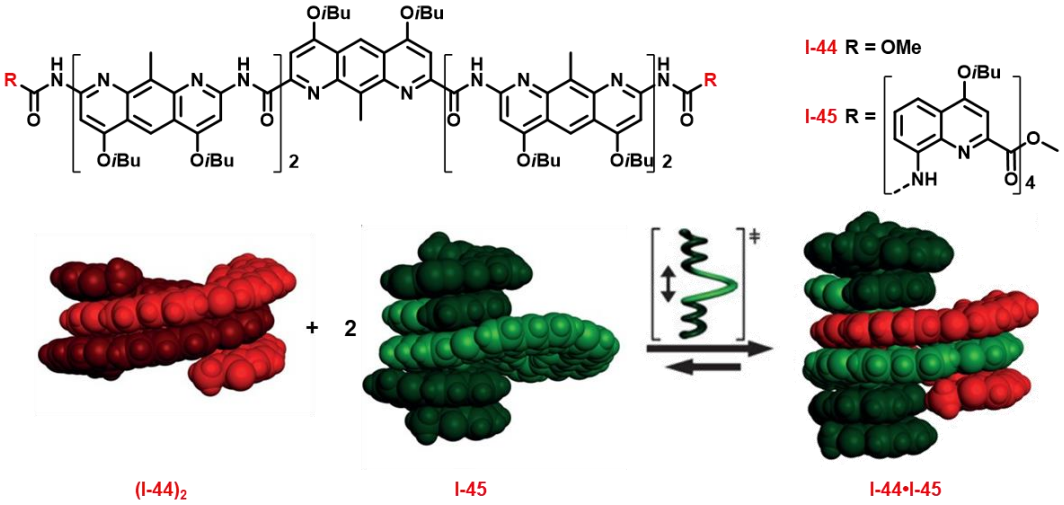


*Figure I–20. Structures of foldamers **I–44** and **I–45**, crystallographic structures of **(I–44)$_2$** in its double helical form, **I–45** in its single helical form and the heteroduplex **I–44•I–45**.*[96]

The formation of heteroduplexes by hybridization of different skeletons was also reported by Wisner and coworkers with the **I–46•I–47** and **I–46•I–48** pairs. This was achieved by taking advantage of hydrogen bond interactions between hydrogen bond donors (**I–47**, **I–**

**48)** and acceptors (**I–46**). The corresponding duplexes were formed in solution state with high dimerization constant ($K_{dim} > 3 \times 10^3$, $CDCl_3$), as well as in the solid (Figure I–21).[122,123]

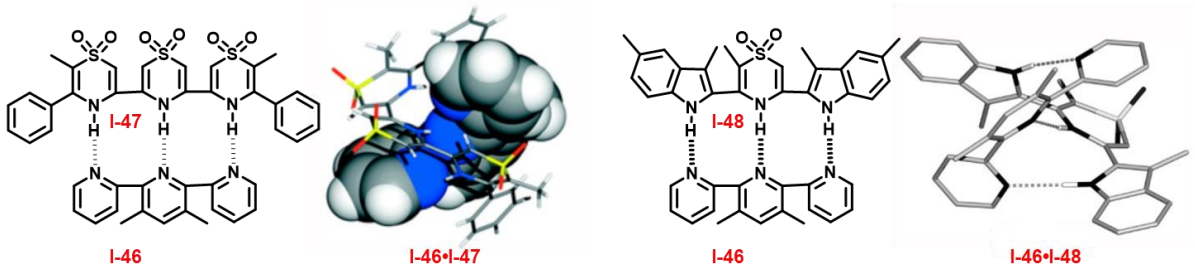


*Figure I–21. Structures of foldamers **I–46**, **I–47** and **I–48** and crystallographic structures of heteroduplexes **I–46•I–47** and **I–47•I–48**.*[122,123]

Eventually, oligoresorcinol **I–30**, which was described in the section dedicated to homoduplexes (IV.A), undergoes a process of dissociation and subsequent reorganization when exposed to linear oligosaccharides **I–49**. This example is quite unique, since this heteroduplex associates strands that have little in common, apart from the presence of hydrogen bond donor and acceptor functions (Figure I–22).[124] This remarkable behavior could be evidenced through circular dichroism spectroscopy, as oligosaccharides induce a preferential handedness of the foldamer backbone.

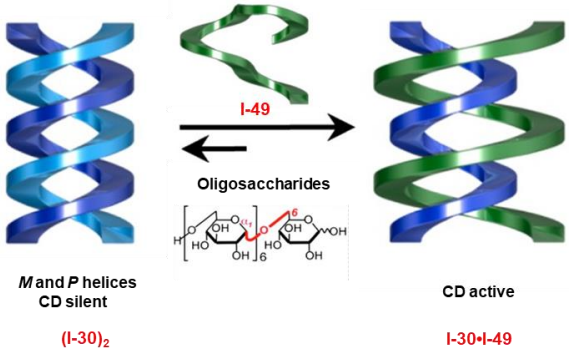


*Figure I–22. Schematic representation of the dissociation of homoduplex **(I–30)₂** in favor to heteroduplex **I–30•I–49** formation upon adding an oligosaccharide **I–49**.*[124]

## C. Hybridization of helical foldamers into multiple helices

Multiple helices, such as triple and quadruple helices, are considerably less common than double helices and, in most of the cases, they are obtained serendipitously. Huc and coworkers described a tetrameric oligomer **I–50** containing 1,8–naphthyridine monomers. X–ray diffraction analyses showed that three strands of this foldamer hybridize in both ‘parallel’ and ‘anti–parallel’ fashion. In other words, the three helices display either identical or non–identical extremities (Figure I–23–a).[19]

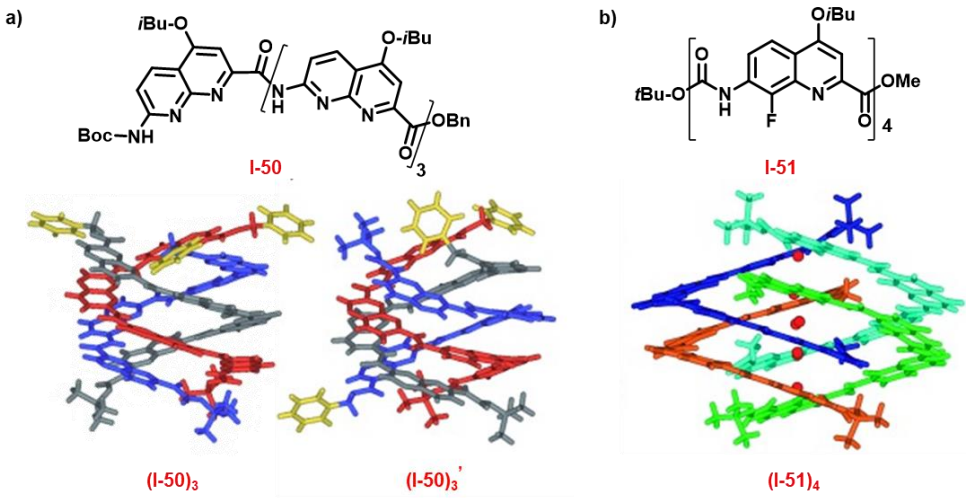


*Figure I–23. a) Structure of foldamer **I–50** and its corresponding triple helical X–ray structures **(I–50)**$_3$, b) Structure of foldamer **I–51** and its second corresponding quadruple helical X–ray structures **(I–51)**$_4$.*[18,19]

The formation of a quadruple helix architecture was reported by Jiang and coworkers in 2008 with foldamer **I–51**. The crystallographic structure of this fluoroquinoline derivative showed the exceptional formation of a quadruple helix with a large cavity, where water molecules were lodged (Figure I–23–b). Thereby, these examples illustrate how even minor variation in the molecular structure can induce unexpected supramolecular arrangements.

## V. π–Functional foldamers: Challenges of the thesis

The rich supramolecular chemistry of foldamers may explain why these structures have found miscellaneous applications in 1) host–guest chemistry, to trap and detect different types of guests,[125,126] 2) molecular machinery, as pseudo–cycles surrounding axles,[127,128] 3) therapeutics and biological applications (ion channelling and cell penetration),[129,130] or 4) catalysis.[23] Besides the established applications of foldamers, it is important to acknowledge that there are additional characteristics to investigate. In this context, the double helices differ from single helices in terms of geometry and potentially, physico–chemical properties. Indeed, controlling the hybridization equilibrium between single and double helices in a reversible manner, without altering the composition of the medium using other strategies than increasing the concentration, lowering the temperature or adding a guest, is still a challenge. Thus, controlling this equilibrium may constitute a strategy to drive the physico–chemical properties of foldamers. This has already been achieved by incorporating responsive units, undergoing conformational or configurational changes upon applying external stimuli, such as light,[35,131,132] redox stimulations[133] or by donor–acceptor interactions.[134,135] This can be advantageous to

develop smart materials and specifically controlling the hybridization equilibrium to elaborate homo– and heteroduplexes in a reversible manner.

## A. Modulating foldamers conformations through redox stimulations

The examples reported so far concerning redox–responsive foldamers, predominantly focus on controlling the conformational changes of individual strands. In this context, introducing electroactive units constitutes a strategy to modulate the conformation of foldamers when applying redox stimulations.

In this context, Heinze and coworkers[136] studied the effect of the redox properties of ferrocene units as a spacer on the behavior of foldamers. The spectroscopic, electrochemical and theoretical studies conducted on **I–52** demonstrated that the oxidation of ferrocene units leads to a conformational change, promoted by electronic repulsions between oxidized redox units.[137] On the other hand, taking advantage from an electroactive spacer able to switch between two conformations, Takata and coworkers[138] described polymer **I–53** comprising chiral spirobifluorene units. This macromolecule can undergo reversible changes from a conformation with a conformational freedom to a rigid planar conformation upon oxidation. This leads to a conformational change of the polymer from its helical structure to a coil–shaped and rigid helix. This highlighted an innovative redox–driven foldamer by modifying the rigidity of the skeleton (Figure I–24).

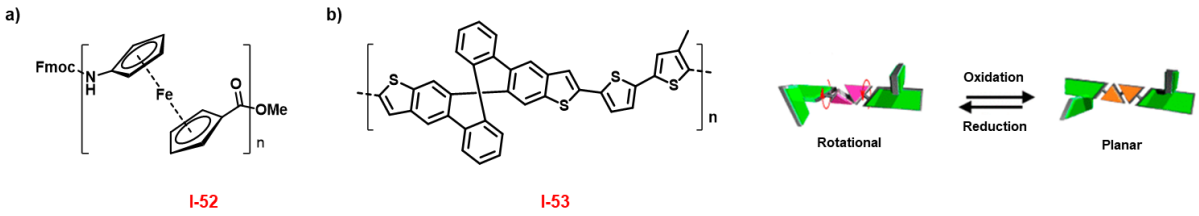


*Figure I–24. Structures of electroactive foldamer **I–52** and **I–53**, and schematic illustration of the conformational change of **I–53** upon oxidation.*[137,138]

Dubreuil, Huc and coworkers[139] demonstrated that the reduction reaction of **I–54** leads to the conversion of a pyridazine ring into a pyrrole one. This irreversible process affected the host–guest chemistry of this foldamer because the association constant with tartaric acid is significantly lower after reduction ($K_{pyridazine} > 10^6$ *vs* $K_{pyrrole} = 1.6 \times 10^4$). However, one will note that this example may lack reversibility.

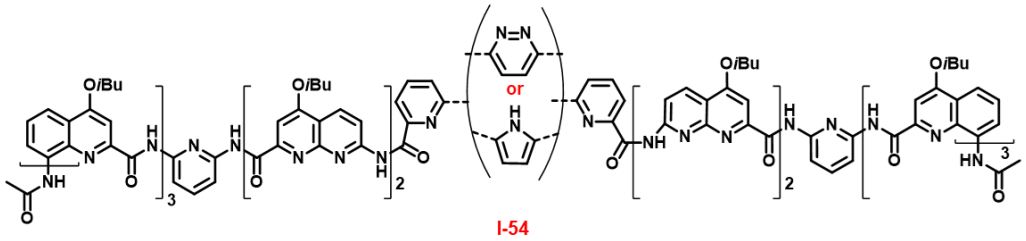


*Scheme I–10. Structure of foldamer **I–53**.*[139]

In this context, the research led by Z.T. Li and coworkers deserves to be highlighted. For instance, this team designed short oligomer **I–55**, which is capable of forming distinct arrangements promoted by inter or intramolecular hydrogen bonds when oxidizing the TTF units.[140] Based on the same concept of radical–cation dimerization, Z.T. Li and coworkers demonstrated that the preferred secondary structure of an oligo(ethylene glycol)–linked bipyridinium $BIPY^{2+}$ radical cation polymers **I–56** depends from inter– or intramolecular radical stacking, which favors homoduplexes or pleated structures, respectively (Scheme I–1).[141,142]

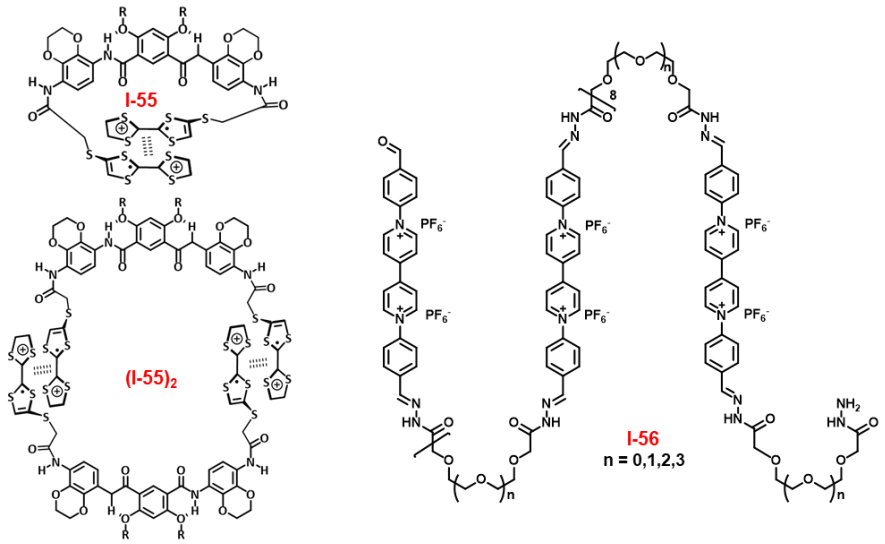


*Scheme I–11. Examples of electroactive foldamers containing tetrathiafulvalene **I–55** and $BIPY^{2+}$ **I–56** units.*[141,142]

Combining both driving forces, radical cation dimerization and donor–acceptor interactions, the same group developed a series of non–helical foldamers containing donor and acceptor electroactive units, such as TTF and bipyridinium ($BIPY^{2+}$) **I–57**,[143] dialkoxynaphthalene (NP) and bipyridinium $BIPY^{2+}$ **I–58**,[144] respectively. On this ground, the authors showed that the folding–unfolding processes can be tuned according to their oxidized/reduced states. This control can be achieved thanks to donor–acceptor interactions and

to radical–cation/anion dimerization of the oxidized/reduced species, respectively (Figure I–25).

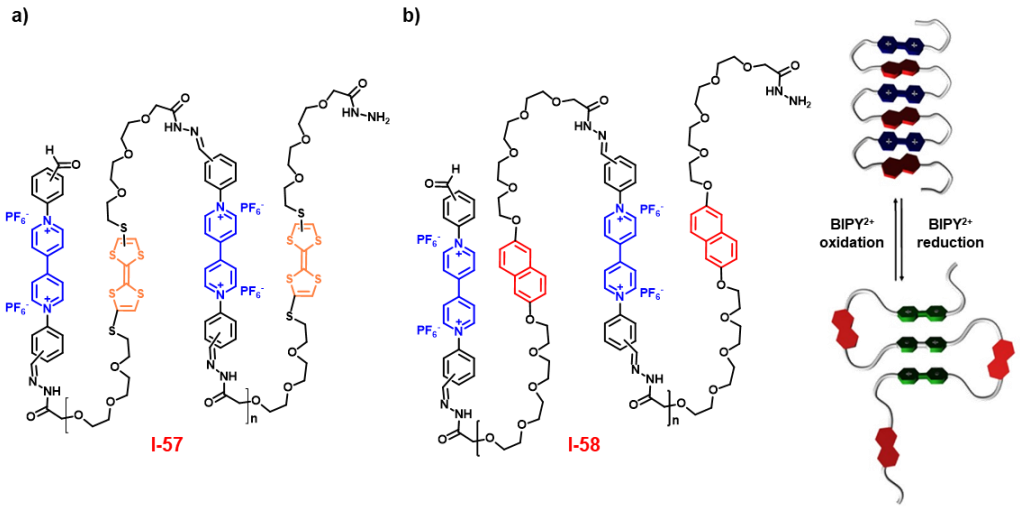


*Figure I–25. Structures of foldamers **I–57** and **I–58** and a representative illustration of the conformational change of **I–58** depending from the redox–state of $BIPY^{2+}$.*[143,144]

This team also went one step further using the same methodology, with the design of a pseudo–rotaxane. In this context, a flexible oligomer incorporating TTF units was synthesized. Taking advantage from the reversible oxidation of TTF units, it was demonstrated that oligomer **I–59** is linear in its neutral state and can interact with $CBPQT^{4+}$ by donor–acceptor interactions. The oxidation of TTF units weakens the corresponding assembly and provokes the dissociation of the axis and macrocycle, since radical cations interact together, which leads to a folded structure (Figure I–26).[145]

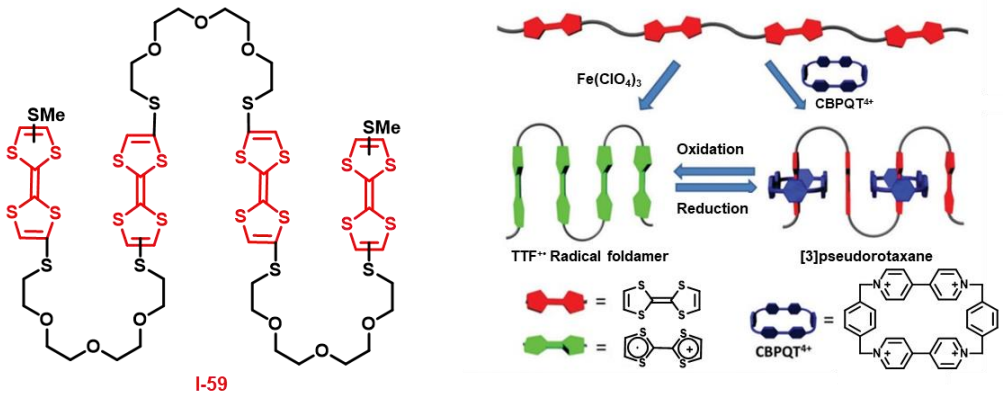


*Figure I–26. Structure of foldamer **I–59** and schematic representation of the involving equilibria depending from the redox states of TTF units.*[145]

Eventually, one will note that our group has also taken advantage of the radical–cation dimerization ability of TTF units to control the hybridization equilibrium of a helical foldamer in a reversible manner. This work will be discussed in detail in the introduction of Chapter 2.

## B. Foldamer based on donor–acceptor interactions

In 1995, Iverson and Lokey[134,135,146] reported the first abiotic and hydrosoluble aromatic foldamer **I–60**. Its pleated secondary structure in solution was ensured by intramolecular aromatic interactions between 1,4,5,8–naphthalenetetracarboxylic diimide (NDI) and 1,5–dialkoxynaphthalene (DAN) rings, which adopt a face–centered stacking arrangement. This was demonstrated by $^{1}$H NMR and UV–visible absorption spectroscopies (Figure I–27–a). Their first result encouraged them to elaborate two additional oligomers containing NDI and DAN (oligo–DAN **I–61** and oligo–NDI **I–62**). Both oligomers intertwined together to give a heteroduplex in aqueous solution (Figure I–27–b).[147] Interestingly, the corresponding red solution (1.5 mM) turned colorless upon heating at 80°C. The disappearance of the absorption band at 526 nm indicated the dissociation of donor–acceptor pairs at high temperature. This spectral modification proved to be irreversible, which shows that heteroduplexes are not formed back after cooling.[148] This example stands as a significant demonstration of the construction of heteroduplexes, potentially serving as an inspiration for chemists to build heteroduplexes with precise reversibility control.

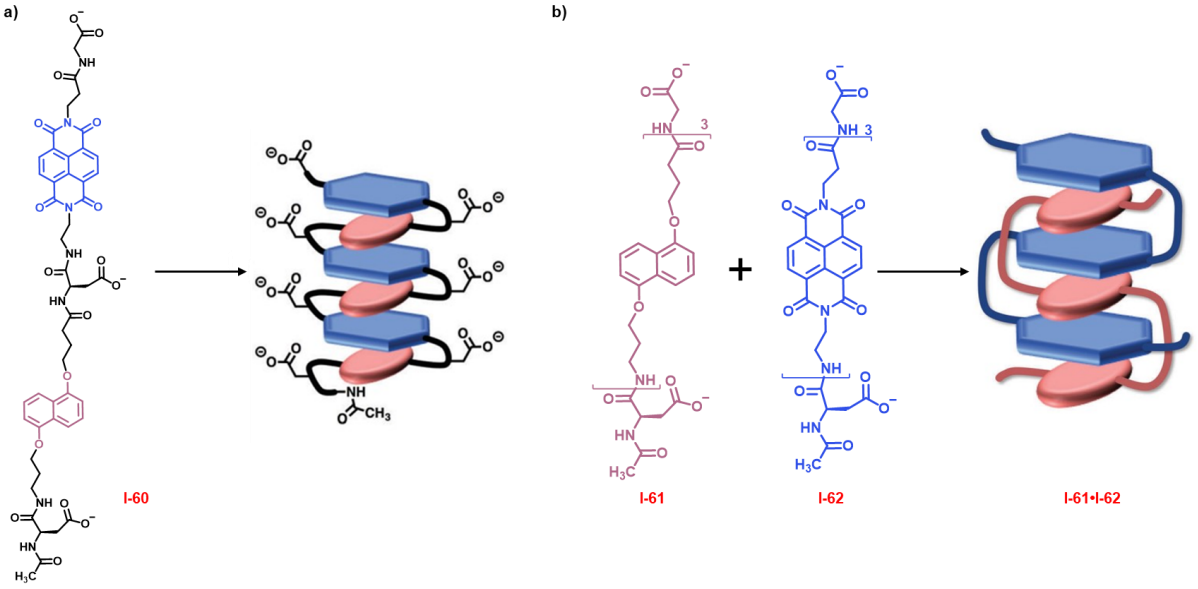


*Figure I–27. Structures of foldamers **I–60** to **I–62**, and schematic representation depicting the formation of the intertwined heteroduplex.*[147,148]

Using a similar strategy, Smietana, Morvan and coworkers recently designed hexamers including NDI (**I–63**) and DAN (**I–64**) units linked by one or two phosphodiesters around a propanediol to ensure the flexibility and hydrophilicity of these hexamers (Figure I–28). UV–visible absorption spectroscopy revealed the formation of a charge transfer complex through intertwining both hexamers in water. This duplex serves as a seed for the assembly into fibers,

which subsequently evolves towards a hydrogel state upon drying.[149] Interestingly, a heterohexamer made of alternating DAN and NDI monomers led to the formation of nanotubes.[150] Altogether, these results show to which extent the obtained microstructures depend on the unimers that self–assemble and how much remains to be done to fully control the bottom–up approaches.

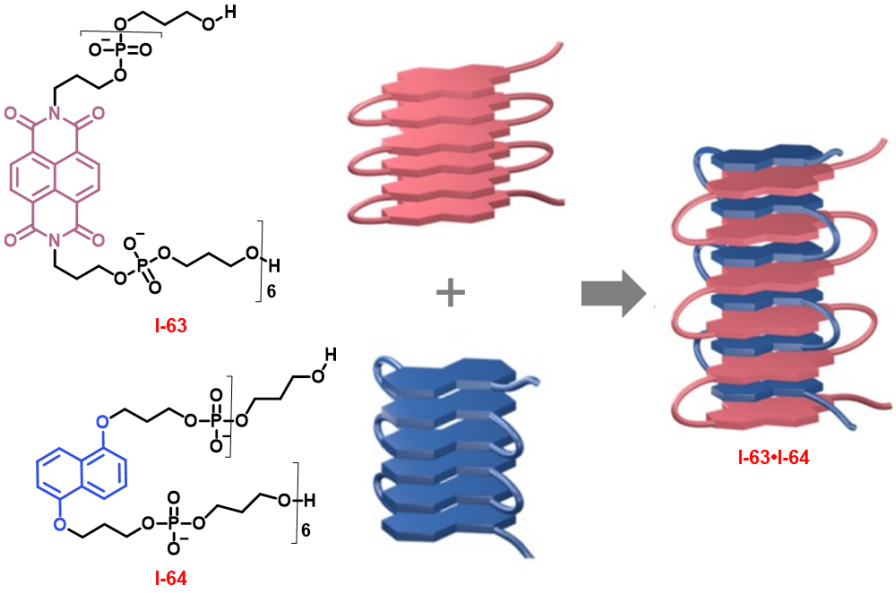


*Figure I–28. Structures of **I–63** and **I–64** and schematic representation of the corresponding heteroduplex **I–63•I–64**.*[149,150]

These previous examples reported the formation of duplexes in water, where charge transfer interactions were found to be strong. This certainly explains why the impact of donor–acceptor interactions on the supramolecular chemistry of foldamers was less explored in organic solvents.

In this context, our group began to develop this strategy after promising preliminary work on this subject. Foldamer **I–65**, endowed with two pyrene units at both extremities acting as donor moieties, was shown to form dimers, as evidenced by $^{1}$H NMR spectroscopy (Figure I–29). Upon adding an electron–deficient substituent (DCTNF, **I–67**), the equilibrium shifted towards the single helical state, most likely because DCTNF is involved into stronger aromatic interactions with the single helices in comparison to the double ones. This process was associated to a color change and logically, to the appearance of a charge transfer absorption band around 650 nm.[151] Furthermore, in unpublished results, it was found that a heteroduplex **I–65•I–66** was detected between pyrene– (**I–65**) and a 3,5–dinitroaniline–containing (**I–66**) foldamers using $^{1}$H NMR spectroscopy and mass spectrometry, despite a clear of selectivity.

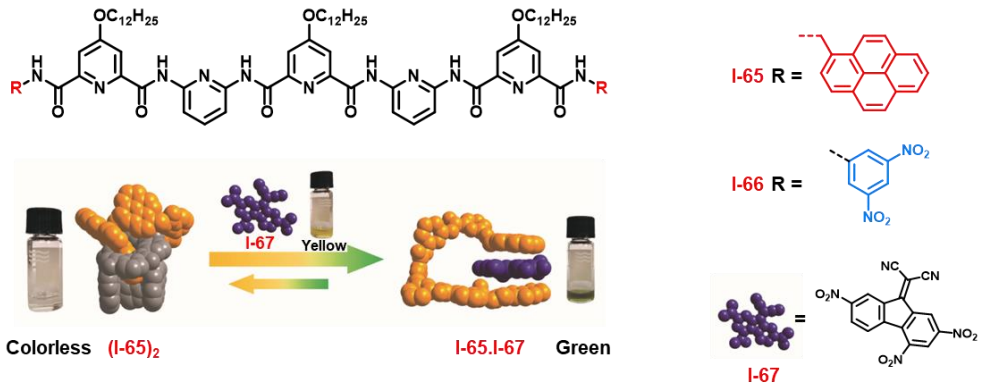


*Figure I–29. Structures of foldamers **I–65** and **I–66**, and schematic representation of the dissociation of the dimer upon adding DCTNF **I–67** to favor the complex **I–65•I–67**.*[151]

Therefore, the unique examples described by Iverson, Smietana and their teams, as well as the little we know about the design of heteroduplexes motivated our group to design heteroduplexes (if possible, in a selective manner) in order to investigate their supramolecular behavior and target new physico–chemical properties.

## VI. Thesis objectives

As evidenced by this introductory chapter, foldamers have been thoroughly studied in the literature and have emerged as potential candidates in a wide variety of applications ranging from biomedicine to materials science. These architectures are obtained from covalently linked monomers, able to fold in different ways through non–covalent interactions. This folding process leads to the formation of sophisticated secondary structures, depending on the backbone design and types of monomers. Some foldamers were shown to form multiplexes, *e.g.* double, triple or even quadruple helices. Devising strategies that can foresee and govern their formation appears relevant, most of them being serendipitously discovered at the time.

As mentioned at the beginning of this chapter, double helices differ from single helices in terms of geometry and physico–chemical properties. This is the reason why controlling the parameters that govern the equilibrium between single and double helices represents a challenge that has to be tackled. The equilibrium between single *vs* double helices depends on solute–solute and solute–solvent interactions. Thus, it can be shifted towards the hybridized species by increasing the concentration, varying the temperature or by taking advantage from the presence of a cavity formed by the helical skeleton.

Switching from single to double helices in a reversible manner can be already reached by controlling the temperature. However, it is challenging to induce this switching process by increasing the concentration, changing the solvent or introducing a guest, without altering the

composition of the medium. Consequently, reaching a reversible control over the equilibrium between single and hybridized helices represents a fundamental exciting challenge and constitutes the central concept of the RECHERCHE project (funded by the National Research Agency). This is why we envisaged to control the equilibrium between helices by applying an external stimuli, which would not affect the composition of the medium.

In this context, Chapter 2 discusses our efforts and successes to control the single–to–double helix equilibrium through redox stimulations. This part of the manuscript focuses on an electroactive foldamer grafted with the tetrathiafulvalene redox switch and its analogues, which helped understanding a particular supramolecular behavior.

Chapter 3 will primarily target the efforts conducted to elaborate heteroduplexes in a selective manner through donor–acceptor interactions. It will detail our efforts to synthesize and characterize electron rich strands (incorporating tetrathiafulvalene, dialkoxynaphthalene, pyrene units), and poor ones (containing trinitrofluorenone, naphthalene diimide functional groups) at the extremities of the foldamer skeleton. This chapter will also focus on the unexpected behavior of the electroactive foldamers and detail our efforts to understand their singular supramolecular chemistry.

(1) Eisenberg, D. The Discovery of the α–Helix and β–Sheet, the Principal Structural Features of Proteins. *Proceedings of the National Academy of Sciences* **2003**, *100* (20), 11207–11210.
(2) Klug, A. The Discovery of the DNA Double Helix. *Journal of Molecular Biology* **2004**, *335* (1), 3–26.
(3) Watson, J. D.; Crick, F. H. Molecular Structure of Nucleic Acids: A Structure for Deoxyribose Nucleic Acid. *Nature* **1953**, *171* (4356), 737–738.
(4) Diener, M.; Adamcik, J.; Sánchez–Ferrer, A.; Jaedig, F.; Schefer, L.; Mezzenga, R. Primary, Secondary, Tertiary and Quaternary Structure Levels in Linear Polysaccharides: From Random Coil, to Single Helix to Supramolecular Assembly. *Biomacromolecules* **2019**, *20* (4), 1731–1739.
(5) Natta, G.; Pino, P.; Corradini, P.; Danusso, F.; Mantica, E.; Mazzanti, G.; Moraglio, G. Crystalline High Polymers of α–Olefins. *Journal of the American Chemical Society* **1955**, *77* (6), 1708–1710.
(6) Gellman, S. H. Foldamers: A Manifesto. *Accounts of Chemical Research* **1998**, *31* (4), 173–180.
(7) Hill, D. J.; Mio, M. J.; Prince, R. B.; Hughes, T. S.; Moore, J. S. A Field Guide to Foldamers. *Chemical Reviews* **2001**, *101* (12), 3893–4012.
(8) Hecht, S.; Huc, I. *Foldamers: Structure, Properties and Applications*; John Wiley & Sons, **2007**.
(9) Rodriguez, J. M.; Hamilton, A. D. Benzoylurea Oligomers: Synthetic Foldamers That Mimic Extended α Helices. *Angewandte Chemie* **2007**, *119* (45), 8768–8771.
(10) Guo, L.; Almeida, A. M.; Zhang, W.; Reidenbach, A. G.; Choi, S. H.; Guzei, I. A.; Gellman, S. H. Helix Formation in Preorganized β/γ–Peptide Foldamers: Hydrogen–Bond Analogy to the α–Helix without α–Amino Acid Residues. *Journal of the American Chemical Society* **2010**, *132* (23), 7868–7869.
(11) Fremaux, J.; Mauran, L.; Pulka-Ziach, K.; Kauffmann, B.; Odaert, B.; Guichard, G. α-Peptide–Oligourea Chimeras: Stabilization of Short α-Helices by Non-Peptide Helical Foldamers. *Angewandte Chemie* **2015**, *127* (34), 9954–9958.
(12) Sebaoun, L.; Maurizot, V.; Granier, T.; Kauffmann, B.; Huc, I. Aromatic Oligoamide β–Sheet Foldamers. *Journal of the American Chemical Society* **2014**, *136* (5), 2168–2174.
(13) Lee, S.; Hua, Y.; Flood, A. H. β–Sheet–like Hydrogen Bonds Interlock the Helical Turns of a Photoswitchable Foldamer to Enhance the Binding and Release of Chloride. *The Journal of Organic Chemistry* **2014**, *79* (17), 8383–8396.
(14) Gellman, S. H. Foldamers: A Manifesto. *Accounts of Chemical Research* **1998**, *31* (4), 173–180.
(15) Kang, Y. K.; Byun, B. J. Computationally Designed B-turn Foldamers of Γ-peptides Based on 2-(Aminomethyl) Cyclohexanecarboxylic Acid. *Biopolymers* **2012**, *97* (12), 1018–1025.
(16) Srinivas, D.; Gonnade, R.; Ravindranathan, S.; Sanjayan, G. J. Conformationally Constrained Aliphatic− Aromatic Amino–Acid–Conjugated Hybrid Foldamers with Periodic β–Turn Motifs. *The Journal of Organic Chemistry* **2007**, *72* (18), 7022–7025.
(17) Tang, Q.; Zhong, Y.; Miller, D. P.; Liu, R.; Zurek, E.; Lu, Z.–L.; Gong, B. Reverse Turn Foldamers: An Expanded β–Turn Motif Reinforced by Double Hydrogen Bonds. *Organic Letters* **2020**, *22* (3), 1003–1007.
(18) Gan, Q.; Bao, C.; Kauffmann, B.; Grélard, A.; Xiang, J.; Liu, S.; Huc, I.; Jiang, H. Quadruple and Double Helices of 8-fluoroquinoline Oligoamides. *Angewandte Chemie International Edition* **2008**, *47* (9), 1715–1718.
(19) Ferrand, Y.; Kendhale, A. M.; Garric, J.; Kauffmann, B.; Huc, I. Parallel and Antiparallel Triple Helices of Naphthyridine Oligoamides. *Angewandte Chemie International Edition* **2010**, *49* (10), 1778–1781.
(20) Sebaoun, L.; Maurizot, V.; Granier, T.; Kauffmann, B.; Huc, I. Aromatic Oligoamide β–Sheet Foldamers. *Journal of the American Chemical Society* **2014**, *136* (5), 2168–2174.
(21) Maier, T.; Przylas, I.; Strater, N.; Herdewijn, P.; Saenger, W. Reinforced HNA Backbone Hydration in the Crystal Structure of a Decameric HNA/RNA Hybrid. *Journal of the American Chemical Society* **2005**, *127* (9), 2937–2943.
(22) Massena, C. J.; Wageling, N. B.; Decato, D. A.; Martin Rodriguez, E.; Rose, A. M.; Berryman, O. B. A Halogen-Bond-Induced Triple Helicate Encapsulates Iodide. *Angewandte Chemie* **2016**, *128* (40), 12586–12590.
(23) Smaldone, R. A.; Moore, J. S. Reactive Sieving with Foldamers: Inspiration from Nature and Directions for the Future. *Chemistry–A European Journal* **2008**, *14* (9), 2650–2657.
(24) Verreault, D.; Moreno, K.; Merlet, É.; Adamietz, F.; Kauffmann, B.; Ferrand, Y.; Olivier, C.; Rodriguez, V. Hyper–Rayleigh Scattering as a New Chiroptical Method: Uncovering the Nonlinear Optical Activity of Aromatic Oligoamide Foldamers. *Journal of the American Chemical Society* **2019**, *142* (1), 257–263.
(25) Suk, J.; Naidu, V. R.; Liu, X.; Lah, M. S.; Jeong, K.–S. A Foldamer–Based Chiroptical Molecular Switch That Displays Complete Inversion of the Helical Sense upon Anion Binding. *Journal of the American Chemical Society* **2011**, *133* (35), 13938–13941.
(26) Le Bailly, B. A.; Clayden, J. Dynamic Foldamer Chemistry. *Chemical Communications* **2016**, *52* (27), 4852–4863.
(27) Berl, V.; Huc, I.; Khoury, R. G.; Krische, M. J.; Lehn, J.–M. Interconversion of Single and Double Helices Formed from Synthetic Molecular Strands. *Nature* **2000**, *407* (6805), 720–723.
(28) Berl, V.; Huc, I.; Khoury, R. G.; Lehn, J.–M. Helical Molecular Programming: Folding of Oligopyridine-dicarboxamides into Molecular Single Helices. *Chemistry–A European Journal* **2001**, *7* (13), 2798–2809.
(29) Dolain, C.; Maurizot, V.; Huc, I. Protonation-Induced Transition between Two Distinct Helical Conformations of a Synthetic Oligomer via a Linear Intermediate. *Angewandte Chemie International Edition* **2003**, *42* (24), 2738–2740.
(30) Helical Molecular Programming: Folding of Oligopyridine-dicarboxamides into Molecular Single Helices. *Chemistry – A European Journal* **2001**, *7* (13), 2798–2809.
(31) Berl, V.; Huc, I.; Khoury, R. G.; Lehn, J.–M. Helical Molecular Programming: Supramolecular Double Helices by Dimerization of Helical Oligopyridine–Dicarboxamide Strands. *Chemistry – A European Journal* **2001**, *7* (13), 2810–2820.
(32) Faour, L.; Adam, C.; Gautier, C.; Goeb, S.; Allain, M.; Levillain, E.; Canevet, D.; Sallé, M. Redox–Controlled Hybridization of Helical Foldamers. *Chem. Commun.* **2019**, *55* (40), 5743–5746.
(33) Tie, C.; Gallucci, J. C.; Parquette, J. R. Helical Conformational Dynamics and Photoisomerism of Alternating Pyridinedicarboxamide/m–(Phenylazo) Azobenzene Oligomers. *Journal of the American Chemical Society* **2006**, *128* (4), 1162–1171.
(34) Khan, A.; Kaiser, C.; Hecht, S. Prototype of a Photoswitchable Foldamer. *Angewandte Chemie International Edition* **2006**, *45* (12), 1878–1881.
(35) King, E. D.; Tao, P.; Sanan, T. T.; Hadad, C. M.; Parquette, J. R. Photomodulated Chiral Induction in Helical Azobenzene Oligomers. *Organic Letters* **2008**, *10* (9), 1671–1674.
(36) Yu, Z.; Hecht, S. Remote Control over Folding by Light. *Chemical Communications* **2016**, *52* (40), 6639–6653.
(37) Yu, Z.; Hecht, S. Reversible and Quantitative Denaturation of Amphiphilic Oligo (Azobenzene) Foldamers. *Angewandte Chemie* **2011**, *123* (7), 1678–1681.

(38) Menke, F. S.; Mazzier, D.; Wicher, B.; Allmendinger, L.; Kauffmann, B.; Maurizot, V.; Huc, I. Molecular Torsion Springs: Alteration of Helix Curvature in Frustrated Tertiary Folds. *Organic & Biomolecular Chemistry* **2023**, 21, 1275-1283.
(39) Menke, F. S.; Wicher, B.; Allmendinger, L.; Maurizot, V.; Huc, I. An Abiotic, Tetrameric, Eight–Helix Bundle. *Chemical Science* **2023**, *14* (14), 3742–3751.
(40) Horne, W. S.; Price, J. L.; Keck, J. L.; Gellman, S. H. Helix Bundle Quaternary Structure from α/β–Peptide Foldamers. *Journal of the American Chemical Society* **2007**, *129* (14), 4178–4180.
(41) Yashima, E.; Ousaka, N.; Taura, D.; Shimomura, K.; Ikai, T.; Maeda, K. Supramolecular Helical Systems: Helical Assemblies of Small Molecules, Foldamers, and Polymers with Chiral Amplification and Their Functions. *Chemical Reviews* **2016**, *116* (22), 13752–13990.
(42) Cheng, R. P.; Gellman, S. H.; DeGrado, W. F. β–Peptides: From Structure to Function. *Chemical Reviews* **2001**, *101* (10), 3219–3232.
(43) Nielsen, P. E.; Haaima, G. Peptide Nucleic Acid (PNA). A DNA Mimic with a Pseudopeptide Backbone. *Chemical Society Reviews* **1997**, *26* (2), 73–78.
(44) Wu, C. W.; Sanborn, T. J.; Zuckermann, R. N.; Barron, A. E. Peptoid Oligomers with α–Chiral, Aromatic Side Chains: Effects of Chain Length on Secondary Structure. *Journal of the American Chemical Society* **2001**, *123* (13), 2958–2963.
(45) Simon, R. J.; Kania, R. S.; Zuckermann, R. N.; Huebner, V. D.; Jewell, D. A.; Banville, S.; Ng, S.; Wang, L.; Rosenberg, S.; Marlowe, C. K. Peptoids: A Modular Approach to Drug Discovery. *Proceedings of the National Academy of Sciences* **1992**, *89* (20), 9367–9371.
(46) Nowick, J. S.; Mahrus, S.; Smith, E. M.; Ziller, J. W. Triurea Derivatives of Diethylenetriamine as Potential Templates for the Formation of Artificial β–Sheets. *Journal of the American Chemical Society* **1996**, *118* (5), 1066–1072.
(47) Seebach, D.; Hook, D. F.; Glättli, A. Helices and Other Secondary Structures of B-and Γ-peptides. *Peptide Science: Original Research on Biomolecules* **2006**, *84* (1), 23–37.
(48) Trabocchi, A.; Guarna, F.; Guarna, A. γ–and δ–Amino Acids: Synthetic Strategies and Relevant Applications. *Current Organic Chemistry* **2005**, *9* (12), 1127–1153.
(49) Hamuro, Y.; Geib, S. J.; Hamilton, A. D. Oligoanthranilamides. Non–Peptide Subunits That Show Formation of Specific Secondary Structure. *Journal of the American Chemical Society* **1996**, *118* (32), 7529–7541.
(50) Huc, I. Aromatic Oligoamide Foldamers. *European Journal of Organic Chemistry* **2004**, *2004* (1), 17–29.
(51) Nelson, J. C.; Saven, J. G.; Moore, J. S.; Wolynes, P. G. Solvophobically Driven Folding of Nonbiological Oligomers. *Science* **1997**, *277* (5333), 1793–1796.
(52) Hou, J.–L.; Shao, X.–B.; Chen, G.–J.; Zhou, Y.–X.; Jiang, X.–K.; Li, Z.–T. Hydrogen Bonded Oligohydrazide Foldamers and Their Recognition for Saccharides. *Journal of the American Chemical Society* **2004**, *126* (39), 12386–12394.
(53) Zhu, J.; Parra, R. D.; Zeng, H.; Skrzypczak–Jankun, E.; Zeng, X. C.; Gong, B. A New Class of Folding Oligomers: Crescent Oligoamides. *Journal of the American Chemical Society* **2000**, *122* (17), 4219–4220.
(54) Sugiura, H.; Nigorikawa, Y.; Saiki, Y.; Nakamura, K.; Yamaguchi, M. Marked Effect of Aromatic Solvent on Unfolding Rate of Helical Ethynylhelicene Oligomer. *Journal of the American Chemical Society* **2004**, *126* (45), 14858–14864.
(55) Tanaka, Y.; Katagiri, H.; Furusho, Y.; Yashima, E. A Modular Strategy to Artificial Double Helices. *Angewandte Chemie International Edition* **2005**, *44* (25), 3867–3870.
(56) Yashima, E.; Maeda, K.; Iida, H.; Furusho, Y.; Nagai, K. Helical Polymers: Synthesis, Structures, and Functions. *Chemical Reviews* **2009**, *109* (11), 6102–6211.
(57) Qi, S.; Zhang, C.; Yan, T.; Yang, F.; Zhang, J.; Mao, S.; Dong, Z. Hybrid Helical Polymer Nanochannels Constructed by Combining Aromatic Amide and Pyridine-Oxadiazole Structural Sequences. *Macromolecular Rapid Communications* **2020**, *41* (24), 2000099.
(58) Chen, F.; Shen, J.; Li, N.; Roy, A.; Ye, R.; Ren, C.; Zeng, H. Pyridine/Oxadiazole-based Helical Foldamer Ion Channels with Exceptionally High K+/Na+ Selectivity. *Angewandte Chemie International Edition* **2020**, *59* (4), 1440–1444.
(59) Nelson, J. C.; Saven, J. G.; Moore, J. S.; Wolynes, P. G. Solvophobically Driven Folding of Nonbiological Oligomers. *Science* **1997**, *277* (5333), 1793.
(60) Stephens, O. M.; Kim, S.; Welch, B. D.; Hodsdon, M. E.; Kay, M. S.; Schepartz, A. Inhibiting HIV Fusion with a β–Peptide Foldamer. *Journal of the American Chemical Society* **2005**, *127* (38), 13126–13127.
(61) Hua, Y.; Flood, A. H. Flipping the Switch on Chloride Concentrations with a Light–Active Foldamer. *Journal of the American Chemical Society* **2010**, *132* (37), 12838–12840.
(62) Ferrand, Y.; Kendhale, A. M.; Kauffmann, B.; Grélard, A.; Marie, C.; Blot, V.; Pipelier, M.; Dubreuil, D.; Huc, I. Diastereoselective Encapsulation of Tartaric Acid by a Helical Aromatic Oligoamide. *Journal of the American Chemical Society* **2010**, *132* (23), 7858–7859.
(63) Zhang, D.–W.; Zhao, X.; Hou, J.–L.; Li, Z.–T. Aromatic Amide Foldamers: Structures, Properties, and Functions. *Chemical Reviews* **2012**, *112* (10), 5271–5316.
(64) Malone, J. F.; Murray, C. M.; Dolan, G. M.; Docherty, R.; Lavery, A. J. Intermolecular Interactions in the Crystal Chemistry of N–N–Diphenylisophthalamide, Pyridine–2, 6–Dicarboxylic Acid Bisphenylamide, and Related Compounds. *Chemistry of Materials* **1997**, *9* (12), 2983–2989.
(65) Hamuro, Y.; Geib, S. J.; Hamilton, A. D. Novel Molecular Scaffolds: Formation of Helical Secondary Structure in a Family of Oligoanthranilamides. *Angewandte Chemie International Edition in English* **1994**, *33* (4), 446–448.
(66) Hamuro, Y.; Geib, S. J.; Hamilton, A. D. Novel Folding Patterns in a Family of Oligoanthranilamides: Non–Peptide Oligomers That Form Extended Helical Secondary Structures. *Journal of the American Chemical Society* **1997**, *119* (44), 10587–10593.
(67) Kolomiets, E.; Berl, V.; Lehn, J.–M. Chirality Induction and Protonation-induced Molecular Motions in Helical Molecular Strands. *Chemistry–A European Journal* **2007**, *13* (19), 5466–5479.
(68) Juwarker, H.; Suk, J.; Jeong, K.–S. Foldamers with Helical Cavities for Binding Complementary Guests. *Chemical Society Reviews* **2009**, *38* (12), 3316–3325.
(69) Juwarker, H.; Jeong, K.–S. Anion–Controlled Foldamers. *Chemical Society Reviews* **2010**, *39* (10), 3664–3674.
(70) Huc, I.; Maurizot, V.; Gornitzka, H.; Léger, J.–M. Hydroxy–Substituted Oligopyridine Dicarboxamide Helical Foldamers. *Chemical Communications* **2002**, No. 6, 578–579.
(71) Garric, J.; Léger, J.–M.; Huc, I. Molecular Apple Peels. *Angewandte Chemie* **2005**, *117* (13), 1990–1994.
(72) Bao, C.; Kauffmann, B.; Gan, Q.; Srinivas, K.; Jiang, H.; Huc, I. Converting Sequences of Aromatic Amino Acid Monomers into Functional Three-Dimensional Structures: Second-Generation Helical Capsules. *Angewandte Chemie International Edition* **2008**, *47* (22), 4153–4156.
(73) Bao, C.; Gan, Q.; Kauffmann, B.; Jiang, H.; Huc, I. A Self-assembled Foldamer Capsule: Combining Single and Double Helical Segments in One Aromatic Amide Sequence. *Chemistry–A European Journal* **2009**, *15* (43), 11530–11536.

(74) Ferrand, Y.; Huc, I. Designing Helical Molecular Capsules Based on Folded Aromatic Amide Oligomers. *Accounts of Chemical Research* **2018**, *51* (4), 970–977.

(75) Ashwell, G.; Morell, A. G. Membrane Glycoproteins and Recognition Phenomena. *Trends in Biochemical Sciences* **1977**, *2* (4), 76–78.

(76) Liu, H.; Wu, J.; Xu, Y.–X.; Jiang, X.–K.; Li, Z.–T. Complexation of Hydrogen Bonding–Driven Preorganized Di–and Hexacationic Bisporphyrin Receptors for C60(CO2)2 in Aqueous and DMSO Media. *Tetrahedron Letters* **2007**, *48* (41), 7327–7331.

(77) Hou, J.–L.; Yi, H.–P.; Shao, X.–B.; Li, C.; Wu, Z.–Q.; Jiang, X.–K.; Wu, L.–Z.; Tung, C.–H.; Li, Z.–T. Helicity Induction in Hydrogen-Bonding-Driven Zinc Porphyrin Foldamers by Chiral C60-Incorporating Histidines. *Angewandte Chemie* **2006**, *118* (5), 810–814.

(78) Wu, Z.–Q.; Shao, X.–B.; Li, C.; Hou, J.–L.; Wang, K.; Jiang, X.–K.; Li, Z.–T. Hydrogen–Bonding–Driven Preorganized Zinc Porphyrin Receptors for Efficient Complexation of C60, C70, and C60 Derivatives. *Journal of the American Chemical Society* **2005**, *127* (49), 17460–17468.

(79) Wu, Z.–Q.; Li, C.–Z.; Feng, D.–J.; Jiang, X.–K.; Li, Z.–T. Foldamer–Based Pyridine–Fullerene Tweezer Receptors for Enhanced Binding of Zinc Porphyrin. *Tetrahedron* **2006**, *62* (48), 11054–11062.

(80) Zhang, D.–W.; Zhao, X.; Hou, J.–L.; Li, Z.–T. Aromatic Amide Foldamers: Structures, Properties, and Functions. *Chemical Reviews* **2012**, *112* (10), 5271–5316.

(81) Hasenknopf, B.; Lehn, J.–M.; Kneisel, B. O.; Baum, G.; Fenske, D. Self-assembly of a Circular Double Helicate. *Angewandte Chemie International Edition in English* **1996**, *35* (16), 1838–1840.

(82) Bell, T. W.; Jousselin, H. Self–Assembly of a Double–Helical Complex of Sodium. *Nature* **1994**, *367* (6462), 441–444.

(83) Koert, U.; Harding, M. M.; Lehn, J.–M. DNH Deoxyribonucleohelicates: Self Assembly of Oligonucleosidic Double–Helical Metal Complexes. *Nature* **1990**, *346* (6282), 339–342.

(84) Barboiu, M.; Lehn, J.–M. Dynamic Chemical Devices: Modulation of Contraction/Extension Molecular Motion by Coupled–Ion Binding/pH Change–Induced Structural Switching. *Proceedings of the National Academy of Sciences* **2002**, *99* (8), 5201–5206.

(85) Rich, A.; Crick, F. H. C. The Molecular Structure of Collagen. *Journal of Molecular Biology* **1961**, *3* (5), 483–IN4.

(86) Langs, D. A. Three–Dimensional Structure at 0.86 Å of the Uncomplexed Form of the Transmembrane Ion Channel Peptide Gramicidin A. *Science* **1988**, 188–191.

(87) Maurizot, V.; Léger, J. M.; Guionneau, P.; Huc, I. Diversity of Interstrand Pp Stacking Motifs in the Double Helices of Pyridinedicarboxamide Oligomers. *Russian Chemical Bulletin* **2004**, *53* (7), 1572–1576.

(88) Berl, V.; Huc, I.; Khoury, R. G.; Lehn, J.–M. Helical Molecular Programming: Supramolecular Double Helices by Dimerization of Helical Oligopyridine-dicarboxamide Strands. *Chemistry–A European Journal* **2001**, *7* (13), 2810–2820.

(89) Haldar, D.; Jiang, H.; Léger, J.–M.; Huc, I. Double versus Single Helical Structures of Oligopyridine–Dicarboxamide Strands. Part 2: The Role of Side Chains. *Tetrahedron* **2007**, *63* (27), 6322–6330.

(90) Baptiste, B.; Zhu, J.; Haldar, D.; Kauffmann, B.; Léger, J.–M.; Huc, I. Hybridization of Long Pyridine-Dicarboxamide Oligomers into Multi-Turn Double Helices: Slow Strand Association and Dissociation, Solvent Dependence, and Solid State Structures. *Chemistry–An Asian Journal* **2010**, *5* (6), 1364–1375.

(91) Berni, E.; Kauffmann, B.; Bao, C.; Lefeuvre, J.; Bassani, D. M.; Huc, I. Assessing the Mechanical Properties of a Molecular Spring. *Chemistry–A European Journal* **2007**, *13* (30), 8463–8469.

(92) Berni, E.; Kauffmann, B.; Bao, C.; Lefeuvre, J.; Bassani, D. M.; Huc, I. Assessing the Mechanical Properties of a Molecular Spring. *Chemistry–A European Journal* **2007**, *13* (30), 8463–8469.

(93) Berni, E.; Garric, J.; Lamit, C.; Kauffmann, B.; Léger, J.–M.; Huc, I. Interpenetrating Single Helical Capsules. *Chemical Communications* **2008**, No. 17, 1968–1970.

(94) Gan, Q.; Ferrand, Y.; Bao, C.; Kauffmann, B.; Grélard, A.; Jiang, H.; Huc, I. Helix–Rod Host–Guest Complexes with Shuttling Rates Much Faster than Disassembly. *Science* **2011**, *331* (6021), 1172–1175.

(95) Gan, Q.; Shang, J.; Kauffmann, B.; Wang, Y.; Bie, F.; Jiang, H. A Highly Stable Double Helix of Aromatic Oligoamide Comprised of Fused Ring Aromatic Units. *Tetrahedron* **2012**, *68* (23), 4479–4484.

(96) Singleton, M. L.; Pirotte, G.; Kauffmann, B.; Ferrand, Y.; Huc, I. Increasing the Size of an Aromatic Helical Foldamer Cavity by Strand Intercalation. *Angewandte Chemie* **2014**, *126* (48), 13356–13360.

(97) Gan, Q.; Li, F.; Li, G.; Kauffmann, B.; Xiang, J.; Huc, I.; Jiang, H. Heteromeric Double Helix Formation by Cross–Hybridization of Chloro–and Fluoro–Substituted Quinoline Oligoamides. *Chemical Communications* **2010**, *46* (2), 297–299.

(98) Syud, F. A.; Stanger, H. E.; Gellman, S. H. Interstrand Side Chain− Side Chain Interactions in a Designed β–Hairpin: Significance of Both Lateral and Diagonal Pairings. *Journal of the American Chemical Society* **2001**, *123* (36), 8667–8677.

(99) Faure, G.; Bornot, A.; de Brevern, A. G. Protein Contacts, Inter–Residue Interactions and Side–Chain Modelling. *Biochimie* **2008**, *90* (4), 626–639.

(100) Berka, K.; Laskowski, R.; Riley, K. E.; Hobza, P.; Vondrasek, J. Representative Amino Acid Side Chain Interactions in Proteins. A Comparison of Highly Accurate Correlated Ab Initio Quantum Chemical and Empirical Potential Procedures. *Journal of Chemical Theory and Computation* **2009**, *5* (4), 982–992.

(101) Spassov, V. Z.; Yan, L.; Flook, P. K. The Dominant Role of Side-chain Backbone Interactions in Structural Realization of Amino Acid Code. ChiRotor: A Side-chain Prediction Algorithm Based on Side-chain Backbone Interactions. *Protein Science* **2007**, *16* (3), 494–506.

(102) Berl, V.; Huc, I.; Khoury, R. G.; Krische, M. J.; Lehn, J.–M. Interconversion of Single and Double Helices Formed from Synthetic Molecular Strands. *Nature* **2000**, *407* (6805), 720–723.

(103) Haldar, D.; Jiang, H.; Léger, J.–M.; Huc, I. Interstrand Interactions between Side Chains in a Double-Helical Foldamer. *Angewandte Chemie* **2006**, *118* (33), 5609–5612.

(104) Berl, V.; Huc, I.; Khoury, R. G.; Lehn, J.–M. Helical Molecular Programming: Folding of Oligopyridine-dicarboxamides into Molecular Single Helices. *Chemistry–A European Journal* **2001**, *7* (13), 2798–2809.

(105) Haldar, D.; Jiang, H.; Léger, J.–M.; Huc, I. Interstrand Interactions between Side Chains in a Double-Helical Foldamer. *Angewandte Chemie* **2006**, *118* (33), 5609–5612.

(106) Saito, N.; Terakawa, R.; Shigeno, M.; Amemiya, R.; Yamaguchi, M. Side Chain Effect on the Double Helix Formation of Ethynylhelicene Oligomers. *The Journal of Organic Chemistry* **2011**, *76* (12), 4841–4858.

(107) Ichinose, W.; Miyagawa, M.; Ito, J.; Shigeno, M.; Amemiya, R.; Yamaguchi, M. Synthesis and Duplex Formation of the Reverse Amidohelicene Tetramer. *Tetrahedron* **2011**, *67* (30), 5477–5486.

(108) Amemiya, R.; Ichinose, W.; Yamaguchi, M. Synthesis and Thermally Stable Helix–Dimer Formation of Amidohelicene Oligomers. *Bulletin of the Chemical Society of Japan* **2010**, *83* (7), 809–815.

(109) Shigeno, M.; Sato, M.; Kushida, Y.; Yamaguchi, M. Aminomethylenehelicene Oligomers Possessing Flexible Two-Atom Linker Form a Stimuli-Responsive Double-Helix in Solution. *Asian Journal of Organic Chemistry* **2014**, *3* (7), 797–804.

(110) Shigeno, M.; Kushida, Y.; Yamaguchi, M. Heating/Cooling Stimulus Induces Three–State Molecular Switching of Pseudoenantiomeric Aminomethylenehelicene Oligomers: Reversible Nonequilibrium Thermodynamic Processes. *Journal of the American Chemical Society* **2014**, *136* (22), 7972–7980.
(111) Kushida, Y.; Saito, N.; Shigeno, M.; Yamaguchi, M. Multiple Competing Pathways for Chemical Reaction: Drastic Reaction Shortcut for the Self–Catalytic Double–Helix Formation of Helicene Oligomers. *Chemical Science* **2017**, *8* (2), 1414–1421.
(112) Shigeno, M.; Kushida, Y.; Yamaguchi, M. Molecular Thermal Hysteresis in Helix-Dimer Formation of Sulfonamidohelicene Oligomers in Solution. *Chemistry–A European Journal* **2013**, *19* (31), 10226–10234.
(113) Kushida, Y.; Shigeno, M.; Yamaguchi, M. Concentration Threshold and Amplification Exhibited by a Helicene Oligomer during Helix-Dimer Formation: A Proposal on How a Cell Senses Concentration Changes of a Chemical. *Chemistry–A European Journal* **2015**, *21* (39), 13788–13792.
(114) Sugiura, H.; Yamaguchi, M. Helix–Dimer–Random–Coil Thermal Switching Process of Ethynylhelicene Heptamer Highly Sensitive to Its Environment. *Chemistry Letters* **2007**, *36* (1), 58–59.
(115) Goto, H.; Katagiri, H.; Furusho, Y.; Yashima, E. Oligoresorcinols Fold into Double Helices in Water. *Journal of the American Chemical Society* **2006**, *128* (22), 7176–7178.
(116) Goto, H.; Furusho, Y.; Yashima, E. Supramolecular Control of Unwinding and Rewinding of a Double Helix of Oligoresorcinol Using Cyclodextrin/Adamantane System. *Journal of the American Chemical Society* **2007**, *129* (1), 109–112.
(117) Li, J.; Wisner, J. A.; Jennings, M. C. A Self–Associating ADADA Hydrogen–Bonded Double Helix. *Organic Letters* **2007**, *9* (17), 3267–3269.
(118) Iida, H.; Shimoyama, M.; Furusho, Y.; Yashima, E. Double–Stranded Supramolecular Assembly through Salt Bridge Formation between Rigid and Flexible Amidine and Carboxylic Acid Strands. *The Journal of Organic Chemistry* **2010**, *75* (2), 417–423.
(119) Yamada, H.; Wu, Z.–Q.; Furusho, Y.; Yashima, E. Thermodynamic and Kinetic Stabilities of Complementary Double Helices Utilizing Amidinium–Carboxylate Salt Bridges. *Journal of the American Chemical Society* **2012**, *134* (22), 9506–9520.
(120) Amemiya, R.; Saito, N.; Yamaguchi, M. Hetero–Double–Helix Formation by an Ethynylhelicene Oligomer Possessing Perfluorooctyl Side Chains. *The Journal of Organic Chemistry* **2008**, *73* (18), 7137–7144.
(121) Zhan, C.; Léger, J.–M.; Huc, I. Cross-Hybridization of Pyridinedicarboxamide Helical Strands and Their N-Oxides. *Angewandte Chemie* **2006**, *118* (28), 4741–4744.
(122) Wang, H.–B.; Mudraboyina, B. P.; Li, J.; Wisner, J. A. Minimal Complementary Hydrogen–Bonded Double Helices. *Chemical Communications* **2010**, *46* (39), 7343–7345.
(123) Wang, H.–B.; Mudraboyina, B. P.; Wisner, J. A. Substituent Effects in Double-Helical Hydrogen-Bonded AAA-DDD Complexes. *Chemistry–A European Journal* **2012**, *18* (5), 1322–1327.
(124) Goto, H.; Furusho, Y.; Yashima, E. Double Helical Oligoresorcinols Specifically Recognize Oligosaccharides via Heteroduplex Formation through Noncovalent Interactions in Water. *Journal of the American Chemical Society* **2007**, *129* (29), 9168–9174.
(125) Juwarker, H.; Suk, J.; Jeong, K.–S. Foldamers with Helical Cavities for Binding Complementary Guests. *Chemical Society Reviews* **2009**, *38* (12), 3316–3325.
(126) Zhu, Y.–Y.; Wang, G.–T.; Li, Z.–T. Molecular Recognition with Linear Molecules as Receptors. *Current Organic Chemistry* **2011**, *15* (9), 1266–1292.
(127) Wang, X.; Gan, Q.; Wicher, B.; Ferrand, Y.; Huc, I. Directional Threading and Sliding of a Dissymmetrical Foldamer Helix on Dissymmetrical Axles. *Angewandte Chemie International Edition* **2019**, *58* (13), 4205–4209.
(128) Wang, X.; Wicher, B.; Ferrand, Y.; Huc, I. Orchestrating Directional Molecular Motions: Kinetically Controlled Supramolecular Pathways of a Helical Host on Rodlike Guests. *Journal of the American Chemical Society* **2017**, *139* (27), 9350–9358.
(129) Chen, F.; Shen, J.; Li, N.; Roy, A.; Ye, R.; Ren, C.; Zeng, H. Pyridine/Oxadiazole-based Helical Foldamer Ion Channels with Exceptionally High K+/Na+ Selectivity. *Angewandte Chemie International Edition* **2020**, *59* (4), 1440–1444.
(130) Iriondo-Alberdi, J.; Laxmi-Reddy, K.; Bouguerne, B.; Staedel, C.; Huc, I. Cellular Internalization of Water-Soluble Helical Aromatic Amide Foldamers. *ChemBioChem* **2010**, *11* (12), 1679–1685.
(131) Tie, C.; Gallucci, J. C.; Parquette, J. R. Helical Conformational Dynamics and Photoisomerism of Alternating Pyridinedicarboxamide/m–(Phenylazo) Azobenzene Oligomers. *Journal of the American Chemical Society* **2006**, *128* (4), 1162–1171.
(132) Khan, A.; Kaiser, C.; Hecht, S. Prototype of a Photoswitchable Foldamer. *Angewandte Chemie International Edition* **2006**, *45* (12), 1878–1881.
(133) Faour, L.; Adam, C.; Gautier, C.; Goeb, S.; Allain, M.; Levillain, E.; Canevet, D.; Sallé, M. Redox–Controlled Hybridization of Helical Foldamers. *Chemical Communications* **2019**, *55* (40), 5743–5746.
(134) Nguyen, J. Q.; Iverson, B. L. An Amphiphilic Folding Molecule That Undergoes an Irreversible Conformational Change. *Journal of the American Chemical Society* **1999**, *121* (11), 2639–2640.
(135) Scott Lokey, R.; Iverson, B. L. Synthetic Molecules That Fold into a Pleated Secondary Structure in Solution. *Nature* **1995**, *375* (6529), 303–305.
(136) Siebler, D.; Förster, C.; Heinze, K. Redox–Responsive Organometallic Foldamers from Ferrocene Amino Acid: Solid–Phase Synthesis, Secondary Structure and Mixed–Valence Properties. *Dalton Transactions* **2011**, *40* (14), 3558–3575.
(137) Siebler, D.; Linseis, M.; Gasi, T.; Carrella, L. M.; Winter, R. F.; Förster, C.; Heinze, K. Oligonuclear Ferrocene Amides: Mixed-Valent Peptides and Potential Redox-Switchable Foldamers. *Chemistry–A European Journal* **2011**, *17* (16), 4540–4551.
(138) Okuda, H.; Koyama, Y.; Uchida, S.; Michinobu, T.; Sogawa, H.; Takata, T. Reversible Transformation of a One–Handed Helical Foldamer Utilizing a Planarity–Switchable Spacer and C 2–Chiral Spirobifluorene Units. *ACS Macro Letters* **2015**, *4* (4), 462–466.
(139) Lautrette, G.; Aube, C.; Ferrand, Y.; Pipelier, M.; Blot, V.; Thobie, C.; Kauffmann, B.; Dubreuil, D.; Huc, I. Tuning the Guest-Binding Ability of a Helically Folded Capsule by In Situ Modification of the Aromatic Oligoamide Backbone. *Chemistry–A European Journal* **2014**, *20* (6), 1547–1553.
(140) Wang, W.–K.; Chen, Y.–Y.; Wang, H.; Zhang, D.–W.; Liu, Y.; Li, Z.–T. Tetrathiafulvalene-Based Macrocycles Formed by Radical Cation Dimerization: The Role of Intramolecular Hydrogen Bonding and Solvent. *Chemistry–An Asian Journal* **2014**, *9* (4), 1039–1044.
(141) Zhang, Y.–C.; Zhang, D.–W.; Wang, H.; Zhou, Y.; Li, Z.–T. Bipyridinium Radical Cation Dimerization–Driven Polymeric Pleated Foldamers and a Homoduplex That Undergo Ion–Tuned Interconversion. *Polymer Chemistry* **2015**, *6* (24), 4404–4408.
(142) Qi, Q.; Yang, B.; Xi, C.–G.; Yang, X.; Zhang, D.–W.; Liu, S.; Li, Z.–T. Doubly, Triply and Multiply Pleated Sheets of Bipyridinium Radical Cation-Incorporated Polymers Tuned by Four Cucurbiturils. *ChemistrySelect* **2016**, *1* (21), 6792–6796.
(143) Chen, L.; Wang, H.; Zhang, D.–W.; Zhou, Y.; Li, Z.–T. Quadruple Switching of Pleated Foldamers of Tetrathiafulvalene–Bipyridinium Alternating Dynamic Covalent Polymers. *Angewandte Chemie International Edition* **2015**, *54* (13), 4028–4031.
(144) Zhang, Y.–C.; Chen, L.; Wang, H.; Zhou, Y.–M.; Zhang, D.–W.; Li, Z.–T. Pleated Polymeric Foldamers Driven by Donor–Acceptor Interaction and Conjugated Radical Cation Dimerization. *Chinese Chemical Letters* **2016**, *27* (6), 817–821.

(145) Zhan, T.–G.; Wu, L.; Zhao, Z.; Zhou, Z.–B.; Yun, M.–Y.; Wei, J.; Zheng, S.–T.; Yin, H.–H.; Zhang, K.–D. Reversible Conversion between a Pleated Oligo–Tetrathiafulvalene Radical Foldamer and Folded Donor–Acceptor [3] Pseudorotaxane under Redox Conditions. *Chemical Communications* **2017**, *53* (39), 5396–5399.

(146) Peebles, C.; Piland, R.; Iverson, B. L. More than Meets the Eye: Conformational Switching of a Stacked Dialkoxynaphthalene–Naphthalenetetracarboxylic Diimide (DAN–NDI) Foldamer to an NDI–NDI Fibril Aggregate. *Chemistry–A European Journal* **2013**, *19* (35), 11598–11602.

(147) Gabriel, G. J.; Iverson, B. L. Aromatic Oligomers That Form Hetero Duplexes in Aqueous Solution. *Journal of the American Chemical Society* **2002**, *124* (51), 15174–15175.

(148) Nguyen, J. Q.; Iverson, B. L. An Amphiphilic Folding Molecule That Undergoes an Irreversible Conformational Change. *Journal of the American Chemical Society* **1999**, *121* (11), 2639–2640.

(149) de Carvasal, K. P.; Vergoten, G.; Vasseur, J.–J.; Smietana, M.; Morvan, F. Supramolecular Recognition of Phosphodiester–Based Donor and Acceptor Oligomers Forming Gels in Water. *Biomacromolecules* **2023**, *24* (2), 756–765.

(150) de Carvasal, K. P.; Aissaoui, N.; Vergoten, G.; Bellot, G.; Vasseur, J.–J.; Smietana, M.; Morvan, F. Folding of Phosphodiester–Linked Donor–Acceptor Oligomers into Supramolecular Nanotubes in Water. *Chemical Communications* **2021**, *57* (34), 4130–4133.

(151) Aparicio, F.; Faour, L.; Allain, M.; Canevet, D.; Sallé, M. A Pyrene–Functionalized Foldamer: Structural Impact and Recognition Properties Supported by Donor–Acceptor Interactions. *Chemical Communications* **2017**, *53* (88), 12028–12031.

# Chapter 2

# A new redox–sensitive foldamer: Synthesis, Supramolecular chemistry and Redox–triggered hybridization into homoduplexes

# I. Introduction

As mentioned in the conclusion of Chapter 1, the general objective of this PhD work lies on the design, the synthesis, and the characterizations of helical electroactive foldamers and the selective synthesis of duplexes. In this context, Chapter 2 details the efforts we made to devise homoduplexes and control their hybridization equilibrium.

Consequently, the following discussion focuses on the development of a new helical electroactive foldamer that was designed to allow for controlling the single *vs* double helix equilibrium in a reversible manner. In fact, the hybridization equilibrium is governed by different parameters, which are related to solute–solute and solute–solvent interactions. Thus, shifting the equilibrium towards the hybridized species is possible by increasing the concentration, lowering the temperature, taking advantage from solvophobic effects or the presence of a guest, and hence by modifying the composition of the medium. Unfortunately reaching reversibility through these strategies seems difficult. For that reason, achieving a reversible control over the equilibrium between single and hybridized helices without altering the composition of the medium constitutes a challenge to overcome. In this context, redox stimulation appeared as a relevant lever to reach our goals.

This concept was initially explored in our research group during the thesis of Dr Lara Faour, focusing on a short oligomer and a flexible linker.[1] The objective of the present work is to extend this study to longer oligomers and a rigid linker, providing further insights into the impact of TTF oxidation on the hybridization process. The following paragraphs will discuss the choices made regarding the foldamer skeleton, the selected electroactive unit, and the linker. The main objectives of this chapter consist in:

- Investigating the behavior of the functionalized foldamer in solution and the impacts of solvents, concentration, temperature and the presence of certain additives.
- Studying the effect of a short linker on the conformation and hence, on the hybridization equilibrium in solution. A particular attention will also be paid to the solid–state.
- Assessing the influence of electrochemical stimulations on the hybridization equilibrium by varying the redox state of electroactive units.

## A. Oligopyridine dicarboxamide foldamers: characteristics and hybridization

Oligopyridine dicarboxamide foldamers are constructed from alternating 2,6–diaminopyridine and 2,6–dicarbonylpyridine units. These oligomers allow for incorporating diverse functionalities units at the $R_1$, $R_{1'}$ and $R_2$ positions (Scheme II–1). This family of foldamers, which was initially developed by Lehn and Huc, adopts a specific helical conformation in solution that is stabilized by a network of hydrogen bonds.[2–4]

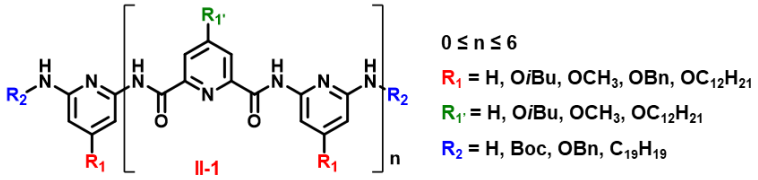


*Scheme II–1. Representative structure of an oligopyridine dicarboxamide foldamer (OiBu: isobutoxy chains, $OCH_3$: methoxy groups, OBn: benzyloxy groups, $OC_{12}H_{21}$: dodecyloxy chains, Boc: tert–butyloxycarbonyl).*

Before going into the details of this PhD work, it also appears important to explain why the present study focuses on this family. Among the wide diversity of available building blocks to construct helical backbones described in the literature (see Chapter 1), this skeleton was selected given several features it displays:

- Its synthesis is well–established and described in the literature; longer oligomers are attainable in a straightforward manner through convergent strategies;[5–7]
- They adopt a helical conformation in their single and double helical forms, with a moderate dimerization constant, and in most organic solvents;[8–12]
- The ease of their characterizations in solution as well in the solid state;[7]
- The functionalization of such foldamers is readily accessible within the core and the extremities;[6,7]
- They exhibit transparency in the visible range and are inactive in a wide range of redox potentials.[13]

### A.1. Characterizations of single and double helices in solution

The supramolecular chemistry of oligopyridine dicarboxamide foldamers in solution is primarily studied by $^1$H NMR spectroscopy. When both single and double helices coexist in solution, two sets of signals corresponding to amide protons are often observed when conducting experiments at variable temperatures and concentrations. The observation of both sets translates the presence of single and double helices that are in slow exchange at the NMR

timescale. Integrating both sets of signals allows the evaluation of the dimerization constant $K_{dim}$. It is noteworthy that the chemical shifts of the double helices are more shielded compared to those of the single helix, because of the increased π–π interactions between helices. In the solid–state, the resolution of crystallographic structures sometimes provides strong evidence for the formation of double helices.[3,4]

To date, the studies carried out on these foldamers have shown that even small changes in the overall structure can result in significant variations in the hybridization phenomenon.[14–17] Indeed, this process can be influenced by various internal (length of foldamer, side chains, terminal functions) and external parameters (temperature, concentration and solvents). These factors can greatly affect the stability of the foldamers and influence their thermodynamic and kinetic properties.

## A.2. Effects of solvents

Solvents generally have a major influence on the supramolecular arrangements adopted by foldamers (single or double helices), depending on their polar, protic, or aprotic natures. Regarding the family of oligopyridine dicarboxamide, chlorinated solvents, such as chloroform, have been proven to support the formation of double helices rather than single helical structure due to their moderate polarity. On the contrary, the presence of polar solvents like DMSO tends to favor the formation of single helices. Noteworthy is also the case of pyridine, which favors the single helical state due to the π–π interactions between the solvent molecules and the pyridine moieties of the foldamer skeleton. Eventually, one will note that oligopyridine dicarboxamide foldamers are generally insoluble in apolar solvents.[15]

## A.3. Impact of the length of foldamers

The length of foldamers can be readily adjusted by varying the number of monomers, and increasing the chain length has a significant impact on the hybridization: the longer the foldamer, the higher the dimerization constant.[18] This length–dependent effect also influences the kinetics of the '*single vs double helices*' equilibrium. In the case of a heptamer, the steady state is generally reached within minutes, whereas a tridecamer may need weeks for the equilibrium to be established.[15]

## B. Tetrathiafulvalene: a singular electroactive unit

The importance of tetrathiafulvalene (TTF) in materials science emerged during 1970s.[19] Since then, TTF has found applications in various fields,[20] thanks to its remarkable structural and electrochemical properties as well as its ease of functionalization.[21–23] TTF is an electroactive moiety that possesses 14 π electrons. It exhibits a quasi–planar and non–aromatic structure in its neutral state. It can undergo reversible oxidation processes to form aromatic radical–cations $TTF^{\bullet+}$ and dication states $TTF^{2+}$ (Figure II–1). The oxidation potentials for these states are typically observed at $E^1_{1/2}$ = 0.37 V and $E^2_{1/2}$ = 0.75 V *vs* a standard calomel electrode (SCE) in acetonitrile.[24]

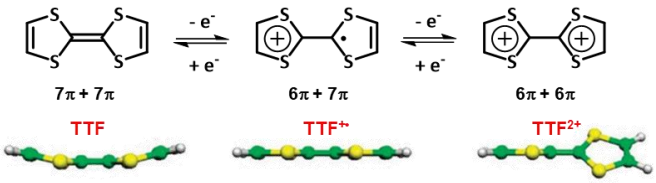


*Figure II–1. The three redox states of tetrathiafulvalene unit and their optimised geometries calculated at the B3P86/6–31G** level.*[24]

Tetrathiafulvalene is often perceived as a planar and rigid structure, but in reality, it exhibits a flexibility, and its conformation is determined by the interactions occurring between its different substituents.[25] The donor properties of TTF unit were initially explored in the solid state by forming crystals through interactions with electron–deficient moieties, resulting in charge transfer complexes. The pioneering example of a charge transfer complex was obtained by combining TTF with TCNQ (tetracyanoquinodimethane), leading to the formation of the first organic–based metallic conductor charge transfer complex.[26,27] The crystals of the TTF–TCNQ complex exhibit separate stacks of donors and acceptors (Figure II–2–*Left*)[28] and the overlapping of orbitals within each stack leads to the formation of a conduction band. However, the conductivity of this material is limited to the direction of the stacking axis, imparting a unidimensional nature to its conduction properties. In that, the use of an analogue of TTF, tetramethyltetraselenafulvalene (TMTSF) has allowed the electrocrystallization of the first superconducting salts of radical cation (Bechgaard salts)[29,30] (Figure II–2–*Right*), which were obtained by electrochemical oxidation of TMTSF in the presence of a supporting electrolyte.

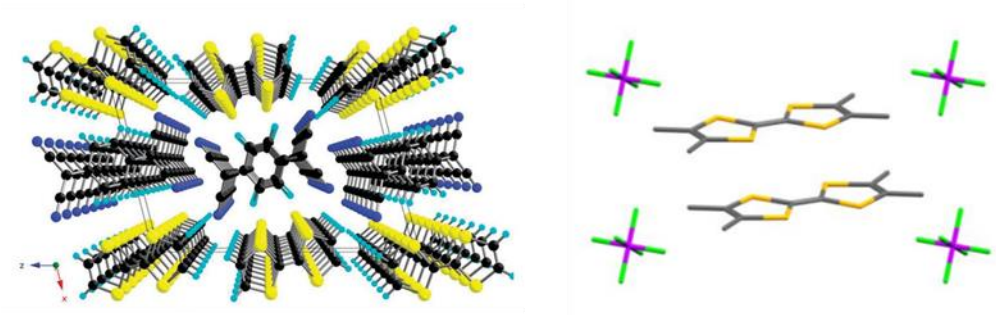

*Figure II–2. Left. Crystallographic structures of the TTF–TCNQ complex,[28] Right. The $(TMTSF)_2PF_6$ Bechgaard salt.[29]*

## B.1. Dimerization of TTF radical–cations

TTF has been highlighted for decades for its capability to establish intermolecular interactions (π–π or sulfur–sulfur interactions) in the neutral state. Indeed, TTF units can form very weak dimers in the neutral state. On the other hand, its particular ability to form stronger dimers in solution upon oxidation was described more recently. Two types of oxidized dimers have to be considered, namely *pimers* and *π–dimers*. The former ones, also called mixed–valence dimers $(TTF_2)^{\bullet+}$, include two TTF units sharing a positive charge, while the second type contains two $TTF^{\bullet+}$ radical cations associated into a $(TTF^{\bullet+})_2$ dimer. Considering TTF–based dimers in the neutral state and their evolution upon a sufficiently slow increase of the redox potential, these species will first undergo a single electron oxidation process leading to *pimer* species and subsequently, a second one–electron oxidation leading to the formation of π–dimers $(TTF^{\bullet+})_2$. Eventually, the oxidation into $TTF^{2+}$ dication species will lead to the dissociation of the dimer (Scheme II–2). Noteworthily, the three different redox states of TTF, as well as the π–dimer and the mixed valence species, can be identified through UV–visible absorption spectroscopy thanks to their distinct spectroscopic signatures.[31,32]

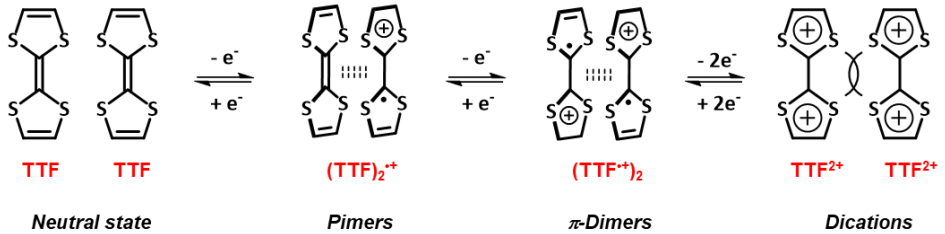


*Scheme II–2. Successive oxidation of TTF unit and plausible modes of interaction.*

The distinct features observed along the π–dimerization of radical cations result from the specific characteristics of this interaction.[33] The overlap of singly occupied molecular orbitals (SOMO) between the interacting monomers results in the formation of a bonding

(HOMO) and an anti–bonding (LUMO) orbitals within the dimer. Along this process, diamagnetic species are formed through radical pairing.

As evidenced by the teams of Mingos and McPartlin,[34] as well as the Novoa and the Miller groups,[35] interplanar distances between $TTF^{\bullet+}$ radical cations involved in a π–dimer are short in the solid state with values about 3.45 Å. Thereby, this bond is not strictly covalent, as the C–C distances are larger than those of a conventional C–C bond, but smaller than the sum of van der Waals radii (3.5 ± 0.5 Å) for organic aromatic compounds.[33,36,37] On this basis, this bond has been described as a covalent and multi–centered bond in the recent literature.[36]

The moderate interaction between $TTF^{\bullet+}$ radical cations explains why the formation of such π–dimers has mainly been observed in the solid state or in concentrated solutions.[38,39] For instance, it was detected at – 48 °C in ethanol (C = 1 mmoL.$L^{-1}$),[40] and its dimerization constant was estimated to $K_{dim}$ = 0.6 at 2°C in acetone (Figure II–3).[32]

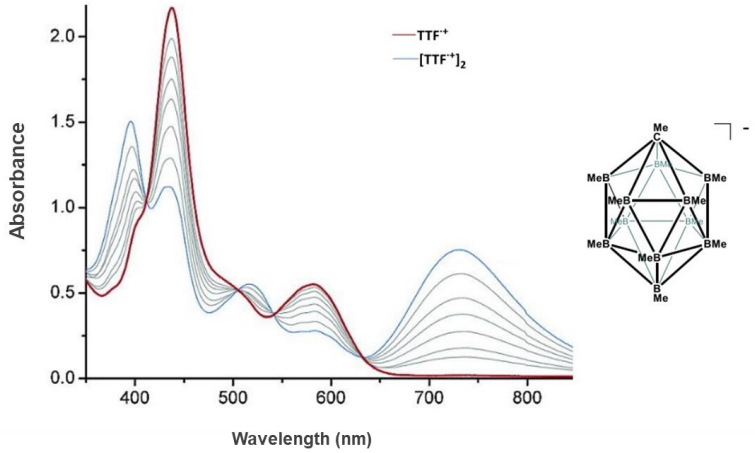


*Figure II–3. Structure of the dodecamethylmethylcarba–closo–dodecarboranate cluster ($CB^-$) and variable temperature UV–visible absorption spectroscopy of a $TTF^{\bullet+}CB^-$ (1.3 mM, acetone). Temperature (in °C, from bottom to top at 740 nm: 20,–40,–55,–63,–70,–78,–85, and–90.*[32]

In order to enhance the stability of the π–dimers at room temperatures, several approaches have been explored. One possibility lies on the confinement of π–dimers within a cavity, such as cucurbiturils[41] or coordination cages.[42] Another strategy was employed by chemists, who took advantage of this weak and redox–sensitive interaction to design stimuli–responsive systems. Consequently, pre–organized structures were synthesized, enabling the preorganization of both radical cations, and thereby facilitating their dimerization.[31,43–45]

## B.2. Redox–responsive supramolecular architectures based on TTF

The reversible oxidations of TTF, along with its ability to form mixed–valence species and π–dimers that have specific spectroscopic signatures, has led to diverse applications in

molecular and supramolecular chemistry. In this context, TTF derivatives have shown their potential in various classes of materials such as molecular receptors,[21] electroactive polymers and dendrimers,[44,46,47] donor–acceptor systems,[48] molecular switches,[49] dynamic interlocked systems (catenane and rotaxane)[50,51] and foldamers.[52] To illustrate that point, and given the wide literature on the topic, a selection of relevant examples will be briefly discussed below.

### B.2.a. Rotaxane and controlled molecular motion

Rotaxanes are mechanically interlocked molecular architectures initially developed by the group of Fraser Stoddart,[53] who shared the Nobel Prize in chemistry in 2016 with Jean–Pierre Sauvage[54] and Bernard L. Feringa[55] for their pioneering work on the design and synthesis of molecular machinery. As illustrated with Figure II–4, Stoddart and coworkers described a remarkable tristable rotaxane featuring three stations: two of them correspond to electron–rich moieties (dioxynaphthalene (DNP) and tetrathiafulvalene (TTF)), while the third station is the electron–deficient viologen ($V^{2+}$).[56] The mobile acceptor ring cyclobis(paraquat–*p*–phenylene) ($CBPQT^{4+}$) undergoes translational movements along the axis of the rotaxane, which depend on the oxidation states of the stations and/or the ring. In the 6+ state, TTF and $CBPQT^{4+}$ are mainly associated due to their preferential interactions. The oxidation of TTF unit to the dicationic state allows the formation of **II–1**$^{8+}$, provokes electrostatic repulsions between $TTF^{2+}$ and $CBPQT^{4+}$ cations, and leads to the motion of the $CBPQT^{4+}$ macrocycle towards the better electron–donating moiety, DNP. Alternatively, when the system undergoes reduction, the reduced ring $CBPQT^{2(\bullet+)}$ moves towards the $V^{\bullet+}$ station, which is facilitated by the pairing of the as–formed radical cations (Figure II–4).

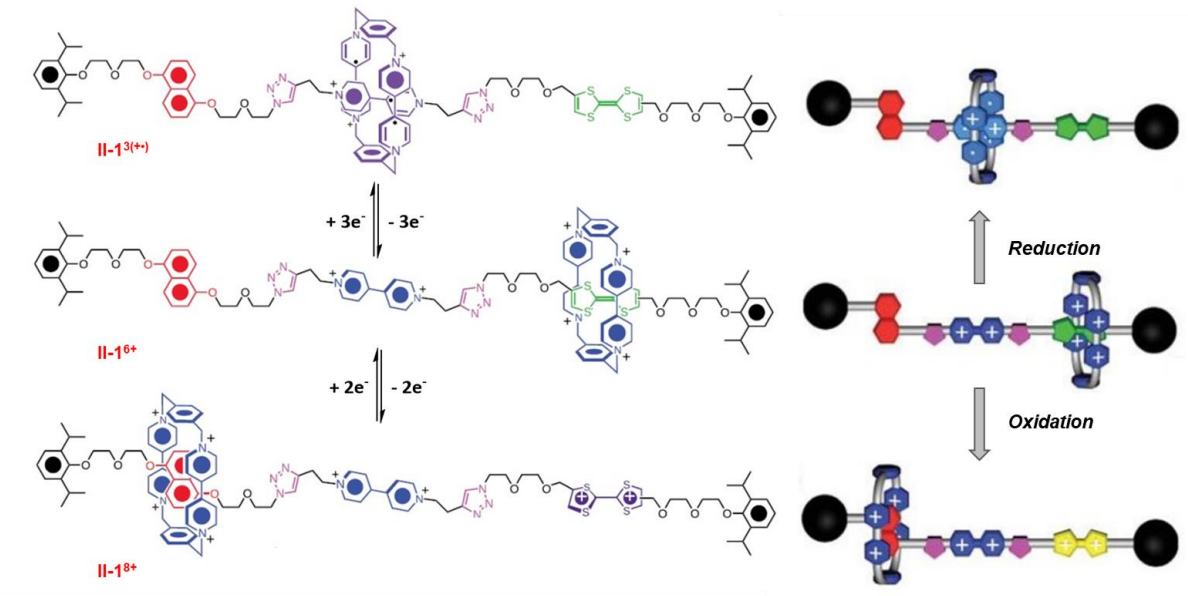


*Figure II–4. Example of tristable rotaxane **II–1** described by Stoddart group.*[56]

### B.2.b. Conformational control in calixarenes through radical–cation dimerization and ion recognition

Calixarenes have been employed as another supramolecular architecture to control the orientation of TTF unit and their interactions. In this context, the behavior of a calixarene endowed with two TTF units **II–2** was described by Sallé and coworkers.[31] Upon oxidation of TTF units, mixed valence $(TTF)_2^{\bullet+}$ dimer and a π–dimer $(TTF^{\bullet+})_2$ were formed (Figure II–5). To study the formation of these species in solution, a titration with the $Na^+$ cation was performed and followed by cyclic voltammetry and spectroelectrochemistry. In this manner, it was shown that the $Na^+$ cation is trapped by the eight oxygen atoms, which leads to a conformational change and hence, to the subsequent dissociation of the dimers. This was evidenced by the disappearance of the absorption bands corresponding to the mixed valence species and π–dimers (1750 and 765 nm, respectively).

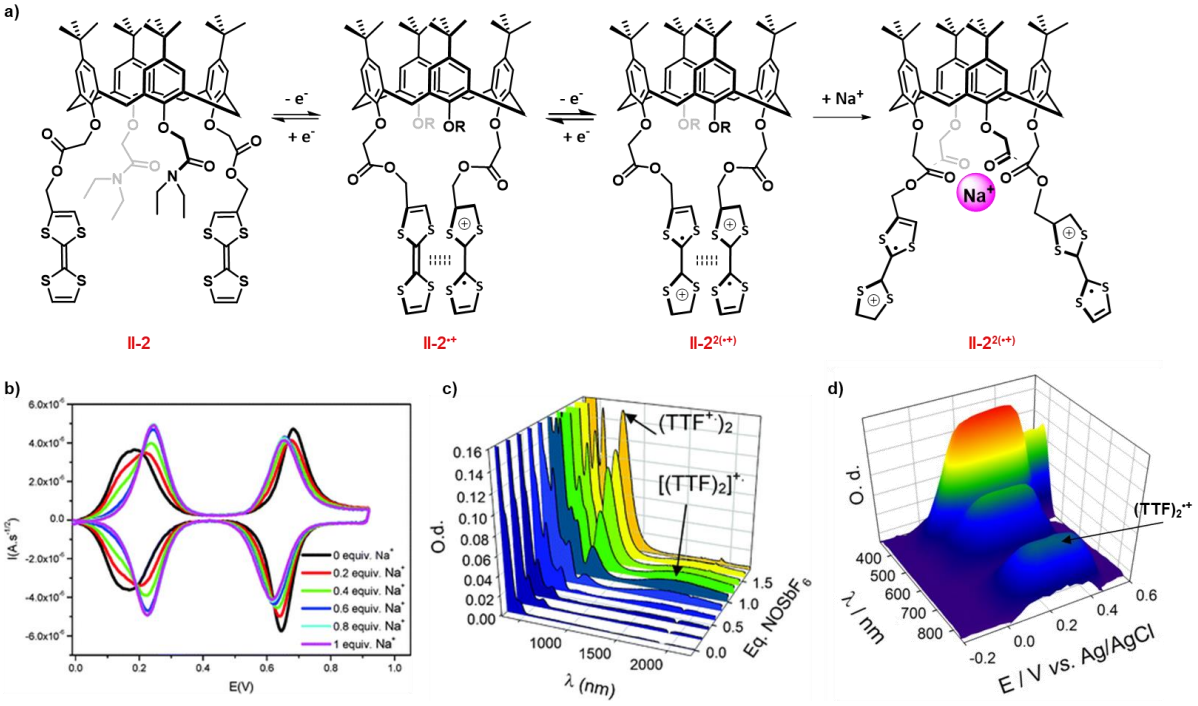


*Figure II–5. a) Structure of the calix[4]arene functionalized with two TTF units **II–2** and representation of the interaction between TTF units depending on the redox state and/or the presence of $Na^+$ ions, b) Evolution of the voltammogram of **II–2** (0.5 mmol.$L^{-1}$, DCM/ACN; 0.1 M n–$Bu_4NPF_6$, Pt, v = 100 mV.$s^{-1}$ vs. AgCl/Ag) in the presence of n equivalents of $Na^+$ cation, c) Absorption spectra in the presence of increasing amounts of oxidizing agent $NOSbF_6$. d) Spectroelectrochemistry in thin layer (d ≈ 50 µm); conditions (Pt, Ø = 2 mm); [**II–2**] = 0.75 mM in $CH_2Cl_2/CH_3CN$ (1/1), $Bu_4NPF_6$ (0.2 mol.$L^{-1}$), scan rate 0.125 mV $s^{-1}$.*[31]

### B.2.c. Supramolecular macrocyclization through radical pairing

The previous examples involve the preorganization of TTF units and their oxidized derivatives within a single molecule. In contrast, the dimerization of radical cations of TTF may serve as a valuable interaction to drive the formation of multi–component systems. The case of short oligoarylamides **II–3** and **II–4**, which include three pyridyl rings and are functionalized with two tetrathiafulvalene units, is particularly relevant to discuss this possibility. As demonstrated by Z.–T. Li and coworkers,[57] the oxidation of the TTF units to the radical cation state may lead to two types of arrangements (Scheme II–3), depending on the intra– or intermolecular nature of the interactions between $TTF^{\bullet+}$ units. In non–polar solvents, such as dichloromethane, intramolecular dimer $(TTF^{+\bullet})_2$ was favored with an estimated association constant $K_a$ of $1.0 \times 10^4$ and $9.7 \times 10^3$ for **II–3** and **II–4**, respectively. When shifting to more polar solvents, intermolecular interactions between oxidized TTF units were favored, leading to the formation of supramolecular macrocycle with an estimated dimerization constant $K_{dim}$ = $5.9 \times 10^2$ for **II–3** ($CH_2Cl_2/CH_3CN$ 1/1).

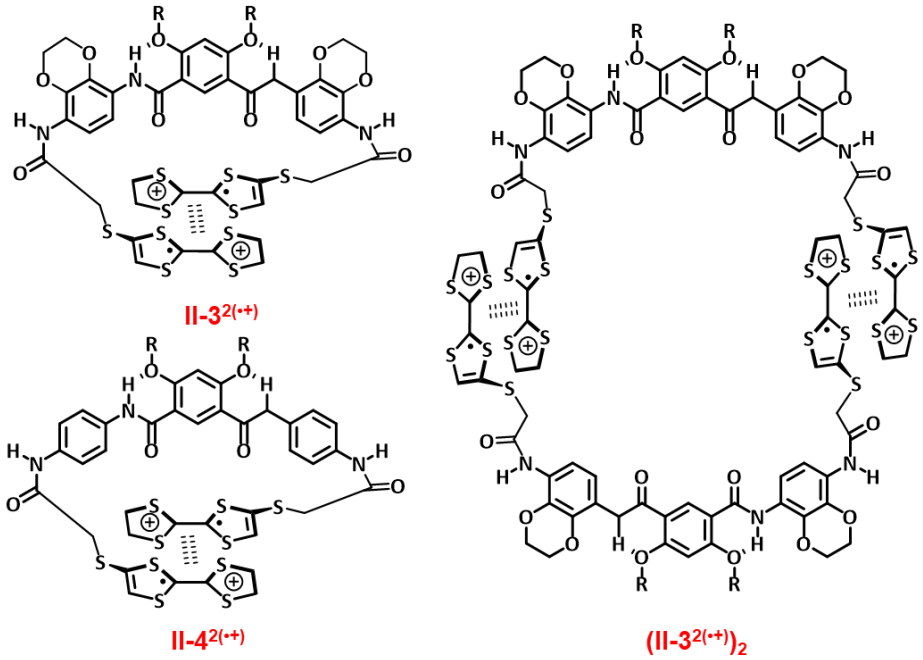


*Scheme II–3. Structures of **II–3** and **II–4**, and the intramolecular and intermolecular interactions modes.*[57]

## B.3. Hybridization of foldamers based TTF

In our group, the concept of "redox–controlled hybridization of foldamers" was first investigated during the thesis of Dr Lara Faour.[1] To do so, TTF units were grafted on an oligoarylamide foldamer containing five pyridyl rings through copper–catalyzed cycloaddition chemistry (CuAAC – Figure II–6). In the neutral state, foldamer **II–5** hybridizes with a moderate dimerization constant, while the oxidation of TTF units increases by two order of magnitude the dimerization constant ($K_{dim}$(**II–5**)$_2^{2(\bullet+)}$) = $10^2 \times K_{dim}$(**II–5**)$_2$) thanks to the radical dimerization process.[58] As a consequence, the π–dimer species were observed at concentrations down to $5 \times 10^{-6}$ M at room temperature thanks to their specific absorption band at λ = 770 nm. This example actually constituted a proof–of–concept to build the *RECHERCHE* ANR project, which funded my PhD fellowship.

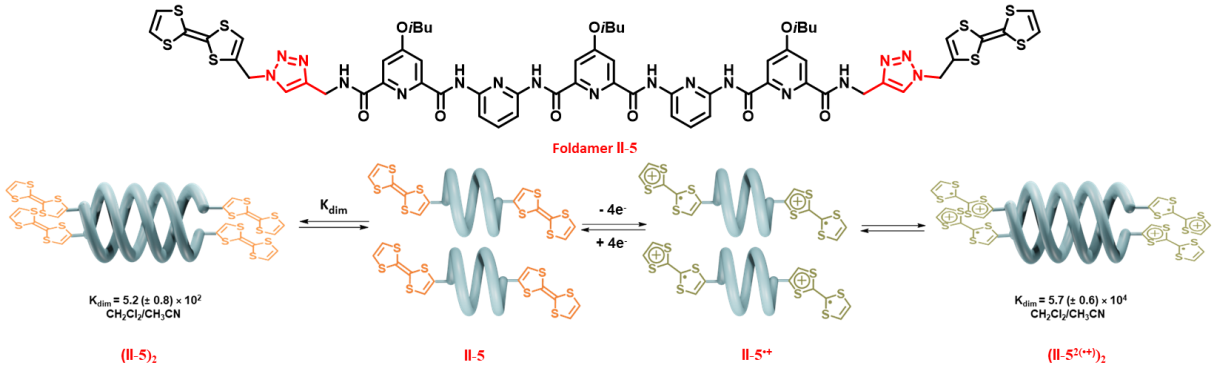


*Figure II–6. Structure of foldamer **II–5**, and schematic representation of the equilibria in its neutral and oxidized states with their relation dimerization constants.*[58]

# II. Results and discussions

## A. Design

As mentioned in paragraph §I.A oligopyridine dicarboxamides were selected for numerous reasons. For such a skeleton, the length of the strand represents a critical parameter to control the hybridization equilibrium. The foldamer skeleton should have a moderate length: 1) not too long, in order to preserve the dynamics between the single and double helices in solution and to avoid extremely high dimerization constants that would preclude any control of the hybridization equilibrium, 2) not too short, in order to guarantee helical conformations and exclude the possibility of obtaining non helical species (as for the case of the pyrene–based foldamer,[59] which was reported by our group). This is the reason why an oligopyridine dicarboxamide foldamer containing seven pyridyl moieties was selected. Such a structure is likely to display a moderate dimerization constant and helical conformations, be that in the single or the double helical state.[18]

Isobutoxy moieties have been chosen as side chains since former studies led by the group[1] showed that 1) oligopyridine dicarboxamide foldamers devoid of side chains showed poor solubility in common organic solvents, 2) introducing long alkyl chains (*e.g. n*–dodecyloxy chains) led to significantly enhanced solubilities but poor propensity to crystallisation. On the contrary, isobutoxy chains provided sufficient solubility, which facilitates the characterisations in the solution phase, and crystallinity, which definitely made simpler the analyses in the solid state. Eventually, one will also note that introducing alkoxy chains leads to an increased electron density on the helical backbone and hence, to significantly higher, but reasonable, dimerization constants.[14,60,61]

As evidenced through §I.B.2, the tetrathiafulvalene electroactive unit constitutes a relevant choice to drive the hybridization through redox stimulations and follow its redox and supramolecular state through UV–vis–NIR absorption spectroscopy thanks to its distinct spectroscopic signatures.

Lastly, we selected a rigid and short linker, an amide connector, between the foldamer skeleton and the electroactive units in order to maximise the impact of redox stimulations on the hybridization equilibrium. Multiple tests had been carried out by Dr Lara Faour during her thesis to synthesize such a foldamer, in vain.[1] In this context, foldamer **A** was defined as a first target molecule; its retrosynthetic scheme is represented below (Scheme II–4). The synthesis of

foldamer **A** involves the preparation of the precursors **II–12** and **II–17**. The crucial step in this synthetic scheme consists in grafting the TTF units on amine **II–14**.

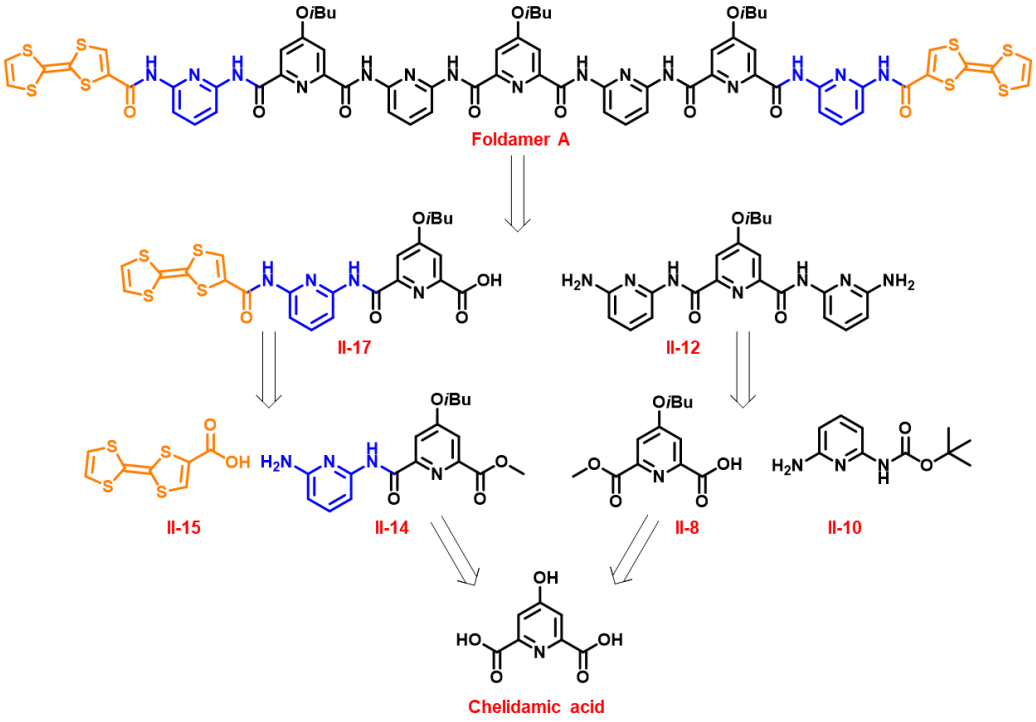


*Scheme II–4. Retrosynthetic scheme of foldamer **A**.*

## A.1. Synthesis of precursors

The synthesis of foldamer **A** started with an esterification reaction of chelidamic acid to give compound **II–6** (Y = 71 %), based on a previously described protocol.[62] The following step allowed the introduction of solubilizing alkoxy chains through nucleophilic substitution (Scheme II–5). This was achieved by reacting diester **II–6** with 1–iodo–2–methylpropane in DMF in the presence of potassium carbonate to give diester **II–7** with a 60 % yield. Diester **II–7** was subsequently converted into mono–acid **II–8** or diacid **II–9**. The mono–saponification reaction was performed in the presence of one equivalent of sodium hydroxide in methanol. The corresponding sodium carboxylate was isolated and subsequently protonated in acidic medium (HCl, 1 M). In this manner, carboxylic acid **II–8** was isolated with a 75 % yield, which appears particularly good considering the presence of two ester functions within **II –7**. In parallel, diacid **II–9** was quantitatively obtained from diester **II–7** after treatment with excess potassium hydroxide and acidification.

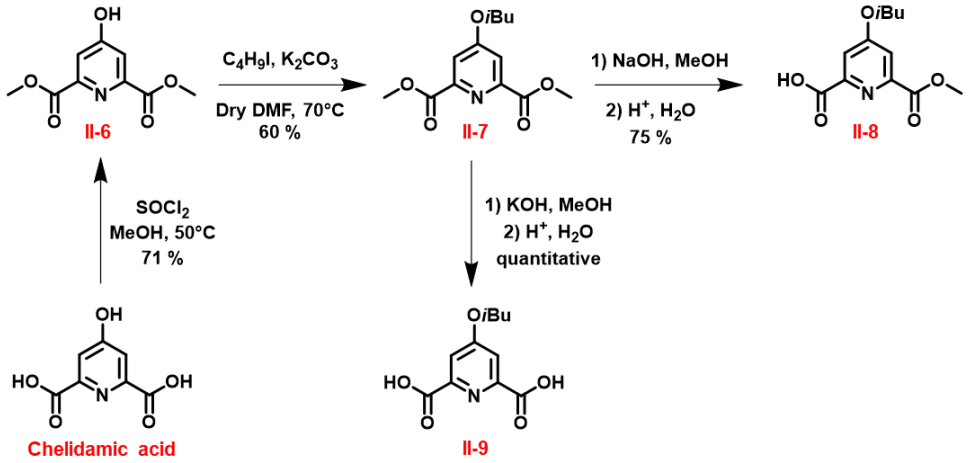


*Scheme II–5. Synthesis of precursors **II–8** and **II–9**.*

## A.2. Preparation of diamine II–12

Diacid **II–9** was subsequently used to prepare the central sequence of the skeleton through two simultaneous amide–coupling reactions (Scheme II–6). In principle, this could have been achieved by reacting diacid **II–9** and an excess of 2,6–diaminopyridine. Nevertheless, a mono–protection reaction was conducted on 2,6–diaminopyridine to improve the yield and selectivity of this reaction and to avoid the formation of longer oligomers. This was led by using di–*tert*–butyl dicarbonate in THF and afforded *tert*–butyl (6–aminopyridin–2–yl)carbamate **II–10** with a 61 % yield. The carboxylic acid functions of **II–9** were then activated by using oxalyl chloride and a catalytic amount of DMF under inert atmosphere. The subsequent addition–elimination of two equivalents of **II–10** in the presence of DIPEA allowed for isolating biscarbamate **II–11** with a particularly good yield (81 %). The desired diamine precursor **II–12** was finally obtained by deprotecting amine functions with trifluororoacetic acid TFA in a quantitative manner (Scheme II–6).[18]

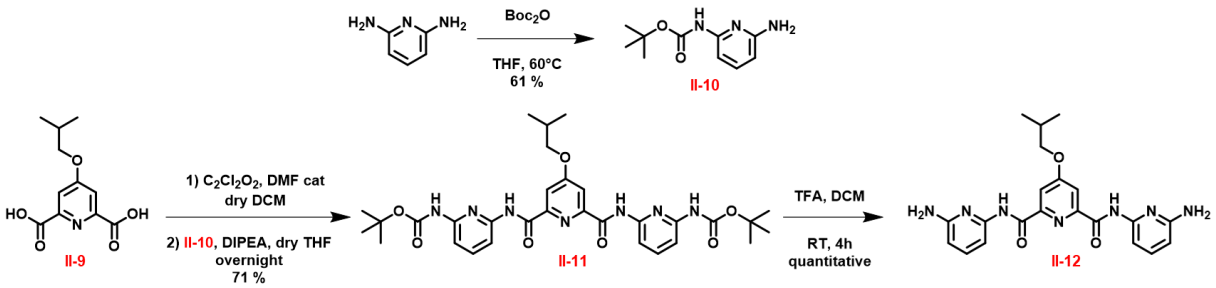


*Scheme II–6. Synthesis of precursors **II–10** and **II–12**.*

## A.3. Synthesis of amine II–14

The peripheral component **II–13** was designed by coupling mono–acid **II–8** to the protected 2,6–diaminopyridine **II–10**, using the same coupling reagent and protocol employed

for constructing the central segment **II–12**, with a high yield of 90 % (Scheme II–7). This intermediate is unique because it can be deprotected on both sides to give an amine or a carboxylic acid, which can then react with complementary functionalities and extend the skeleton on both sides. Once compound **II–13** synthesized, it was converted to amine **II–14** by using TFA to yield **II–14** quantitatively.

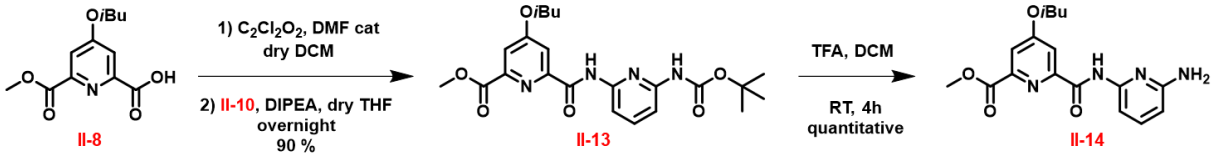


*Scheme II–7. Synthesis of amine **II–14**.*

## A.4. Synthesis of carboxytetrathiafulvalene II–15

The synthesis of carboxyTTF was led according to the protocol described by Garín and coworkers.[63] After an acid–base reaction involving TTF and lithium diisopropylamide (LDA) in anhydrous diethyl ether at –78°C, carbon dioxide (gas) was introduced to form the corresponding carboxylate, which was finally protonated in aqueous medium (Y = 90 %) to give carboxyTTF **II–15** (Scheme II–8).

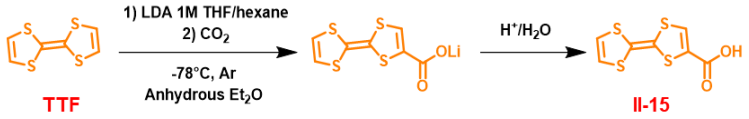


*Scheme II–8. Synthesis of carboxyTTF **II–15**.*

## A.5. Incorporating the TTF unit at the outer segment

The coupling between carboxyTTF **II–15** and compound **II–14** represents a key step in the synthesis, which turned out to be quite challenging! Various types of activating agents were employed in order to form the desired amide linker. Multiple tests have been conducted by employing the standard carboxylic acid activation reagents, namely oxalyl chloride and thionyl chloride in various solvents such as dichloromethane, chloroform and tetrahydrofuran, with and without heating (30°C). However, the desired product could not be obtained in such conditions. Considering these results and the sensitivity of TTF to acidic conditions, Ghosez reagent (1–chloro–*N*,*N*,2–trimethyl–1–propenylamine) was selected as an activating reagent to convert the carboxylic acid function to an acid chloride one, ensuring the absence of hydrogen chloride release.[64] To do so, carboxyTTF **II–15** was dissolved in dry dichloromethane and Ghosez reagent (6 equivalents) was added under argon atmosphere. The corresponding acid chloride was obtained by evaporating the solvent under reduced pressure and anhydrous tetrahydrofuran

was introduced. The corresponding solution was added to a mixture of compound **II–14** and dry DIPEA, resulting in a 22 % yield of the expected compound **II–16** (Scheme II–9).

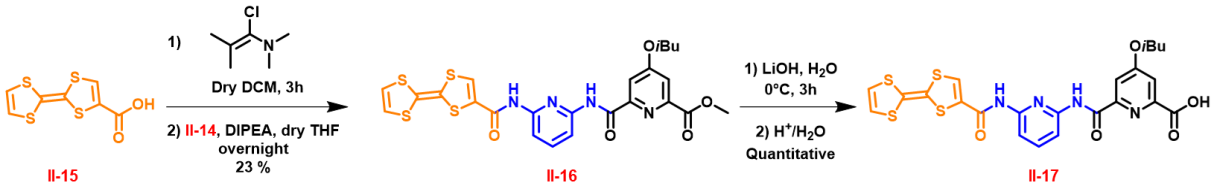


*Scheme II–9. Synthesis of block **II–17**.*

Given this first achievement, we tried to improve the yield of this reaction by testing other mild activating agents. In this context, acid **II–15** was converted into the corresponding *O*–acylurea intermediate by using dicyclohexylcarbodiimide (DCC) and 4–dimethylaminopyridine (DMAP) under argon atmosphere in anhydrous dichloromethane.[65] Then, the activated species underwent an addition–elimination reaction with amine **II–14**, to afford amide **II–16** with a significantly increased yield of 53 %. The purification of this compound caused difficulties due to the extremely low solubility of this intermediate, which may be responsible for this moderate yield. Nevertheless, amide **II–16** could be isolated at a 200 mg scale, which further allowed its saponification using lithium hydroxide to give carboxylic acid **II–17** with a quantitative yield.

## A.6. Synthesis of compound II–18

By analogy to compound **II–16**, amide **II–18** was synthesized by peptidic coupling between carboxyTTF **II–15** and protected diaminopyridine **II–10** by using DCC and DMAP with a 52 % yield (Scheme II–10). This compound will serve as reference for subsequent characterizations.

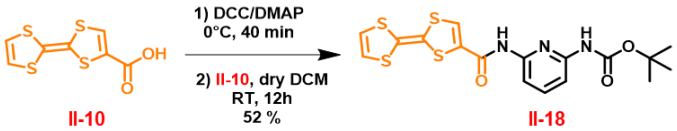


*Scheme II–10. Synthesis of reference compound **II–18**.*

## A.7. Synthesising target foldamer A

The final step of this synthesis involves diamine **II –12** and carboxylic acid **II –17**. Given the presence of the acid–sensitive TTF unit in **II –17**, Ghosez reagent appeared as a relevant choice to prepare target foldamer **A**. While dichloromethane was found to be unsuitable for this coupling, the highest yield was calculated when carrying out the reaction in anhydrous

THF (42 mg– 37% – Scheme II–11). The purification of foldamer **A** also proved challenging: multiple attempts using silica gel chromatography and crystallization were ineffective to separate the mono–adduct from the bis–adduct. Actually, we had to employ a recycling size exclusion and high–performance liquid chromatography (recycling SEC–HPLC,– eluent: chloroform) to achieve this separation successfully.

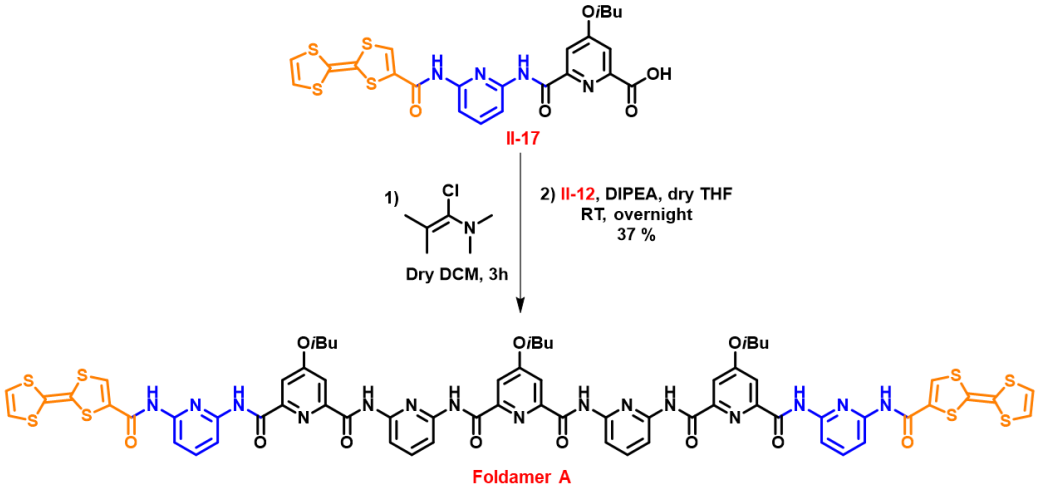


*Scheme II–11. Synthesis of foldamer **A**.*

Eventually, one will note that another type of activating reagent was tested (DCC and DMAP), and although the desired product was detected by mass spectrometry, its isolation could not be achieved because of an extremely low yield.

## B. Solid–state analysis of foldamer A

### B.1. Analysis at the molecular level

Monocrystals of foldamer **A** were successfully obtained from solvents of diverse polarities, including dimethylsulfoxide, and dimethylformamide through crystallization, as well as tetrahydrofuran, chloroform and a mixture of chloroform and methanol through slow evaporation. All the crystallographic structures evidence a single helical secondary structure, which correlates with this family of oligopyridine dicarboxamide foldamer.[3] In all cases, the stability of the helix is maintained by a network of intramolecular hydrogen bonds formed between the NH protons of the amide functions and the nitrogen atom of the pyridine units, with bonds length ranging from 2.19 to 2.45 Å (pale blue dotted lines– Figure II–7).

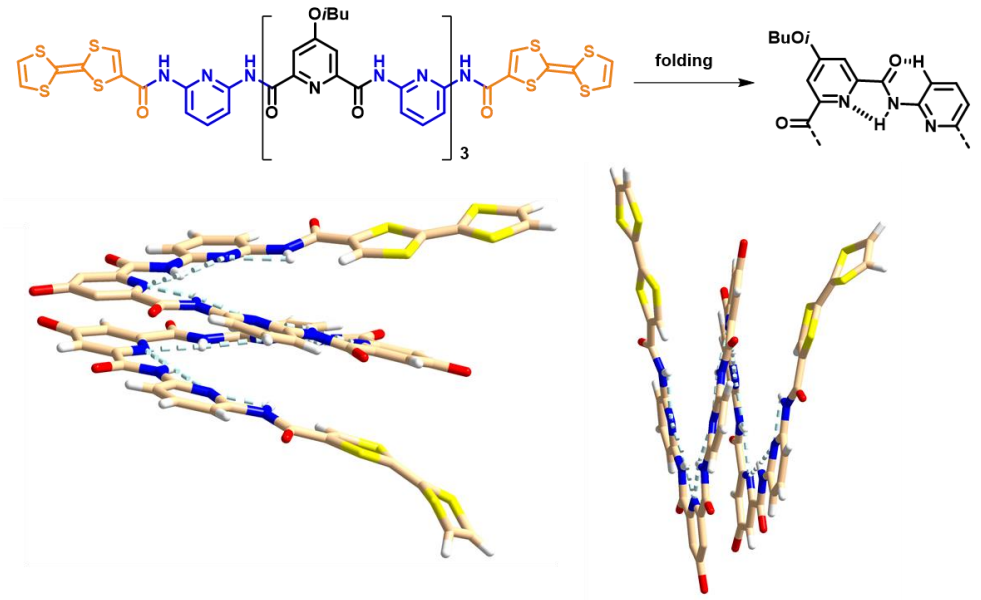


*Figure II–7. Chemical structure representing the folding mode by intramolecular hydrogen bonds, the corresponding crystallographic structure and the NH–N intramolecular hydrogen bonds (isobutoxy side chains are omitted for clarity for all the crystallographic structures).*

In the five crystallographic structures, TTF units are part of the helix, which is in sharp contrast with the crystallographic structure of foldamer **II–5** (see chemical structure §I.B.3):[58] in the case of **II–5**, triazole rings are quasi–perpendicular to the helical structure and TTF units do not interact with the foldamer skeleton (Figure II–8); on the contrary, short TTF–skeleton distances were measured in all cases for foldamer **A** (below 4 Å). Thereby, the helical pitch will be defined as the distance between TTF unit and the fourth pyridine unit within the foldamer skeleton.

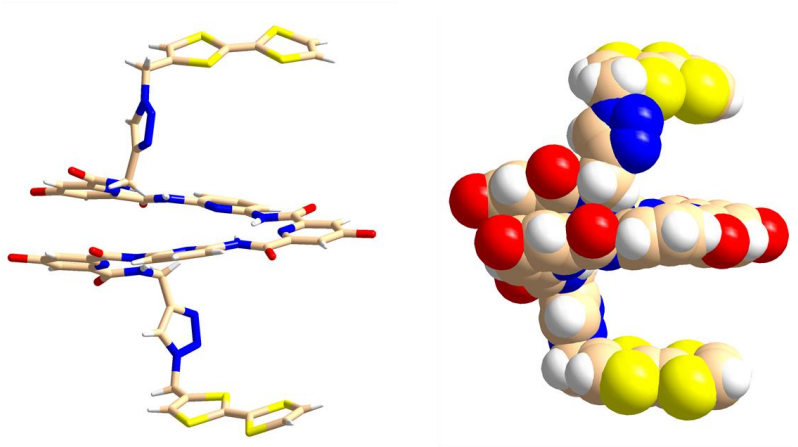

*Figure II–8. Crystallographic structure of foldamer **II–5** that includes triazole–containing linkers.*

Considering the structures obtained from DMSO, DMF, THF and $CHCl_3$, the helical pitch is calculated based on the internal cycle of the TTF unit, which is adjacent to the amide function and the values are 3.56, 3.59, 3.66 and 3.52 Å, respectively. The situation appeared

different for the structure obtained from a mixture of $CHCl_3$/MeOH. Indeed, both cycles of the TTF units are involved in the helical structure and defined a helix pitch of 3.57 Å (Figure II–9).

The folding into a single helix also promotes the appearance of an elliptical cavity with approximate dimensions 8 Å × 5.5 Å in all structures. The orientation of amide protons to the center contributes to the overall polarity of the cavity, which permits interactions with polar molecules.

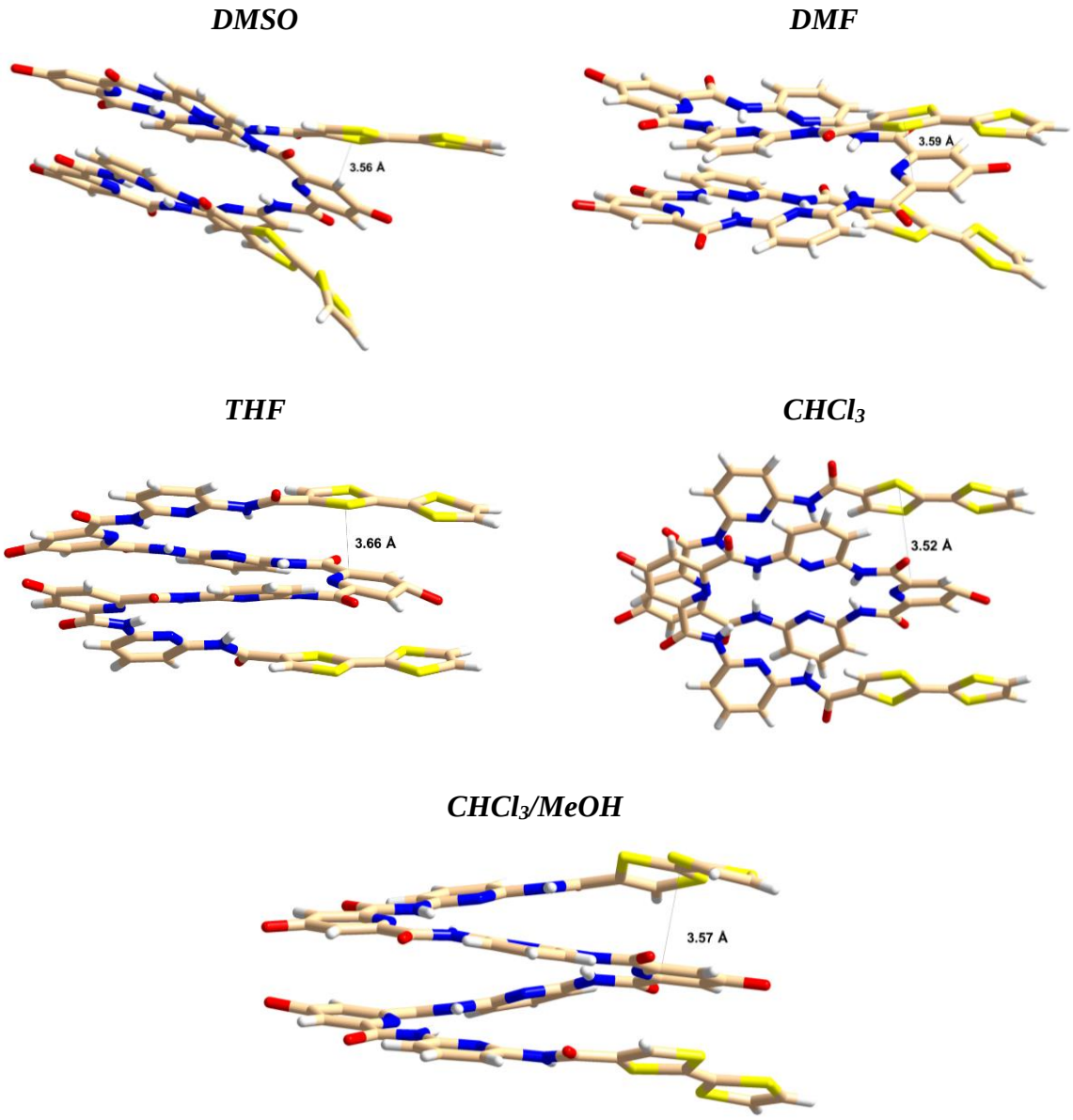


*Figure II–9. The five X–ray structures obtained of foldamer **A** in the solid state in five different solvents as single helix form.*

Upon examining the crystallographic structures, we observed that the orientation of TTF units are different and that these units deviate from planarity in some cases. These observations and differences detected between the structures support the need for a separate discussion on the packing within the crystal lattice for each structure. For the subsequent discussion, we defined the cycles of TTF unit as external and internal (adjacent to the amide functions) cycles. Since foldamer **A** exhibits a chiral structure due to its helical conformation and since is does not include chiral centers, solutions of **A** contains equal amounts of *M* (left–handed) and *P* (right–handed) helices. Thereby, *M* and *P* helices systematically co–crystallized in a head–to tail fashion. Figure II–9 shows four examples for *M* helices in DMSO, THF, $CHCl_3$ and $CHCl_3$/MeOH and one example for a *P* helical conformation in DMF.

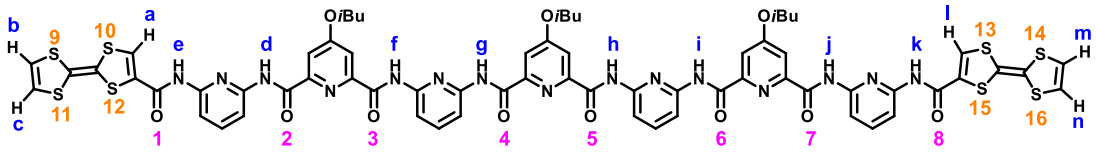

*Scheme II–12. Structure of foldamer **A** with the protons, the oxygen and the sulfur atoms numbered to facilitate further interpretations.*

## B.2. Impact of the solvent on the packing of foldamer A

### B.2.a. Crystallization from DMSO

The crystallographic structure obtained from monocrystals grown by crystallization in DMSO revealed the presence of one water and two DMSO molecules in the polar cavity of the helix (Figure II–10). The water molecule acts as hydrogen bond donor, forming hydrogen bonds between its hydrogen atoms and the nitrogen atoms of the pyridine units. It also acts as hydrogen bond acceptor, since an interaction is observed between its oxygen atom and the protons of amide functions connected to the central pyridine ring. In addition, the oxygen atom of the sulfoxide function of DMSO interacts with the protons of amide function (H (e), H (g), H (h) and H (k)) through intermolecular hydrogen bonds.

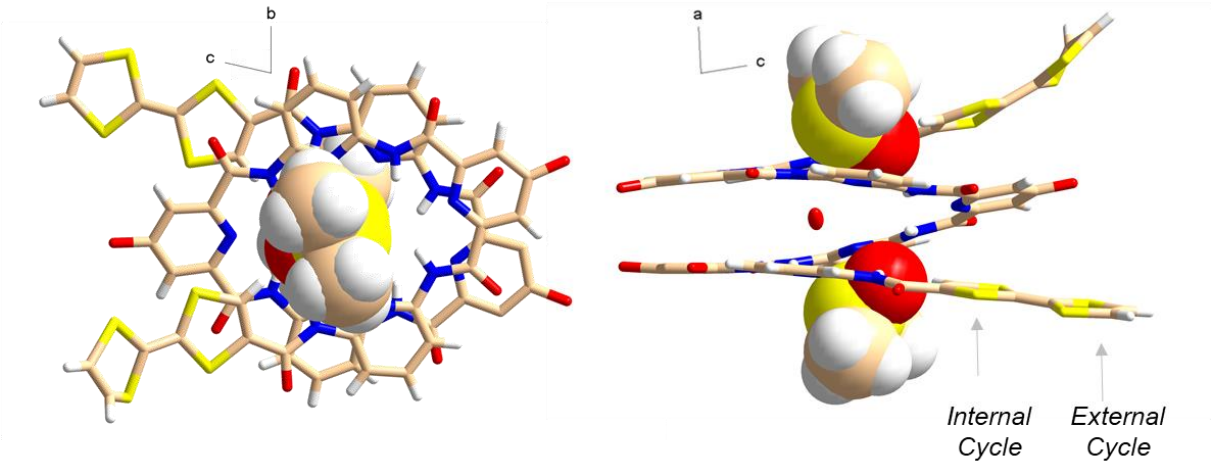


*Figure II–10. X–ray structure of foldamer **A** obtained by crystallization in DMSO. A water molecule and two DMSO molecules are in the cavity of the helix. The packing in the lattice viewed form a axis (left), b axis (right).*

While it is generally known that TTF units are planar and rigid, there can be exceptions where TTF units undergo substantial non–planarity. In this crystal structure and along the b axis, it appears that one TTF unit deviates from planarity by 30°, while the second one remains planar (Figure II–11). At this stage, one will note that S–S (16) intermolecular interactions were detected between planar TTF units with a value of 3.65 Å (violet dotted lines), while no S–S interaction was evidenced for non–planar units (Figure II–11).

Three observations may deserve attention to explain the distortion phenomenon: 1) a hydrogen bond (2.47 Å, blue dotted lines) is set up between the hydrogen atom H (b) of the external 1,3–dithiole cycle of TTF and the oxygen of the carbonyl group (4) of an adjacent helix; 2) this oxygen atom (4) is also engaged in intermolecular hydrogen bonds (2.36 Å, green dotted lines) with the H (n) hydrogen atom of a neighbouring planar TTF unit; 3) CH–π interactions also occurred between the H (c) hydrogen atom of a distorted TTF and the external cycle of a planar TTF unit from an adjacent helix (3.35 Å, which corresponds to a strong CH–π interaction – dotted orange lines). Thereby, this crystallographic structure shows that these hydrogen bonds differ by the relative orientation of TTF C–H bonds with regard to the complementary carbonyl functions: no distortion is observed when the 1,3–dithiole ring and the carbonyl function are in the same plan, while distorted TTF units involve interactions between rings and carbonyl functions that do not belong to the same plan.

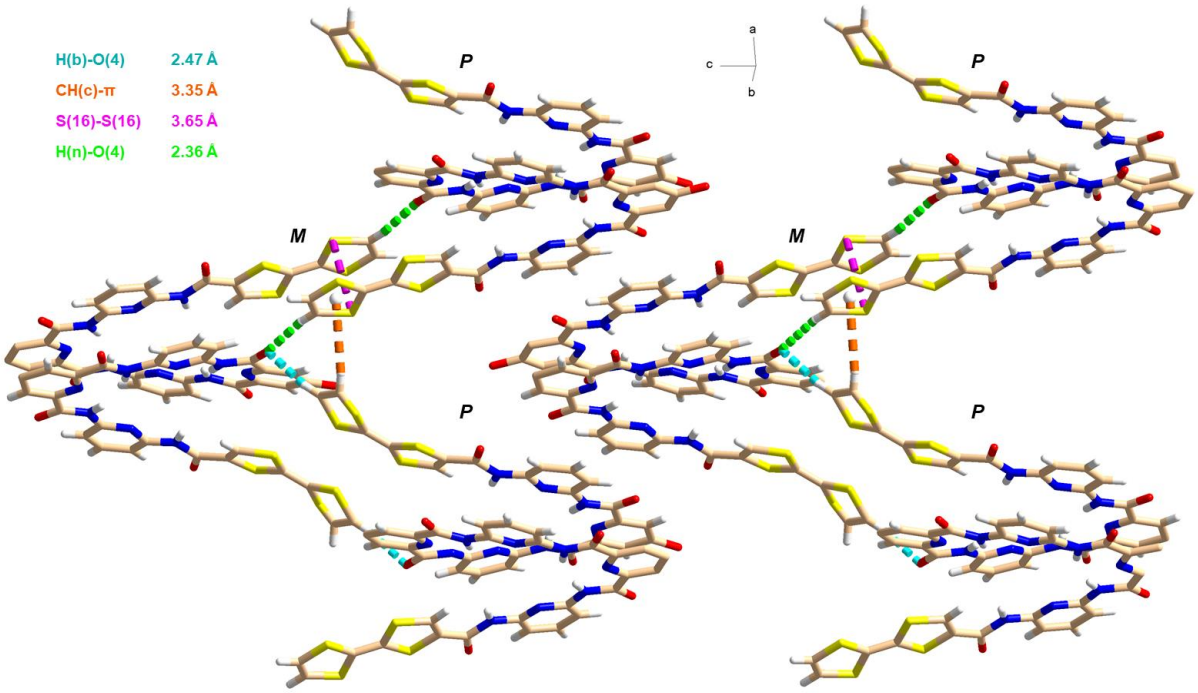


*Figure II–11. Packing of foldamer **A** in the lattice: hydrogen bonds 2.47 Å (blue dotted lines) and 2.36 Å (green dotted lines), CH–π interactions 3.35 Å (orange dotted lines) and S–S contacts 3.65 Å (violet dotted lines).*

### B.2.b. Crystallization from DMF

The crystallographic structures obtained from crystals grown in DMF and DMSO have similarities: the monoclinic crystal system is the same, and one water molecule and two solvent molecules, which interact with the foldamer skeleton through hydrogen bonds, are detected within the cavity (Figure II–12). Considering the planarity of TTF units, both deviate from planarity with a value of 12.43° (containing H (m) and H (n)) and 15.86° (containing H (b) and H (c)), which is clearly less pronounced than in DMSO.

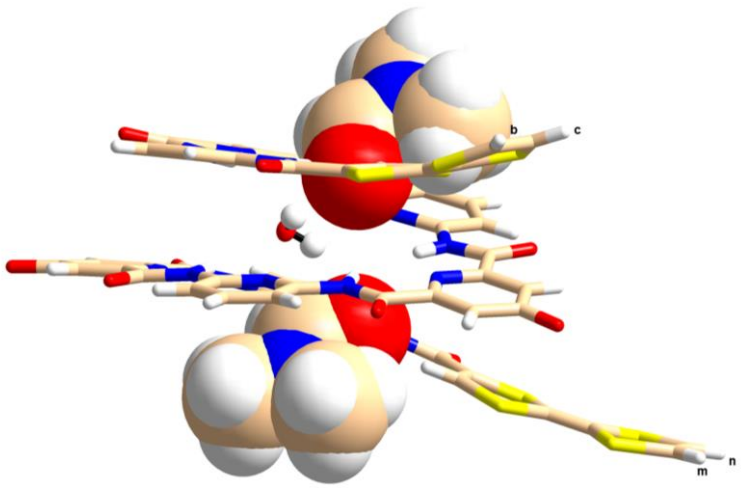


*Figure II–12. X–ray structure of foldamer **A** obtained from crystallization from DMF containing one molecule $H_2O$ and two molecules of DMF.*

The arrangement of the single helices in the solid state in DMF differs from the structure observed in DMSO. In this packing (Figure II–13), a hydrogen bond with a length of 2.23 Å (blue dotted lines) occurs between the hydrogen atom H (n) and the oxygen atom O (7) of the amide function. This hydrogen bond takes place between neighbouring *M* helices within the adjacent columns. Two distinct CH–π interactions have been observed in the packing. The first interaction involves the hydrogen atom H (m) of a TTF unit from *P* helices, which interacts with the external cycle of another TTF unit (containing H (a) and H (b)) from the neighbouring *M* helices in different columns. This interaction is characterized by a distance of 3.96 Å (orange dotted lines). The second CH–π interaction, with a length of 3.86 Å (green dotted lines) takes place between H (n) of TTF units in the *M* helices and the second pyridine units of the foldamer skeleton in the *P* helices. These CH–π interactions occur between the *M* and *P* helices within the same column. Furthermore, π–π stacking interactions were observed between the foldamer skeletons. Specifically, a stacking distance of 3.78 Å was detected between the second pyridyl monomers of the *P* helices and the first pyridyl units of the *M* helices. These aromatic interactions occur between helices from different columns (violet dotted lines). Herein, no S–S contact was observed.

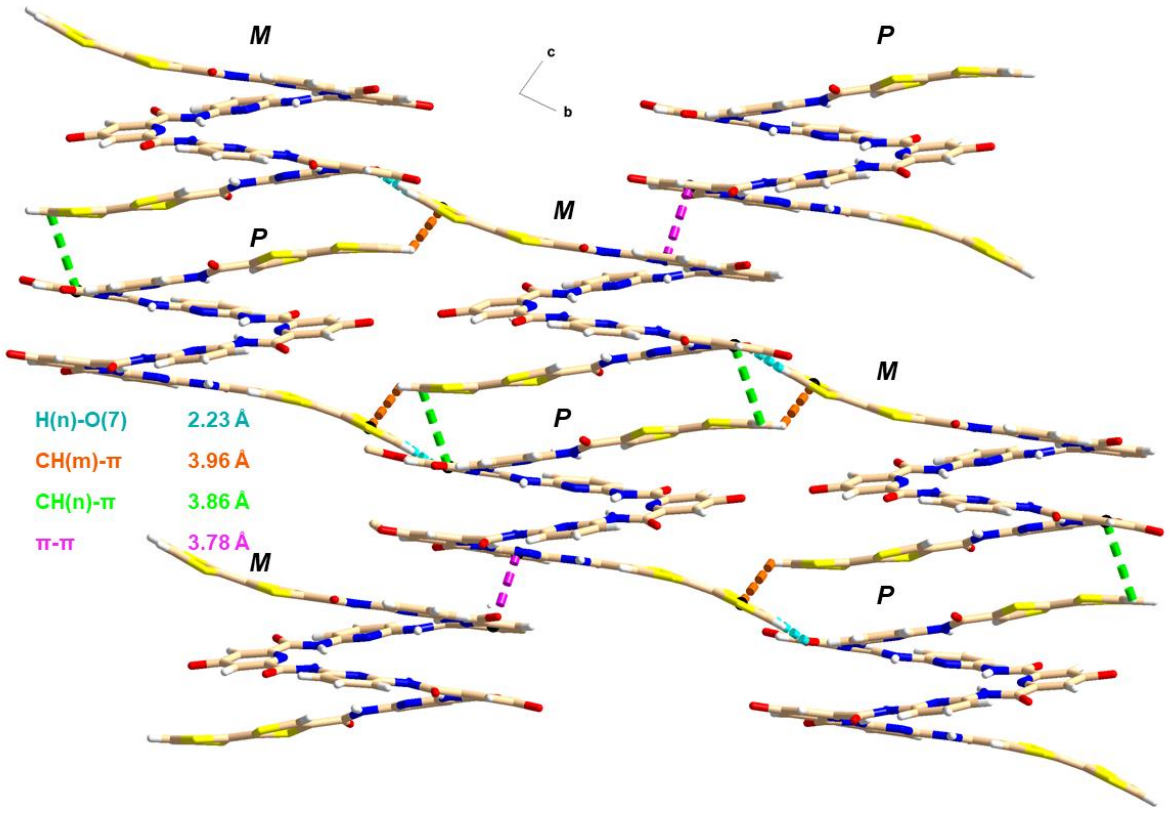


*Figure II–13. Packing of foldamer **A** in the lattice: hydrogen bonds 2.23 Å (blue dotted lines), CH–π interactions 3.96 Å (orange dotted lines) and CH–π 3.86 Å (green dotted lines) and π–π contacts 3.78 Å (violet dotted lines).*

### B.2.c. Slow evaporation from THF

The monocrystals obtained by slow evaporation of THF also revealed the presence of a single helical structure for foldamer **A** containing two water molecules in its cavity (Figure II–14). The TTF units were found to be slightly tilted in comparison to the foldamer skeleton. The orientation of TTF units can be explained by investigating their arrangement within the lattice.

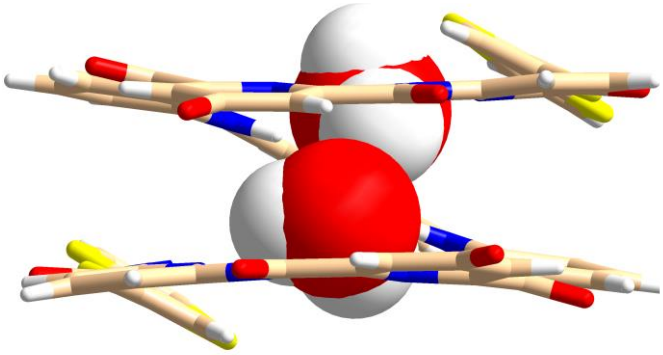

*Figure II–14. X–ray structure of foldamer **A** obtained by slow evaporation from THF containing two water molecules.*

At first glance, the observation of the crystallographic structure along the b axis revealed that TTF units are not coplanar to the neighbouring pyridyl units that constitute the foldamer skeleton. This deviation can be attributed to the presence of strong hydrogen bonds, measuring 2.35 and 2.43 Å, between the hydrogen atoms of the first cycle of TTF units H (a), H (i) and the oxygen atoms O (6) and O (3) of the amide function of the adjacent helices, respectively (indicated by red and dark green dotted lines – Figure II–15). This type of intermolecular hydrogen bond was not observed in the previous structures, where the TTF units were in the same plane as the foldamer skeleton.

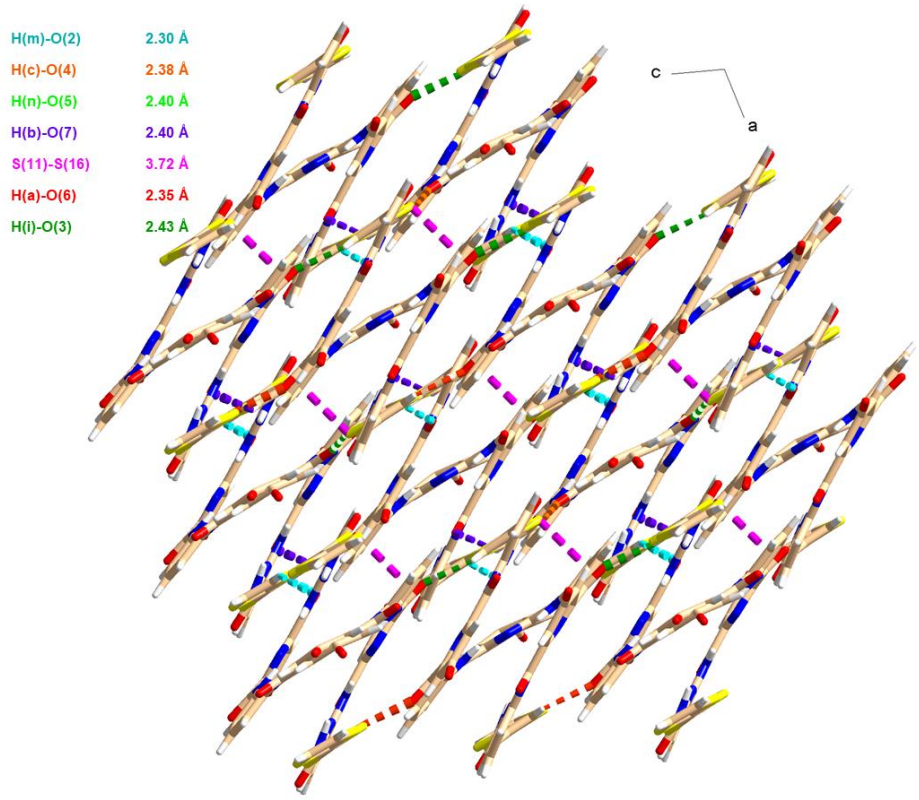


*Figure II–15. Packing of foldamer **A** in the lattice (direction b axis): hydrogen bonds 2.30 Å (blue dotted lines), 2.34 Å (green dotted lines), 2.38 Å (orange dotted lines), 2.40 Å (purple dotted lines), S–S contact 3.72 Å (violet dotted lines).*

Furthermore, the other hydrogen atoms of both TTF units were involved in hydrogen bonds with the oxygen atoms of adjacent helices: 1) H (b) with O (7) d = 2.40 Å (purple dotted lines), 2) H (c) with O (4) d = 2.38 Å (orange dotted lines), 3) H (n) with O (5) d = 2.40 Å (green dotted lines), 4) H (m) with O (2) d = 2.30 Å (blue dotted lines). Note that all these intermolecular hydrogen bonds took place between the hydrogen atoms of *M* helices and the oxygen atoms of *P* helices, and vice versa. Additionally, S–S contacts were observed between S (11) of the *M* helices and S (16) of the *P* helices with a length value of 3.72 Å (violet dotted lines – Figure II–16). CH–π interactions could not be evidenced in this structure.

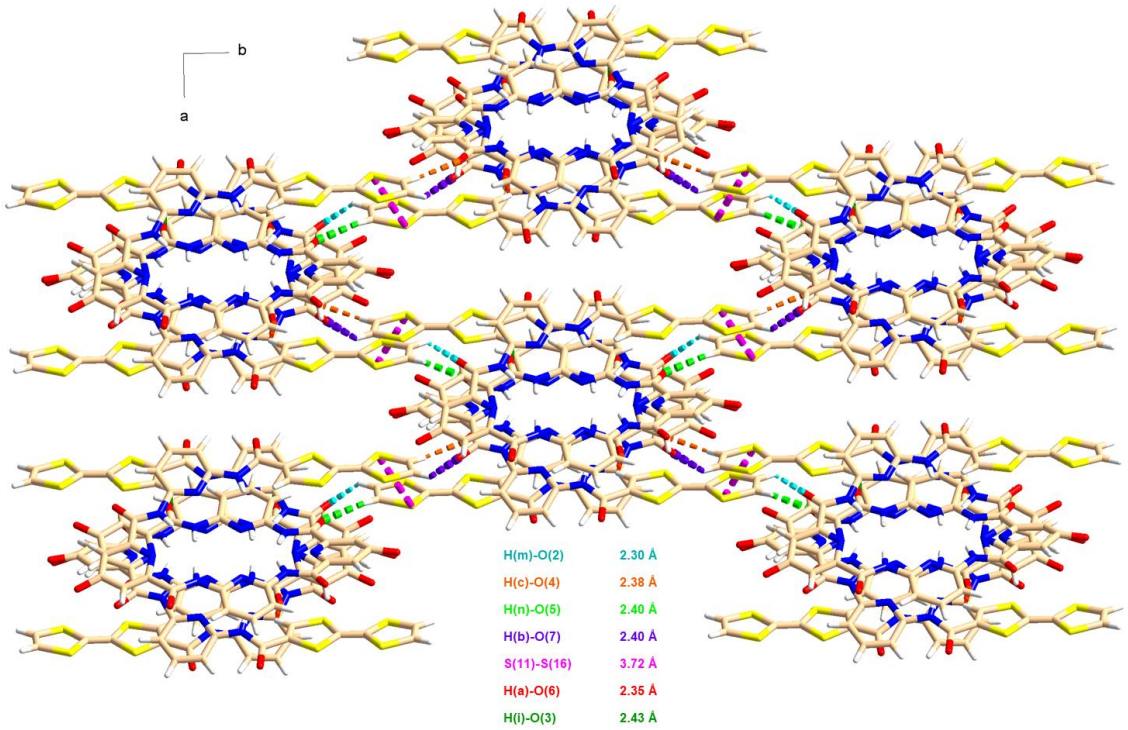


*Figure II–16. Packing of foldamer **A** in the lattice (direction axis c): hydrogen bonds 2.35 Å (dark green dotted lines) 2.43 Å (red dotted lines).*

### B.2.d. Slow evaporation from $CHCl_3$

The slow evaporation of a chloroform solution of foldamer **A** allowed the formation of single crystals. These were studied by X–ray diffraction analyses, which showed once again the crystallization of the single helical form. In the solid state, helices are organized in a head to tail fashion (Figure II–17). Though the resolution of the obtained crystals was insufficient to reach a sufficient spatial resolution, electroactive units do seem to interact with the foldamer skeleton. New crystals are currently being grown to perform a proper resolution of this crystallographic structure.

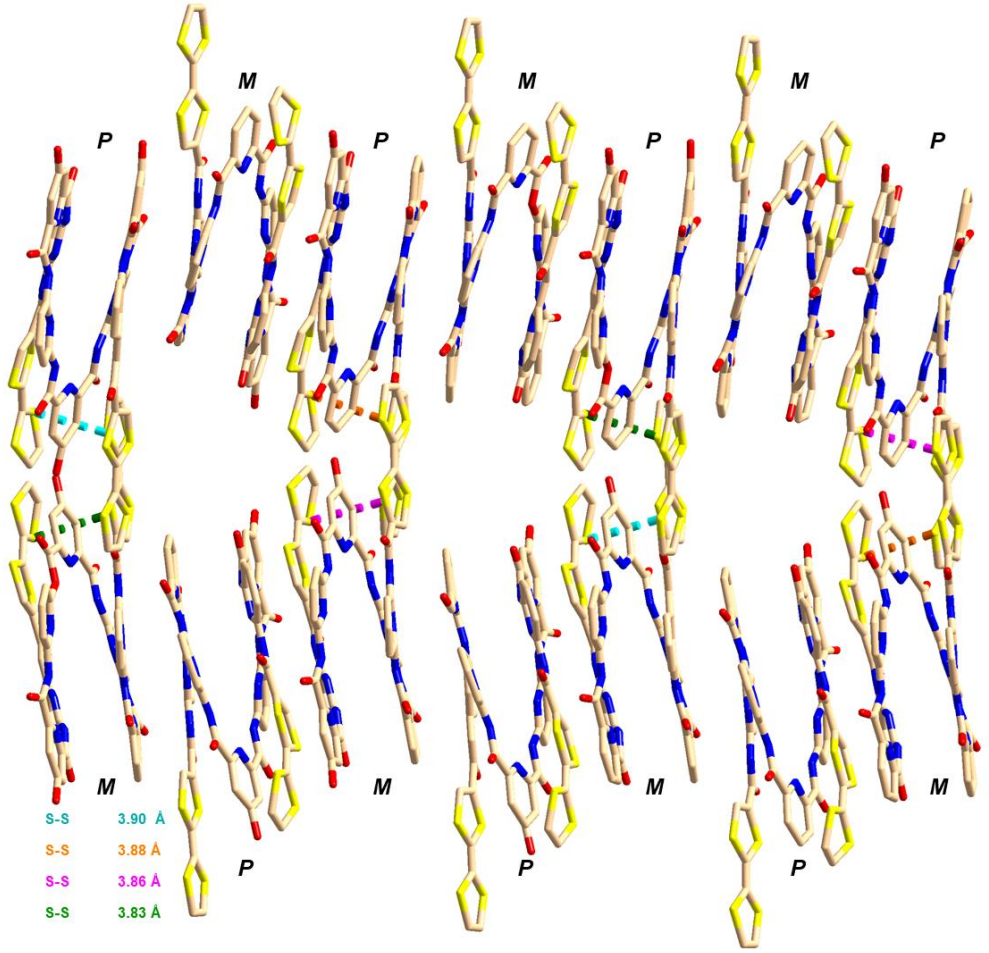


*Figure II–17. Part of the packing of foldamer **A** in the lattice: S–S contact 3.83, 3.86, 3.88, and 3.90 Å between S (11) and S (16) (green, violet, orange and blue dotted lines, respectively).*

### B.2.e. Structure from a mixture of $CHCl_3$/MeOH

In the polar cavity of this single helix (Figure II–18), three methanol molecules were found and involved into hydrogen bonds. The main difference between this structure and the others relies on the orientation of the TTF units. This may be attributed to the positioning of the hydrogen atoms in the internal cycle of TTF units (H (a) and H (l)), which are oriented towards the external side of the cavity, while the H (a) and H (l) protons are oriented towards the center of the cavity in the above–mentioned crystallographic structures. These hydrogen atoms participate to intramolecular hydrogen bonding with the adjacent amide oxygen atoms (O (1)). The presence of this hydrogen bond may influence the orientation of TTF units and promote contact between the external cycle of TTF and the foldamer skeleton, which induces a deviation from planarity of 25.74°. The hydrogen atom (a) of non–planar TTF is involved in intermolecular hydrogen bond (2.45 Å – orange dotted lines) with an oxygen (3) of the adjacent helix in the packing (*P* helices). The H (c) proton of the *P* helices is involved in hydrogen bonds (2.31 Å) with O (8) of the *M* helices (blue dotted lines) and H (n) with O (6) 2.48 Å (green

dotted lines) between *P* helices. In this case, no intermolecular S–S interaction could be highlighted.

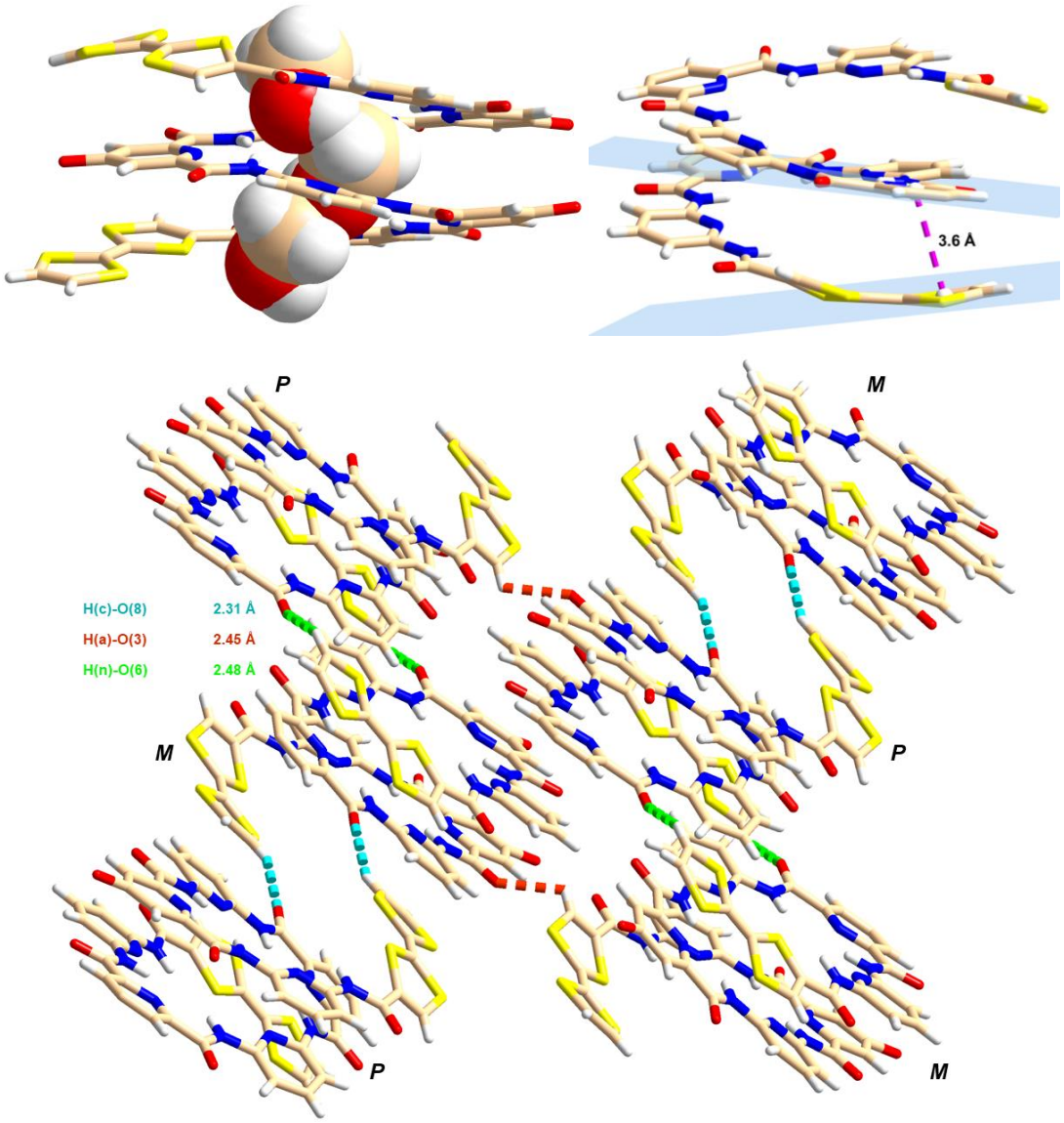


*Figure II–18. Up. X–ray structure of foldamer* ***A*** *obtained from slow evaporation from a mixture of* $CHCl_3$*/MeOH as single helix. The cavity contains three methanol molecules. Down. Packing of foldamer* ***A*** *in the lattice: hydrogen bonds 2.31 Å (blue dotted lines) and 2.48 Å (green dotted lines), 2.45 Å (orange dotted lines).*

## B.3. Solid state analysis of compound of II–16

Compound **II–16**, which served as a reference, includes a TTF unit as well as two pyridyl rings. Consequently, **II–16** cannot fold to form helical structures. This molecule crystallized in the triclinic P–1 space group by crystallization in DMSO (Figure II–19). The crystallographic structure highlighted the formation of a pseudo–cavity involving two pyridyl units interacting through hydrogen bonds. A DMSO molecule was also found to interact with the compound through hydrogen bonding. These molecules organize in the lattice in a head–

to–tail fashion. It is noteworthy that all four sulfur atoms were involved into S–S interactions (3.91 Å). Additionally, H (b) was involved in hydrogen bond with a value of 2.32 Å with the oxygen atom O (2) of the amide function of the adjacent molecule.

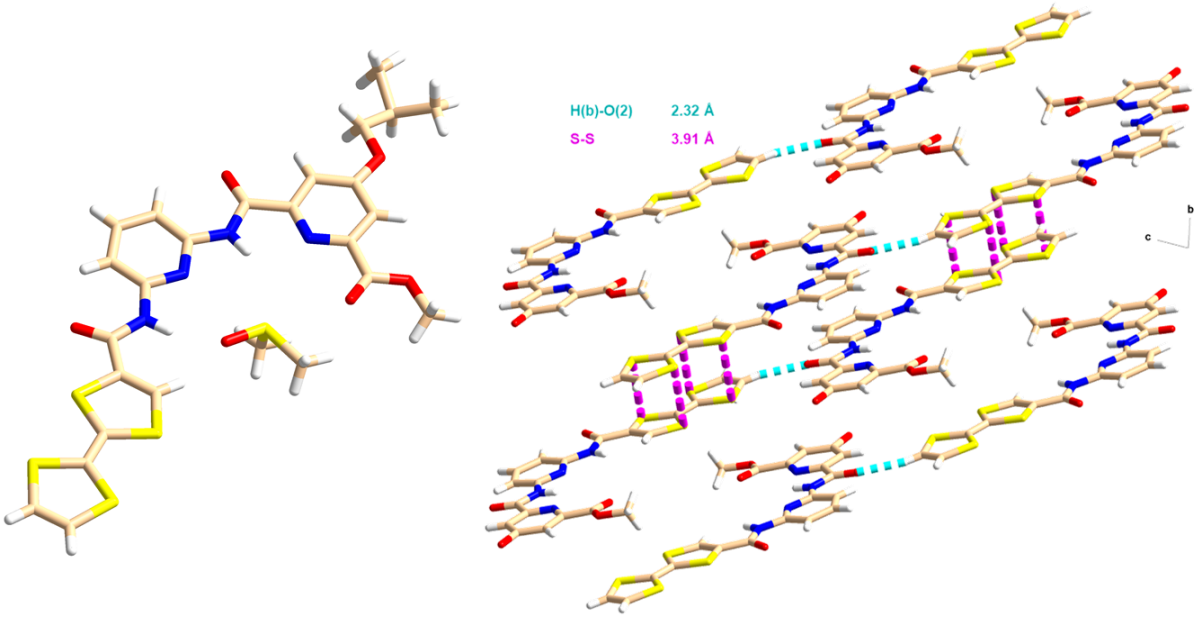


*Figure II–19. X–ray structure of **II–18** and the packing in the lattice showing S–S contacts 3.9 Å (violet dotted lines) and hydrogen bonds 2.32 Å (blue dotted lines).*

## C. Analysis of foldamer A in solution in the neutral state

### C.1. Characterization of single and double helices and determination of the dimerization constant

The most commonly used technique for the characterization of single and double helices is $^{1}$H NMR spectroscopy. Since these species are most often in slow equilibrium at the NMR timescale, two distinct series of signals can be observed for amide and sometimes aromatic protons. The integration of the signals can be used to determine the dimerization constant $K_{dim}$ following the equation:

$$[M] = \frac{-1 + \sqrt{1 + 8K_{dim}C_t}}{4K_{dim}}$$

*[M] = concentration of simple helix, $C_t$ = [M] + 2[D] (total concentration in foldamer), [D] = concentration of double helix*

In order to assess this dimerization constant in a rigorous manner, dilution experiments are generally led to determine the proportions of single and double helices at different concentrations. In this manner, one can perform a non–linear regression analysis using the

above–mentioned equation and estimate the dimerization constant, on condition that the thermodynamic equilibrium is reached.

## C.2. Impact of solvent composition on solutions of foldamer A

In general, the conformation of foldamers in solution is influenced by the nature of solvent. However, oligopyridine dicarboxamide foldamers maintain a robust helical conformation in solution, which is not affected by the solvent nature.[66] However, the solvent properties significantly affect the hybridization equilibrium in most cases.

### C.2.a. $^1$H NMR analysis of foldamer A in different solvents

Given the complexity of the structure, an interpretation of the $^1$H NMR spectrum in DMSO–$d_6$ will be given firstly to assign all the signals. This polar and hydrogen bond acceptor solvent is actually known to favor the single helical state. This was further confirmed in the case of foldamer **A**, since a single set of signals was observed. In these conditions, foldamer **A** displays a symmetric structure that helps assigning the four signals of the eight amide protons (10.47, 10.44, 10.35 and 10.27 ppm at 7 mmol.L$^{-1}$ – Figure II–20). This attribution was assisted through 2D NMR spectroscopy ($^1$H COSY and $^1$H NOESY).

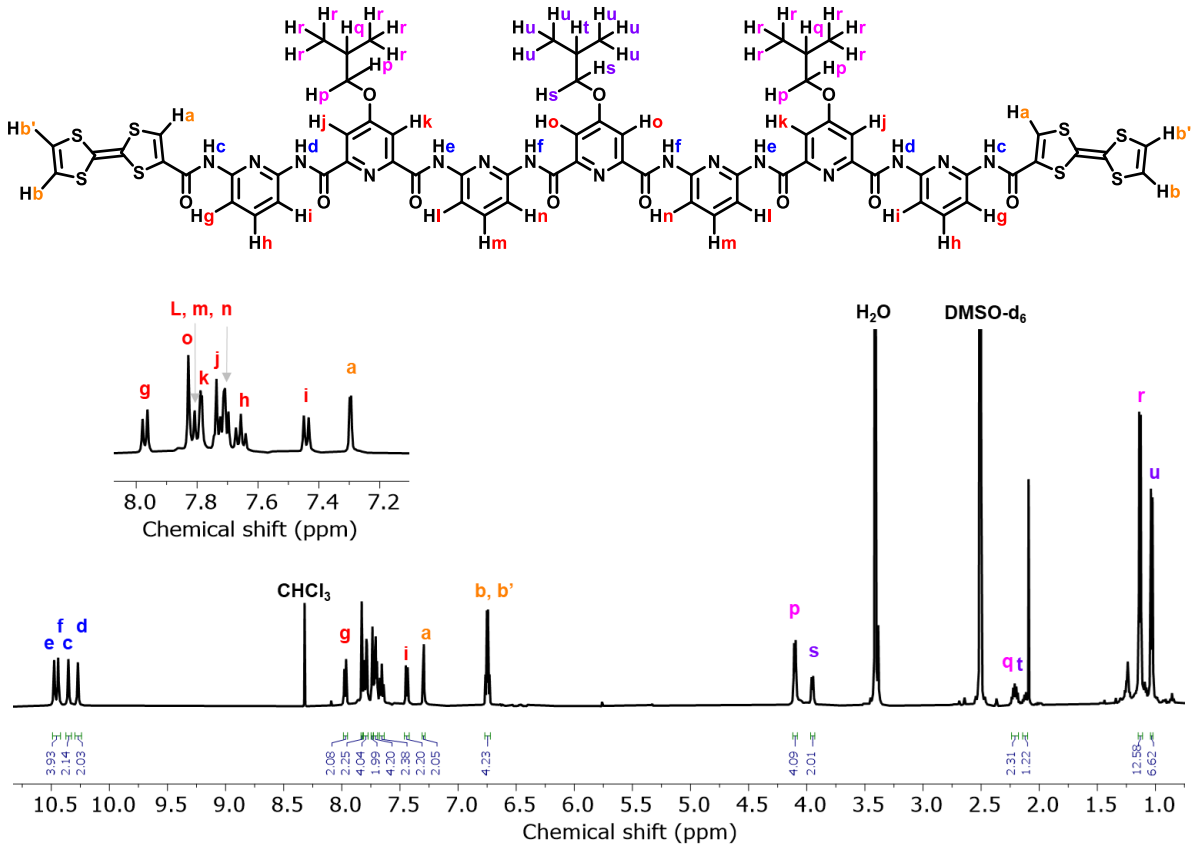


*Figure II–20. Chemical structure of foldamer **A** and detailed $^1$H NMR spectrum of foldamer **A** in DMSO.*

In order to explore the influence of solvents on the behavior of foldamer **A** in solution, $^{1}$H NMR spectra were recorded in six different solvents selected for their more or less polar features, and their protic or aprotic nature. These analyses were conducted at a concentration of 4 mmol.L$^{-1}$ (due to its moderate solubility), at room temperature and using a 500 MHz Bruker (Figure II–21). A single set of signals was systematically observed for amide protons, which are deshielded. These signals are comparable to those detected in DMSO–$d_6$, which indicates that foldamer **A** adopts a single helical state and this, whatever the solvent under consideration. One will note that this observation may correlate with the single helical structures that were systematically obtained in the solid state, though crystallization experiments were attempted in a variety of solvents and conditions.

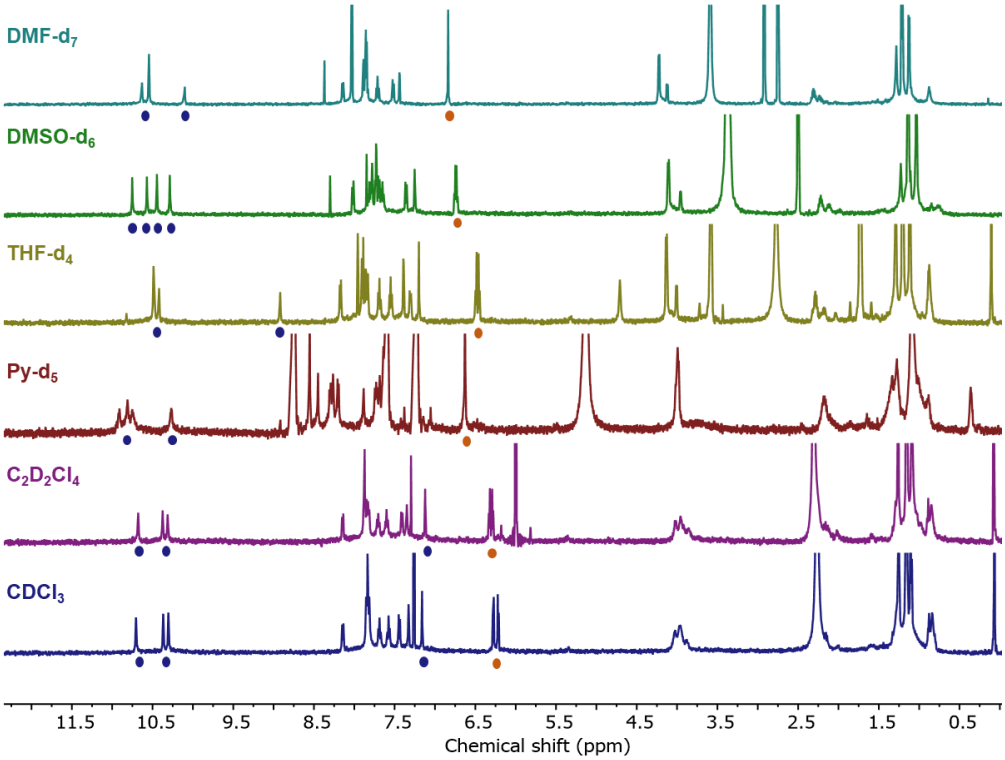


*Figure II–21. $^{1}$H NMR spectra of foldamer **A** in various solvents: blue circles correspond to the amide protons and orange circles correspond to the TTF protons (4 mM, 298 K, 500 MHz).*

### C.2.b. $^{1}$H NMR analysis of foldamer A in deuterated chloroform

Chloroform is well–known for studying the hybridization equilibrium of oligopyridine dicarboxamide foldamers.[18,66,67] This prompted us to perform a variable–concentration $^{1}$H NMR experiment in deuterated chloroform. Due to the moderate solubility of foldamer **A**, the maximum concentration that could be reached was 5.2 mmol.L$^{-1}$. The corresponding spectra revealed the presence of a single set of signals at relatively high chemical shifts, and consequently suggest the absence of double helical structures in solution (Figure II–22).

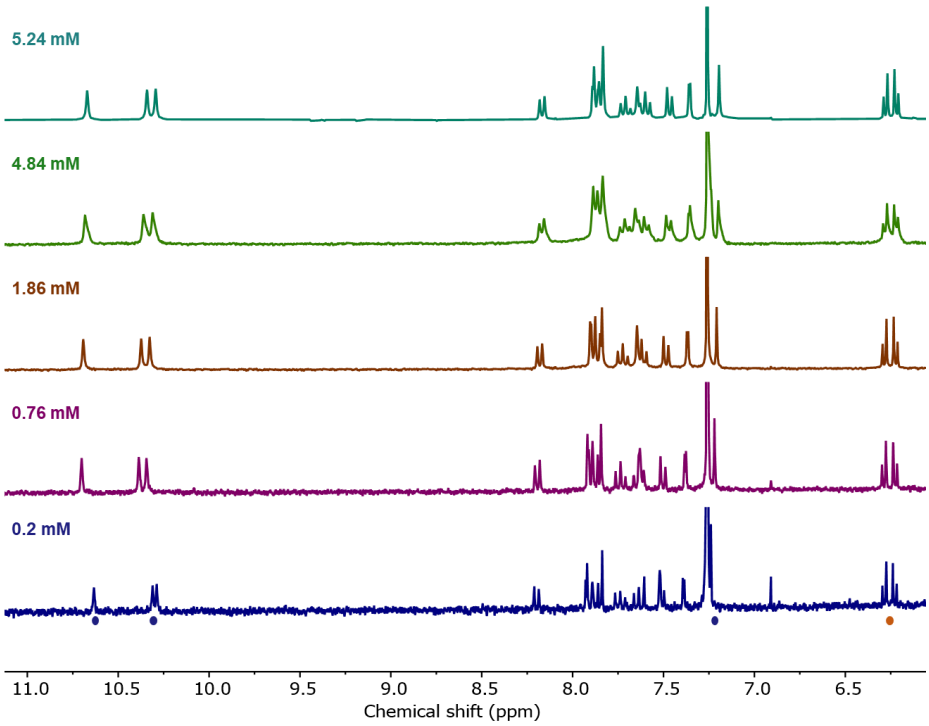


*Figure II–22. $^{1}$H NMR spectra of foldamer **A** at different concentrations: blue circles correspond to the amide protons and orange circles correspond to the TTF protons ($CDCl_3$, 298 K, 300 MHz).*

The behavior of foldamer **A** was unexpected because its analogue containing isobutoxy chains and lacking electroactive units **II–19** (Scheme II–13) exhibits a high solubility and a significant dimerization constant ($31 \times 10^3$ in $CDCl_3$ at 20°C).[18] On the other hand, when compared to **II–20**,[1] which displays the same skeleton and linkers with a different functional unit (*i.e.* Disperse red), the latter showed a remarkably high solubility in chlorinated solvents and a moderate dimerization constant ($126 \pm 3$, $CDCl_3$, 298 K). In this case, signals corresponding to double helices could be observed at concentrations down to 0.5 $mmol.L^{-1}$. Furthermore, an X–ray crystal structure of the double helix $(\mathbf{II–20})_2$ was obtained in different mixtures, and notably in a DMSO/ACN mixture, despite the presence of DMSO that tends to dissociate double helices.

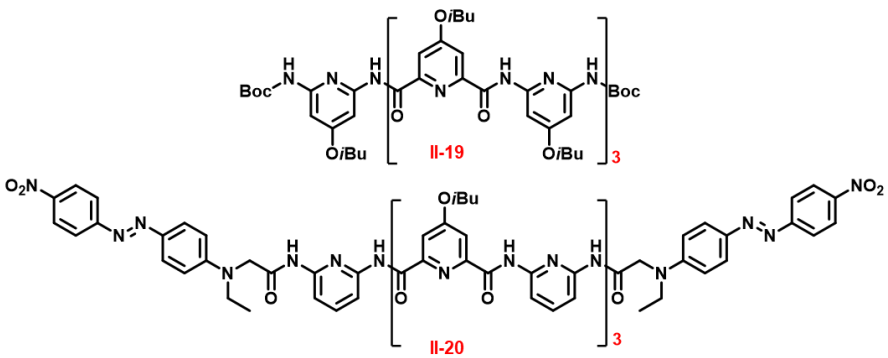


*Scheme II–13. Chemical structures of foldamers **II–19** and **II–20**.*

Based on these observations, two hypotheses were envisaged:

1) Foldamer **A** displays such a strong hybridization ability that the signals of single helices are not observed, even at low concentrations;
2) The single set of signals is attributed to the single helical structures; the nature of the linker and/or the electroactive unit stabilizes the single helical state and prevents the hybridization process. This unexpected supramolecular behavior prompted us to perform various complementary experiments, which are discussed below.

## C.3. Influence of the temperature

Temperature constitutes an external parameter, which can affect the hybridization, like solvents and concentrations.[2] The above–mentioned analyses (dilution) were conducted using a Bruker 300 MHz spectrometer. To account for the possibility of fast exchange and in order to improve the resolution of low concentration solutions, the following $^{1}$H NMR spectra were recorded using a Bruker 500 MHz spectrometer.

The $^{1}$H NMR spectra recorded in $CDCl_3$ at 5.2 mmol.L$^{-1}$ as a function of temperature (Figure II–23) showed the presence of a single set of signals for the amide protons at low (273 K) and high temperatures (323 K). Consequently, one can conclude that the composition of the medium does not change. Since double helices of these types of foldamers are known to dissociate at high temperatures because of weakened inter–strand interactions,[2] it seems rather reasonable to assign those signals to single helical species. Moreover, the signals of TTF protons are neither upfield or downfield shifted, indicating the absence of interactions involving the electroactive units.

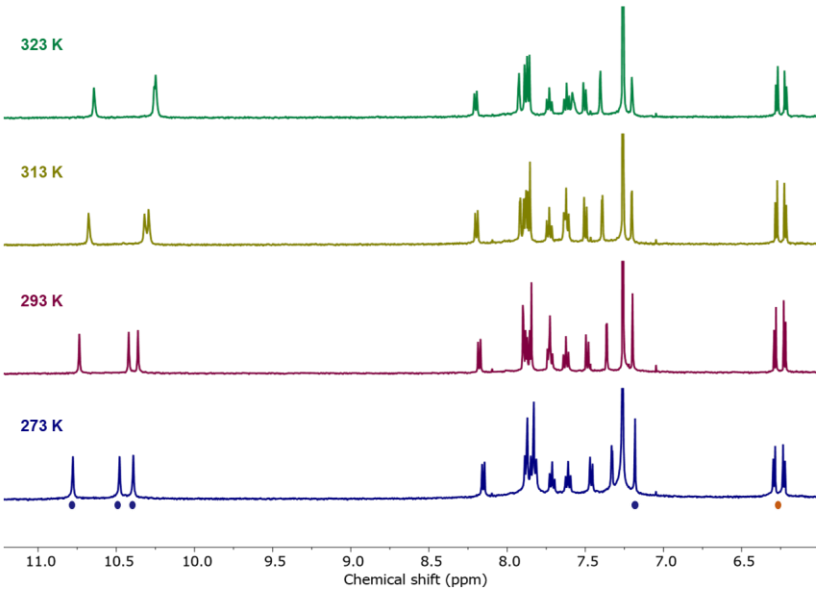


*Figure II–23. $^{1}H$ NMR spectra of foldamer **A** at different temperatures (5.2 mM, $CDCl_3$, 500 MHz).*

On the other hand, the slight variation in the chemical shift observed for amide signals could be attributed to conformational changes in solution upon heating or to weaker interactions with water molecules at high temperatures.

## C.4. Effect of anions on foldamer A

As discussed in the first chapter, the family of oligoarylamides exhibits recognition abilities. The corresponding recognition process can occur within their cavity, where small guests, such as anions, cations and neutral molecules, can be accommodated. In our case, this assertion is further supported by crystallographic structures that reveal the presence of molecules, such as water or solvent molecules bound through hydrogen bonds.

Along the preparation of her PhD, Dr Lara Faour performed a series of experiments on oligopyridine dicarboxamide functionalized with photoactive units, using different types of anions, to investigate the effect of these guests on the hybridization phenomenon. She demonstrated that upon adding halide anions, the equilibrium between single and double helices was shifted towards the formation of single helices. This is due to the fact that the complexation process between the single helix and the anions is favored. The first equilibrium between single and double helices was found to be slow at the NMR timescale, whereas the equilibrium between a single helix, anions and the complex formed among them was fast. Conversely, no complexation was detected between double helices and anions.[1]

Based on these results, the titration with anions appeared as a viable approach to determine the nature of the single set of signals observed for the amide protons. Upon titration of foldamer **A** with tetrabutylammonium chloride (Figure II–24), the signals corresponding to amide protons were progressively downfield shifted and no second set of signals appeared. This indicates the occurrence of a fast exchange at the NMR timescale, which is characteristic of the anion–single helix association. Our attempts to fit the experimental data to the mathematical model corresponding to a 1:1 stoichiometry failed, which indicates that this stoichiometry can be ruled out. Instead, a reasonable agreement was found when fitting the data to a 1:2 stoichiometry model. The collected dataset was not sufficient to properly estimate the equilibrium constants $K_1$ and $K_2$. However, it appears reasonable to state that the overall binding constant $\beta = K_1 \times K_2$ is comprised between $10^4$ and $10^5$.

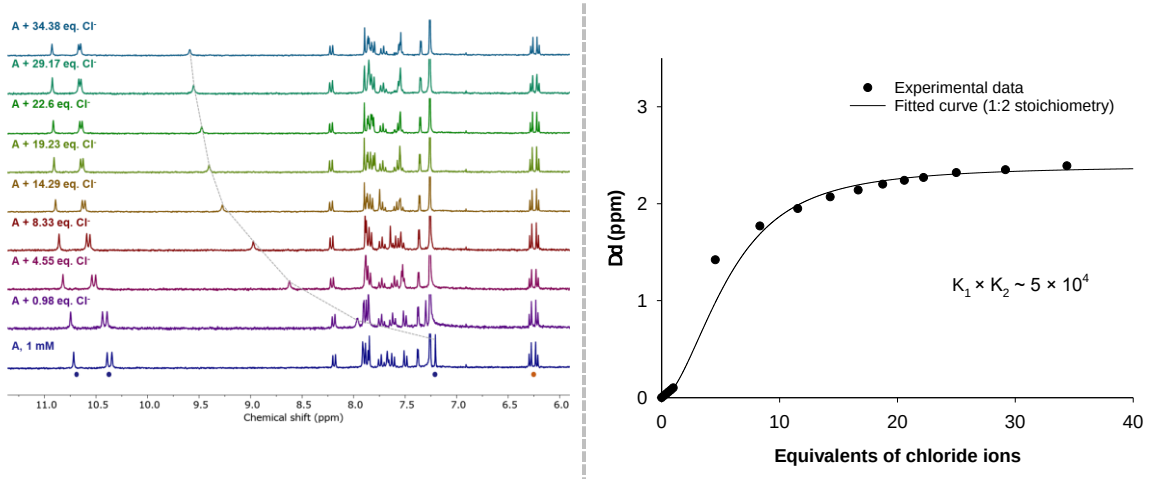


*Figure II–24. Left. $^1$H NMR spectra of foldamer **A** (1 mM) in $CDCl_3$ titrated with a solution of n–$Bu_4NCl$ (50 mM, 298 K, 500 MHz) containing **A** (1 mM). Right. Evolution of the chemical shift of an amide proton ($\delta_0$ = 7.20 ppm) as a function of the concentration of chloride ions and the corresponding fit (1:2 stoichiometry).*

## C.5. Effect of acceptors on donor TTF

As evidenced by the analyses led in solution and in the solid state, the single helix of foldamer **A** exhibits a high stability, which hinders its ability to hybridize. At this stage, we suspected that strong aromatic interactions between TTF and the foldamer skeleton take place. Thus, employing a competitive interaction to weaken the single helical state and favor hybridization appeared relevant. Since TTF is known for forming charge transfer complexes with electron–deficient derivatives such as NDI,[68–70] and TCNQ, two solutions of foldamer **A** (1 mmol.L$^{-1}$) in $CDCl_3$ were titrated with a solution of *N*,*N*–dimethylnaphthalene diimide (NDI) and tetracyanoquinodimethane TCNQ, respectively. The experiments were followed by $^1$H NMR spectroscopy ($CDCl_3$, [**A**] = 1 mM, Figure II–25). Unfortunately, the chemical shifts of TTF protons (6.25 ppm), NDI protons (8.72 ppm) and TCNQ (7.55 ppm) remained unchanged

in these conditions, even in the presence of eight and ten equivalent of the acceptors (limit of solubility). One should also note that no color change was observed upon adding NDI or TCNQ, which also translates the absence of interaction.

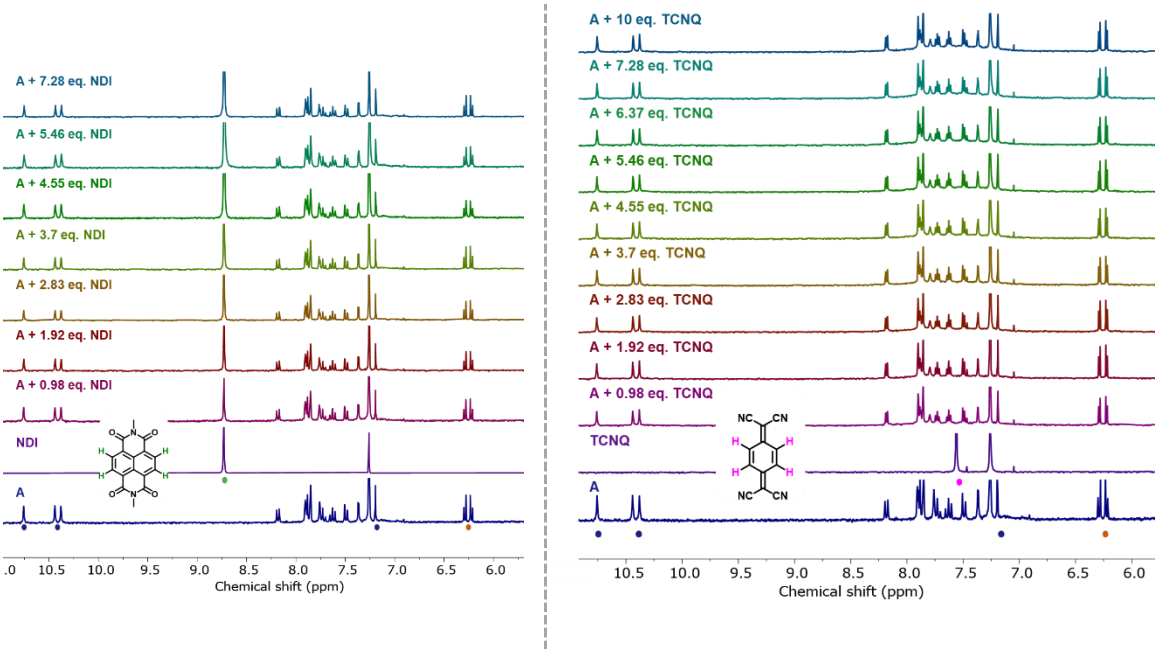


*Figure II–25. Titration of foldamer **A** (1 mM, $CDCl_3$, 298 K, 300 MHz) with acceptors NDI and TCNQ containing **A** (1 mM).*

In conclusion, foldamer **A** definitely shows a singular behavior in comparison to other oligomers from the same family. As evidenced by $^1$H NMR spectroscopy, it does not hybridize into duplexes, suggesting that it may be kinetically trapped. Our inability to obtain crystals from the duplex, as well as the obtaining of five crystallographic structures of single helices are in line with this assertion. Moreover, the X–ray diffraction analyses showed systematic aromatic interactions between the TTF units and the foldamer backbone. This is likely to lead to the occurrence of a high energetical barrier preventing the interconversion between single and double helices. In this context, the temperature sensitivity of the TTF–based foldamer constituted a limit to surpass the corresponding activation energy. This behavior appears facilitated by the short amide linker that directs the orientation of the TTF unit and makes the latter part of the helical structure. All these effects combined render this foldamer unable to hybridize in the neutral state.

## D. Electrochemical analyses

All the analyses conducted on foldamer **A** have confirmed its single helical state, when TTF units are in the neutral state. In this section, we will examine the electrochemical behavior of TTF unit in order to assess its impact on the hybridization phenomenon.

## D.1. Choice of the electrolyte

As mentioned previously, foldamers may interact with certain anions within their cavity. Therefore, when selecting an electrolyte, it is important to avoid anions that can readily react with the foldamer cavity. In organic solvents, the most common electrolyte is *n*–tetrabutylammonium hexafluorophosphate (*n*–$Bu_4NPF_6$). A titration of foldamer **A** (Figure II–26) with a solution of *n*–$Bu_4NPF_6$ was performed to confirm that the anion does not interact within the cavity of the foldamer. All the proton signals remained unaffected during this titration, which further supports the selection of *n*–$Bu_4NPF_6$ as the suitable electrolyte.

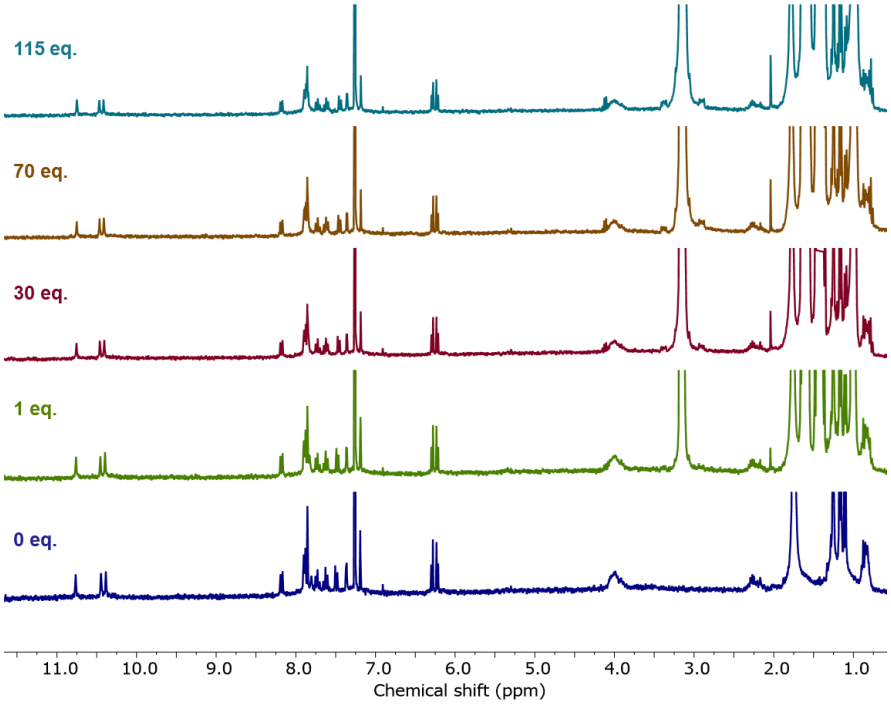


*Figure II–26. $^1H$ NMR spectra of foldamer **A** (1 mM) in $CDCl_3$ titrated with a solution of n–$Bu_4NPF_6$ (120 mM, 298 K, 300 MHz).*

## D.2. Choice of the solvents and concentrations

In order to facilitate the comparison with its neutral state, the initial voltammetry analyses were performed in chloroform. Under these conditions, foldamer **A** exhibits an adsorption phenomenon onto the electrode surface upon oxidation of the TTF units to the dicationic state. To prevent this adsorption, the study was subsequently conducted in a mixture of chloroform and acetonitrile (*1/1 (v/v)*). Due the limited solubility of foldamer **A**, determining the appropriate concentration was an intricate challenge due to the precipitation, especially when considering the presence of acetonitrile. Consequently, to address solubility issues, the samples were prepared 24 hours before the measurement in order to ensure complete solubility

during the measurement. The selected concentration was $1.25 \times 10^{-4}$ mol.L$^{-1}$ in a mixture of chloroform/acetonitrile (*1/1*).

The voltammogram of foldamer **A** displays two reversible oxidation waves associated to the formation of radical–cation $TTF^{\bullet+}$ and dication state $TTF^{2+}$ (Figure II–27), respectively ($E_{½}^{1}$ = 0.29 V, $E_{½}^{2}$ = 0.73 vs $Ag/AgNO_3$). These values are found to be higher than the TTF–based foldamer **II–5** ($E_{½}^{1}$ = 0.13 V, $E_{½}^{2}$ = 0.56 V vs $AgNO_3/Ag$), which correlates with the electronic effect of the directly attached carbonyl substituent. Furthermore, the linear evolution of the peak intensity with the square root of the scan rate confirmed that oxidized species do not adsorb onto the electrode surface.

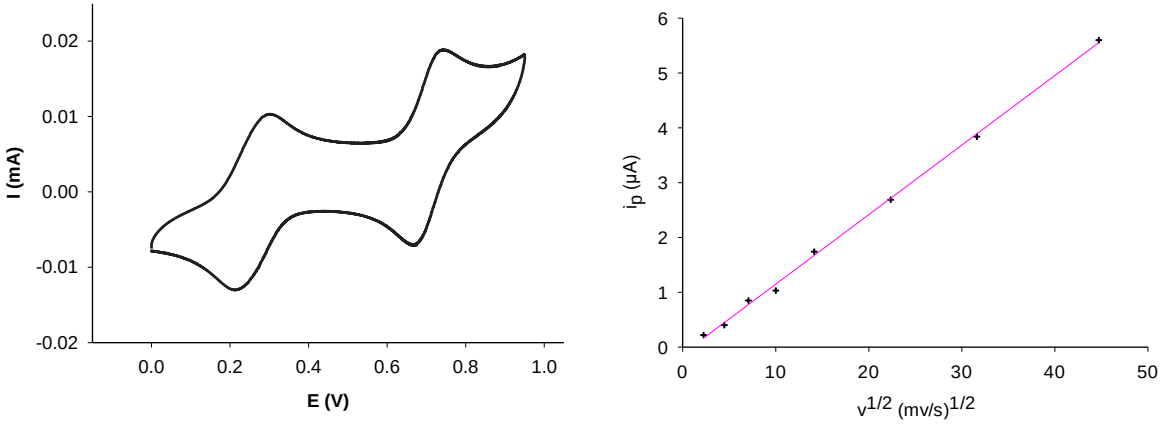


*Figure II–27. Left. Cyclic voltammogram of foldamer **A** (Pt, C = 1.25 × 10$^{-4}$ M, $CHCl_3$/ACN (1/1), 0.1 M, $Bu_4NPF_6$, v = 100 mV.s$^{-1}$, E vs $Ag/AgNO_3$ (0.01 M). Right. Evolution of the peak intensity $i_p$ as a function of the square root of the scan rate.*

Reference compounds **II–16** and **II–18** were also characterized in order to understand the electrochemical behavior of foldamer **A**. The derivatives include the terminal part of the foldamer skeleton, *i.e.* one TTF unit and a portion of the foldamer skeleton that is unable to fold into a helix. Therefore, when TTF units are oxidized, the observation of π–dimers would only result from supramolecular dimerization or polymerization.

Due to its limited solubility in a 1/1 mixture of chloroform and acetonitrile, **II–16** was finally excluded from this study. To ensure a rigorous comparison, the cyclic voltammogram of compound **II–18** was recorded under the same conditions as those for foldamer **A**. It displayed the expected reversible oxidation waves associated to the formation of radical–cation $TTF^{\bullet+}$ and dication $TTF^{2+}$, ($E_{½}^{1}$ = 0.21 V, $E_{½}^{2}$ = 0.62 *vs* $Ag/AgNO_3$ – Figure II–28). The first oxidation wave appeared thinner in comparison to the case of foldamer **A**, which suggests the occurrence of interactions involving the $TTF^{\bullet+}$ units of **A**.

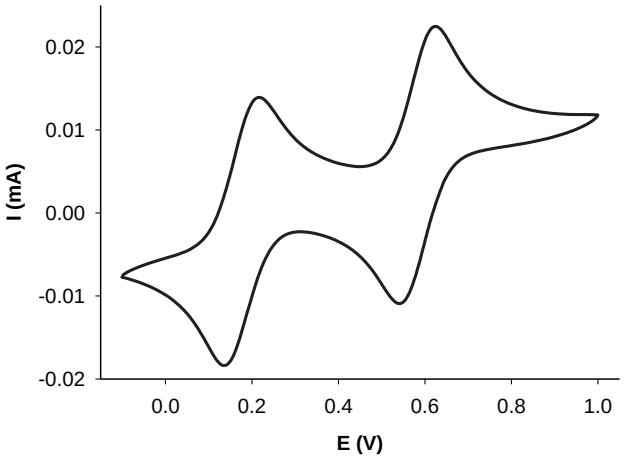


*Figure II–28. Voltammogram of compound **II–18** (Pt, C = 1.25 × $10^{-4}$ M, $CHCl_3$/ACN (1/1), 0.1 M, $Bu_4NPF_6$, v = 100 mV.$s^{-1}$, Ag/$AgNO_3$ (0.01 M)).*

A deconvolution of the voltammogram of foldamer **A** was carried out in order to subtract the contribution of the diffusion to the measured current (Figure II–29). This mathematical treatment showed that the areas are similar in oxidation and reduction, and the first oxidation wave is clearly enlarged. Thus, the oxidation process is reversible, and some interactions occur between the electroactive units along the first electrochemical process, which is commonly noticed when forming oxidized TTF dimers. Interestingly, such interactions can be set up in an intramolecular or an intermolecular manner and may allow for developing redox–controlled macrocyclization, polymerization or hybridization, in the case of helical foldamers.

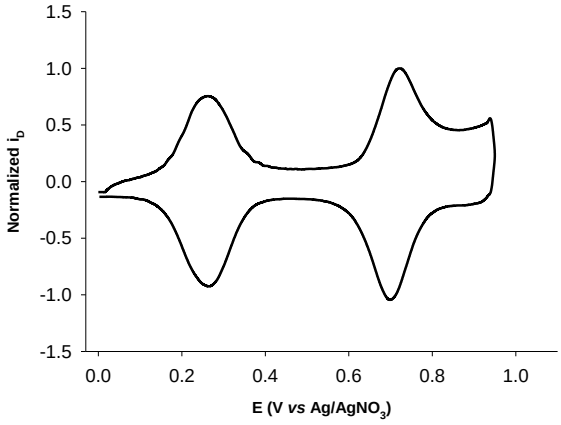


*Figure II–29. Deconvoluted version of the cyclic voltammogram of foldamer **A** presented in Figure II–27.*

## E. Towards redox–induced hybridization

The oxidation of TTF units appears as a potentially effective approach to control the stability of the helix. Through oxidation, the properties of TTF units (charge, electron density) evolve, which can lead to the dissociation of non–covalent bonds between TTF and the neighbouring units. Considering the widening of the first electrochemical process and hence,

the possible formation of radical cation dimers, we anticipated that this process could indeed affect the single–to–double helix equilibrium.

Spectroelectrochemistry is a technique that combines electrochemistry and spectroscopy (such as UV–vis, fluorescence, FTIR…) to study the behavior of electroactive species in solution or on surfaces in real time and *in–situ*. It involves the simultaneous monitoring of spectroscopic properties (such as absorbance, emission or vibrational modes) of molecules, while subjecting the latter to a varying or constant potential at an electrode. *The spectroelectrochemical measurements were performed at the MOLTECH–Anjou laboratory in collaboration with Dr. Christelle Gautier and Dr. Eric Levillain.*

These experiments were carried out in the same conditions as for the cyclic voltammetry in a mixture of chloroform ($CHCl_3$) and acetonitrile (ACN) in a 1/1 (*v/v*) ratio, and in the presence of *n*–tetrabutylammonium hexafluorophosphate (0.1 M).

Due to solubility issues, foldamer **A** could not be studied at concentrations over 1 $mmol.L^{-1}$. Hence, the first spectroelectrochemical measurement was acquired at this concentration. However, an adsorption phenomenon occurred on the electrode surface, which impeded the harnessing of reliable data. Consequently, the solution was diluted to 0.66 $mmol.L^{-1}$, and then diluted twice after each subsequent dilution.

The obtained spectra (Figure II–30–*Left*) clearly demonstrates the presence of an absorption band centered at 770 nm, which is a distinctive spectroscopic feature of π–dimers $(TTF^{\bullet+})_2$.[71] Remarkably, this signature is observed at concentrations as low as $10^{-5}$ M. This result highlights the notable ability of foldamer **A** to form π–dimers after oxidation, even at very low concentrations.

Normalizing the variation of absorption at $\lambda$ = 580 nm, the corresponding $\Delta A_{770}$ value were plotted as a function of the total concentration. This study revealed a nonlinear evolution, which shows the intermolecular character of the interactions between oxidized species (Figure II–30–*Right*). Though we do not dispose of a large dataset, we can affirm that the dimerization constant of the oxidized species is in the range of $10^4$, which indicates a strong propensity of foldamer **A** to form radical cation dimers.

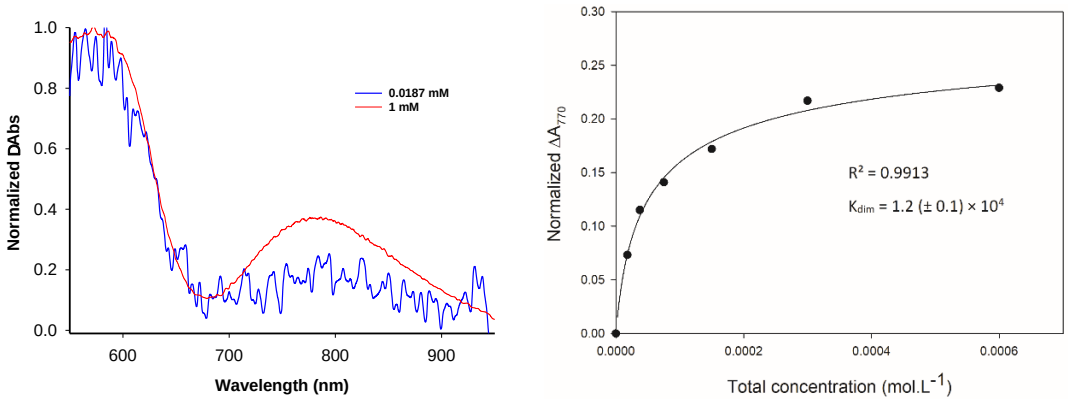


*Figure II–30. Left. 2D sections extracted at 0.65 V vs Ag/$AgNO_3$ (0.1 M) from spectroelectrochemical experiments performed at different concentrations of foldamer **A** in $CHCl_3$/$CH_3CN$ 1/1, n–$Bu_4NPF_6$ (0.1 M) at 50 mV.$s^{-1}$, under thin layer conditions. Absorbance values are normalized with the normalization coefficient obtained for the band located at 580 nm. Right. The evolution of the dimer/monomer ratio as a function of concentration.*

On this ground, three plausible arrangements can be envisioned: the formation of a supramolecular polymer, a macrocycle or the generation of double helices (Figure II–31).

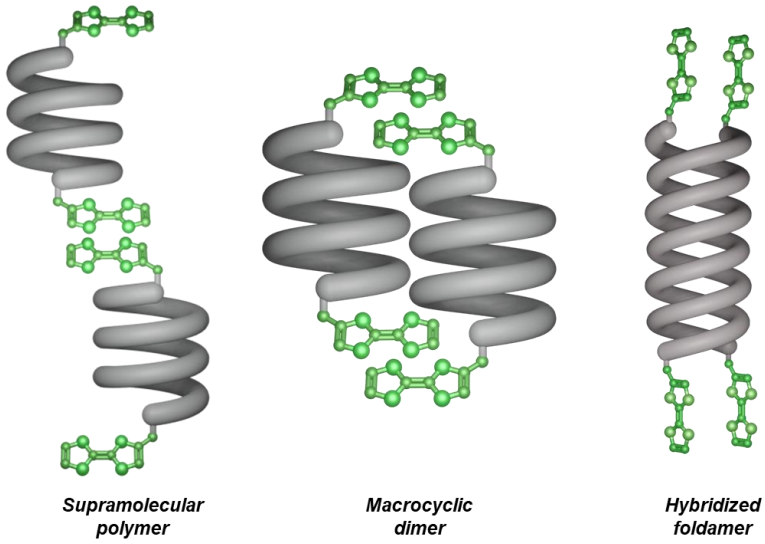


*Figure II–31. Possible supramolecular arrangements of foldamer **A** upon the oxidation of TTF units.*

To get insight on the possible formation of a supramolecular polymer, spectroelectrochemical analyses were performed on reference compound **II–18**, which cannot form macrocycles or duplexes. This was performed by using the same experimental conditions as those applied for the analysis of foldamer **A**. The corresponding spectroelectrochemical studies revealed that the interactions between TTF radical cations only occur at high concentrations (> 7.5 mM – Figure II–32–*Right*). Furthermore, by comparing the spectroelectrochemical data of foldamer **A** at 1 mM to that of reference compound **II–18** at 1.2 mM, we can clearly conclude that the concentration of π–dimers is significantly more pronounced in the case of foldamer **A** (Figure II–32–*Left*).

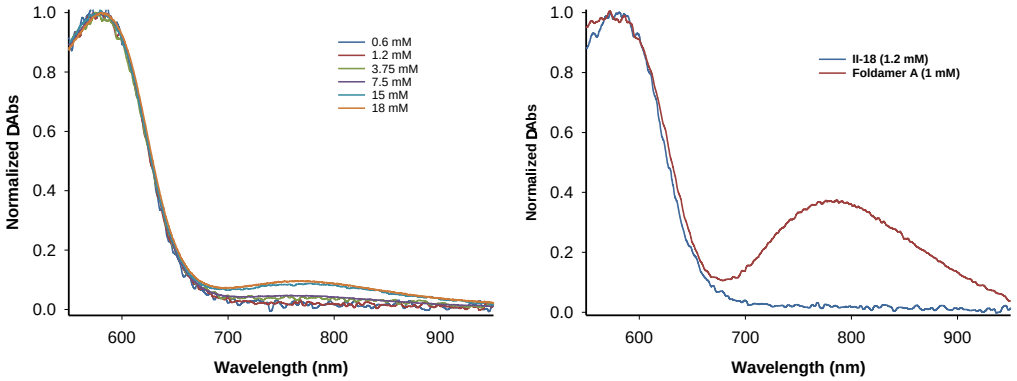


*Figure II–32. Right. Spectroelectrochemistry of reference compound **II –18**. Left. Comparison of the spectroelectrochemical spectra between foldamer **A** at 1 mM and **II–18** at 1.2 mM.*

From a more quantitative point of view, Figure II–33 demonstrates that foldamer **A** forms π–dimers at concentrations that are two orders of magnitude lower than reference **II–18**. These results exclude the supramolecular polymerization of foldamer **A**.

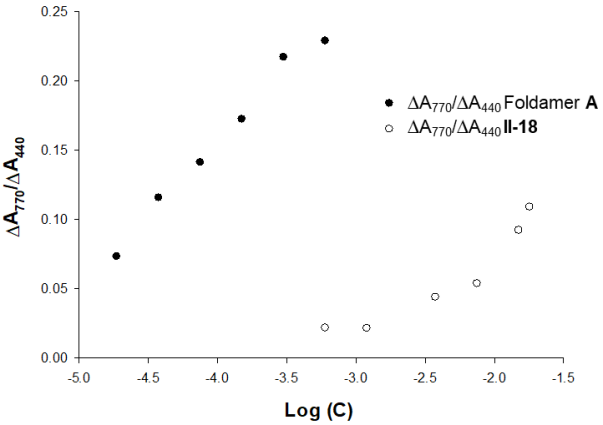


*Figure II–33. Comparison of the evolution of the dimer/monomer ratio between foldamer **A** and **II–18** as function of log(C).*

Considering *i)* the structure of foldamer **A** (see X–ray diffraction analyses), the network of hydrogen bonds and aromatic interactions that stabilize its helical conformation and, the relative orientation of TTF units, as well as *ii)* the fact that the well–preorganized systems described by Zhang–Ting Li and coworkers (see Scheme II–3) solely display a dimerization constant of *ca.* 100 in the same solvent system,[72] we consider the formation of supramolecular macrocycle very unlikely. Thus, the redox–triggered hybridization of foldamer **A** into homoduplexes appears as a rational explanation to justify the formation of π–dimers at very weak concentrations and in the absence of any additive known for stabilizing these supramolecular assemblies.

# III. Conclusions

The field of stimuli–responsive foldamers based on redox stimulations is still in its early stages of development. Along this work, we synthesized a new foldamer derived from the oligopyridine dicarboxamide skeleton endowed with tetrathiafulvalene units through amide linkers. The synthesis of this foldamer **A** appeared quite challenging and much effort was made to optimize the conditions of synthesis and purification that allowed the successful preparation of foldamer **A** after thirteen steps. All the studies conducted in solution in the neutral state highlighted the stability of foldamer **A** in its single helical arrangement and showed that it does not hybridize in this state.

This assertion was further supported by solid–state analyses. Despite dedicating much time to crystallization experiments, five crystallographic structures could be solved for foldamer **A**, all of them corresponding to single helices. The analysis of these structures highlighted the role of the amide linker in the orientation of TTF units, which forces the latter to be part of the helix through several intra– and intermolecular interactions.

The oxidation of TTF units affects their properties and weakens the stability of the single helix. Through spectroelectrochemical measurements, we showed that the dimerization of radical cations was more efficient for the foldamer in comparison to the reference molecule, highlighting the contribution of the foldamer skeleton to the formation and stabilization of π–dimers. In this context, the nature of the linker proved to be an important parameter that affects the overall behavior of a foldamer functionalized with electroactive units. Additional insights on this result will be given in chapter 3 with the synthesis and characterization of another TTF–containing foldamer, among others.

To our knowledge, foldamer **A** constitutes the first example of "redox–triggered hybridization process" and this, without any alteration of the medium composition.

(1) Faour, L. Architectures Stimulables à Base de Foldamères Photo–et Électroactifs, Université d'Angers, 2018.
(2) Berl, V.; Huc, I.; Khoury, R. G.; Krische, M. J.; Lehn, J.–M. Interconversion of Single and Double Helices Formed from Synthetic Molecular Strands. *Nature* **2000**, *407* (6805), 720–723.
(3) Berl, V.; Huc, I.; Khoury, R. G.; Lehn, J.–M. Helical Molecular Programming: Folding of Oligopyridine-dicarboxamides into Molecular Single Helices. *Chemistry–A European Journal* **2001**, *7* (13), 2798–2809.
(4) Berl, V.; Huc, I.; Khoury, R. G.; Lehn, J.–M. Helical Molecular Programming: Supramolecular Double Helices by Dimerization of Helical Oligopyridine-dicarboxamide Strands. *Chemistry–A European Journal* **2001**, *7* (13), 2810–2820.
(5) Zhang, D.–W.; Zhao, X.; Hou, J.–L.; Li, Z.–T. Aromatic Amide Foldamers: Structures, Properties, and Functions. *Chemical Reviews* **2012**, *112* (10), 5271–5316.
(6) Huc, I. Aromatic Oligoamide Foldamers. *European Journal of Organic Chemistry* **2004**, *2004* (1), 17–29.
(7) Baptiste, B.; Zhu, J.; Haldar, D.; Kauffmann, B.; Léger, J.–M.; Huc, I. Hybridization of Long Pyridine-Dicarboxamide Oligomers into Multi-Turn Double Helices: Slow Strand Association and Dissociation, Solvent Dependence, and Solid State Structures. *Chemistry–An Asian Journal* **2010**, *5* (6), 1364–1375.
(8) Berl, V.; Huc, I.; Khoury, R. G.; Lehn, J.–M. Helical Molecular Programming: Folding of Oligopyridine-dicarboxamides into Molecular Single Helices. *Chemistry–A European Journal* **2001**, *7* (13), 2798–2809.
(9) Berl, V.; Huc, I.; Khoury, R. G.; Lehn, J.–M. Helical Molecular Programming: Supramolecular Double Helices by Dimerization of Helical Oligopyridine-dicarboxamide Strands. *Chemistry–A European Journal* **2001**, *7* (13), 2810–2820.
(10) Berl, V.; Huc, I.; Khoury, R. G.; Krische, M. J.; Lehn, J.–M. Interconversion of Single and Double Helices Formed from Synthetic Molecular Strands. *Nature* **2000**, *407* (6805), 720–723.
(11) Haldar, D.; Jiang, H.; Léger, J.–M.; Huc, I. Interstrand Interactions between Side Chains in a Double-Helical Foldamer. *Angewandte Chemie* **2006**, *118* (33), 5609–5612.
(12) Helical Molecular Programming: Folding of Oligopyridine-dicarboxamides into Molecular Single Helices. *Chemistry– A European Journal* **2001**, *7* (13), 2798–2809.
(13) Gellman, S. H. Foldamers: A Manifesto. *Accounts of Chemical Research* **1998**, *31* (4), 173–180.
(14) Jiang, H.; Léger, J.–M.; Huc, I. Aromatic δ–Peptides. *Journal of the American Chemical Society* **2003**, *125* (12), 3448–3449.
(15) Haldar, D.; Jiang, H.; Léger, J.–M.; Huc, I. Double versus Single Helical Structures of Oligopyridine–Dicarboxamide Strands. Part 2: The Role of Side Chains. *Tetrahedron* **2007**, *63* (27), 6322–6330.
(16) Haldar, D.; Jiang, H.; Léger, J.–M.; Huc, I. Interstrand Interactions between Side Chains in a Double–Helical Foldamer. *Angewandte Chemie International Edition* **2006**, *45* (33), 5483–5486.
(17) Hamuro, Y.; Geib, S. J.; Hamilton, A. D. Novel Molecular Scaffolds: Formation of Helical Secondary Structure in a Family of Oligoanthranilamides. *Angewandte Chemie International Edition in English* **1994**, *33* (4), 446–448.
(18) Baptiste, B.; Zhu, J.; Haldar, D.; Kauffmann, B.; Léger, J.–M.; Huc, I. Hybridization of Long Pyridine-Dicarboxamide Oligomers into Multi-Turn Double Helices: Slow Strand Association and Dissociation, Solvent Dependence, and Solid State Structures. *Chemistry–An Asian Journal* **2010**, *5* (6), 1364–1375.
(19) Wudl, F.; Wobschall, D.; Hufnagel, E. J. Electrical Conductivity by the Bis (1, 3–Dithiole)–Bis (1, 3–Dithiolium) System. *Journal of the American Chemical Society* **1972**, *94* (2), 670–672.
(20) Bryce, M. R. Functionalised Tetrathiafulvalenes: New Applications as Versatile π–Electron Systems in Materials Chemistry. *Journal of Materials Chemistry* **2000**, *10* (3), 589–598.
(21) Jana, A.; Bähring, S.; Ishida, M.; Goeb, S.; Canevet, D.; Sallé, M.; Jeppesen, J. O.; Sessler, J. L. Functionalised Tetrathiafulvalene–(TTF–) Macrocycles: Recent Trends in Applied Supramolecular Chemistry. *Chemical Society Reviews* **2018**, *47* (15), 5614–5645.
(22) Segura, J. L.; Martín, N. New Concepts in Tetrathiafulvalene Chemistry. *Angewandte Chemie International Edition* **2001**, *40* (8), 1372–1409.
(23) Canevet, D.; Sallé, M.; Zhang, G.; Zhang, D.; Zhu, D. Tetrathiafulvalene (TTF) Derivatives: Key Building–Blocks for Switchable Processes. *Chem. Commun.* **2009**, 17, 2245–2269.
(24) Martín, N. Tetrathiafulvalene: The Advent of Organic Metals. *Chemical Communications* **2013**, *49* (63), 7025–7027.
(25) Wang, C. S.; Bryce, M. R.; Batsanov, A. S.; Howard, J. A. Synthesis of Pyrazinoporphyrazine Derivatives Functionalised with Tetrathiafulvalene (TTF) Units: X-Ray Crystal Structures of Two Related TTF Cyclophanes and Two Bis (1, 3-Dithiole-2-Thione) Intermediates. *Chemistry–A European Journal* **1997**, *3* (10), 1679–1690.
(26) Bloch, A. N.; Ferraris, J. P.; Cowan, D. O.; Poehler, T. O. Microwave Conductivities of the Organic Conductors TTF–TCNQ and ATTF–TCNQ. *Solid State Communications* **1973**, *13* (7), 753–757.
(27) Kwak, J. F.; Chaikin, P. M.; Russel, A. A.; Garito, A. F.; Heeger, A. J. Anisotropic Thermoelectric Power of TTF–TCNQ. *Solid State Communications* **1975**, *16* (6), 729–732.
(28) Kistenmacher, T. J.; Phillips, T. E.; Cowan, D. O. The Crystal Structure of the 1: 1 Radical Cation–Radical Anion Salt of 2, 2'–Bis–l, 3–Dithiole (TTF) and 7, 7, 8, 8–Tetracyanoquinodimethane (TCNQ). *Acta Crystallographica Section B: Structural Crystallography and Crystal Chemistry* **1974**, *30* (3), 763–768.
(29) Jérome, D.; Mazaud, A.; Ribault, M.; Bechgaard, K. Superconductivity in a Synthetic Organic Conductor (TMTSF)2PF6. *Journal de Physique Lettres* **1980**, *41* (4), 95–98.
(30) Andrieux, A.; Duroure, C.; Jérome, D.; Bechgaard, K. The Metallic State of the Organic Conductor TMTSF–DMTCNQ at Low Temperature under Pressure. *Journal de Physique Lettres* **1979**, *40* (15), 381–383.
(31) Lyskawa, J.; Sallé, M.; Balandier, J.–Y.; Le Derf, F.; Levillain, E.; Allain, M.; Viel, P.; Palacin, S. Monitoring the Formation of TTF Dimers by Na+ Complexation. *Chemical communications* **2006**, No. 21, 2233–2235.
(32) Rosokha, S. V.; Kochi, J. K. Molecular and Electronic Structures of the Long–Bonded π–Dimers of Tetrathiafulvalene Cation–Radical in Intermolecular Electron Transfer and in (Solid–State) Conductivity. *Journal of the American Chemical Society* **2007**, *129* (4), 828–838.
(33) Miller, J. S.; Novoa, J. J. Four–Center Carbon− Carbon Bonding. *Accounts of Chemical Research* **2007**, *40* (3), 189–196.
(34) Yan, Y.–K.; Mingos, D. M. P.; Kurmoo, M.; Li, W.–S.; Scowen, I. J.; McPartlin, M.; Coomber, A. T.; Friend, R. H. Synthesis, Structure and Physical Properties of Tetrathiafulvalenium Salts of the Ferracarborane Complex Commo–[3, 3′–Fe {1–(C 4 H 3 S)–1, 2–C 2 B 9 H 10} 2]. *Journal of the Chemical Society, Dalton Transactions* **1995**, No. 17, 2851–2860.
(35) Capdevila-Cortada, M.; Novoa, J. J.; Bell, J. D.; Moore, C. E.; Rheingold, A. L.; Miller, J. S. Unusually Long, Multicenter, Cationδ+··· Anionδ− Bonding Observed for Several Polymorphs of [TTF][TCNE]. *Chemistry–A European Journal* **2011**, *17* (34), 9326–9341.

(36) Novoa, J. J.; Lafuente, P.; Del Sesto, R. E.; Miller, J. S. Exceptionally Long (≥ 2.9 Å) C− C Bonds between [TCNE]− Ions: Two-Electron, Four-Center Π*–Π* C− C Bonding in Π-[TCNE] 22. *Angewandte Chemie International Edition* **2001**, *40* (13), 2540–2545.

(37) Hunter, C. A.; Sanders, J. K. The Nature of Pi–Pi. Interactions. *Journal of the American Chemical Society* **1990**, *112* (14), 5525–5534.

(38) Khodorkovsky, V.; Shapiro, L.; Krief, P.; Shames, A.; Mabon, G.; Gorgues, A.; Giffard, M. Do π–Dimers of Tetrathiafulvalene Cation Radicals Really Exist at Room Temperature? *Chemical Communications* **2001**, 24, 2736–2737.

(39) Huchet, L.; Akoudad, S.; Levillain, E.; Roncali, J.; Emge, A.; Bäuerle, P. Spectroelectrochemistry of Electrogenerated Tetrathiafulvalene–Derivatized Poly (Thiophenes): Toward a Rational Design of Organic Conductors with Mixed Conduction. *The Journal of Physical Chemistry B* **1998**, *102* (40), 7776–7781.

(40) Bozio, R.; Zanon, I.; Girlando, A.; Pecile, C. Vibrational Spectroscopy of Molecular Constituents of One-dimensional Organic Conductors. Tetrathiofulvalene (TTF), TTF+, and (TTF+) 2 Dimer. *The Journal of Chemical Physics* **1979**, *71* (5), 2282–2293.

(41) Ziganshina, A. Y.; Ko, Y. H.; Jeon, W. S.; Kim, K. Stable π–Dimer of a Tetrathiafulvalene Cation Radical Encapsulated in the Cavity of Cucurbit [8] Uril. *Chemical communications* **2004**, 7, 806–807.

(42) Yoshizawa, M.; Kumazawa, K.; Fujita, M. Room–Temperature and Solution–State Observation of the Mixed–Valence Cation Radical Dimer of Tetrathiafulvalene,[(TTF) 2]+•, within a Self–Assembled Cage. *Journal of the American Chemical Society* **2005**, *127* (39), 13456–13457.

(43) Hasegawa, M.; Daigoku, K.; Hashimoto, K.; Nishikawa, H.; Iyoda, M. Face–to–Face Dimeric Tetrathiafulvalenes and Their Cation Radical and Dication Species as Models of Mixed Valence and π–Dimer States. *Bulletin of the Chemical Society of Japan* **2012**, *85* (1), 51–60.

(44) Christensen, C. A.; Becher, J.; Goldenberg, L. M.; Bryce, M. R. Synthesis and Electrochemistry of a Tetrathiafulvalene (TTF) 21–Glycol Dendrimer: Intradendrimer Aggregation of TTF Cation Radicals. *Chemical Communications* **1998**, 4, 509–510.

(45) Bejger, C.; Davis, C. M.; Park, J. S.; M. Lynch, V.; Love, J. B.; Sessler, J. L. Palladium Induced Macrocyclic Preorganization for Stabilization of a Tetrathiafulvalene Mixed–Valence Dimer. *Organic letters* **2011**, *13* (18), 4902–4905.

(46) Inagi, S.; Naka, K.; Chujo, Y. Functional Polymers Based on Electron–Donating TTF and Derivatives. *Journal of Materials Chemistry* **2007**, *17* (39), 4122–4135.

(47) Segura, J. L.; Martín, N. New Concepts in Tetrathiafulvalene Chemistry. *Angewandte Chemie International Edition* **2001**, *40* (8), 1372–1409.

(48) Bergkamp, J. J.; Decurtins, S.; Liu, S.–X. Current Advances in Fused Tetrathiafulvalene Donor–Acceptor Systems. *Chemical Society Reviews* **2015**, *44* (4), 863–874.

(49) Frei, M.; Diederich, F.; Tremont, R.; Rodriguez, T.; Echegoyen, L. Tetrathiafulvalene (TTF)-Bridged Resorcin [4] Arene Cavitands: Towards New Electrochemical Molecular Switches. *Helvetica Chimica Acta* **2006**, *89* (9), 2040–2057.

(50) Schröder, H. V.; Schalley, C. A. Tetrathiafulvalene–a Redox–Switchable Building Block to Control Motion in Mechanically Interlocked Molecules. *Beilstein journal of organic chemistry* **2018**, *14* (1), 2163–2185.

(51) Nielsen, M. B.; Li, Z.–T.; Becher, J. Tetrathiafulvalenophanes and Their Catenanes. *Journal of Materials Chemistry* **1997**, *7* (7), 1175–1187.

(52) Chen, L.; Wang, H.; Zhang, D.–W.; Zhou, Y.; Li, Z.–T. Quadruple Switching of Pleated Foldamers of Tetrathiafulvalene–Bipyridinium Alternating Dynamic Covalent Polymers. *Angewandte Chemie International Edition* **2015**, *54* (13), 4028–4031.

(53) Stoddart, J. F. Mechanically Interlocked Molecules (MIMs)—Molecular Shuttles, Switches, and Machines (Nobel Lecture). *Angewandte Chemie International Edition* **2017**, *56* (37), 11094–11125.

(54) Sauvage, J.–P. From Chemical Topology to Molecular Machines (Nobel Lecture). *Angewandte Chemie International Edition* **2017**, *56* (37), 11080–11093.

(55) Feringa, B. L. The Art of Building Small: From Molecular Switches to Motors (Nobel Lecture). *Angewandte Chemie International Edition* **2017**, *56* (37), 11060–11078.

(56) Trabolsi, A.; Khashab, N.; Fahrenbach, A. C.; Friedman, D. C.; Colvin, M. T.; Cotí, K. K.; Benítez, D.; Tkatchouk, E.; Olsen, J.–C.; Belowich, M. E. Radically Enhanced Molecular Recognition. *Nature Chemistry* **2010**, *2* (1), 42–49.

(57) Wang, W.–K.; Chen, Y.–Y.; Wang, H.; Zhang, D.–W.; Liu, Y.; Li, Z.–T. Tetrathiafulvalene-Based Macrocycles Formed by Radical Cation Dimerization: The Role of Intramolecular Hydrogen Bonding and Solvent. *Chemistry–An Asian Journal* **2014**, *9* (4), 1039–1044.

(58) Faour, L.; Adam, C.; Gautier, C.; Goeb, S.; Allain, M.; Levillain, E.; Canevet, D.; Sallé, M. Redox–Controlled Hybridization of Helical Foldamers. *Chemical Communications* **2019**, *55* (40), 5743–5746.

(59) Aparicio, F.; Faour, L.; Allain, M.; Canevet, D.; Sallé, M. A Pyrene–Functionalized Foldamer: Structural Impact and Recognition Properties Supported by Donor–Acceptor Interactions. *Chemical Communications* **2017**, *53* (88), 12028–12031.

(60) Sanchez–Garcia, D.; Kauffmann, B.; Kawanami, T.; Ihara, H.; Takafuji, M.; Delville, M.–H.; Huc, I. Nanosized Hybrid Oligoamide Foldamers: Aromatic Templates for the Folding of Multiple Aliphatic Units. *Journal of the American Chemical Society* **2009**, *131* (24), 8642–8648.

(61) Delsuc, N.; Léger, J.–M.; Massip, S.; Huc, I. Proteomorphous Objects from Abiotic Backbones. *Angewandte Chemie* **2007**, *119* (1-2), 218–221.

(62) Di Antonio, M.; McLuckie, K. I.; Balasubramanian, S. Reprogramming the Mechanism of Action of Chlorambucil by Coupling to a G–Quadruplex Ligand. *Journal of the American Chemical Society* **2014**, *136* (16), 5860–5863.

(63) Garin, J.; Orduna, J.; Uriel, S.; Moore, A. J.; Bryce, M. R.; Wegener, S.; Yufit, D. S.; Howard, J. A. Improved Syntheses of Carboxytetrathiafulvalene, Formyltetrathiafulvalene and (Hydroxymethyl) Tetrathiafulvalene: Versatile Building Blocks for New Functionalised Tetrathiafulvalene Derivatives. *Synthesis* **1994**, *1994* (05), 489–493.

(64) Montalbetti, C. A.; Falque, V. Amide Bond Formation and Peptide Coupling. *Tetrahedron* **2005**, *61* (46), 10827–10852.

(65) Neises, B.; Steglich, W. Simple Method for the Esterification of Carboxylic Acids. *Angewandte Chemie International Edition in English* **1978**, *17* (7), 522–524.

(66) Berl, V.; Huc, I.; Khoury, R. G.; Lehn, J.–M. Helical Molecular Programming: Folding of Oligopyridine-dicarboxamides into Molecular Single Helices. *Chemistry–A European Journal* **2001**, *7* (13), 2798–2809.

(67) Berl, V.; Huc, I.; Khoury, R. G.; Lehn, J.–M. Helical Molecular Programming: Supramolecular Double Helices by Dimerization of Helical Oligopyridine–Dicarboxamide Strands. *Chemistry– A European Journal* **2001**, *7* (13), 2810–2820.

(68) Schröder, H. V.; Hupatz, H.; Achazi, A. J.; Sobottka, S.; Sarkar, B.; Paulus, B.; Schalley, C. A. A Divalent Pentastable Redox-Switchable Donor–Acceptor Rotaxane. *Chemistry–A European Journal* **2017**, *23* (12), 2960–2967.

(69) Tan, L.; Zhang, G.; Zhang, D.; Zhu, D. Linear and Cyclic Tetrathiafulvalene–Naphthalenediimide Donor–Acceptor Molecules: Metal Ions–Promoted Electron Transfer. *The Journal of Organic Chemistry* **2011**, *76* (21), 9046–9052.

(70) Beldjoudi, Y.; Narayanan, A.; Roy, I.; Pearson, T. J.; Cetin, M. M.; Nguyen, M. T.; Krzyaniak, M. D.; Alsubaie, F. M.; Wasielewski, M. R.; Stupp, S. I. Supramolecular Tessellations by a Rigid Naphthalene Diimide Triangle. *Journal of the American Chemical Society* **2019**, *141* (44), 17783–17795.

(71) Torrance, J. B.; Scott, B. A.; Welber, B.; Kaufman, F. B.; Seiden, P. E. Optical Properties of the Radical Cation Tetrathiafulvalenium (TT F+) in Its Mixed–Valence and Monovalence Halide Salts. *Physical Review B* **1979**, *19* (2), 730.

(72) Wang, W.–K.; Chen, Y.–Y.; Wang, H.; Zhang, D.–W.; Liu, Y.; Li, Z.–T. Tetrathiafulvalene-Based Macrocycles Formed by Radical Cation Dimerization: The Role of Intramolecular Hydrogen Bonding and Solvent. *Chemistry–An Asian Journal* **2014**, *9* (4), 1039–1044.

# Chapter 3

# Helical foldamers grafted with electron poor and rich aromatics: From kinetically–trapped systems to heteroduplexes

# I. Towards heteroduplex formation through aromatic donor–acceptor interactions

As elaborated in the concluding section of the first chapter, heteroduplexes remain rather scarce in the literature. These supramolecular architectures are formed by intertwining of two non–identical strands. As a result, they differ not only geometrically from single helices, but also in terms of physico–chemical properties. For instance, double helices showed applications in different domains of biology, for permitting the penetration of lipid cells[1] or to act as ion channels.[2] Additionally, the difference in geometry sometimes permits the encapsulation of molecules in their single helical form and their release upon the formation of double helices or vice–versa.[3] Moreover, their structures, geometry, chirality may have potential in promoting reactions by acting as catalysts.[4,5] These particular features encouraged us to target the control of the equilibrium between single and double helices in a reversible manner.

On the other hand, associating different strands can lead to a wide variety of duplexes, each with unique characteristics. For example, the cavity formed during hybridization of distinct strands could vary in size, potentially accommodating guests that would not fit within the cavity of homoduplexes. Moreover, the polarity of these duplexes cavity could differ, affecting their capacity to trap guests. On the other hand, one could imagine the transfer of chirality from a chiral strand to another distinct achiral one, potentially leading to the discovery of new compounds in the field of catalysis. Thereby, the formation of heteroduplexes with novel and unique properties represents a promising field to explore.

Achieving the selective formation of heteroduplexes relies on suitable level of complementarity between the strands forming the duplexes. Thus, taking advantage of driving force appears as a relevant strategy to favor hybridization into heteroduplexes rather than homoduplexes. In this context, this chapter will focus on the efforts conducted to prepare heteroduplexes in a selective manner through aromatic interactions between electron rich and electron poor units. This asymmetric interaction will serve as a tool to build non–identical strands. In order to accomplish this goal, a series of electroactive foldamers functionalized with electron–deficient and electron–donating units were synthesized and characterized.

## A. Generalities

Charge transfer (CT) occurs when electron density located in the highest occupied molecular orbital (HOMO) of a donor region is shifted towards the moiety bearing the lowest

unoccupied molecular orbital (LUMO) of an acceptor counterpart. Along this process, a new absorption band, called charge transfer band, appears and can be monitored by UV–visible absorption spectroscopy. One will note that molar absorption coefficients of broad CT bands are most often low, which makes it challenging to characterize them in diluted solutions, where the dissociation of the complex is favored.[6] Thus, increasing the concentration of one or both components will increase the chance to detect the CT band. The appearance of the corresponding species is accompanied by a color change, generally observable with the naked eye. Furthermore, CT interactions are also detectable by NMR spectroscopy techniques. Indeed, the alternate face–to–face D–A stacking induces an upfield shift of the aromatic protons for both the donor and acceptor electroactive units.[7] 2D NMR Tools, such as NOE spectroscopy, can also probe this contact by evidencing through–space couplings between protons.[8]

Charge transfer interaction displays comparable features with hydrogen bonding regarding its complementarity between D and A, but this interaction occurs through non–directional electrostatic attraction between electron–rich and electron–deficient cores (Figure III–).[9]

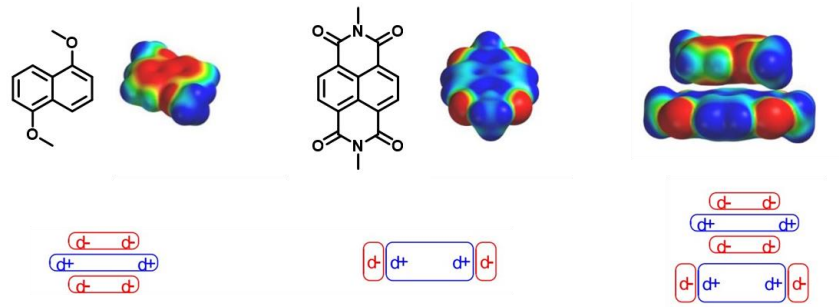

*Figure III–1. Models of the electrostatic potential of an electron–rich (DAN) and electron–deficient (NDI) chromophores and their corresponding D–A complex.*

The association constant of this charge transfer interaction is generally weak or moderate even for the most suitable D–A pairs. In this context, it is important to note that the suitability of D–A pairs depends on several parameters rather than just their structures. Indeed, the binding affinities of these chromophores relies on different factors such as 1) the functionalization of the donor and acceptor compounds, which influences their electrostatic potential maps, 2) the nature of the solvent and 3) the suitable match between the π surfaces of the D–A chromophores. Since aromatic interactions are generally associated to moderate equilibrium constants, additional non–covalent interactions are often employed to build supramolecular structures involving the formation of CT complexes.[10,11]

## B. Supramolecular assemblies stabilized by D–A interactions

Supramolecular assemblies of π–conjugated systems,[12–23] may be constructed from molecules by non–covalent interactions, such as hydrogen bonds, π–π stacking, hydrophobic interactions and others. In this context, aromatic interactions between donor and acceptor units have emerged as a significant tool for developing the field of supramolecular chemistry.[24–31] Thus, various supramolecular systems based on such interactions (Figure III–2) were designed and reported such as gels,[32–45] amphiphilic systems (micelles and vesicles),[46–57] molecular machines (catenanes and rotaxanes),[26–28] supramolecular polymers,[58–66] foldamers,[67–70] and others.[24–27,29–31]

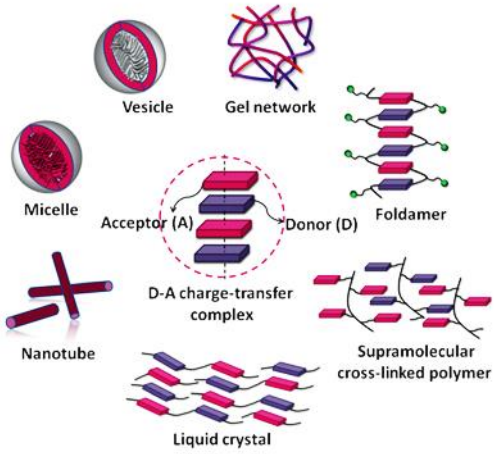


*Figure III–2. Different kinds of D–A supramolecular assemblies.*[6]

## C. Objectives

Since the duplex differs from the single helices in terms of geometry and physico–chemical properties, the obtained heteroduplex will present new physico–chemical characteristics. Interestingly, this aspect remains relatively unexplored in the field of foldamers, though few examples were reported in the fields of molecular machinary,[71] host–guest chemistry[72] or catalysis.[73] Taking advantage from the moderate dimerization constant of oligopyridine dicarboxamide foldamers and charge transfer interactions between donor and acceptor moieties grafted on helical foldamers, we aimed to design and synthesize heteroduplexes in a selective manner with a higher dimerization constant (Figure III–3–*Left*). Furthermore, this will constitute a novel strategy to control the hybridization equilibrium through redox stimulations in a reversible manner (Figure III–3–*Right*).

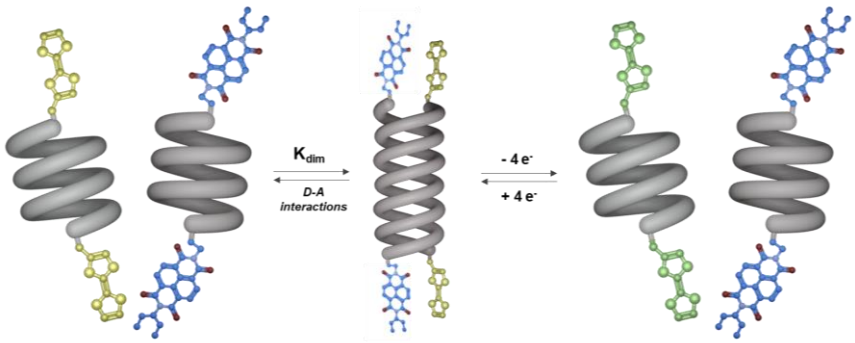


*Figure III–3. Schematic representation of the formation of heteroduplex in the neutral state and the redox–controlled association–dissociation equilibrium presented in the case of TTF– and NDI– based foldamers.*

## D. Design

The design of foldamers able to hybridize into heteroduplexes should take into consideration several important aspects. First, the elaboration of heteroduplexes requires the synthesis of two distinct and complementary strands able to hybridize. In addition, the hybridization process is likely to be promoted because of donor–acceptor interactions. As discussed in the second chapter, the choice of the foldamer skeleton, the electroactive units, as well as the type of the linker between them constitutes a crucial choice for the design of foldamers.

### D.1. Choice of the foldamer skeleton

Oligoarylamides were selected as the skeleton for the foldamer series in this chapter as well. As previously discussed, oligopyridine dicarboxamide oligomers exhibit diverse advantages, including their relatively straightforward synthesis, the stability and predictability of their secondary structures, their propensity to crystallise and most importantly, their ability to reversibly hybridize into double helical structures with a moderate dimerization constant.[74] Over the last years, our team has also developed extensive knowledge and know–how related to their synthesis. Altogether, these points prompted us to pursue this study with this family, at least to make proofs–of–concept. In this context, a foldamer containing seven pyridyl units was selected. As mentioned in the second chapter, the foldamer skeleton should have a moderate length to prevent excessively high dimerization constants, slow kinetics of association–dissociation.

Considering the significant impact of the rigid amide linker on the behavior of foldamer **A** in the second chapter and the large time needed to synthesize a foldamer with the same design, selecting an appropriate linker for this study constituted a challenge to overcome.

Firstly, an efficient overlap between the orbitals of the donor and acceptor chromophores must be possible in the hybridized state. Hence, the selection of a flexible and sufficiently long linker appeared necessary. Secondly, synthesizing strands endowed with different electroactive units have to be designed to target different pairs of D–A foldamers. Therefore, functionalizing the foldamer skeleton with the electroactive units along the last step appears advantageous in terms of convergence and to limit the number of difficult purification steps.

Eventually, the electroactive units will be introduced at the extremities of the foldamer skeleton. This offers advantages in terms of symmetry, which simplifies the process of characterizations and comprehension of these intricate systems. Furthermore, this strategy has been developed by our group, which now developed an expertise regarding the functionalization of foldamers. In this context, linking the foldamer backbone to the electroactive units through copper–catalyzed azide–alkyne cycloaddition (CuAAC)[75–77] appeared relevant (Scheme III–1).

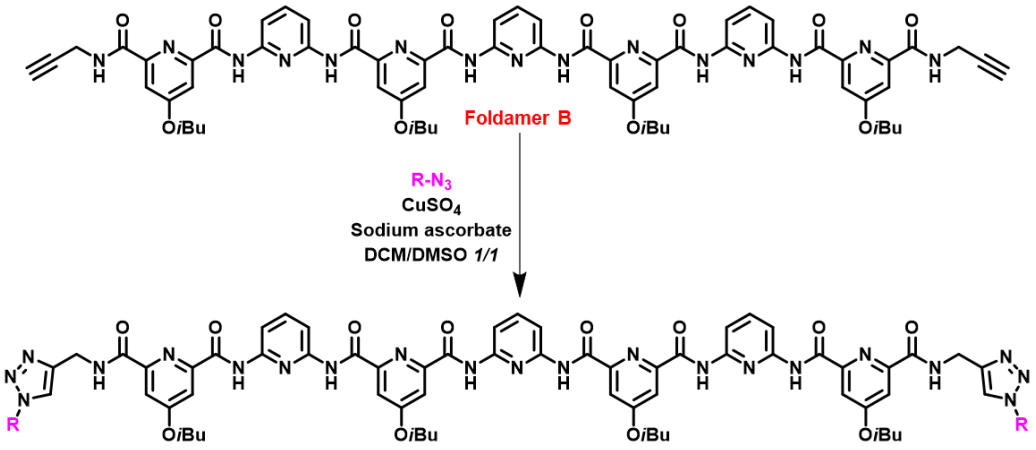


*Scheme III–1. Representative scheme for the functionalized foldamer via click chemistry (R: electroactive unit).*

## D.2. Choice of the electroactive units and pairs

Among the various aromatic compounds depicted in Figure III–4, several pairs were chosen based on different criteria detailed in the next paragraphs.

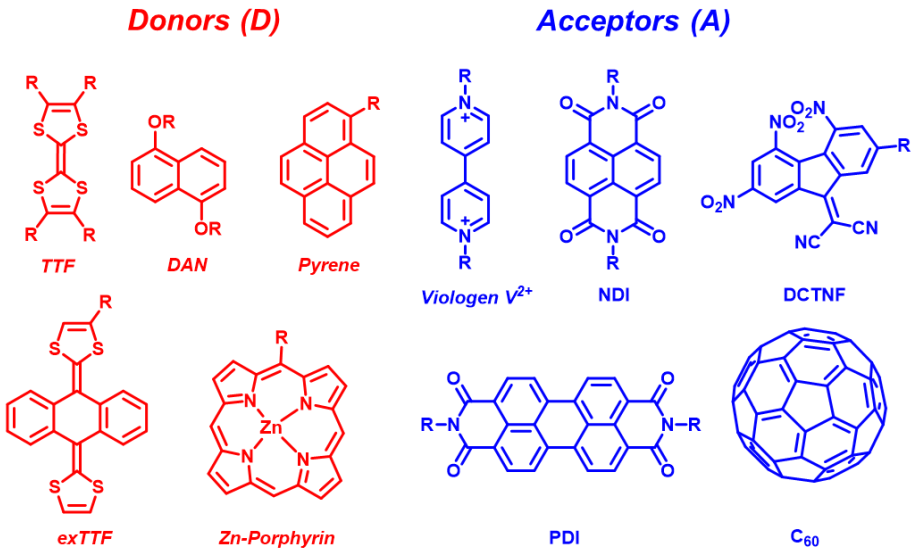


*Figure III–4. Structures of representative donor and acceptor chromophores (TTF: tetrathiafulvalene, DAN: dialkoxynaphthalene, exTTF: extended–tetrathiafulvalene, NDI: naphthalene diimide, DCTNF: trinitrofluorenone derivative, PDI: perylene diimide, $C_{60}$: fullerene).*

In order to start with a well–known system and to allow comparisons with Chapter 2, the first selected electroactive unit was tetrathiafulvalene (TTF). The comparison between two foldamers bearing tetrathiafulvalene units that differ by the nature of the linker (amide for foldamer **A** (see chapter 2) and a triazole–containing one (in chapter 3) will provide additional evidence on the influence of the linker on the behaviors of foldamers in solution. Furthermore, TTF exhibits strong electron donating properties[79–81] and is appealing for the construction of charge transfer complexes.[82,83] On the other hand, the DCTNF acceptor constitutes an electron withdrawing system, which readily forms D–A pairs with TTF.[78–80]

Dialkoxynaphthalene (DAN) and naphthalene diimide (NDI) compounds are well–known for the construction of D–A complexes.[6] This chapter will primarily focus on this pair of chromophores, choice that will be thoroughly explained in paragraph §III.

Eventually, pyrene unit was selected for its singular spectroscopic features and its ability to undergo CT interactions with NDI unit.[6,81]

At this stage, it is nonetheless important to remind that they exhibit planar aromatic neutral cores and present excellent abilities for π–stacking. In most cases, these derivatives can be functionalized in a symmetric or a dissymmetric manner, providing a variety of structures.[82–85] This possibility facilitates a straightforward connection with other species and, affords derivatives that are soluble in a wide range of solvents.[86] Chapter 3 will be organized according to the donor–acceptor pair under consideration.

### D.3. Choice of solvents

Multiple cross–hybridization tests will be tackled in various solvents and at different concentrations. The aim of these tests will consist in finding the best compromise to promote both hybridization and charge transfer complexation between electroactive units to obtain heteroduplexes in a selective manner. This appears quite challenging since the hybridization process of oligopyridine dicarboxamide generally occurs in solvents displaying moderate polarities, such as chlorinated solvents.[87–89] While charge transfer complexes are commonly formed in polar solvents such as $H_2O$, MeOH, and DMSO, in which they exhibit high association constants.[90] Nonetheless, it has already been shown that the hybridization process can take place in more polar solvents, such as DMSO, when an additional driving force can be set up between foldamer strands (*e.g.* aromatic interactions).[91,92] In a reciprocal manner, we also anticipated that charge transfer complexes could be formed in less polar solvents, thanks to the ability of oligopyridine dicarboxamide foldamers to hybridize. Therefore, taking advantage from both phenomena, we envisaged combining two driving forces, hybridization and donor–acceptor interactions to synthesize heteroduplexes in a selective manner.

## II. Pair of TTF– and DCTNF–based foldamers

### A. Synthesis of foldamer dialkyne B

#### A.1. Retrosynthesis

The synthesis of foldamer **B** relies on the retrosynthesis presented in Scheme III–2. In contrast to foldamer **A** (see Chapter 2), foldamer **B** features a diacid central block (**III–2**) instead of a diamine one. Eventually, the extremities of foldamer **B** consist of carboxamide functional groups instead of amine groups (**III–3**). Consequently, foldamer **B** is constituted by seven pyridyl rings in an inverted arrangement in comparison to foldamer **A**.

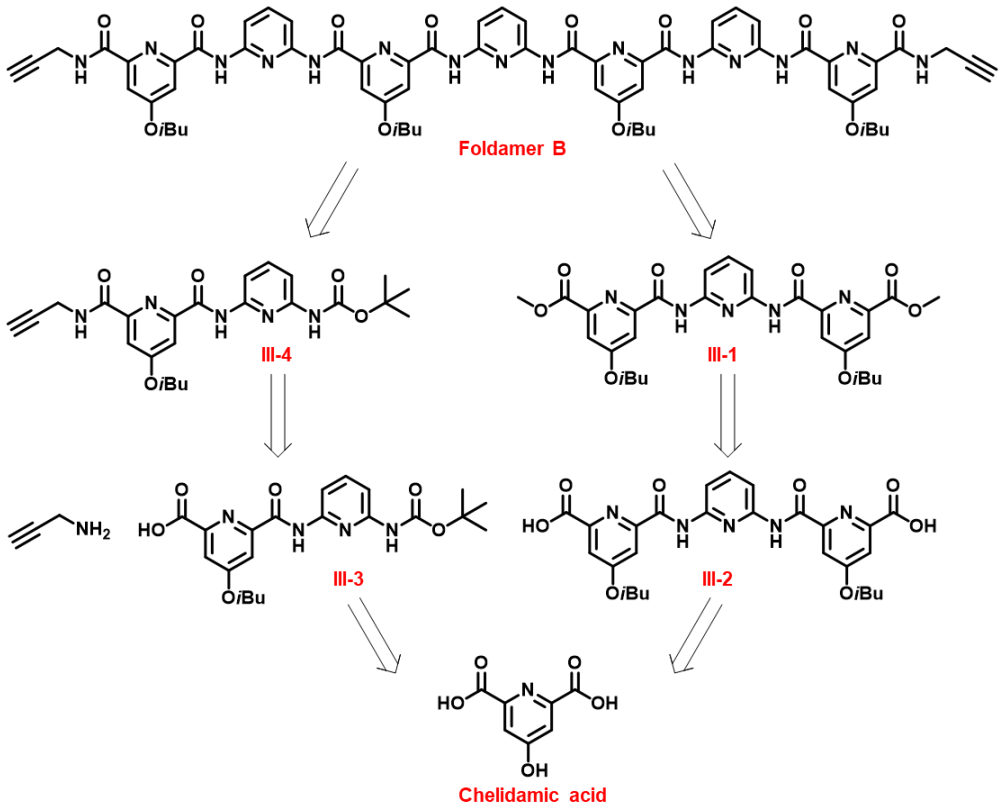


*Scheme III–2. Retrosynthetic scheme of foldamer **B**.*

## A.2. Synthesis of diacid III–2

The synthesis of diacid **III–2** was achieved according to a two–step procedure (Scheme III–3). Carboxylic acid **II–3** was activated into the corresponding acid chloride using oxalyl chloride and a catalytic amount of DMF in distilled dichloromethane under argon atmosphere. An addition–elimination reaction of 2,6–diaminopyridine in the presence of *N*,*N*–diisopropylethylamine subsequently allowed for isolating diester **III–1** in a 75 % yield.[93] Eventually, diacid **III–2** was obtained quantitatively by saponification of diester **III–1** using lithium or sodium hydroxide as a base.

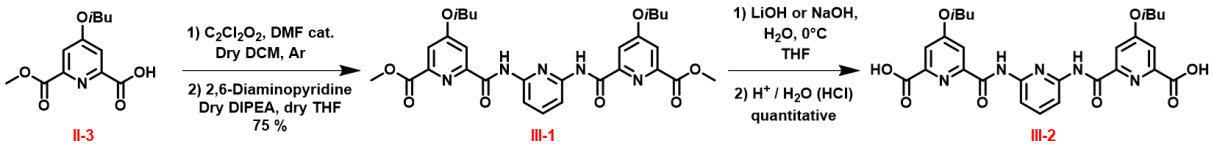


*Scheme III–3. Synthesis of compound **III–2**.*

## A.3. Synthesis of the peripheral block

The synthesis of amine **III–5**, which will eventually be coupled to diacid **III–2**, starts with a quantitative saponification reaction of ester **II–8** using sodium hydroxide to afford the desired carboxylic acid **III–3** after acidification of the medium (Scheme III–4). Then, Ghosez

reagent allowed for preparing the corresponding acid chloride, while avoiding the release of hydrogen chloride along this activation step.[94] In this manner, the dropwise addition of propargylamine and DIPEA led to the isolation of precursor **III–4** with a particularly high yield (94 %). The last step consists in a deprotection reaction of the amine function to afford quantitatively the desired amine **III–5** using trifluoroacetic acid.

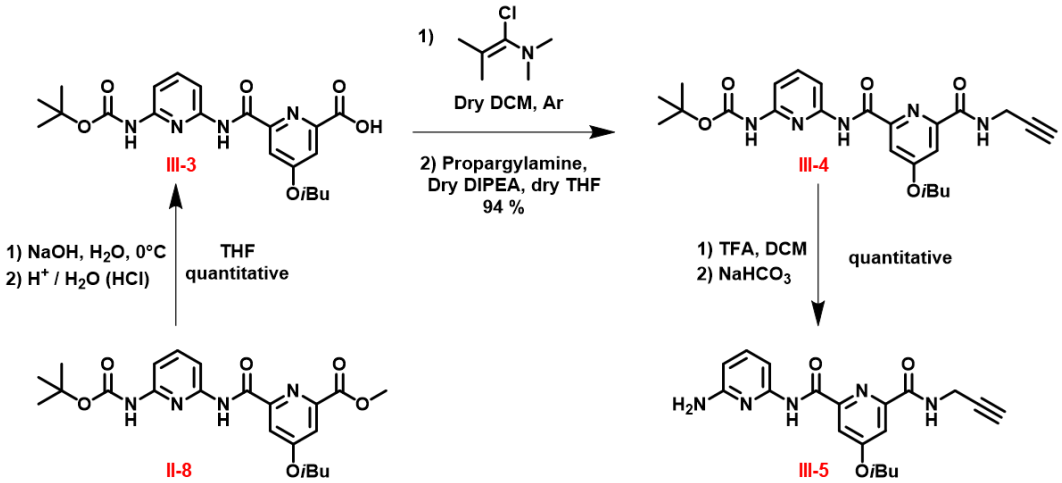


*Scheme III–4. Synthesis of compound **III–5**.*

## A.4. Synthesis of foldamer B

The last step towards the formation of foldamer **B** relies on a peptidic coupling between **III–2** and **III–5**. This allowed for isolating foldamer **B** with a high yield of 84 %, especially considering the poor nucleophilicity of arylamines and the considerable steric hindrance once the first coupling performed (Scheme III–5). Moreover, this sequence could be led on a one gram–scale, which constitutes a clear asset for future developments.

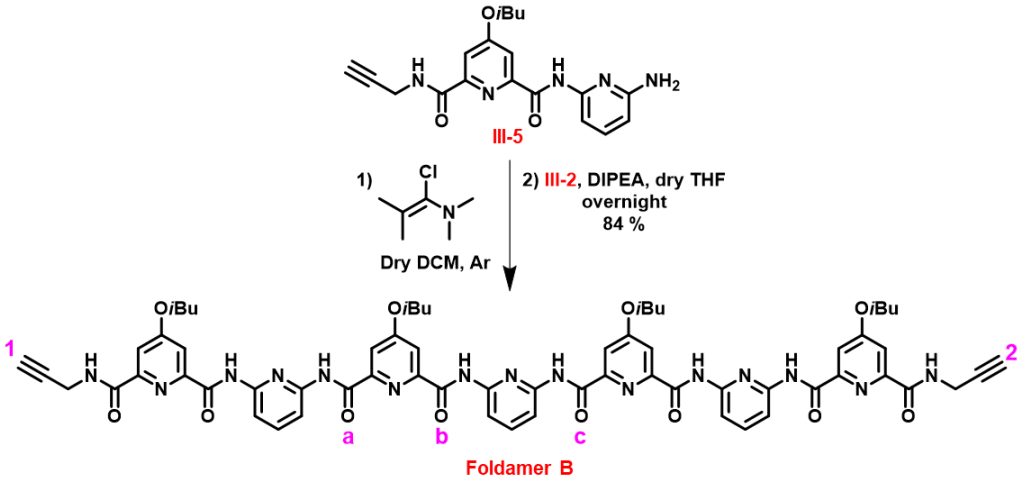


*Scheme III–5. Synthesis of foldamer **B**.*

## A.5. Solid state analysis of foldamer B

Monocrystals of foldamer **B** were obtained through slow evaporation from a solution of DMF. X–ray diffraction analysis showed the crystallization of single helical structures from this polar solvent.[95] The stability of the single helical structure is ensured by a network of hydrogen bonds ranging from 2.21 to 2.37 Å. The polar cavity accommodates a water molecule and a DMF one, which interact with the foldamer skeleton through hydrogen bonds (Figure III–5).

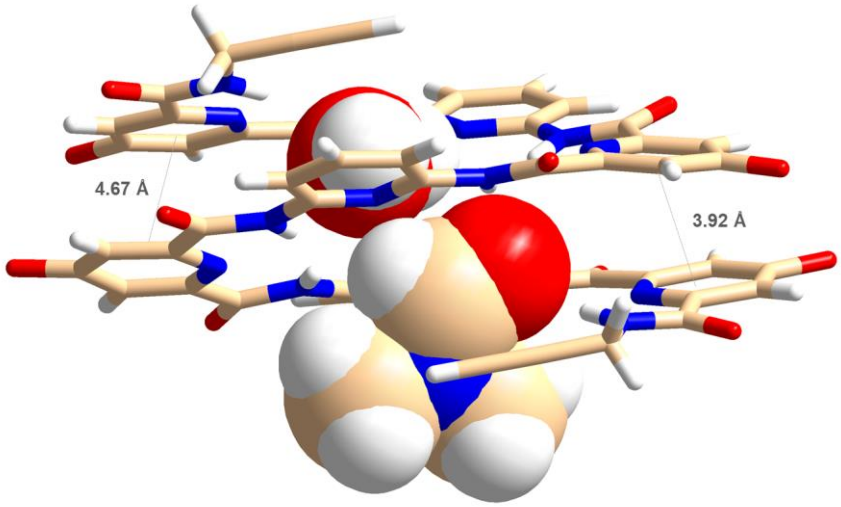


*Figure III–5. X–Ray crystal structure of foldamer **B** (monocrystals obtained from DMF) as a single helix. The cavity contains one water and one DMF molecules (isobutyl chains omitted for clarity).*

With this family of foldamers, the helical pitch can be defined as the distance between the first and the fifth pyridyl rings. In the case of foldamer **B**, the helical pitch was not constant along the strand, depending on the pyridyl ring that was considered as first: distances of 4.67 Å from one extremity and 3.92 Å from the other extremity were indeed measured. Apart from the interaction with DMF and water molecules, this difference could arise from intermolecular interactions between foldamer strands. The hydrogen atoms of the alkyne groups are involved in intra– and intermolecular interactions (Figure III–6): 1) hydrogen atom H (1) interacts with the oxygen atom O (b) of the amide function of the adjacent helices through hydrogen bonds with a value of 2.45 Å (blue dotted lines); 2) the hydrogen atom H (2) participates to intermolecular hydrogen bonds with O (a) (2.53 Å - orange dotted lines) and intramolecular CH–π interactions with the fourth pyridyl rings with a value of 3.55 Å (violet dotted lines).

Eventually, one will note that this X–ray crystallographic structure affords interesting data concerning the orientation of the acetylenic moieties. Herein, –C≡C–H terminal groups

constitute a part of the helix, in contrast to their orientation in an analogous structure containing five pyridyl rings, where these groups were perpendicular to the helix.[96]

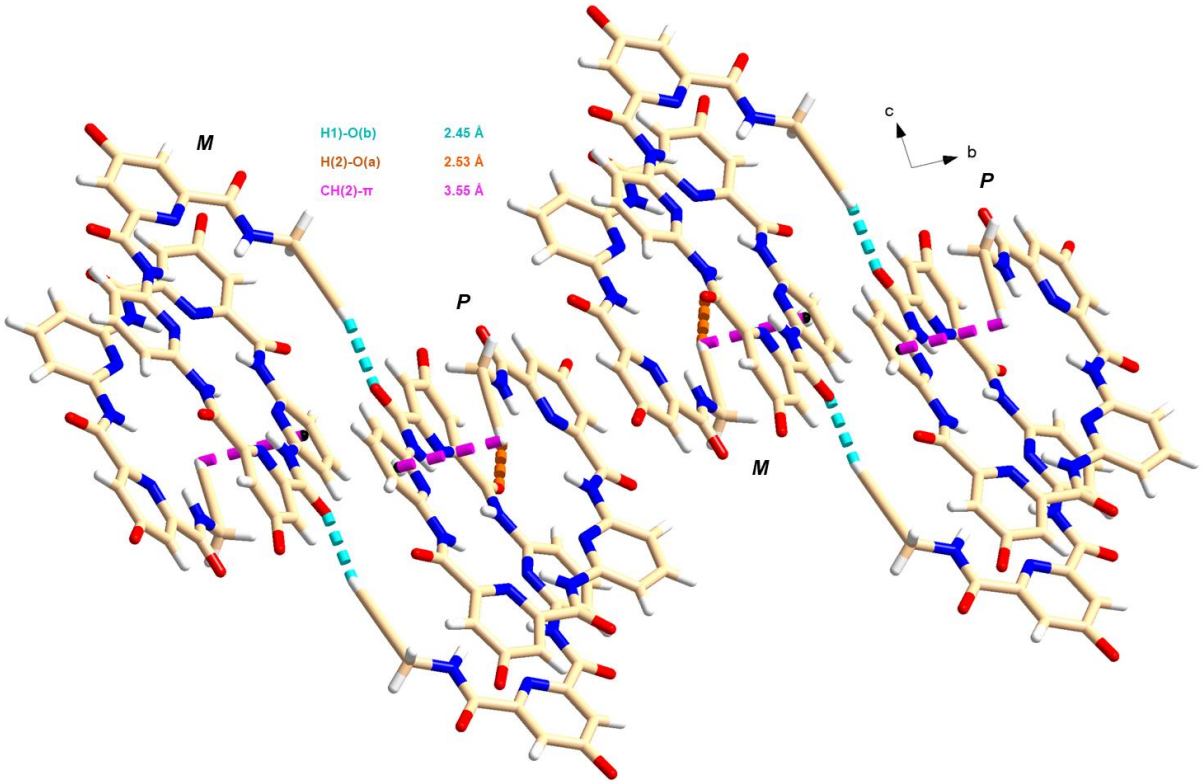


*Figure III–6. Packing of foldamer **B** in the lattice: hydrogen bonds 2.45 Å (blue dotted lines), 2.53 Å (orange dotted lines), and CH–π 3.55 Å (violet dotted lines), top: view following the c axis, down: view following the a axis. Isobutyl chains were omitted for the sake of clarity.*

## B. Synthesis of TTF– and DCTNF–based azides and the corresponding foldamers

### B.1. Synthesis of azides III–8 and III–11

The preparation of azide **III–8** was conducted through three steps (Scheme III–6). The first one consists in the formylation of TTF, which is followed by a reduction of formyltetrathiafulvalene **III–6** according to a protocol described in the literature.[97] The desired azide **III–8**[98] was obtained by treating **III–7** with diphenylphosphoryl azide, 1,8–diazabicyclo[5.4.0]undec–7–ene (DBU) and sodium azide in anhydrous DMF (90 %).

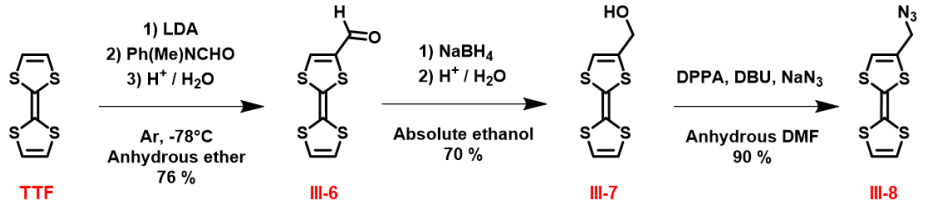


*Scheme III–6. Synthesis of azide **III–8**.*

On the other hand, the synthesis of **III–11** was conducted using a different protocol. First, a nitration reaction was led on the commercially available 9–fluorenone–2–carboxylic acid in a mixture of sulfuric acid and nitric acid, according to a protocol described in the literature.[99] The carboxylic acid function was activated as acid chloride using oxalyl chloride and a catalytic amount of DMF in distilled DCM. After addition–elimination of 2–azidoethan–1–amine in the presence of DIPEA in THF, **III–10** was isolated with a 54 % yield. The last step consisted in grafting the malonitrile group through Knoevenagel reaction[80] to give **III–11** (Scheme III–7), which was only detected by mass spectrometry because of its very low solubility and air sensitivity. Therefore, we decided to perform the CuAAC reaction using **III–10** before condensing malonitrile on the trinitrofluorenone units.

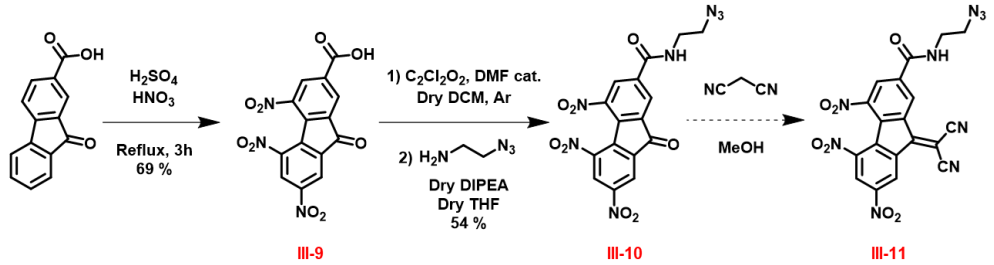


*Scheme III–7. Synthesis of azide **III**–11.*

## B.2. Copper–catalyzed azide–alkyne cycloaddition (CuAAC)

The synthesis of foldamers **C** and **D** was finally achieved by coupling the corresponding azides **III–8** and **III–10** (4 equivalents), respectively with foldamer **B** through copper–catalyzed azide–alkyne cycloaddition. These reactions were conducted in the presence of copper sulfate and sodium ascorbate in a mixture of DCM/DMSO (*1/1*) to ensure the solubility of the reactants Scheme III–8). This represents a valuable strategy for synthesizing a foldamer endowed with tetrathiafulvalene units, with a significantly higher yield of 85 %, in stark contrast to the amide linking (37 %).

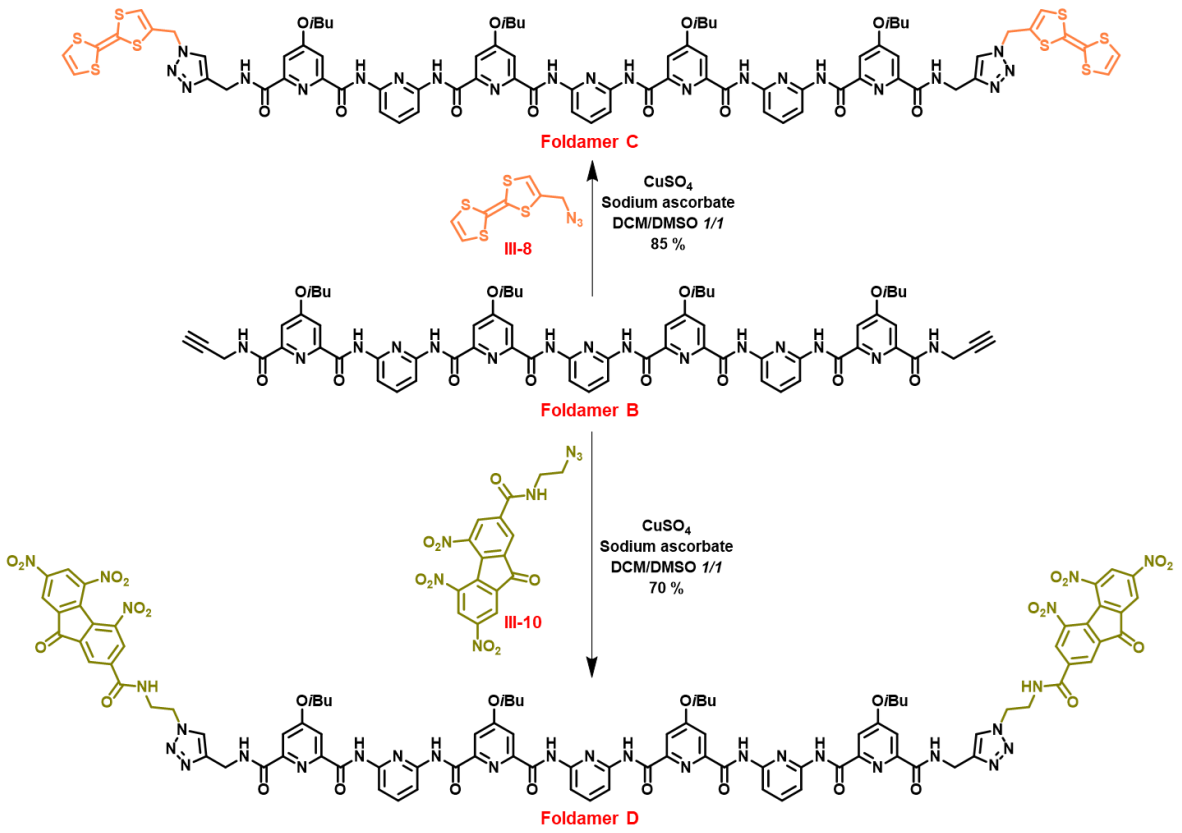


*Scheme III–8. Synthesis of target foldamer **C** and **D**.*

## B.3. Analysis in solution

To compare foldamers **C** and **A** (see chapter 2) using the same conditions, chloroform appeared as a solvent of choice for analytical purposes. The corresponding measurements evidenced the high solubility of foldamer **C** in chloroform, which is commonly used for studying the hybridization process of oligopyridine dicarboxamide foldamers.[87] These experiments revealed the presence of two sets of signals for amide protons, which shows that two species are in slow equilibrium at the NMR timescale (Figure III–7). This observation correlates well with previously reported analogous foldamers containing seven pyridyl rings.[88,89] The signals of both single and double helices can be readily identified. At lower concentrations, the signals corresponding to the amide protons of the single helical structure remain (10.77, 10.53, 10.36 and 8.97 ppm, with each signal integrating for two protons), which is consistent with the central symmetry of the single helix. On the contrary, when considering higher concentrations, a new set of four signals appeared at lower chemical shifts (9.74, 9.65, 9.42 and 8.71 ppm). These correspond to the formation of the double helical structure in solution in the neutral state. *The estimation of the dimerization constant $K_{dim}$ for this series of foldamer was not performed; this will be explained in the subsequent paragraphs.*

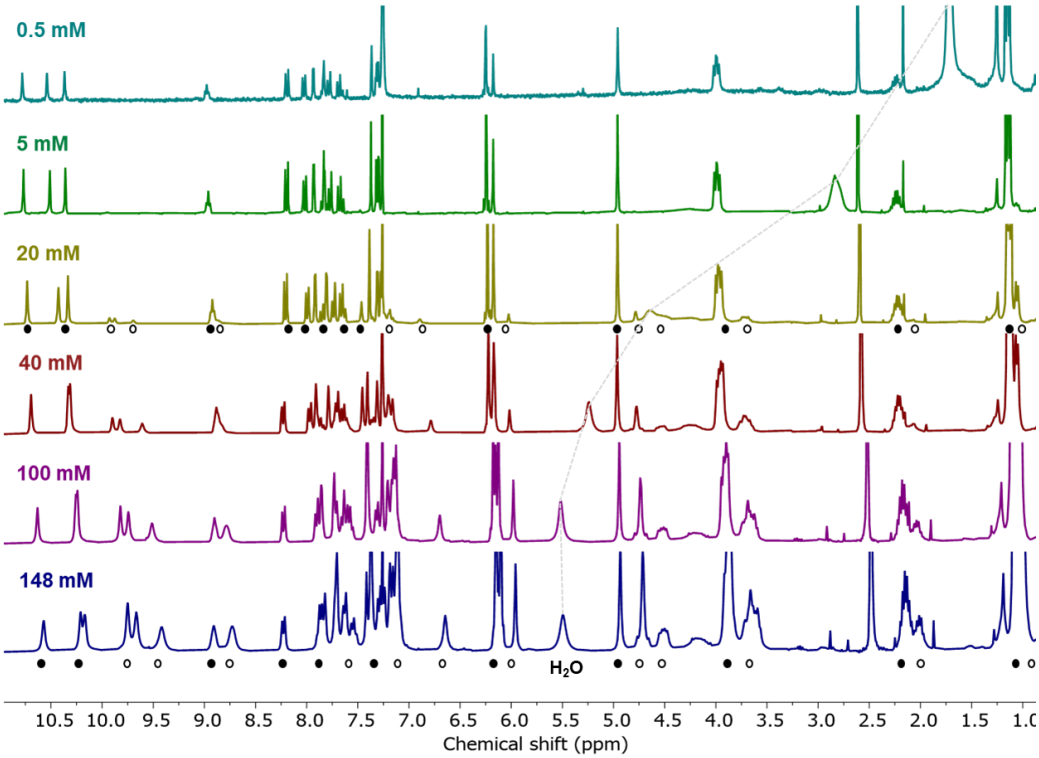


*Figure III–7. Evolution of the $^{1}H$ NMR spectrum of a solution of foldamer **C** upon dilution: single helix (filled circles) and double helix (empty circles) ($CDCl_3$, 298 K, 300 MHz).*

The hybridization process of foldamer **C**, functionalized with TTF units through triazole linkers, occurred in the neutral state, in contrast to foldamer **A** (see chapter 2) where an amide function was used as linker. This relevant result confirmed our hypothesis and analysis conducted on foldamer **A**. The short amide linker promotes intramolecular interactions between TTF units and the foldamer skeleton of **A**, which results in an increased stability of the single helical state. Considering that, comparing the crystallographic structures of **A** and **C** would be particularly valuable. Important efforts have been dedicated to crystallization tests with foldamer **C**. These were performed through slow evaporations, liquid–liquid diffusion, or liquid–gas diffusions. However, these attempts remained vain.

The high sensitivity of foldamer **D** to oxygen due to the presence of TNF units leads to its rapid degradation (around two weeks), which demands careful handling and storage under controlled conditions. Unfortunately, this aspect poses a significant challenge for studying its behavior in solution and performing further characterizations. In addition, the TTF–based foldamer proved to be unstable above 40°C. This rapidly prompted us to select new donor and acceptor functional units, which are benchmark derivatives in that context: dialkoxynaphthalene and naphthalene diimide units, respectively.[6,24]

# III. Pairs of DAN– and NDI–based foldamers: overcoming challenges and outcomes

## A. Functional foldamers incorporating DAN and the first NDI moieties

### A.1. Synthesis

#### A.1.a. Synthesis of azides III–13 and III–17

The functionalization of the commercially available naphthalene tetracarboxylic dianhydride (NDA) in a dissymmetric manner was performed according to two steps and through simple amine condensation (Scheme III–9). Firstly, imide **III–12** was obtained by reacting NDA with propan–1–amine in the presence of DIPEA,[100] and then, the desired azide (**III–13**) was isolated after condensation of 2–azidoethan–1–amine in the presence of DIPEA.

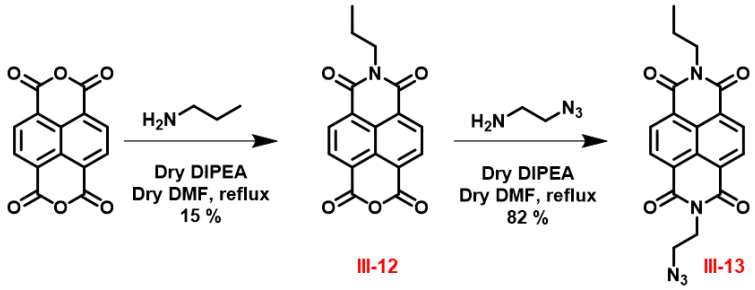


*Scheme III–9. Synthesis of azide **III–13**.*

The synthesis of azide **III–17** was successfully achieved through four steps according to the protocol reported for the TTF–based azide **III–8** (Scheme III–10). The dissymmetrical functionalization of the 1,5–dihydroxynaphthalene was conducted through two successive nucleophilic substitutions using potassium carbonate as a base, and iodomethane and 2–bromoethan–1–ol as electrophilic reagents, to afford compound **III–15**. Subsequently, the latter was treated with diphenyl phosphoryl azide and 1,8–diazabicyclo[5.4.0]undec–7–ene (DBU) to give intermediate **III–16** with a 79 % yield. It should be noted that, in contrast to hydroxylmethylTTF **III –7**, synthesizing azide **III–17** with a high–yield required the isolation of phosphoryl ester **III–16**. The desired azide was finally obtained after a nucleophilic substitution involving sodium azide and intermediate **III–16** in DMF/water (9/1) affording **III–17** with a global yield of 16 %.

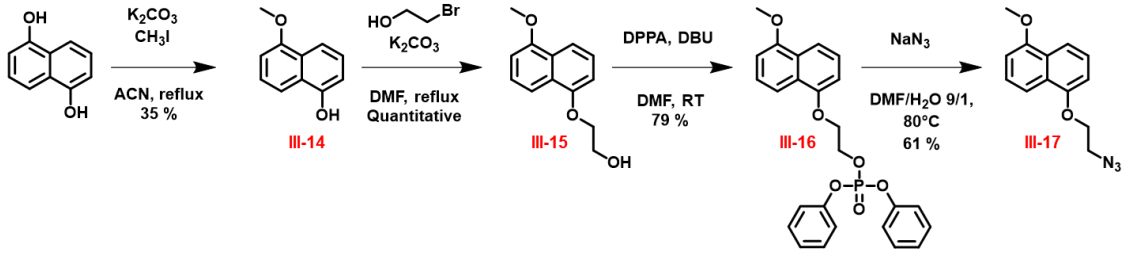


*Scheme III–10. Synthesis of compound **III–17**.*

### A.1.b. Synthesis of foldamers

Foldamers **E** and **F** were obtained as previously described (see paragraph §II.B.2) by reacting **B** and azides **III–13** and **III–17** with a 65 % yield for both (Scheme III–11). Noteworth is the fact that azide **III–17** was less reactive, which prompted us to perform the synthesis of foldamer **F** upon heating at 40°C.

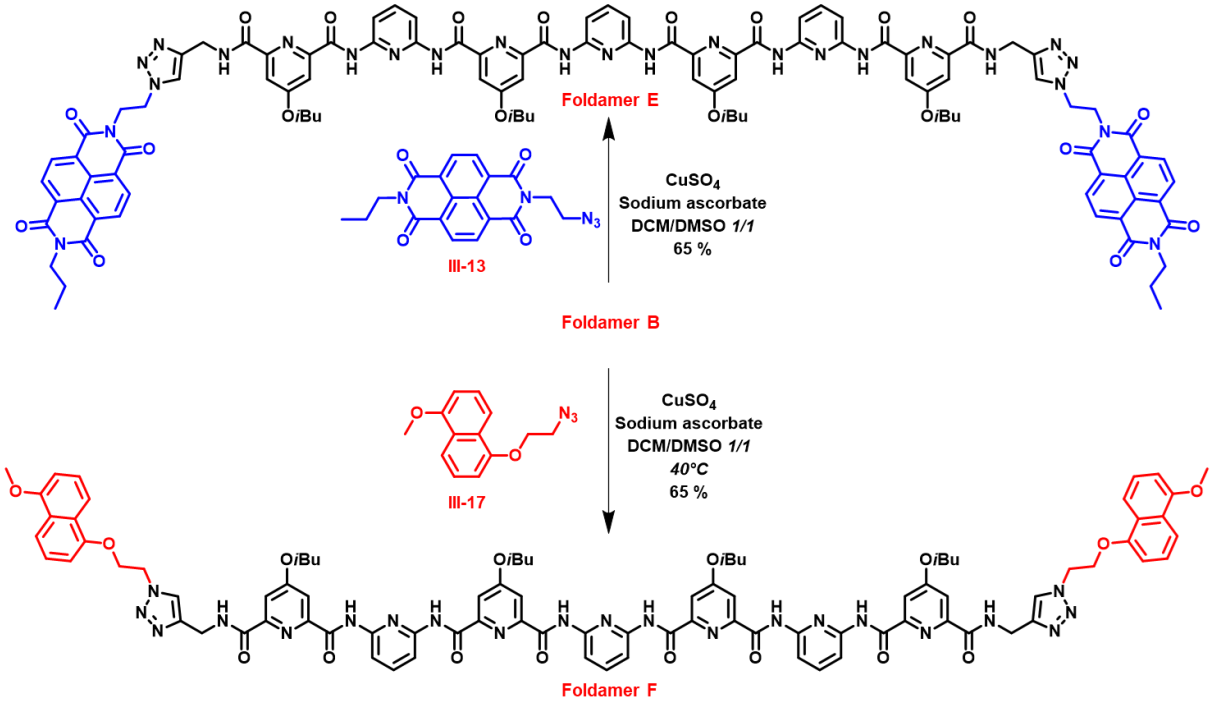


*Scheme III–11. Synthesis of foldamers **E** and **F**.*

## A.2. Solid state analysis

### A.2.a. Analysis of foldamer E in the solid state

Monocrystals of foldamer **E** were obtained by slow evaporation from a solution of DMF in a triclinic P–1 space group. The crystallographic structure revealed the crystallization of foldamer **E** in its single helical form and both *M* and *P* helices co–crystallize together. The polar cavity accommodates two water molecules interacting together and with the foldamer skeleton through hydrogen bonds. Intramolecular hydrogen bond was observed between the H atom of

one triazole unit and the oxygen atom of a neighbouring amide function with a value of 2.57 Å (violet dotted lines, Figure III–8–a). Intramolecular aromatic interactions occurred between pyridyl units and defined a helical pitch of 3.56 Å. Single helices stack together, leading to intermolecular π–π stacking with a value of 3.65 Å (green dotted lines) between NDI and foldamer skeleton within the adjacent blue and red helices and hence, on both sides. However, the triazole rings adopt two different orientations: 1) on one side, they are part of the helix, favoring a π–π stacking between NDI unit and the third pyridyl ring (3.71 Å, orange dotted lines); and 2) on the other side, they are orientated perpendicularly, and in this case, a DMF molecule is present between the foldamer skeleton and the NDI unit within the same helix (Figure III–8–b).

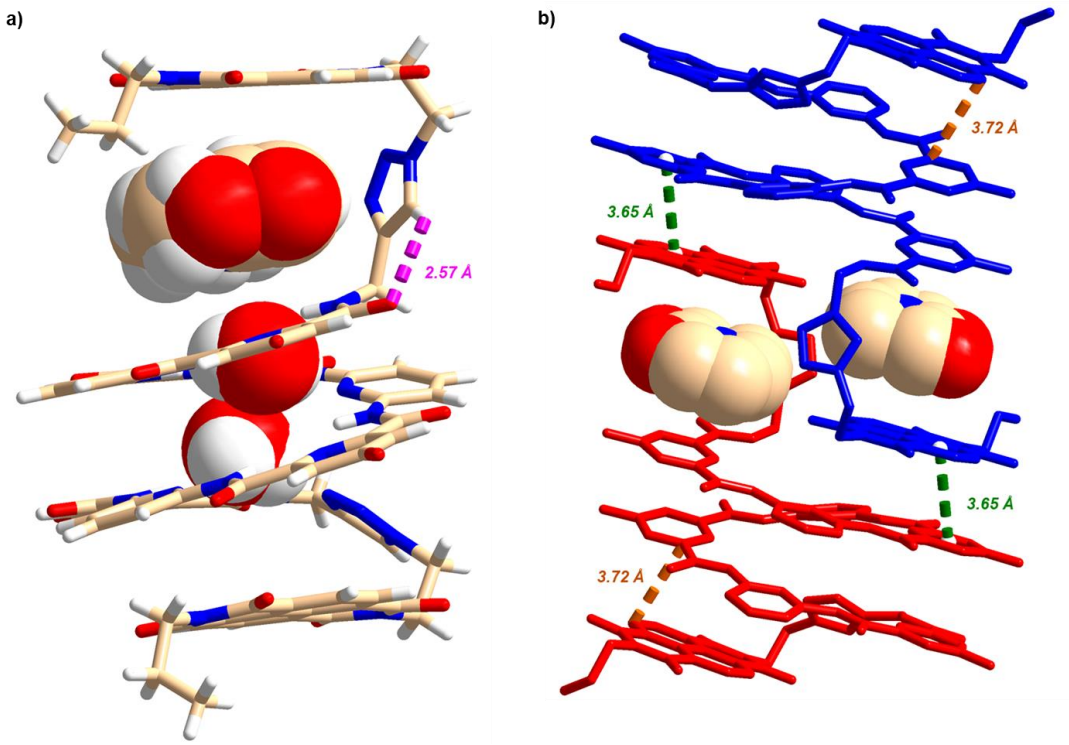


*Figure III–8. a) X–ray structure of foldamer **E** obtained from slow evaporation from DMF as single helix. The cavity contains two water molecules, b) Packing of foldamer **E** in the lattice: π–π stacking between NDIs and pyridine of adjacent helices 3.65 Å (green dotted lines). Isobutyl chains were omitted for the sake of clarity.*

### A.2.b. Solid state analysis of foldamer F

Monocrystals of foldamer **F** were obtained by slow evaporation from a solution of DMSO in a monoclinic P 1 21/c space group. X–Ray diffraction analyses revealed the crystallization of the single helical form. The polar cavity of the foldamer accommodates two DMSO molecules, where the oxygen atoms of these molecules interact with the hydrogen atom of the both peripheral amide functions through hydrogen bonds with a value ranging from 2.14 to 2.36 Å, and a helical pitch of 3.67 Å (Figure III–9–*Left*). An intermolecular hydrogen bond

was also detected between the hydrogen atom (C–H) of triazole and the oxygen atom (C=O) of the adjacent amide function with a value of 2.52 Å (violet dotted lines). Unlike foldamer **E**, both triazoles are perpendicular to the helix axis. Furthermore, CH–π interactions were observed within the lattice occurring between the helices. The first CH–π interaction is strong and it was identified between H (b) and the core of DAN (1) with a value of 3.02 Å (blue dotted lines). Additionally, a second CH–π interaction was detected between H (a) of the *M* helices and the core of the DAN (2) unit of the adjacent *P* helices with a value of 3.72 Å (violet dotted lines) and vice versa (Figure III–9–*Right*). These CH–π interactions highlighted a herringbone organisation between DAN and pyridyl rings. One should also notice that no 'DAN–DAN' or 'DAN–foldamer skeleton' aromatic interaction could be evidenced in this crystallographic structure.

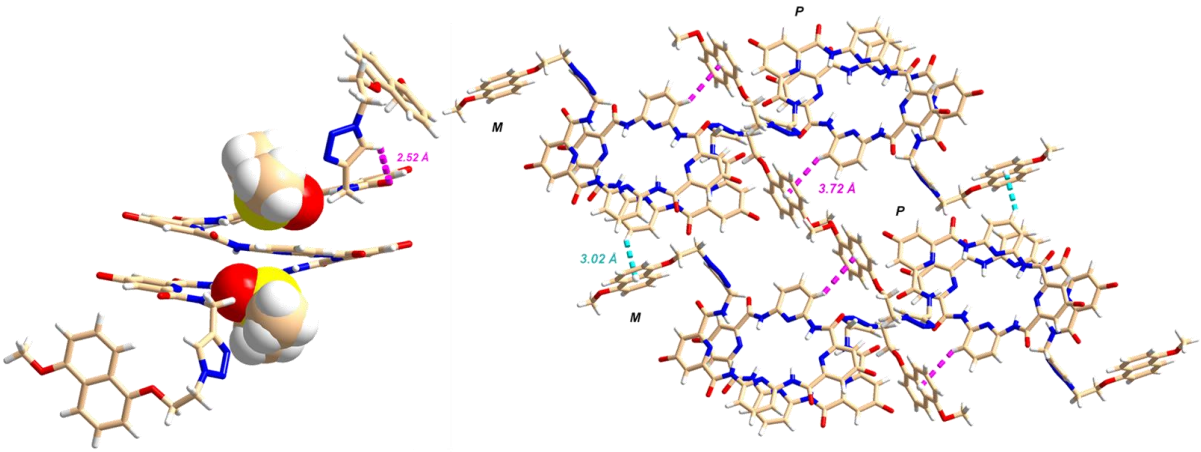


*Figure III–9. Left. X–ray crystal structure of foldamer **F** obtained by slow evaporation from DMSO as single helix. The cavity contains two DMSO molecules. Right. Packing of foldamer **F** in the lattice: CH–π interactions 3.02 Å (blue dotted lines), and 3.72 Å (violet dotted lines). Isobutyl chains were omitted for the sake of clarity.*

## A.3. Cross–hybridization between foldamers E and F

Foldamers **E** and **F** were mixed together in different solvents as well at different concentrations. The most pronounced color change were observed in chloroform and toluene. When foldamers **E** and **F** were dispersed in toluene at room temperature (10 mM, weighing solids together and then, adding the solvent), a pink precipitate was formed. Upon heating the obtained suspensions, particles disappeared and the medium became a yellow solution. Allowing the solution to return to room temperature resulted once again in the precipitation of a pink solid (Figure III–10).

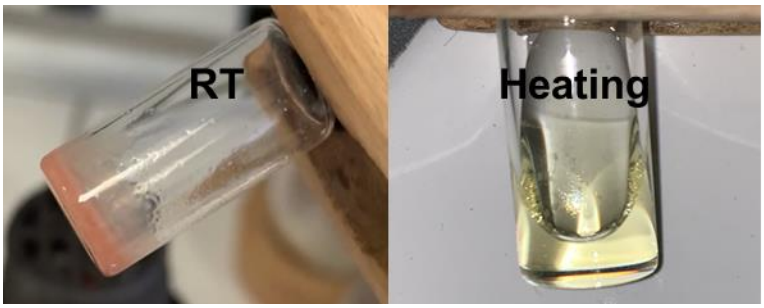


*Figure III–10. Left. Precipitate formed upon mixing foldamers **E** and **F** at room temperature. Right. Yellow solution obtained upon heating the pink precipitate.*

To get insight on this phenomenon, the different steps were followed by $^{1}$H NMR spectroscopy. A suspension containing equimolar amounts of foldamers **E** (n = 8.3 mmol) and **F** (n = 8.3 mmol) was prepared in deuterated toluene (V = 0.3 mL) and then, different suspensions were prepared at lower 'concentrations' by dilution. At 25°C, the resolution was poor at high concentrations and good, at low ones. However, a careful look at the NMR spectrum recorded for a theoretical concentration C = [**E**] = [**F**] = 1.7 mM shows that NDI signals are significantly smaller than those of DAN. This indicates a clear lack of solubility for the corresponding foldamer, which prompted us to study the samples at higher temperatures. Therefore, solutions were heated to 60°C, which was accompanied by an improvement of the resolution. While the signals of foldamer **E** appeared at high temperatures, these proved to disappear once again upon increasing the concentration (Figure III–11). On the contrary, the DAN–containing foldamer **F** remained soluble and hence, performing reliable cross–hybridization experiments in these conditions appeared difficult.

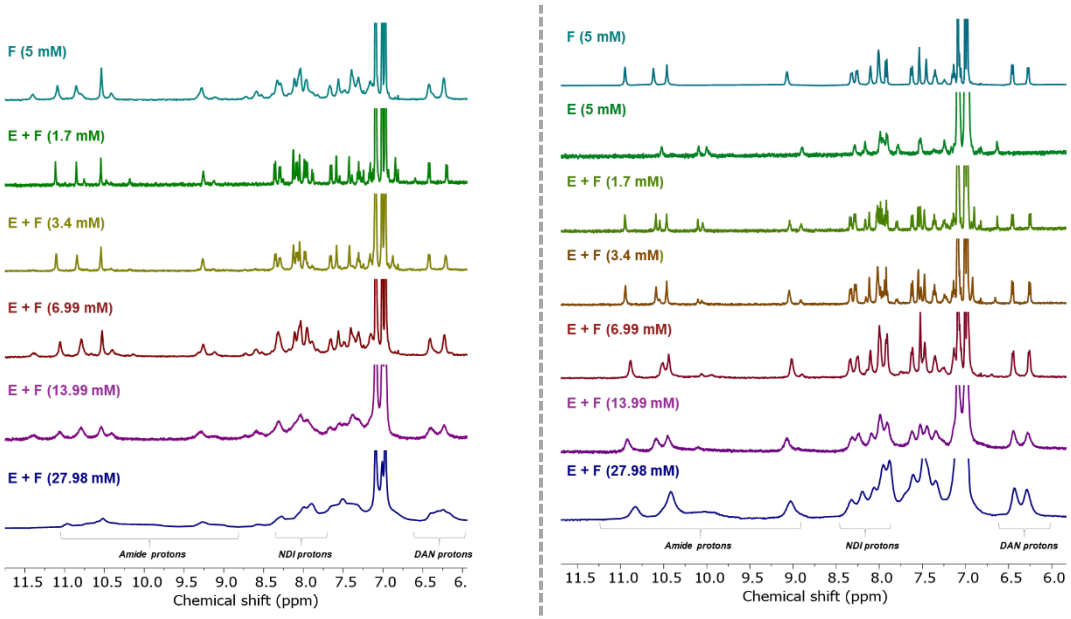


*Figure III–11. Evolution of the $^{1}$H NMR spectra of foldamers **E** and **F** and their mixture at 25°C (left) and 60°C (right) (Toluene–$d_8$, 500 MHz).*

## B. Functional foldamers incorporating DAN and the second NDI moieties

Considering the encouraging results obtained with foldamer **E** (color change) and yet, the manifest lack of solubility when mixing donor and acceptor strands, we envisaged to synthesize foldamer **G**, which is endowed with branched alkyl chains. This appeared especially relevant, since foldamers **B**, **C**, **D** and **F** display high solubilities. Therefore, reconsidering our design to limit NDI–NDI contacts appeared logical. On the other hand, given the complexity of these architectures, we decided to synthesize 1) references **III–20** and **III–21** (Scheme III–12), which mimic the extremities of **F** and **G** and can solely form a supramolecular polymer through a single aromatic interactions, and 2) references **III–23** and **III–24**, which include two electroactive units (like **F** and **G**) but cannot hybridize to form double helices.

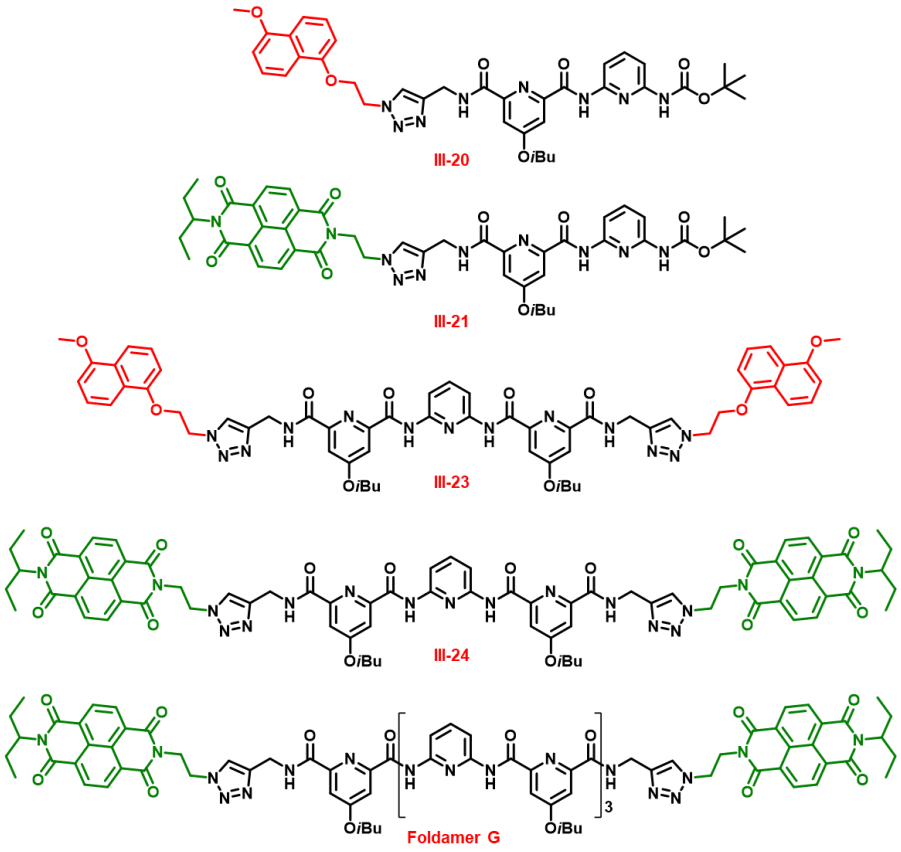


*Scheme III–12. Chemical structures of reference compounds **III–20**, **III–21**, **III–23**, **III–24** and foldamer **G**.*

## B.1. Towards heteroduplex formation

### B.1.a. Synthesis

#### B.1.a.i. Synthesis of azide III–19

Azide **III–19** was synthesized by employing a similar protocol as for **III–13** and by replacing the linear alkyl chain by the branched pentan–3–amine (Scheme III–13).

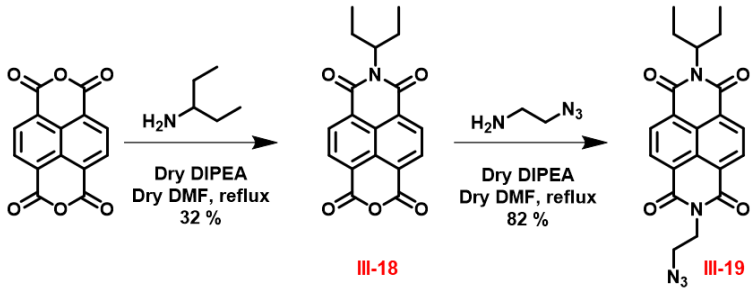


*Scheme III–13. Synthesis of compound **III–19**.*

#### B.1.a.ii. Synthesis of reference compounds

The reference compounds were synthesized according to the protocols developed for foldamers. **III–20** and **III–21** were obtained by coupling azide **III–17** and **III–19**, respectively with intermediate **III–4** through *click* reaction, with a good yield of 84 and 96 % (Scheme III–14).

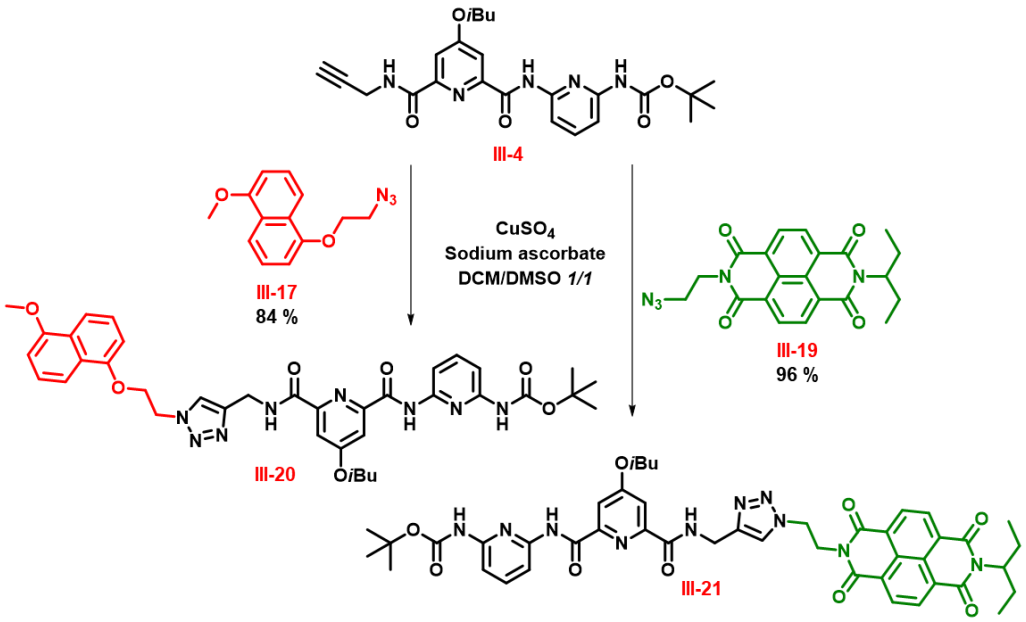


*Scheme III–14. Synthesis of reference compounds **III–20** and **III–21**.*

The synthesis of compounds **III–23** and **III–24** required the preparation of a new intermediate, **III–22**. The latter was synthesized by activating carboxylic acid **III–2** into acid

chloride by Ghosez reagent followed by the addition of propargylamine using the same protocol (Scheme III–15). The crude was purified by silica gel chromatography (eluent DCM/EP 80/20), resulting in a yield of 87 % for **III–22**. Then, a copper–catalyzed cycloaddition was performed on bis–alkyne **III–22** in the presence of azides **III–17** and **III–19,** to give **III–23** and **III–24** with 78 and 90 % yields, respectively.

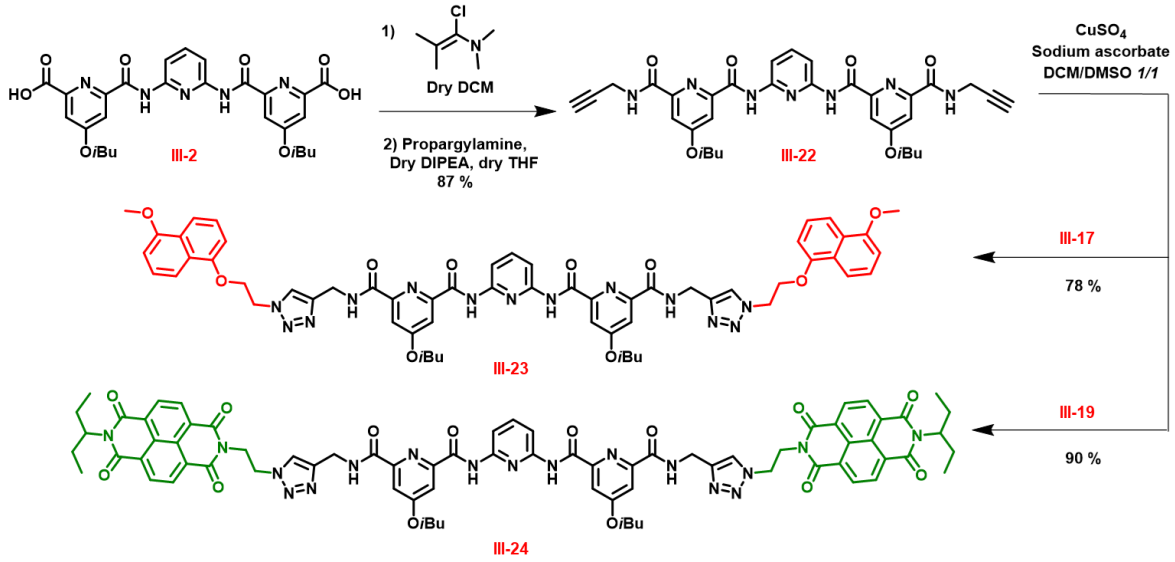


*Scheme III–15. Synthesis of reference compounds **III–23** and **III–24**.*

### B.1.a.iii. Synthesis of foldamer G

Eventually, foldamer **G** could be synthesized following the standard CuAAC protocol and isolated with a high yield (85 % – Scheme III–16).

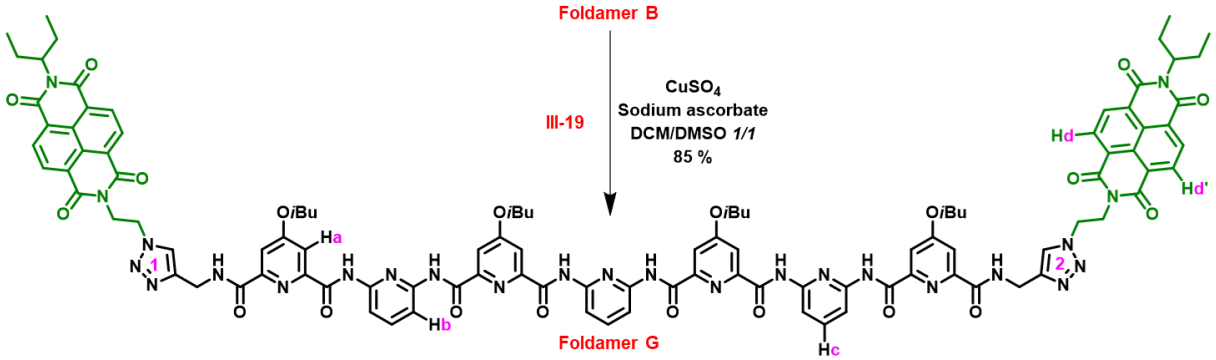


*Scheme III–16. Synthesis of foldamer **G**.*

Foldamer **G** displays excellent solubilities in chlorinated solvents, allowing for reaching concentrations up to 100 mmol.L$^{-1}$, which confirms the relevance of our strategy. Therefore, all the following cross–hybridization analyses were led with foldamer **G** as the acceptor strand.

### B.1.b. Solid state characterization

#### B.1.b.i. Solid state of reference compound

Multiple attempts of crystallization were carried out in order to crystallize the reference compounds individually and the corresponding D–A mixture. Only monocrystals of **III–21** were obtained from a solution containing a mixture of **III–20** and **III–21**. This molecule crystallized in the triclinic P–1 space group by slow evaporation from 1,1,2,2–tetrachloroethane. X–ray diffraction analysis showed the crystallization of this molecule in a sandwich form, where π–π interactions were detected between the NDI core and the peripheral pyridyl ring with a value of 3.55 Å (blue dotted lines – Figure III–12). These observations highlighted the flexibility of the –$CH_2$–triazole–$CH_2$–NH– linker in comparison to the amide connector. Indeed, TTF **II–11** in the second chapter with the amide linker crystallized in a planar form. The amide linker was rigid and short enough to prevent any contact between the TTF unit and the pyridyl rings. On the contrary, the triazole–containing spacer appears more flexible, which permits the establishment of contacts 3.55 Å. Regarding the packing in the lattice, π–π stacking of 3.54 Å was also found between the adjacent molecules according to the b axis between the NDI core and the pyridyl unit (violet dotted lines).

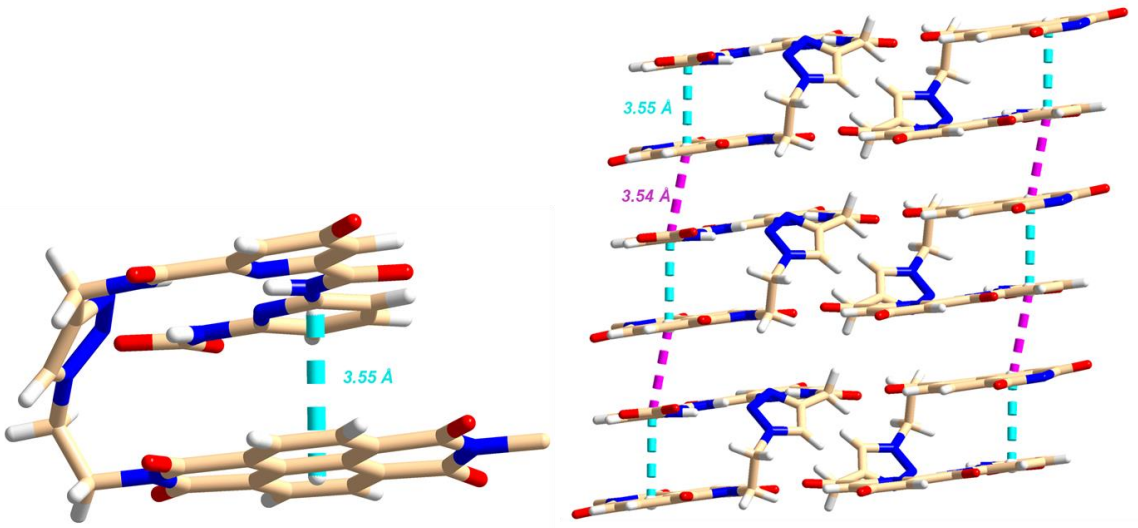


*Figure III–12. Crystallographic structure of reference compound **III–21**. π–π Stacking 3.55 Å (blue dotted lines) and 3.54 Å (violet dotted lines). Isobutyl chains were omitted for the sake of clarity.*

#### B.1.b.ii. Solid state of foldamer G

Monocrystals of foldamer **G** were obtained by slow diffusion of methanol into a solution of **G** in 1,1,2,2–tetrachloroethane. The crystallographic structure (P–1 space group) revealed the crystallization of foldamer **G** in its single helical form. Aromatic interactions were detected

between pyridyl units and defined a helical pitch of 3.67 Å (Figure III–13). Intramolecular hydrogen bond was observed between the hydrogen C–H atom of one triazole unit and the oxygen atom of a neighbouring amide function with a value of 2.87 Å (violet dotted lines). Like analogous foldamer **E**, the orientation of the triazole groups differs, leading in different orientation of NDI units that are more or less distant from the foldamer skeleton. One NDI unit is planar and parallel to the second pyridyl ring, where intramolecular π–π interaction was detected between both moieties (3.77 Å, blue dotted lines). This one is engaged in strong intermolecular π–π interaction within adjacent helix (3.45 Å, orange dotted lines – Figure III–14). On the other hand, CH–π interaction was detected between H (d) of the second NDI and the core of its adjacent pyridyl unit with a value of 3.37 Å (green dotted line).

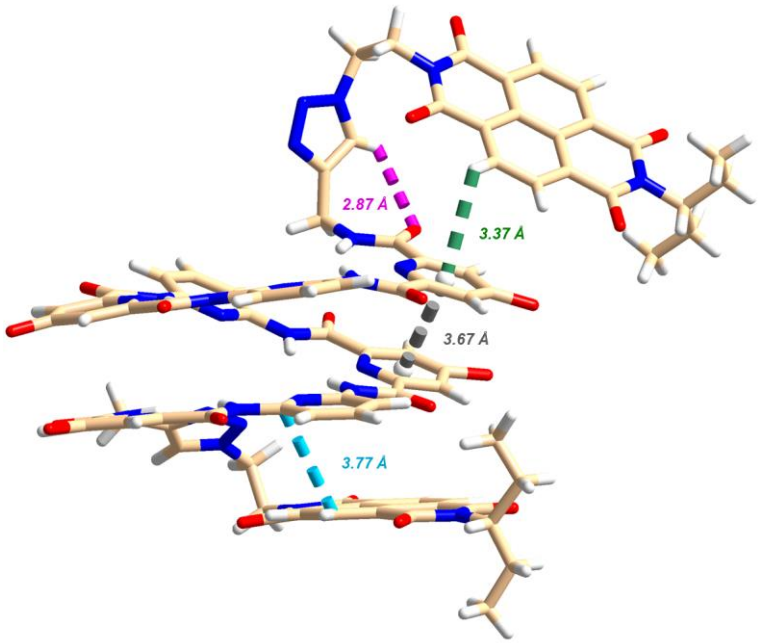


*Figure III–13. X–Ray crystal structure of foldamer **G** obtained from a monocrystal grown by slow diffusion of methanol into a solution of 1,1,2,2–tetrachloromethane, as single helix. CH–π stacking 3.37 Å (green dotted lines) and π–π stacking 3.67 Å (gray dotted lines). Isobutyl chains were omitted for the sake of clarity.*

The latter NDI was involved into aromatic interactions with the adjacent NDI core of the neighbouring helix, maintaining a distance of 3.83 Å (Figure III–14). This interaction displays a slipped face–centered (off–set) geometry as predicted by Hunter and Sanders model for the electron–deficient aromatics.[101] This interaction occurred between *P* and *M* helices (red dotted line between red NDIs). CH–π Interactions were also observed within the lattice occurring between the helices. The first CH–π interaction was identified between the H (c) of the *P* helices and the core of the red NDI of *M* helices with a value of 3.43 Å (blue dotted line). The triazole linker 2 was also engaged in intermolecular CH–π interactions with the H (a) proton of the adjacent helix with a value of 3.38 Å (violet dotted lines).

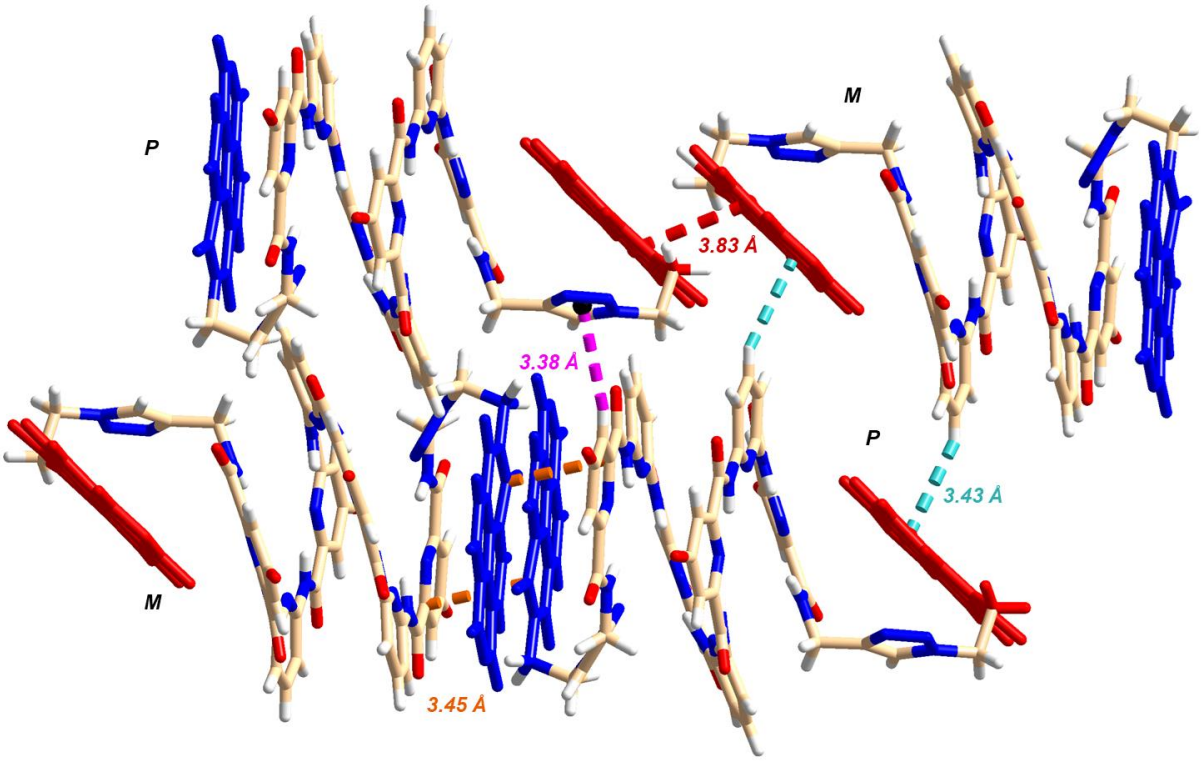


*Figure III–14. Packing of foldamer **G** in the lattice: NDI–NDI π–π interaction 3.83 Å (red dotted lines) and 3.45 Å (orange dotted lines), CH–π interactions: 3.43 Å (blue dotted lines), and 3.38 Å (violet dotted lines). Alkyl chains are omitted for clarity; Blue NDIs are in the same plane.*

### B.1.c. Analysis of reference compounds in solution

#### B.1.c.i. UV–vis absorption spectroscopy

A mixture of the reference compounds **III–20**/**III–21** and **III–23**/**III–24** was prepared upon adding chloroform to the corresponding solids, in order to make rigorous comparisons with foldamer mixtures. Regarding compounds **III–20** (60 mM) and **III–21** (60 mM), the solution of the mixture exhibited a slightly different color (orange) in comparison to the solution of each individual compound (Figure III–15–*Left*). This was further confirmed by UV–visible absorption spectroscopy, which shows a weak shoulder at 550 nm for [**III–20**] = [**III–21**] = 60 mM and a clear CT band at higher concentrations ([**III–20**] = [**III–21**] = 100 mM). On the other hand, for compounds **III–23** (80 mM) and **III–24** (80 mM), a suspension was obtained upon adding the solvent on a mixture of both solids. This originates from the very low solubility of compound **III–23**. The suspension was then diluted until complete solubilization and concentrated to lead to a red solid. The latter was dissolved in a given volume affording a solution with the desired concentration ([**III–23**] = [**III–24**] = 80 mM).

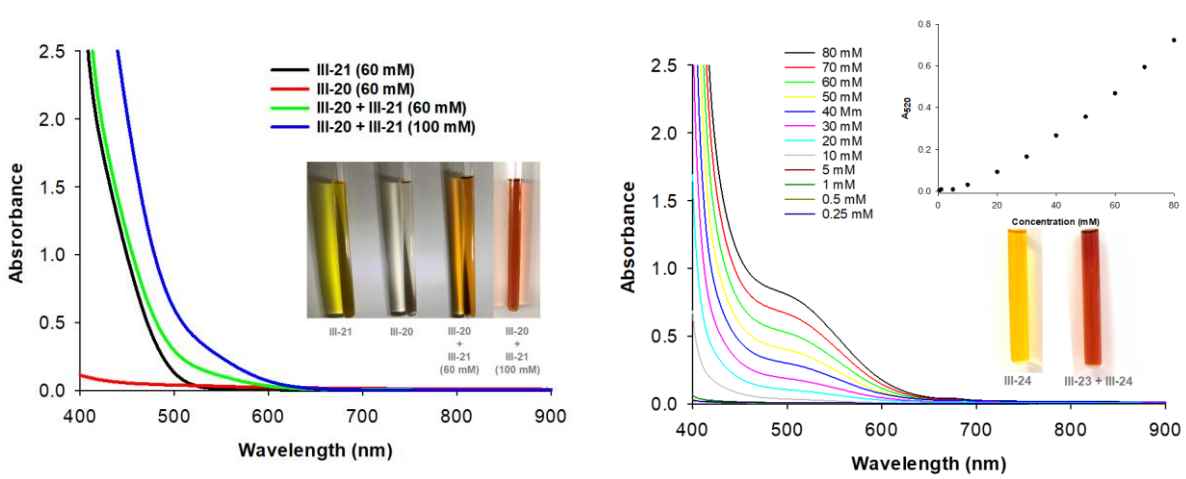


*Figure III–15. Left. UV–vis absorption spectra of reference compounds **III–20** (60mM), **III–21** (60mM) and their mixture (60 and 100 mM) in $CHCl_3$ at RT. Right. UV–vis absorption spectra of reference compounds **III**–23 (80 mM), **III**–24 (80 mM) and their mixture ([**III–23**] = [**III–24**] = 80 mM) in $CHCl_3$ at RT.*

This sample displays a reddish color, indicating the occurrence of aromatic interactions between the donor and the acceptor units (Figure III–15–*Right*). This color change resulted actually from the appearance of a strong charge–transfer absorption band around 520 nm, which disappeared upon dilution. This indicates the dissociation of the charge transfer complex at low concentration. The presence of two electroactive units in each compound, along with a preorganization thanks to the V–shaped oligomer (Figure III–16),[102] promotes the formation of the charge transfer complex. On the other hand, the absence of a charge transfer band for the solutions of both **III–20** and **III–21** can be attributed to the presence of only one electroactive unit in each compound and to the fact that no additional driving force takes place to enhance the donor–acceptor contacts (*e.g.* hybridization of the foldamers). Thereby, the pre –organized V –shape conformation of **III–23** and **III–24**, as well as the number of electroactive units, favor the formation of the DAN–NDI associations.

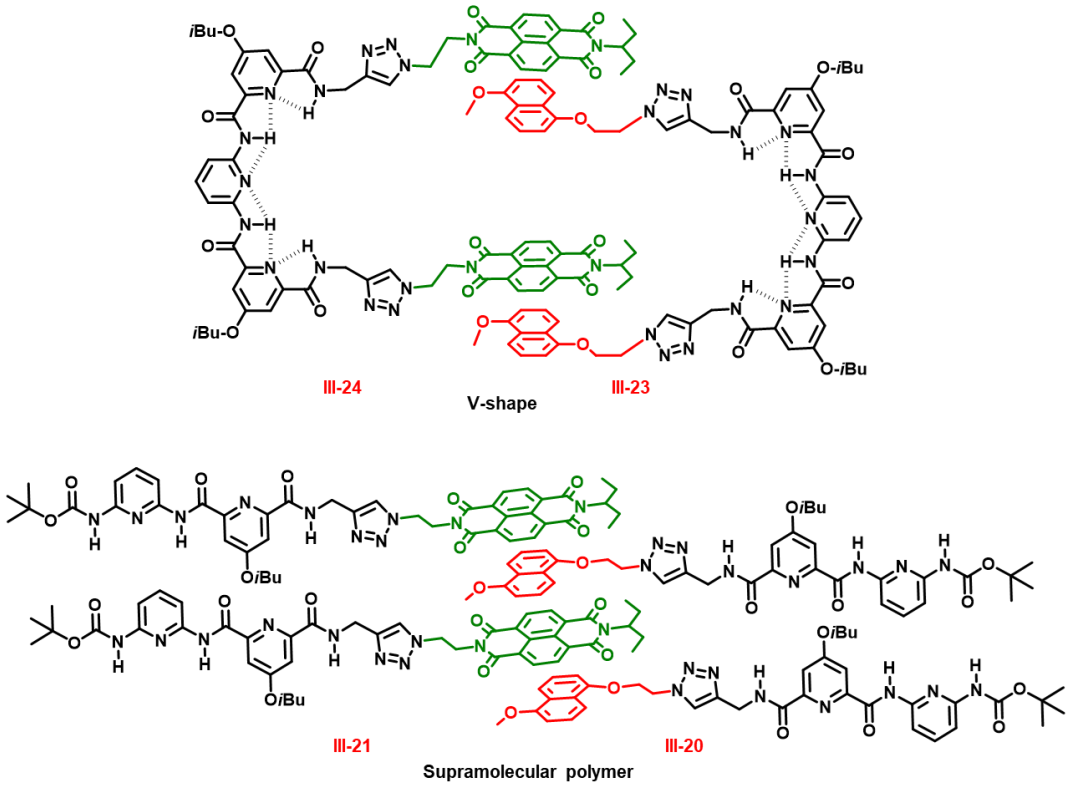


*Figure III–16. Representative chemical structures of V–shape of **III–23** and **III–24** and supramolecular polymer of **III–20** and **III–21**.*

### B.1.c.ii. NMR spectroscopy

A fast exchange at the NMR timescale was observed along the dilution experiments of mixtures **III–20**/**III–21** and **III–23**/**III–24** in $CDCl_3$. A comparison between **III–20** and **III–21**, as well as their mixture, revealed slight variations in the chemical shifts of the amide and aromatic protons (Figure III–17–*Left*). Notably, the aromatic protons of the electroactive units of NDI and DAN displayed variations in the chemical shifts, indicating a modification of their environment. Additionally, a small shift in the chemical shift ($\Delta\delta$ = 0.04 ppm for $^1$H NDI and $\Delta\delta$ = 0.06 ppm for $^1$H DAN at 60 mM) was detected (Figure III–17–*Right*). These observations suggest the presence of weak aromatic interactions between the donor and acceptor, which are constructed through stacking between the compounds, forming a supramolecular polymer.

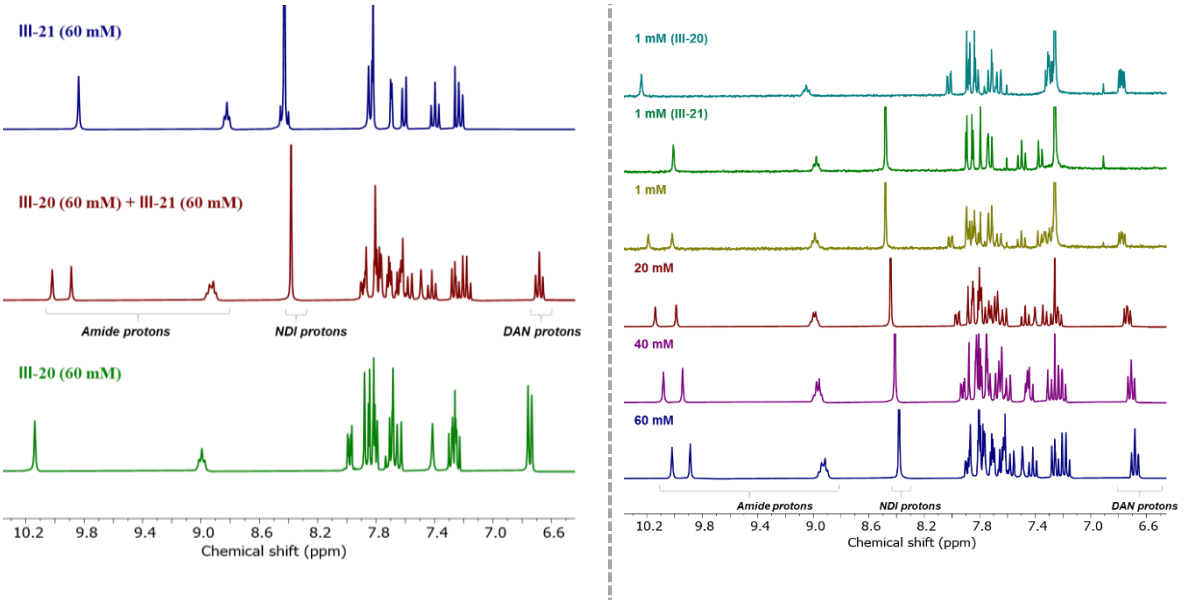


*Figure III–17. Left. Comparison between **III–20** (60 mM) and **III–21** (60 mM) and their mixture. Right. Evolution of the $^{1}$H NMR spectra of a solution of **III–20** and **III–21** upon dilution, and comparison with the individual compounds at 1 mM ($CDCl_3$, 298 K, 300 MHz).*

On the other hand, considering compounds **III–23** and **III–24**, the multiplicity of DAN and NDI protons are not the same in comparison to compounds **III–20** and **III–21**, which indicates different arrangements and environments (Figure III–18). This is consistent with the UV–visible absorption observations. The evolutions of the chemical shifts of NDI protons as reference suggests that there are more aromatic contacts in the case of **III–23** and **III–24**.

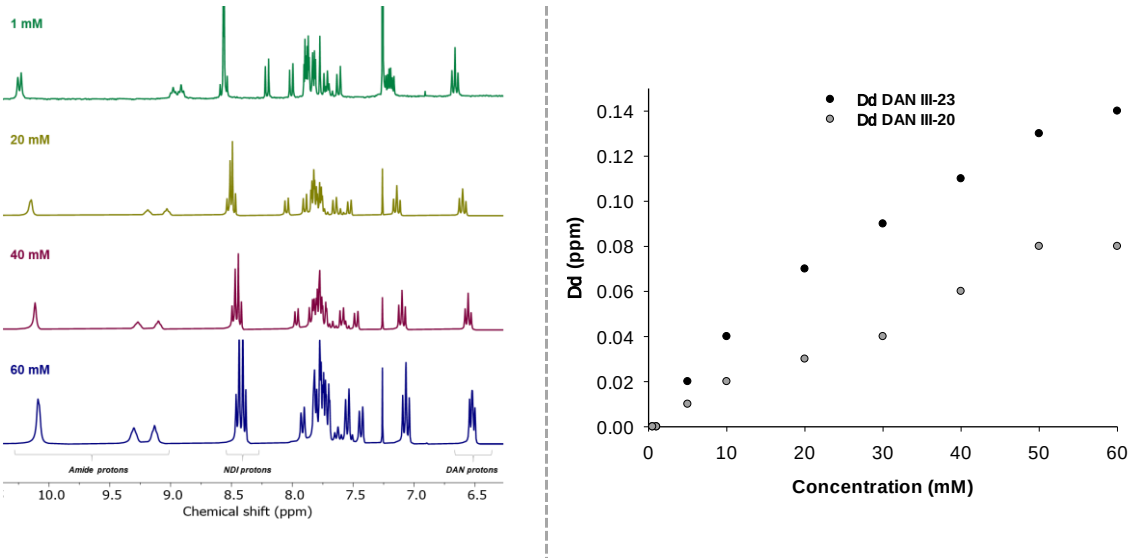


*Figure III–18. Evolution of the $^{1}$H NMR spectra of a solution of **III–23** and **III–24** ($CDCl_3$, 298 K, 300 MHz). The concentration on the x axis corresponds to the concentration of each compound.*

### B.1.d. Cross–hybridization between foldamers F and G

#### B.1.d.i. UV–visible absorption analysis

Foldamers **F** and **G** were combined in various solvents and at different concentrations (such as $CHCl_3$, $CH_2Cl_2$, $C_2H_2Cl_4$, THF, toluene, pyridine from 1 to 5 mM) and systematically showed a color change. The latter was observed in cyclic polar, solvent such as THF, in non–polar aromatic solvents, such as toluene, at low concentrations and in polar aromatic solvents, such as pyridine (Table III–1).

| ***Solvents*** | ***Results*** |
|---|---|
| *$CDCl_3$ / DCM / TCE* | *Reddish–pink solution* |
| *THF* | *Pink suspension* |
| *Toluene* | *Pale pink suspension* |
| *DMSO* | *Orange solution* |
| *Pyridine* | *Pink solution* |
| *Pyridine + Acetone* | *Pink suspension* |
| *Pyridine + Acetonitrile* | *Pink suspension* |
| *Nitrobenzene* | *Pink solution* |
| *Nitromethane* | *Yellow suspension* |
| *DMF* | *Pink solution* |

*Table III–1. Mixtures of foldamers **F** and **G** in various solvents and the observations.*

In THF and toluene, this color change was not pronounced due to the low solubility of foldamer **G** in these solvents and therefore the low concentration achieved for the mixture. On the other hand, the most pronounced color change was detected in chlorinated solvents, such as dichloromethane, chloroform and 1,1,2,2–tetrachloroethane. In these solvents, the solution of foldamers **F** (10 mM) and **G** (10 mM) displayed a reddish–pink color, which is distinct from the colour of individual foldamers: beige for foldamer **F** and yellow for foldamer **G**. Up to the literature,[81,90,103,104] the formation of a CT complex between DAN and NDI moieties is predominantly influenced by the solvent and in most cases driven by solvophobic effects. Our system proves to be original in this regard, since the formation of CT complex was observed in polar and apolar solvents. This assessment is especially true for chloroform which efficiently solvates aromatic species. This demonstrates that the interactions between the donor and the acceptor are driven by other forces, which may originate from the organized architectures due to the presence of foldamer skeleton.

In this context, chloroform was selected as the solvent of study for several reasons. Firstly, chloroform is commonly used for the hybridization analysis of oligopyridine dicarboxamide foldamers.[87–89] Therefore, employing the same solvent for UV–visible absorption and $^{1}$H NMR studies will facilitate the comparison of the obtained results. Secondly, its boiling point is moderate, allowing for heating up to 60°C, and evaporation under reduced pressure after the analysis.

UV–visible absorption analyses were conducted on each foldamer alone and a solution containing both foldamers, at concentrations lower than 5 mmol.L$^{-1}$ in chloroform. Hence, no charge transfer absorption band was detected in diluted solutions. However, at higher concentrations, a red solution of a mixture of foldamers **F** (60 mM) and **G** (60 mM) was obtained, indicating the formation of charge transfer complexes between the donor and acceptor moieties. This was confirmed by the appearance of a broad band around 520–530 nm (Figure III–19–*Left*). This result aligns with previously reported charge transfer complexes observed between DANs and NDIs in the literature.[104–107] Furthermore, the dilution of the mixture of foldamers **F** and **G** at 60 mmol.L$^{-1}$ demonstrated the disappearance of the charge transfer band, and therefore, the absence of the charge transfer complex at low concentrations (Figure III–19–*Right*).[81] This result can explain why we did not observe an evolution for the earlier experiments of cross hybridization at low concentrations (between foldamers **E** and **F** paragraph III.A.3).

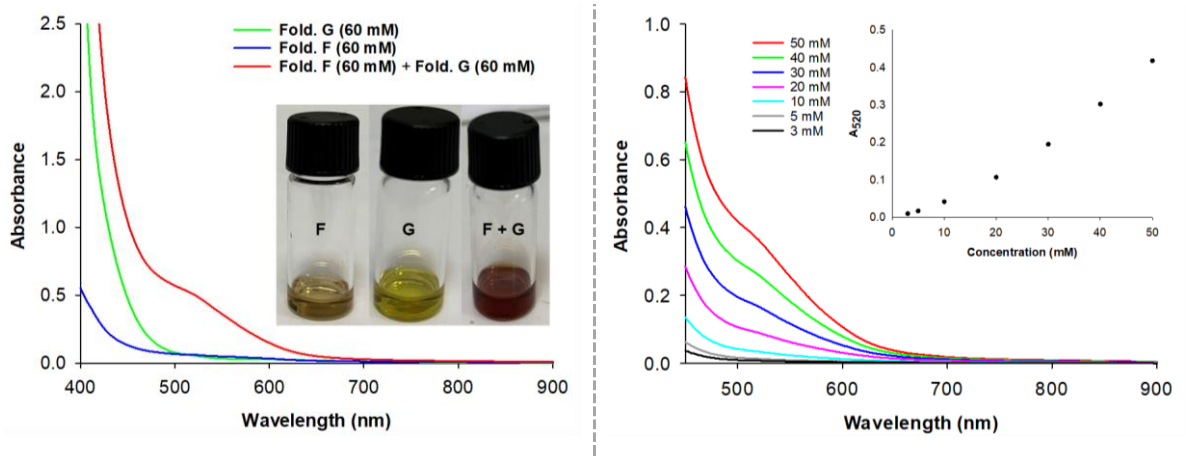


*Figure III–19. Left. UV–vis absorption spectra of foldamers **F**, **G** and their mixture (60 mM) in $CHCl_3$ at RT. Right. Evolution of the absorption spectrum of a solution of foldamers **F** and **G** upon dilution ($CHCl_3$, 298 K), the evolution of the absorption at 520 nm as function of the concentration.*

With regard to variable–concentration UV–visible absorption spectroscopy, it seems important to mention that foldamers present a behavior that is comparable to reference compounds **III–23** and **III–24**, and different from **III–20** and **III–21**. This highlights the effect of pre–organization in orienting functional units and promoting D–A contacts.

D–A interactions between the donor unit DAN and the acceptor unit NDI can occur through the hybridization of both helices, resulting in the formation of the desired heteroduplex. Alternatively, they can take place through interactions between single helices, leading to the formation of a supramolecular polymer composed of inter–connected single helices (Figure III–20). Therefore, in order to identify the supramolecular arrangement occurring in solution and leading to the formation of the charge transfer complex, $^{1}$H NMR spectroscopy analyses were led.

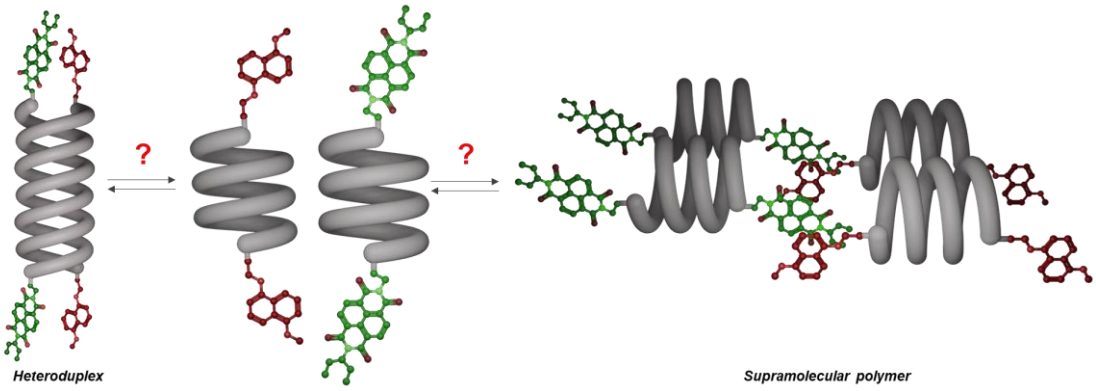


*Figure III–20. Suggestion for the arrangement of foldamers **F** and **G** in solution.*

### B.1.d.ii. $^{1}$H NMR spectroscopy analysis

#### B.1.d.ii.1) Preparation and analysis of the sample

In order to minimize errors and achieve the most accurate concentration measurement, foldamers **F** (60 mM) and **G** (60 mM) were directly weighed into the NMR tube and the powder was dissolved in a given volume of deuterated chloroform to obtain the desired concentration at room temperature. The evolution of the $^{1}$H NMR spectra of the mixture of foldamers **F** and **G** upon dilution revealed the presence of a single set of signals for amide protons, which are in fast exchange at the $^{1}$H NMR timescale. At high and low concentrations, these signals (10.69 (2H), 10.52 (4H), 10.29 (4H), 10.07 (2H), 8.95 (2H) and 8.83 ppm (2H)) integrated for 16 protons corresponding to the amide protons of the single helical structure of both foldamers (Figure III–21). These observations and the lack of a second set of signals, demonstrated that the formation of CT complex did not take place through hybridization, but through the formation of a supramolecular polymer: singles helices interact together through aromatic interactions between functional units. Furthermore, the aromatic protons of DAN and NDI exhibited upfield shifts at high concentration indicating once again D–A interactions, which is consistent with the expected ring current effects for face to face stacking between D and A chromophores.[8] A $^{1}$H NMR DOSY experiment showed the presence of enormous species

(hydrodynamic radius estimated to 33.2 Å) for this mixture (Figure III–21). This suggests that discrete objects, such as single and double helices, are not formed. Instead, the intermolecular interactions enforce the formation of larger aggregates with a lower diffusion coefficient (1.15 × $10^{-10}$ $m^2.s^{-1}$).

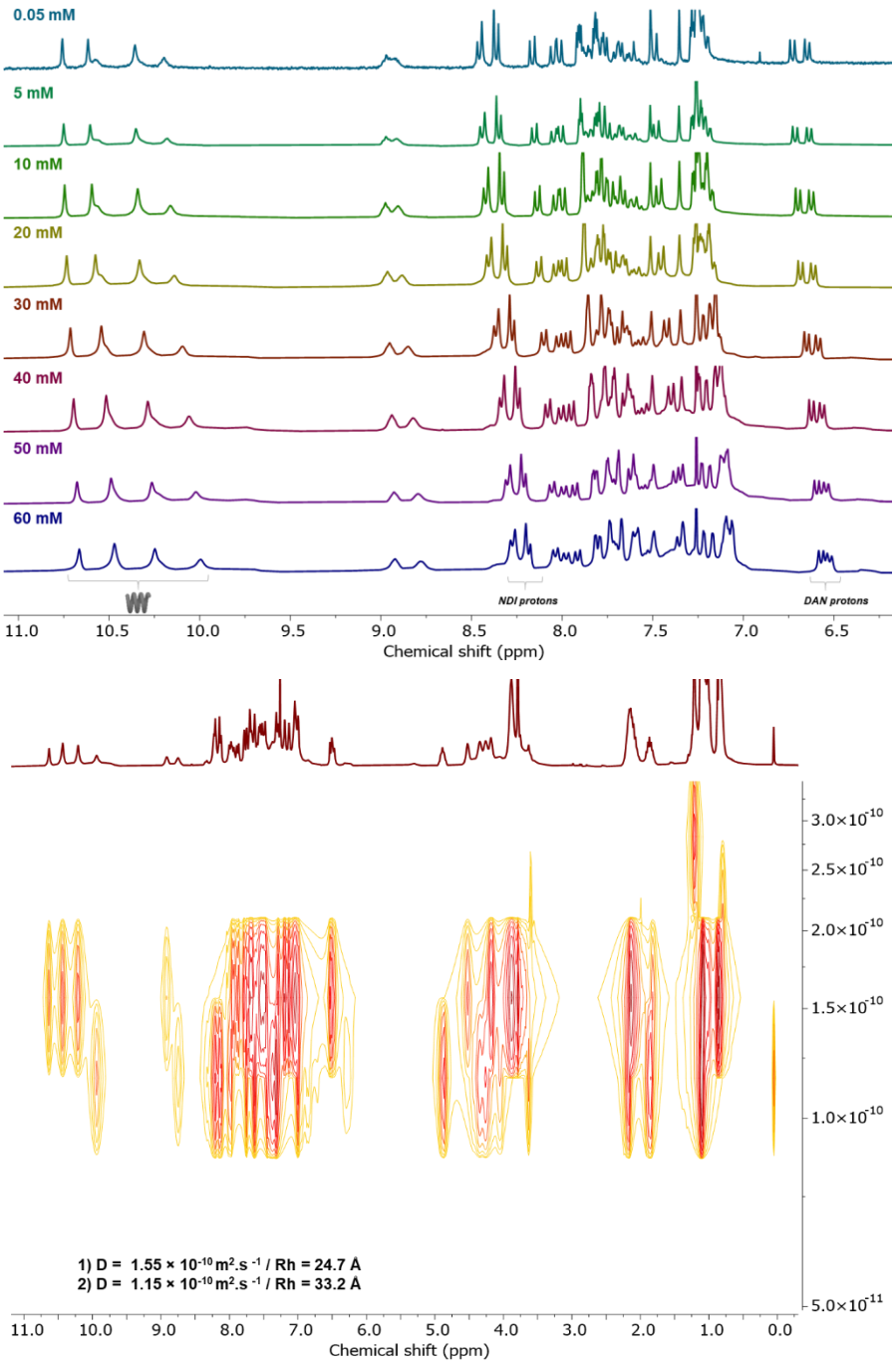


*Figure III–21. Evolution of the $^1$H NMR spectra and $^1$H NMR DOSY experiment of a solution of foldamers **F** (60 mM) and **G** (60mM) in $CDCl_3$ (298 K, 300 MHz).*

As a consequence, the results obtained from UV–visible absorption, 1D and 2D NMR spectroscopies confirmed the formation of a charge transfer complex through donor–acceptor

interactions together with the formation of a supramolecular polymer (NMR studies). These observations constitute an interesting result to explore in the future. However, our main goal consisted in elaborating heteroduplexes through hybridization. Thereby, we dedicated much effort to identify the parameters allowing to shift the 'single–to–double helix' equilibrium, and form heteroduplexes. Given the size of these architectures and the possibility for steric hindrance to impede hybridization, we considered the possibility that the sample's history could be significant and that we might be dealing with an out of equilibrium system.

#### B.1.d.ii.2) Towards out of equilibrium system

All the results presented above were obtained by direct dispersions of foldamers isolated by silica gel chromatography or recycling SEC HPLC. These experiments were led using the initial batches of solids obtained after synthesis. Given the surprising results we obtained, *i.e.* lack of foldamer hybridization, the experiments were repeated using samples that had been diluted before to test the importance of their chemical history. Therefore, we took the same sample, transferred it to a flask, evaporated the solvent on the rotavapor (temperature 45°C), and prepared a solution by dissolving the red corresponding powder in a given volume of $CDCl_3$. The $^1H$ NMR spectra recorded after this second dispersion experiment revealed major differences in terms of composition. Indeed, two species in slow equilibrium at the NMR timescale could be detected (Figure III–22). In particular, new signals appeared in the 9.0–10.0 ppm range, which translates the formation of double helical structures.[108] The $^1H$ NMR DOSY experiment showed three populations displaying significantly smaller hydrodynamic radius (18.5 Å), in comparison to the one measured for the mixture after the first dispersion. An estimation of their hydrodynamic radii showed that their sizes are consistent with single (13.9 Å) and double helical structures (18.5 Å).

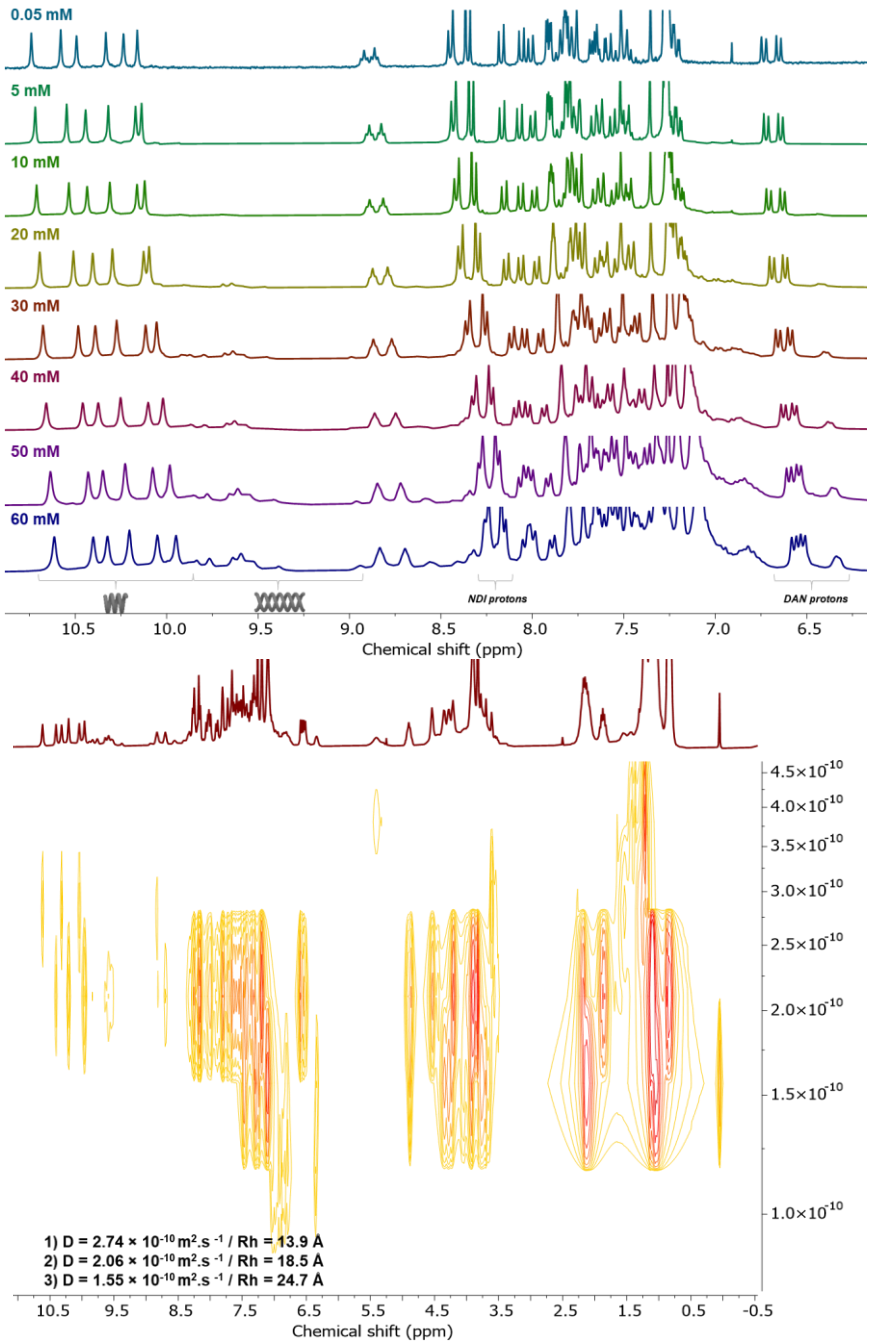


*Figure III–22. Evolution of the $^{1}H$ NMR spectra and $^{1}H$ NMR DOSY experiment of the same solution of foldamers **F** (60 mM) and **G** (60 mM) upon the second dispersion in $CDCl_3$ (298 K, 300 MHz).*

2D NMR spectroscopy was also involved in order to investigate the specific $^{1}H/^{1}H$ contacts between DAN and NDI. The NOESY spectrum of a solution of foldamers **F** and **G** at 60 mmol.L$^{-1}$ highlights coupling between the aromatic protons of NDIs and Hc and Hc' of DAN units (Figure III–23). No additional interaction was observed for Ha,a' and Hb,b'. This lack of interactions may be attributed to the intricate structure of the foldamers and the presence of numerous aromatic protons of pyridine rings, which may complicate the analysis. This differs from other examples reported in the literature where the structures of NDI and DAN are less

complex, resulting in H/H contacts between NDI and DAN aromatic protons being observed consistently.[69]

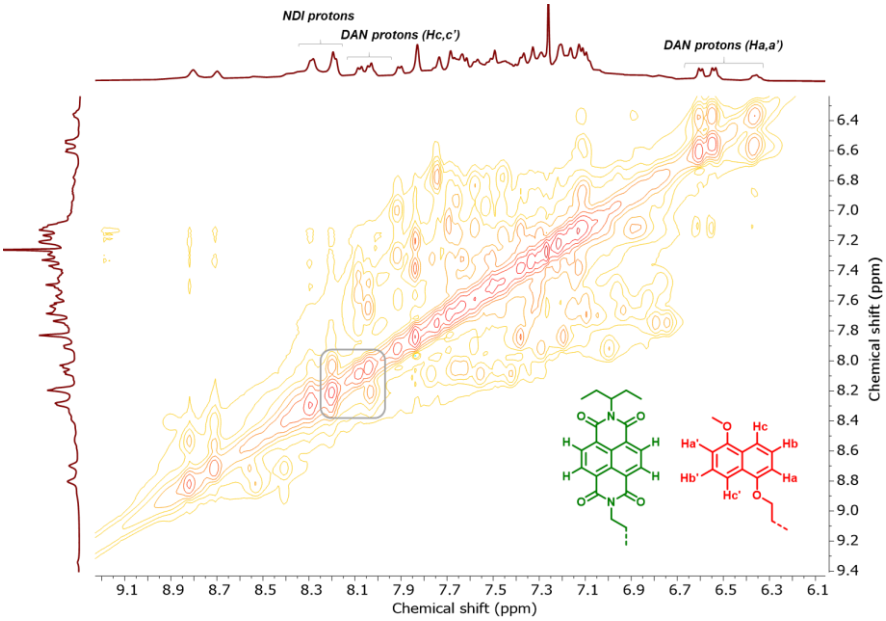


*Figure III–23. H/H contact between DAN and NDI aromatic protons by NOE spectroscopy (**F** (60 mM) and **G** (60 mM) in $CDCl_3$).*

These unexpected results suggest that heteroduplex formation may be favored after a second dispersion. This rapidly raised the question of whether the same applies to each foldamer alone. Hence, by analogy to the analysis conducted on the mixture of foldamers **F** and **G**, solutions of individual foldamers **F** and **G** were prepared from as–synthesized batches, directly in the NMR tube at a high concentration of 80 mmol.$L^{-1}$ and at room temperature.

The $^{1}$H NMR spectra of solution of foldamer **F**, revealed the presence of one set of signals for the amide protons of foldamer **F**, which are in fast equilibrium at the NMR timescale and integrate for 8 protons (80 mM: 10.73 (2H), 10.55 (2H), 10.31 (2H) and 8.99 (2H) ppm *vs* 0.5 mM: 10.76 (2H), 10.57 (2H), 10.35 (2H) and 8.97 (2H) ppm) (Figure III–24–*Left*). These observations evidence the absence of double helical structures. However, when performing a second dilution experiment on the same batch (after concentration *in vacuo*), two distinct sets of signals were observed for the amide protons indicating the occurrence of a slow equilibrium between single and double helices in solution (Figure III–24–*Right*). Interestingly, the percentage of double helix increased from approximately 0 % in the first dilution to 40 % in the second one.

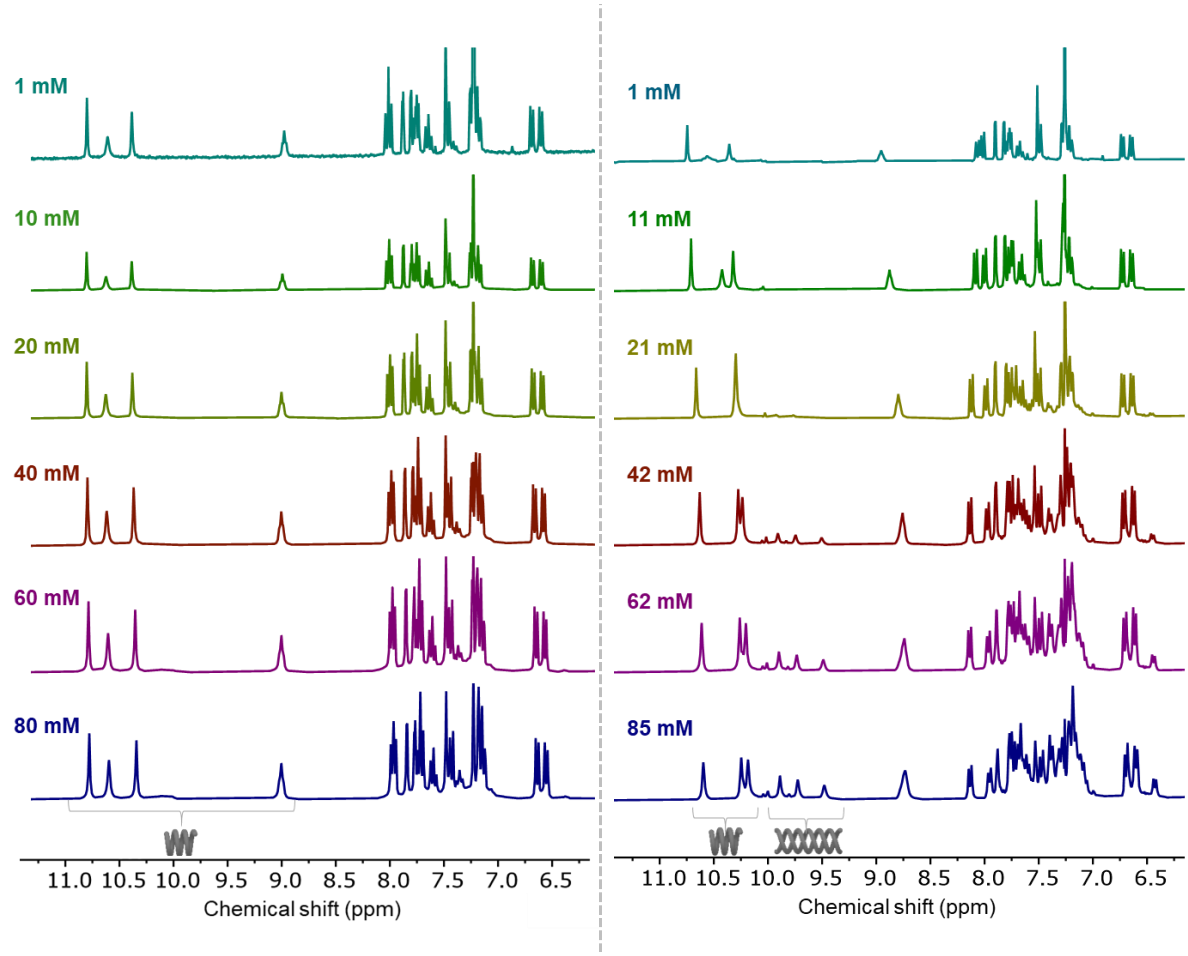


*Figure III–24. Left. First dispersion of foldamer **F** (80 mM). Right. Second dispersion of foldamer **F** (85 mM) in $CDCl_3$ (298 K, 300 MHz).*

The first dilution of foldamer **G** highlighted the occurrence of two equilibrium: a fast one, indicating the formation of a supramolecular polymer through interactions between single helices, and a slow equilibrium, with a second set of signals appearing at high concentrations and revealing the presence of double helices (Figure III–25–*Left*). The formation of double helices is very pronounced during the second dilution; the percentage of double helix increased from 22 % in the first dilution to 48 % in the second one (Figure III–25–*Right*).

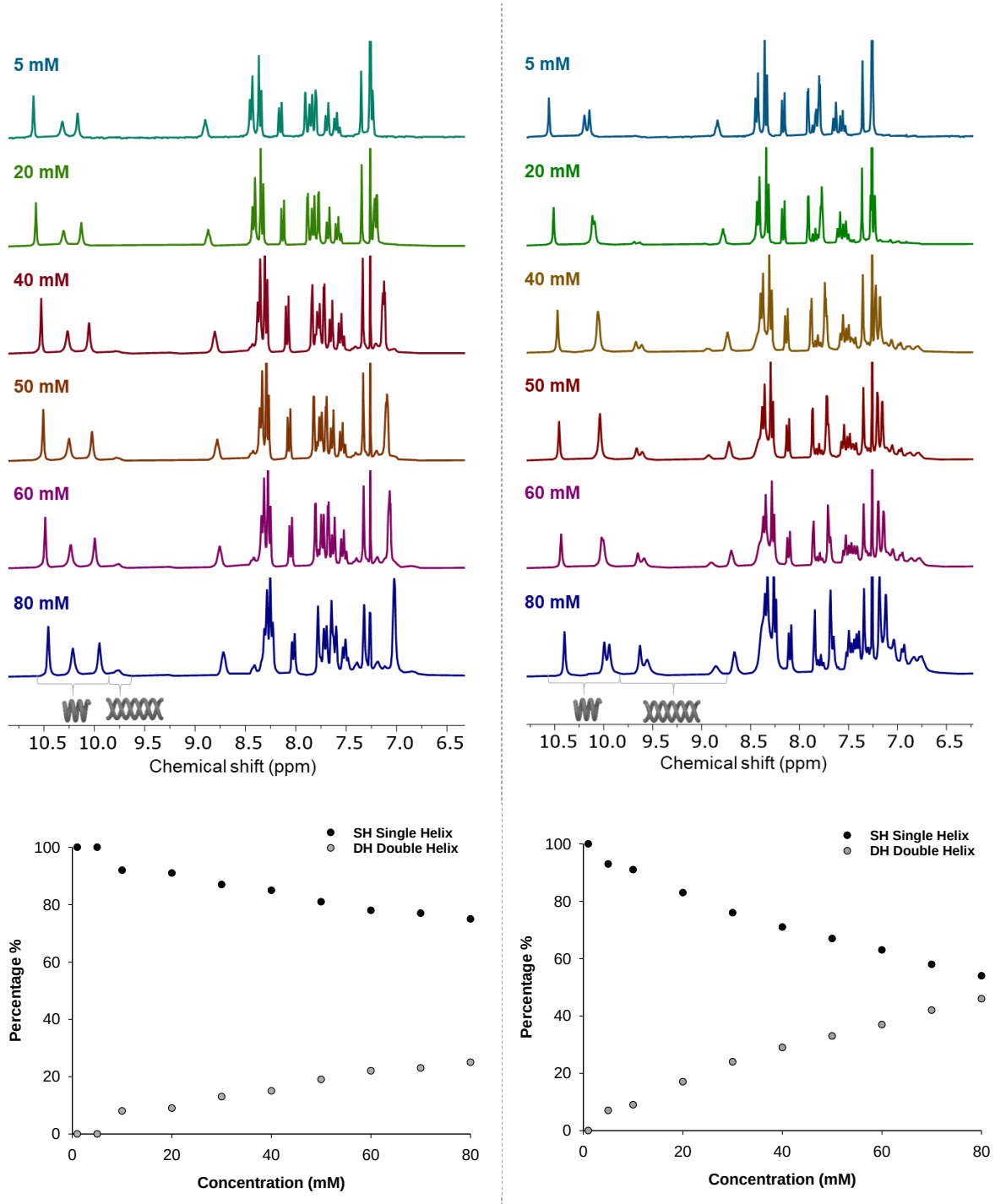


*Figure III–25. Left. First dispersion of foldamer **G** (80 mM) and the evolution of the percentage of SH vs DH as function of the concentration. Right. Second dispersion of foldamer **G** and the evolution of SH vs DH as function of concentration ($CDCl_3$, 298 K, 300 MHz).*

In order to assign these signals, a comparison was made between the spectra of foldamers **F** and **G** individually and a mixture of both foldamers at a concentration of 60 mmol.$L^{-1}$ (Figure III–26). This comparison indicated that the second set of signals in the mixture did not correspond to the second set of signals of either duplex $\mathbf{F}_2$ or duplex $\mathbf{G}_2$, and specifically when considering the aromatic protons of the chromophores. Therefore, it can be concluded that the second set observed in the mixture corresponds to the formation of new

species in solution that were not present when the foldamers were analysed individually. Given the results obtained from mass spectrometry, $^{1}$H NMR and DOSY experiments, it appears reasonable to state that heteroduplexes were formed through the hybridization of complementary strands **F** and **G**.

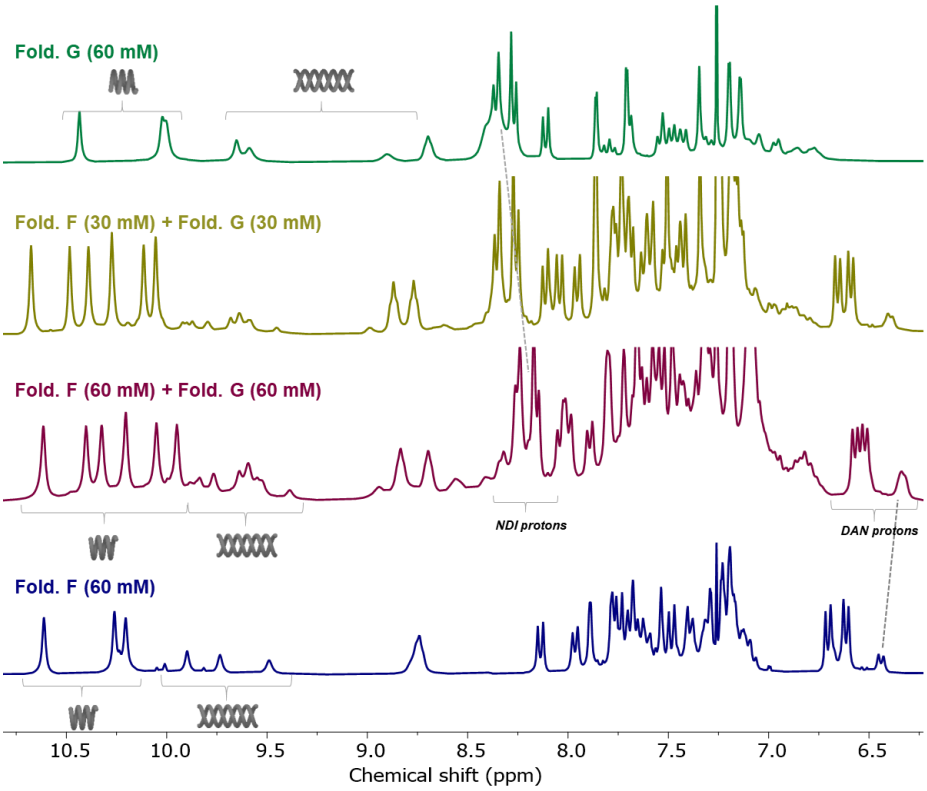


*Figure III–26. Comparison between foldamers **F** (60 mM), **G** (60 mM) and their mixture at 30 and 60 mM ($CDCl_3$, 298 K, 300 MHz).*

Making a comparison with the reference compounds, the variations of the chemical shifts of NDI protons are bigger (Figure III–27), which may reflect the contribution of the foldamer skeleton in favoring the contact between the donor and the acceptor.

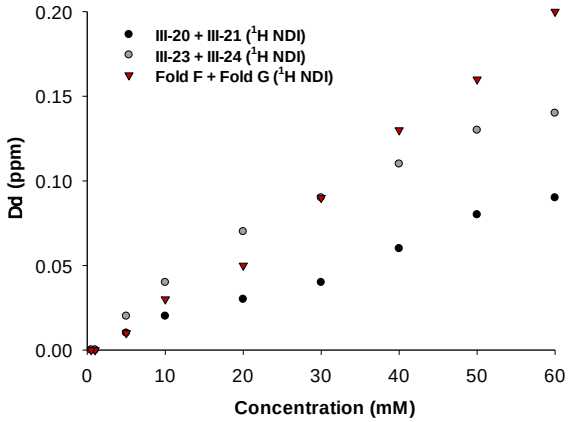


*Figure III–27. Comparison of the evolution of the chemical shift of a NDI proton between the mixture of reference compounds (**III–20/III–21** and **III–23/III–24**) and the mixture of foldamers **F** and **G** as function of the concentration.*

### B.1.d.ii.3) ESI–MS

To study the formation of duplexes by ElectroSpray Ionization mass spectrometry (ESI–MS), a solution containing both **F** and **G** was prepared using a 1/1 DCM/ACN mixture targeting a concentration C = [**F**] = [**G**] = 5 mmol.$L^{-1}$. Unfortunately, this led to a precipitation phenomenon, which impeded further measurements. In order to work at sufficiently high concentrations and circumvent the solubility issue, we envisaged the possibility to introduce additives, namely tetrabutylammonium chloride (*n*–$Bu_4NCl$, 0.5 eq.) and copper (II) sulfate. Forming anion complexes through hydrogen bonds with chloride or cation complexes with $Cu^{2+}$ indeed appeared as a track to improve the solubility of the foldamers and incidentally generate charged species. In this manner, F•G•2 $Cu^{+}$ and F•G•2 $Cl^{-}$ were detected in the positive and negative modes, which constitutes another valuable hint regarding the kind of supramolecular structures formed from **F** and **G**.

Altogether, these results show that the behavior of these foldamers strongly depends on the chemical history of the samples. Consequently, the system does not reach the thermodynamic equilibrium. In other words, these foldamers are under kinetic control.

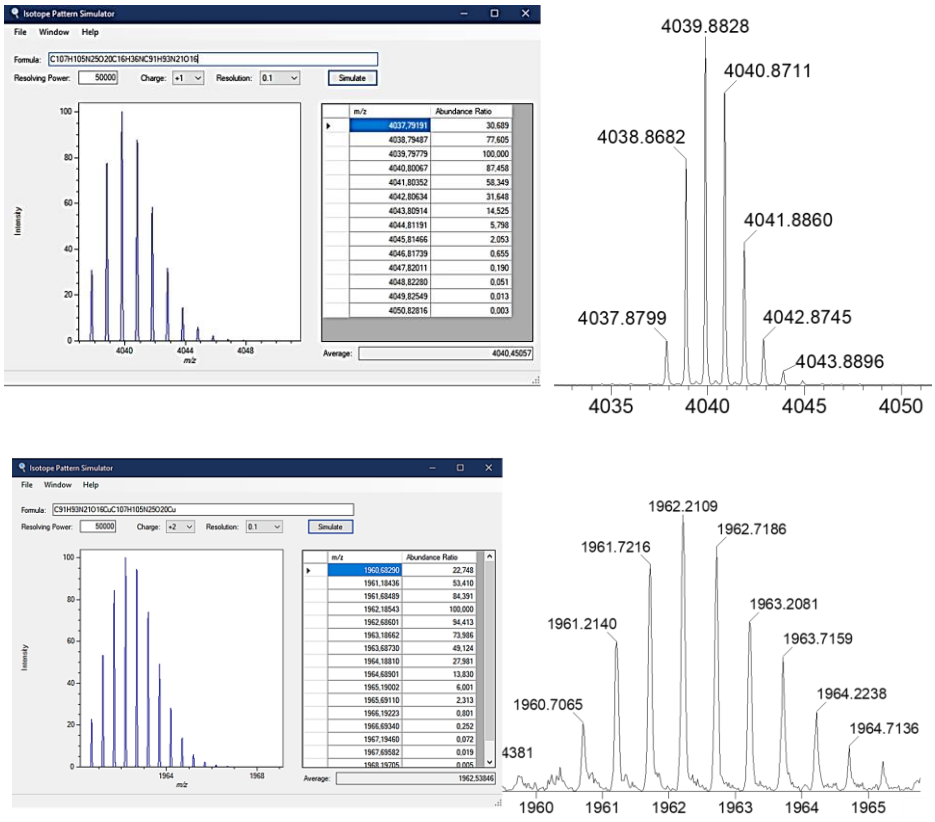

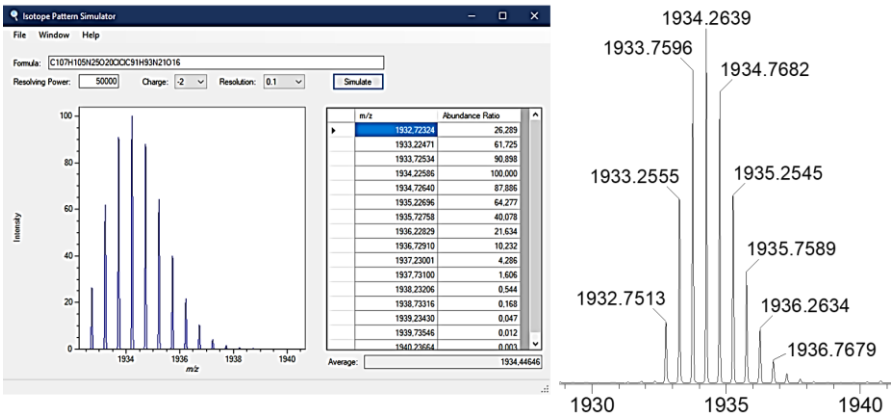


*Figure III–28. ESI MS of heteroduplex foldamers **F** and **G** in the presence of copper sulfate and n–Bu$_4$NCl (positive and negative mode). Left: simulations and right: experiments.*

## B.2. Understanding the kinetics of an out–of–equilibrium system

### B.2.a. Introduction

In the literature, molecules under kinetic control are well–known in the field of supramolecular polymerization.[109–112] This concept leads to introduce a new term defined as 'pathway complexity', a notion that arises when a given molecular building block engaged in multiple competing pathways.[109,113–117] In general, when molecules self–assemble and organize themselves into the most stable supramolecular system, the thermodynamic equilibrium is reached (Figure III–29).[118–122] However, when non–covalent interactions interfere in the process of the self–assembly and generate a high energy barrier, the chemical system may not reach the most stable organization. This leads to kinetically–trapped or metastable state, where the molecules are trapped in a local minimum of the energy landscape. At a given temperature, metastable states slowly evolve towards the ground state, while the composition of kinetically–trapped systems does not evolve because of a particularly high activation energy. These states can be defined as non–dissipative, because they are confined in a local minimum of the energy landscape and need an energy of activation to shift from a state to another one. On the other hand, dissipative non–equilibrium state needs a continuous flux of energy or matter (such as chemical fuel or light for example) to inhibit the relaxation into the minimum energy landscape, because there is relatively no energy activation barrier to overcome.[109–111,113,117]

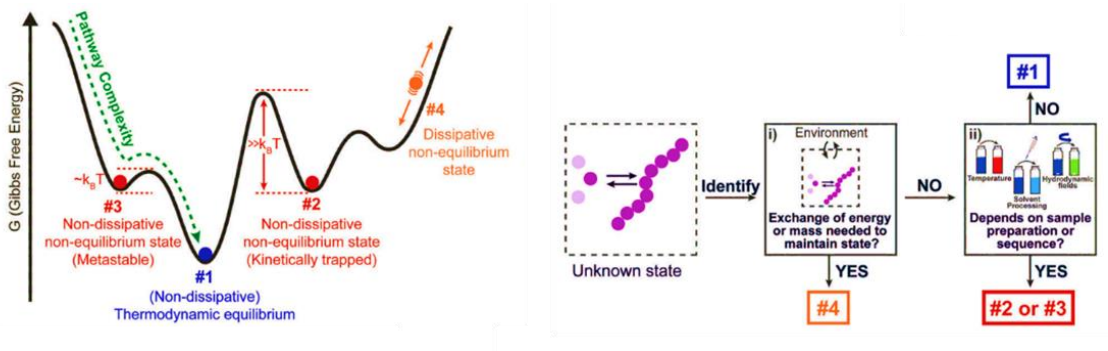


*Figure III–29. Different states of the energy landscape: thermodynamic and the non–equilibrium states.*[109]

Different strategies for controlling pathways in self–assembly were employed. These are based on as the so–called internal and external forces.[109,113,116] Internal forces rely on the construction of the building blocks such as the length,[123–127] and the placement of functional groups. These factors can give rise to additional attractive or repulsive interactions.[128–134] Specifically, these forces have often depended on the competition between inter– and intramolecular hydrogen bonding.[135–145] Furthermore, the external factors that control the kinetic pathways and depend from internal forces could be summarized as temperature and cooling rate,[113–115] concentration,[146,147] solvent composition,[148,149] time,[150,151] and pH responsive monomers or guests.[109,152–156]

Consequently, a number of physico–chemical parameters may influence the composition of the medium. The following paragraph (§III.B.2.b.) describes our efforts to assess the influence of concentration, temperature, and time on the behavior of foldamers in solution. At this stage, one will note that foldamer **G** was selected for these experiments due to its large available quantity. In addition, a comprehensive study also aimed at identifying the structural parameters that are responsible for the formation of kinetically–trapped species. The corresponding results are discussed in paragraph §III.B.3.

### B.2.b. Analysis of kinetic parameters on foldamer G

The experiments described in §III.B.1.d. show that our foldamers are kinetically–trapped as single helices along the first dilution, and that somehow, an activation barrier has been overcome between the first and the second dispersion, making the formation of double helices possible. In this context, the physico–chemical history of the samples appears critical. Hence, the reader should probably have in mind to which events were subjected the samples:

1) the foldamers were isolated through silica gel chromatography and then, by recycling HPLC (eluent: $CHCl_3$ stabilized over ethanol); 2) the chloroform was evaporated under vacuum (bath

temperature ~ 45 °C); 3) a first concentrated solution (C ~ 80 mM, solvent $CDCl_3$, solid before liquid) was prepared before performing the first dilution experiment; 4) all the solutions were gathered and concentrated *in vacuo*, T ~ 45°C; 5) the corresponding solid was dispersed in deuterated chloroform (C ~ 80 mM) for the second dispersion experiment.

### B.2.b.i. Effect of the concentration

Since we suspected that foldamers could be trapped in the single helical state because of supramolecular polymerization through aromatic interactions (Figure III–21,Figure III–24,Figure III–25), we decided to study the impact of the sample history at different concentrations. To do so, solutions of foldamer **G** (from the same batch) were prepared in deuterated chloroform at the following concentrations: 0.5, 1.0, 10, 40 and 80 mM. The $^1$H NMR spectra of these solutions were recorded, the samples were diluted down to 0.1 mM and separately concentrated *in vacuo* in the same conditions (45°C). The corresponding solids were dispersed a second time in deuterated chloroform at the same concentrations and the $^1$H NMR spectra were recorded a second time.

When comparing the spectra recorded at a concentration of 40 mM or lower, no significant variation was observed (Figure III–30–*Left*), which indicates that the foldamer strands remain in the single helical state. For the most concentrated solution (80 mM), the situation proved different (Figure III–30–*Right*): new signals appeared in the 9.75–9.00 ppm range, which is expected along the formation of double helical structures. Since the concentration of double helix appears relatively high at 80 mM (2$^{nd}$ measurement), and that 40 and 80 mM concentrations have the same order of magnitude, it appears rational to consider that at concentrations of 40 mM and below, the concentration is simply not high enough to shift the equilibrium towards the double helical structure. In this context, the dilution experiments presented in Figure III–25 are especially interesting, since it evidences the presence of double helices at concentrations down to 20 mM for a solution, which was diluted for the second time. This observation, which may seem contradictory at first, actually suggests that the kinetics of dissociation of the double helix were actually too slow along the dilution experiment to reach the equilibrium and fully dissociate the double helices. This also raises an important question: did we observe the double helix signals in the concentrated solutions because the concentration was sufficiently high to shift the equilibrium OR, were these double helices observed because they are formed at very high concentrations (when concentrating the samples *in vacuo*) but did not have the time to dissociate?

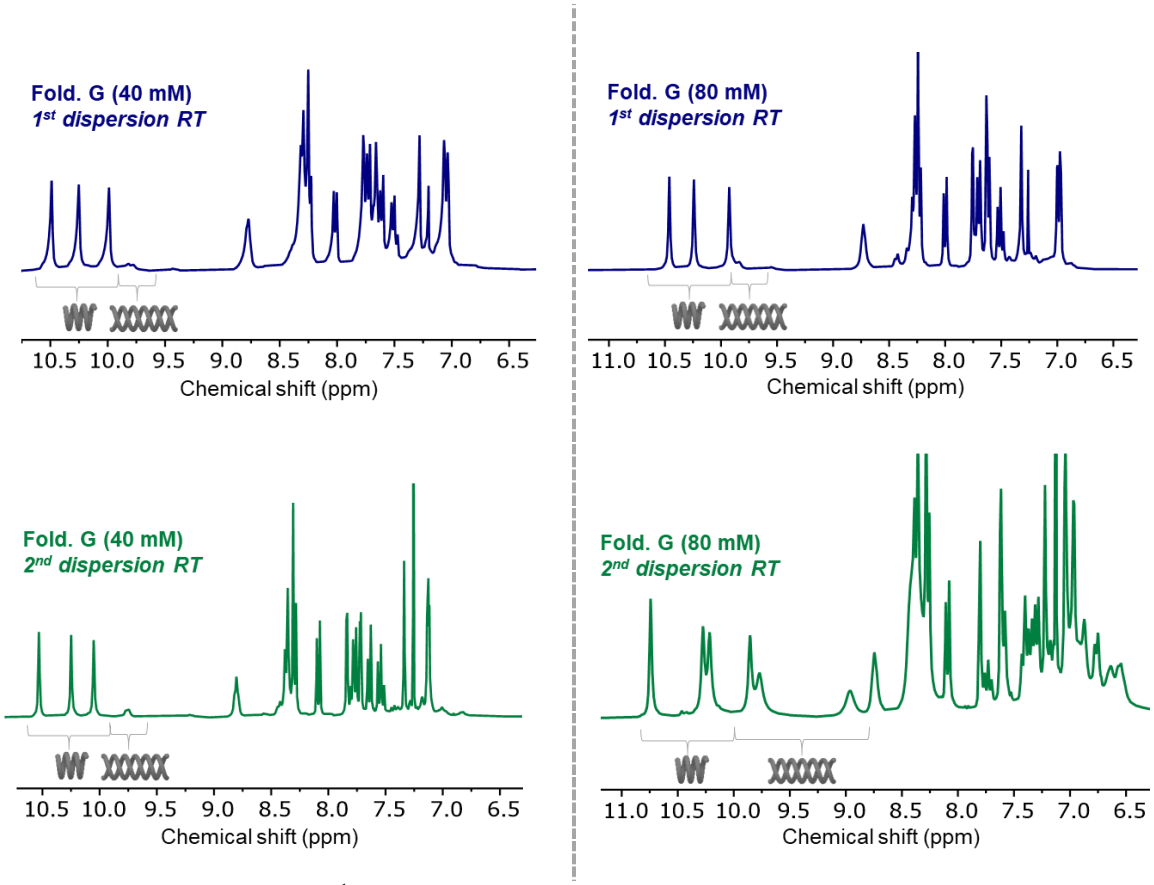


*Figure III–30. Evolution of the $^{1}$H NMR spectra of foldamer **G** at 40 mM (left) and at 80 mM (right) under different conditions ($CDCl_3$, 298 K, 300 MHz).*

### B.2.b.i.1) Impact of time and temperature at high concentration

To answer the question concluding paragraph §B.2.b.i, the evolution of the concentrations of single and double helices was studied as a function of time and temperature for an 80 mM solution of foldamer **G** dispersed in deuterated chloroform for the second time.

In this context, we first measured the $^{1}$H NMR spectrum of this solution after 24 hours at room temperature (~ 20°C) and then, upon heating at 45°C (Figure III–31). While no significant variation was observed at room temperature, modest but significant variations were evidenced at 45°C. Indeed, the integrals of the signals assigned to the double helical state slightly increased (from 33 % to 39 % estimated by integration of single and double helical signals), which suggests that heating the samples at this temperature is actually enough to make this 'apparently frozen system at room temperature' dynamic. Therefore, it appears reasonable to state that the double helix signals observed after the second dispersion process are not solely the result from double helices formed at higher concentrations along the evaporation process (before the second dispersion), but are indeed stable in these experimental conditions.

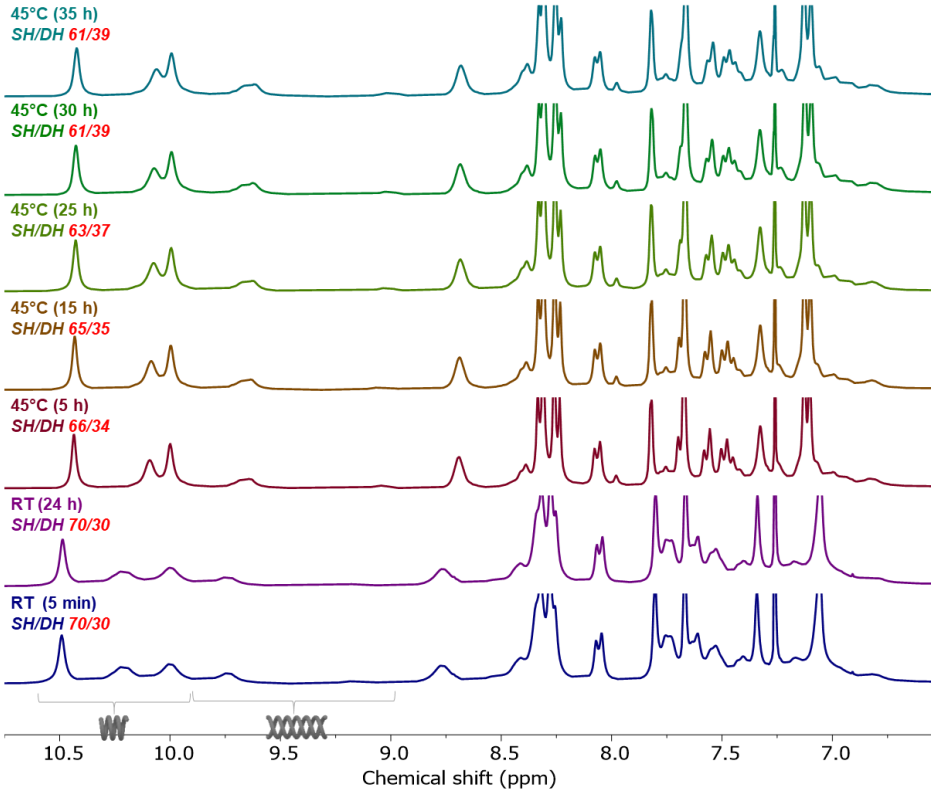


*Figure III–31. Evolution of the $^{1}H$ NMR spectra of foldamer **G** at 80 mM after 5 minutes and 24 hours at RT, and upon heating at 45°C as function of time ($CDCl_3$, 298 K, 300 MHz).*

### B.2.b.i.2) Effect of the evaporation process

Through paragraphs §B.2.b.i and §B.1.a.ii, it was shown that: 1) double helices were observed after the second dispersion, on condition that the concentration of **G** reaches 80 mM in $CDCl_3$; 2) the kinetics of association and dissociation of helical strands in these conditions are slow (kinetically–trapped at room temperature, and metastable at 45°C); 3) the maximum measured concentration of double helix in these conditions corresponded to 39 % of the total foldamer concentration.

Thereby, we anticipated three important points:

- First, that reaching higher concentrations at sufficiently high temperatures could lead to higher concentrations of double helices;
- That a solution at room temperature and containing a high concentration of double helix would remain quite a long time out of equilibrium given the observed slow kinetics of association–dissociation;
- And hence, that concentrating the samples under vacuum and upon heating would allow for preparing samples displaying higher concentrations of double helices. Presumably, such observations could also be made from solutions prepared at higher concentrations,

but the required amount of compound is already very important at 80 mM (for V = 0.4 mL and foldamer **G** (M = 2060 g.mol$^{-1}$), the necessary weight is 66 mg).

With this in mind, a mother solution of foldamer **G** (first dispersion in $CDCl_3$ after isolation) was prepared at a concentration of 80 mM. This solution was divided into two samples, named A and B ([**G**] = 80 mM), which were subsequently diluted with chloroform down to 1 × 10$^{-8}$ mmol.L$^{-1}$ to ensure the full dissociation of double helices and supramolecular polymers. For solution A, chloroform was evaporated under vacuum using a rotavapor and a water bath set at 20°C. For solution B, the same process was followed with a water bath set at 45°C (the evaporation time was significantly shorter). The corresponding solids were subsequently dispersed in deuterated chloroform to afford 80 mM solutions, which were directly analysed by $^1$H NMR spectroscopy. For solution A, the percentage of double helices increased from 22 % for the mother solution to 27 % after evaporation at 20°C. For solution B, this percentage increased up to 50 % after evaporation at 45°C (Figure III–32). This result confirmed our initial assumptions: increased concentrations of double helices may be reached at higher concentrations on condition that samples are heated to surpass the activation barrier that makes the system kinetically–trapped at room temperature.

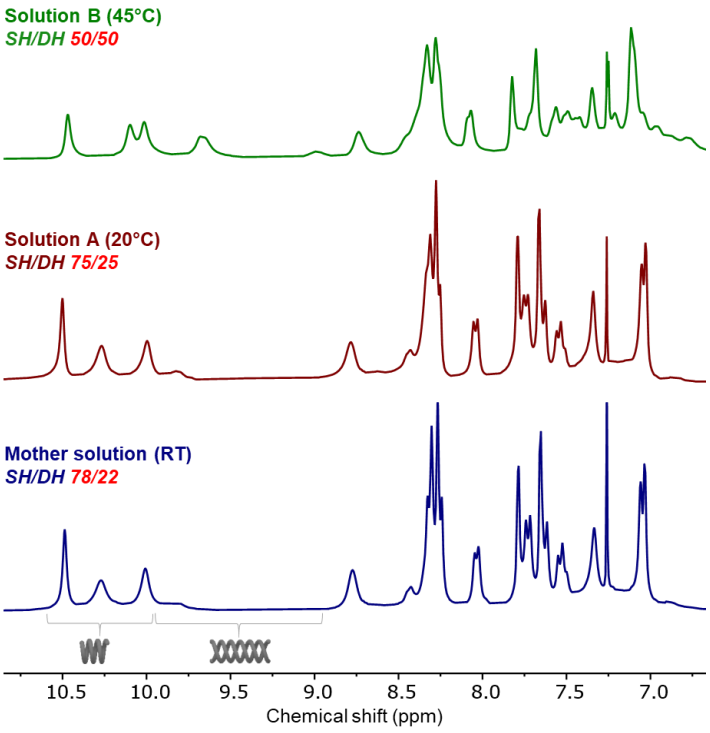


*Figure III–32. Evolution of the $^1$H NMR spectra of foldamer **G** at 80 mM when evaporating without heating at 20°C (solution A) and with heating at 45°C (solution B) ($CDCl_3$, 300 MHz).*

In order to assess the impact of the dilution step that was led before concentration under vacuum, similar tests ([**G**] = 80 mM, solvent: $CDCl_3$) were performed in NMR tubes without prior dilution. Chloroform was evaporated at 20°C and 45°C for tubes A and B, respectively. As far as the corresponding solids are concerned, these prove to have different colors: A was pale yellow, while B was substantially darker. One will note that such a difference could arise from different packing (H or J aggregate[157]), as previously evidenced by Banerjee *et al.*[158]

When dissolving the corresponding solids in deuterated chloroform, a major difference was observed: in tube A, the percentage of double helix increased by 5 % in comparison to the initial solution, while it increased by about 30 % for the heated sample (Figure III–33). By comparing these results with those obtained after dilution and concentration under vacuum, this experiment shows that the dilution step, which had for objective to dissociate aggregates, does not have a major impact on the composition of the medium and hence, in the sample history. Consequently, temperature and time appear as critical parameters to control the hybridization process and hence, the sample composition.

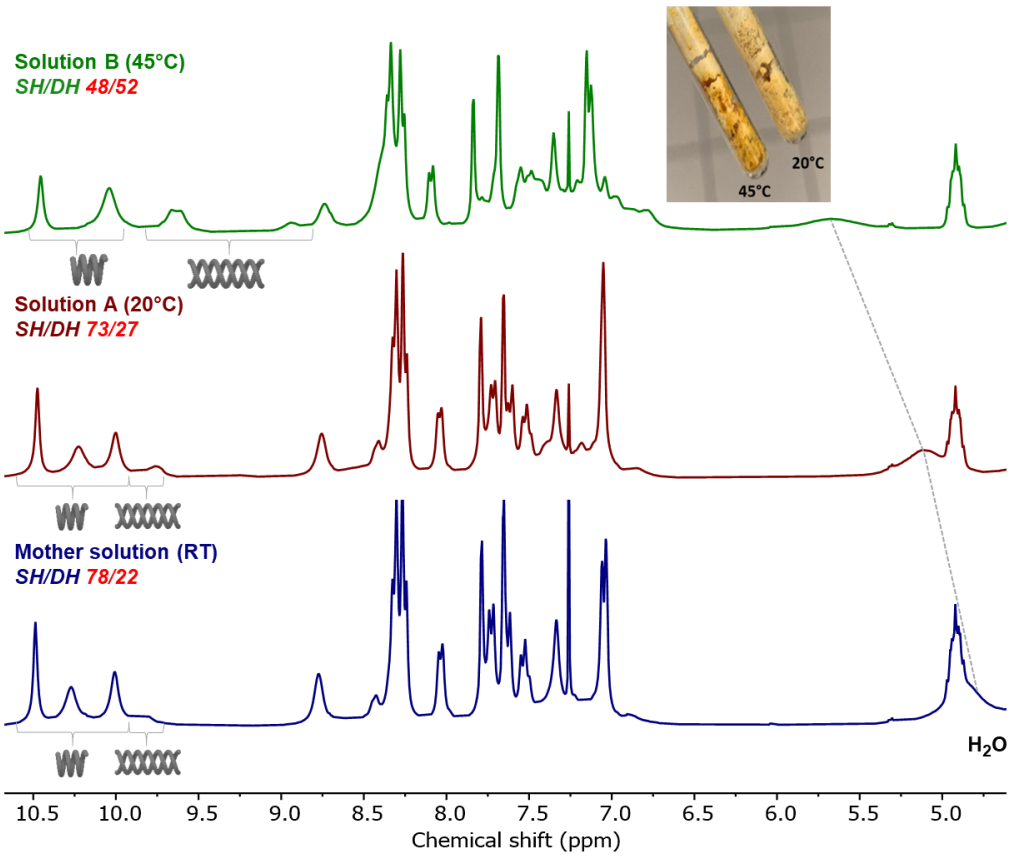


*Figure III–33. Evolution of the $^1H$ NMR spectra of foldamer **G** at 80 mM when evaporating directly in the NMR tube at 20°C (without heating – solution A) and with heating at 45°C (solution B) ($CDCl_3$, 298 K, 300 MHz).*

## B.3. Understanding the kinetic trapping from a structural point of view

### B.3.a. Research hypothesis

As demonstrated through paragraph §B.2, the behavior of these helical foldamers largely depends on kinetic parameters: indeed, these species do not reach the thermodynamic equilibrium at room temperature. In this context, we decided to dedicate efforts to identify the structural parameters impeding this system from reaching the equilibrium.

As reported in the literature,[113,116] out–of–equilibrium systems may be obtained because of intra– and/or intermolecular interactions. Indeed, non–covalent bonds may lead to the formation of inactive species that prevent the rapid formation of the thermodynamic products. In our case, it is noteworthy that the non–dissipative non–equilibrium state of these foldamers is kinetically trapped, because the system requires an additional '*help*', *i.e.* heating, to escape its trap. Indeed, our foldamers are not in a metastable state, which would evolve towards the most stable one with time, on condition that the activation barrier from the metastable state to the thermodynamic state can be surpassed thanks to thermal energy.

Since such a behavior had never been reported for short oligomers,[95,102,159] we presumed that the foldamer skeleton could not be responsible for the observation of a kinetically trapped state and therefore, that the distinguishing features of these foldamers, *i.e.* the presence of triazole rings and electroactive moieties was behind these unexpected results. On this ground, three lines of enquiry were explored:

1) The formation of a supramolecular polymer through π–π interactions between electroactive units could prevent hybridization;
2) The presence of a strong intramolecular or intermolecular π–π interactions between the electroactive units and the pyridyl rings of the foldamer skeleton could lead to kinetically–trapped state;
3) Since triazole is known as hydrogen bond donor, this ring could be involved into hydrogen bonds and hence, lead to the formation of inactive species.

In this context, the following paragraphs describe our efforts to understand the behavior of these out–of–equilibrium foldamers. To do so, two strategies appeared complementary: the first one consists in a careful examination of the obtained crystallographic structures (§B.3.b) and the second one lies on the synthesis and characterizations of control compounds (§B.3.c).

### B.3.b. Overview on the crystallographic structures

Reviewing the obtained crystallographic structures (Figure III–8, III–Figure III–9, Figure III–13), we observed that intermolecular aromatic interactions take place between NDI units of adjacent helices in the case of foldamer **G**. This observation aligns with our first hypothesis, which lies on the formation of kinetically trapped foldamer–based supramolecular polymers through interactions between electroactive units. Furthermore, intramolecular aromatic interactions were also detected in the X–ray crystal structure of foldamer **G** between an electroactive NDI unit and a pyridyl ring of the adjacent helix. This interaction was also detected within foldamer **E** and compound **III–21**, both in an intra and intermolecular manner. This finding matches with the second hypothesis (*interactions between electroactive units and foldamer skeleton*).

On the contrary, all the crystallographic structures obtained from this family of foldamers show the presence of a seven–membered pseudo–cycle formed by intramolecular hydrogen bond. The formation of this pseudo cycle involves the hydrogen atom of the triazole linker and the oxygen atom of the closest amide function, with values of 2.57, 2.52 and 2.87 Å for foldamers **E**, **F** and **G**, respectively (Figure III–34). These observations align with the third hypothesis and make this hypothesis quite convincing. In this context, it seems reasonable to consider that the formation of these stabilized pseudo–cycles hinders the hybridization process. This also explains why heating, *i.e.* weakening this hydrogen bond, leads to increased concentrations of double helical structures.

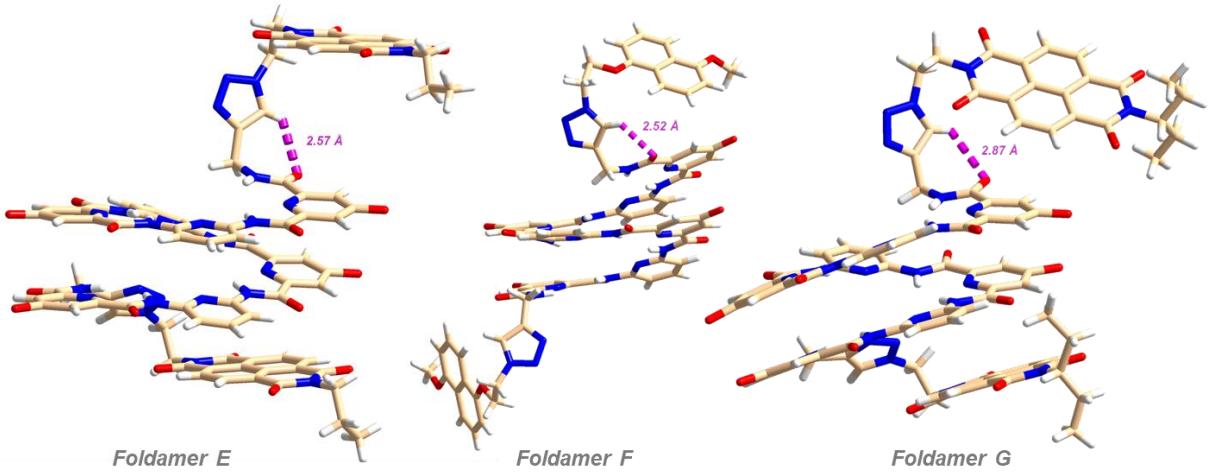


*Figure III–34. Crystallographic structures of foldamers **E**, **F** and **G** and the representative intramolecular hydrogen bonds forming a seven–membered pseudo–cycle.*

### B.3.c. Understanding kinetically–trapped foldamers through a structural approach

In order to understand the structural parameters governing the kinetic trapping of our foldamers, foldamer **B** was selected, as it lacks both the triazole and electroactive units, while foldamer **H** (Scheme III–17) was chosen because it only contains triazole linkers. Designing an electroactive foldamer, endowed with triazole rings but unable to form the seven–membered pseudo–cycle through hydrogen bond also appeared exciting. This is the reason why foldamer **J** and **K** (Scheme III–17) were also synthesized and characterized. By adding a methylene group between the triazole ring and the closest amide function, one can indeed expect the absence or the weakening of the corresponding intramolecular hydrogen bond.

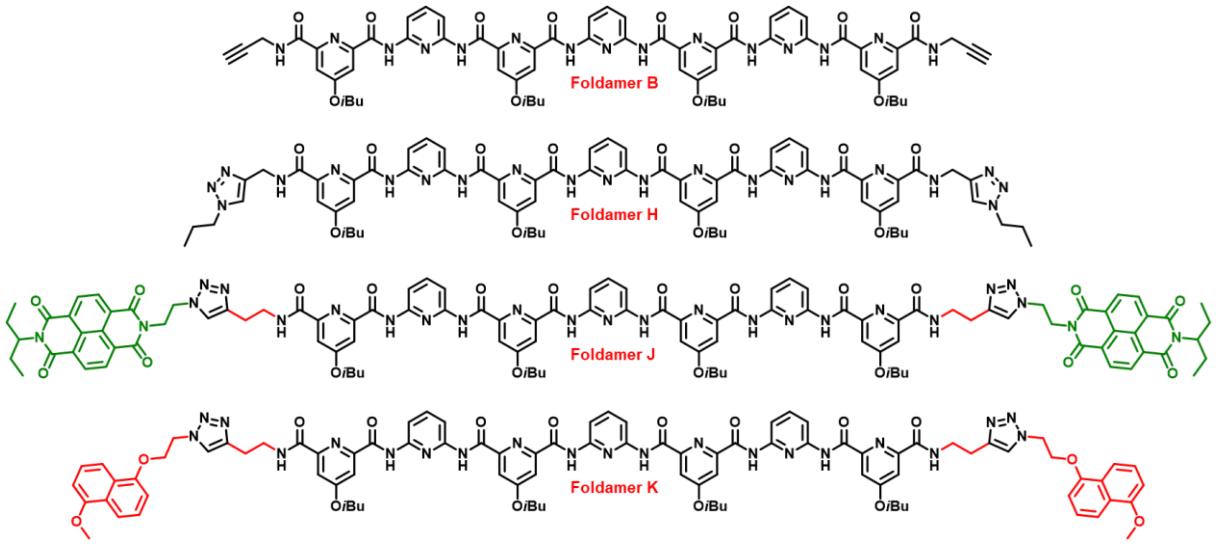


*Scheme III–17. Chemical structures of foldamers **B**, **H**, **J** and **K**.*

#### B.3.c.i. Synthesis

##### B.3.c.i.1) Synthesis of foldamer H

Foldamer **H** was prepared in two steps from foldamer **B**. 1–Azidopropane **III–25** was obtained from 1–bromopropane in the presence of sodium azide in a mixture of THF/$H_2O$ to reflux.[160] Then, foldamer **H** was obtained through CuAAC reaction between **B** and azide **III–25** with a yield of 65 % (Scheme III–18).

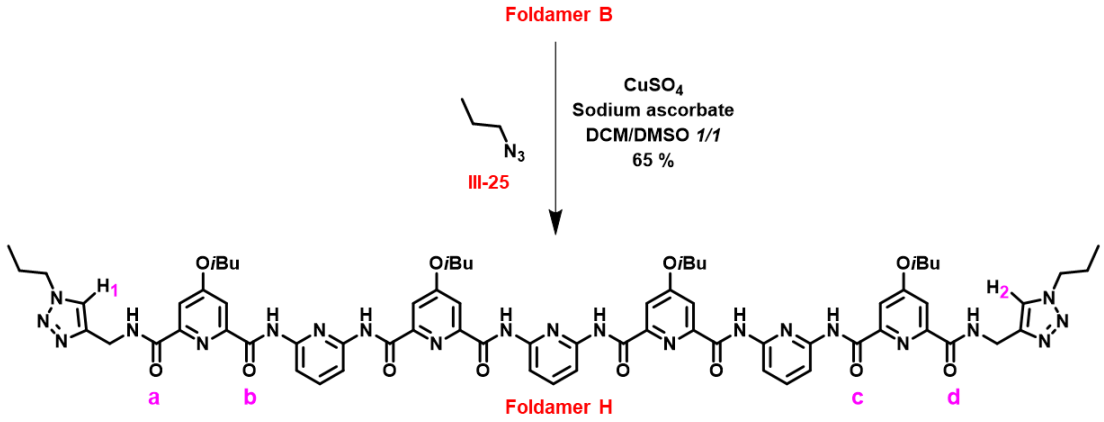


*Scheme III–18. Synthesis of foldamer **H**.*

### B.3.c.i.2) Synthesis of foldamer J and K

To synthesise bis(alkyne) **I**, carboxylic acid **III–3** was first activated into its acid chloride analogue with Ghosez reagent. The addition of a solution of but–3–yn–1–amine and dry DIPEA in dry THF subsequently allowed the formation of **III–26**, which was isolated with a yield of 80 % (Scheme III–19). The amine function of **III–26** was deprotected in the presence of trifluoroacetic acid to yield quantitatively **III–27**. Eventually, the latter was added to the acid chloride obtained from **III–2** to afford foldamer **I** with a yield of 64 %.

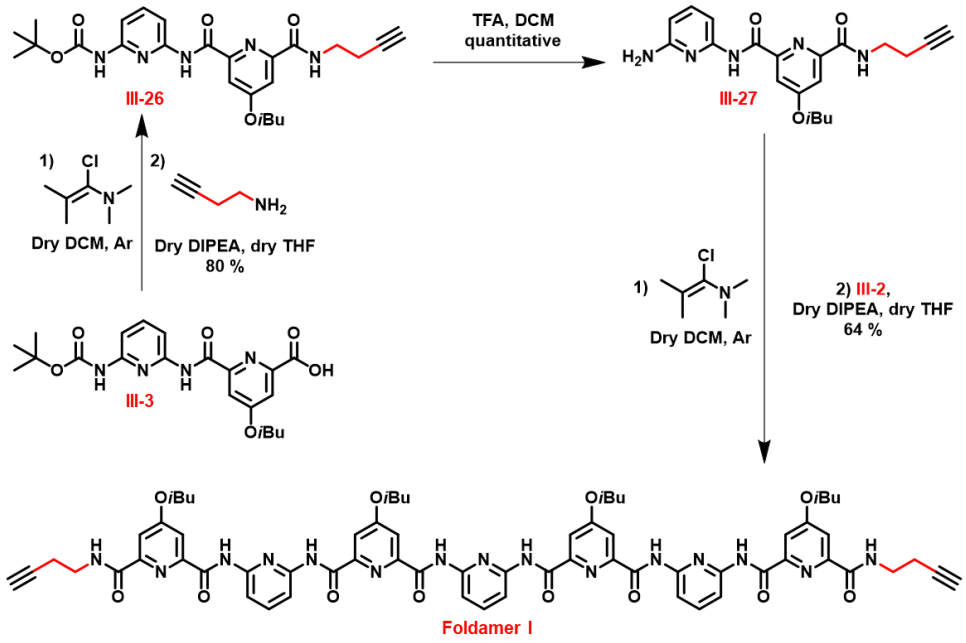


*Scheme III–19. Synthetic scheme of foldamer **I**.*

The grafting process of NDI and DAN units was finally achieved through CuAAC reaction between foldamer **I** and azides **III–19** and **III–17** to give foldamers **J** and **K** with 85 and 81 % of yield, respectively (Scheme III–20).

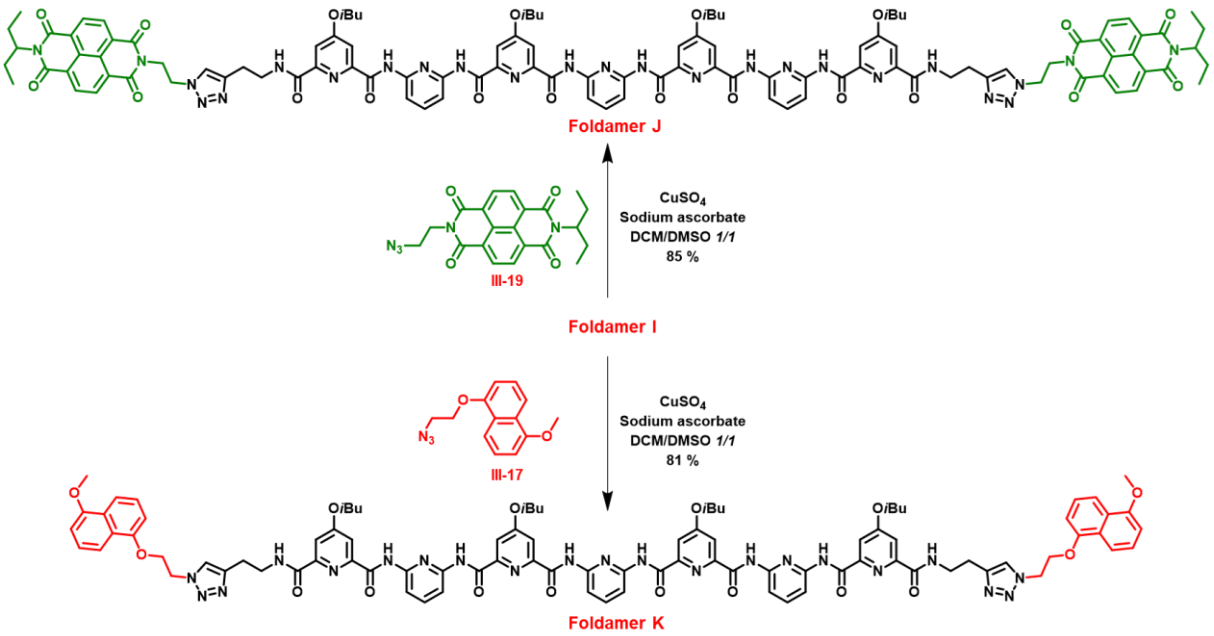


*Scheme III–20. Synthesis of foldamers **J** and **K** via CuAAC reaction.*

### B.3.c.ii. Solid state analysis of foldamer H

Monocrystals of foldamer **H** in its single helical state were obtained by slow evaporation from a solution of DMSO in a triclinic P–1 space group. The polar cavity accommodates two DMSO molecules within the foldamer skeleton through hydrogen bonds between the oxygen atom of DMSO molecules and the hydrogen atoms of two amide functions at the extremities with values ranging from 1.97 to 2.37 Å. Aromatic interactions were detected between pyridyl units and defined a helix pitch of 3.69 Å. A weak hydrogen bond of 2.96 Å was detected between H (1) and the oxygen atom O (a) of the adjacent amide function (see Scheme III–18), which forms a seven–membered pseudo–cycle (Figure III–35–a). Furthermore, intermolecular hydrogen bonds were detected between H (1) of the triazole function and the oxygen atom O (d) of the adjacent helix with a value of 2.55 Å (green dotted lines) and H (2) and O (b) with a value of 2.54 Å (blue dotted lines – Figure III–35–b). It is noteworthy that both triazole groups are perpendicular to the foldamer skeleton unlike the cases of electroactive foldamers specifically NDIs, for which the orientation of the triazole group depends from the interactions between the electroactive units.

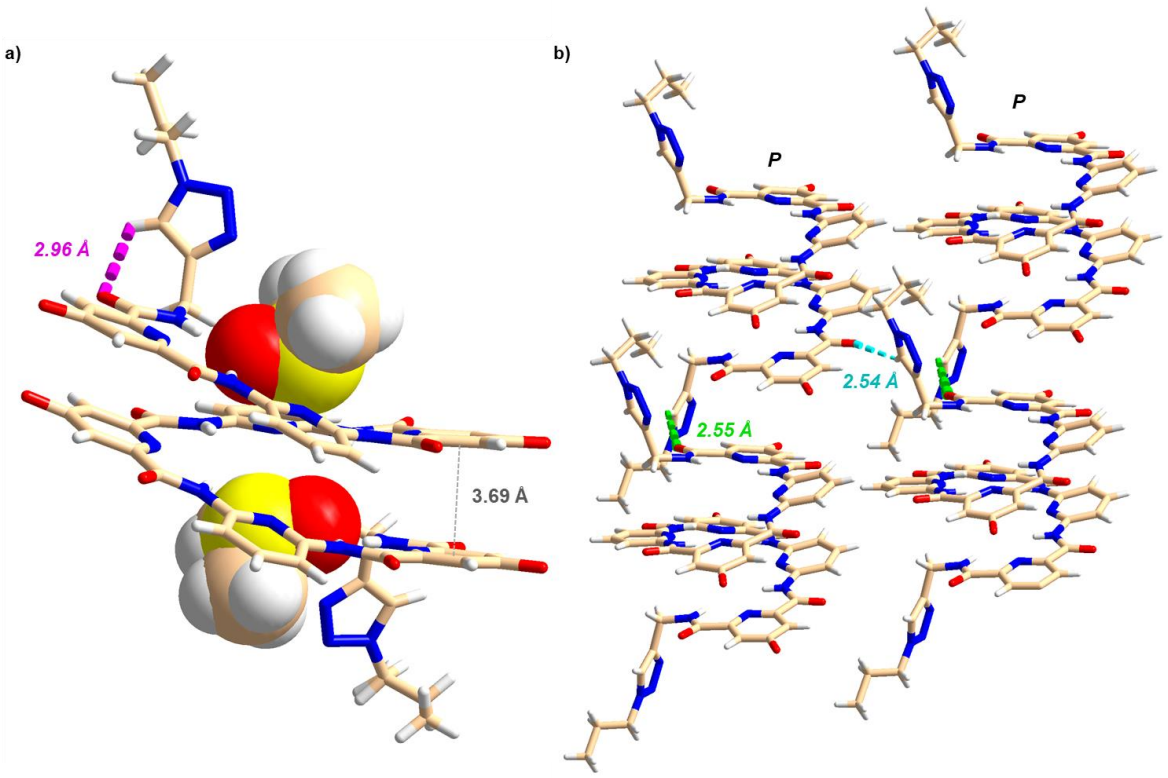


*Figure III–35. a) X–ray crystal structure of foldamer **H** obtained by slow evaporation from a solution of DMSO, which contains two DMSO molecules, b) Packing of foldamer **H** in the lattice. Hydrogen bonds of 2.55 Å (green dotted lines) and 2.54 Å (blue dotted lines) are represented. M helices and isobutoxy chains are omitted for clarity.*

### B.3.c.iii. Analysis in solution

#### B.3.c.iii.1) Foldamer B and I (lacking electroactive unit)

A single set of signals was observed by $^{1}$H NMR spectroscopy (300 MHz) for solutions of foldamers **B** and **I** whatever the concentration. This underlines their very low propensities **B** (Figure III–36 and Figure III–37) to form duplexes (very weak signals appeared at 80 mM). No variation was detected between the first and the second dilutions that were performed. $^{1}$H NMR DOSY experiments led on **B**, confirmed the presence of the same species in solution during both the first and second dispersion, as evidenced by the consistent diffusion coefficient obtained for each ($D = 3.79 \times 10^{-10}$ m$^2$s$^{-1}$, $R_h = 10.10$ Å). This value corresponds to the presence of single helical form in solution at these concentrations. These observations confirm that the foldamer skeleton alone does not play a significant role in the formation of kinetically–trapped molecules.

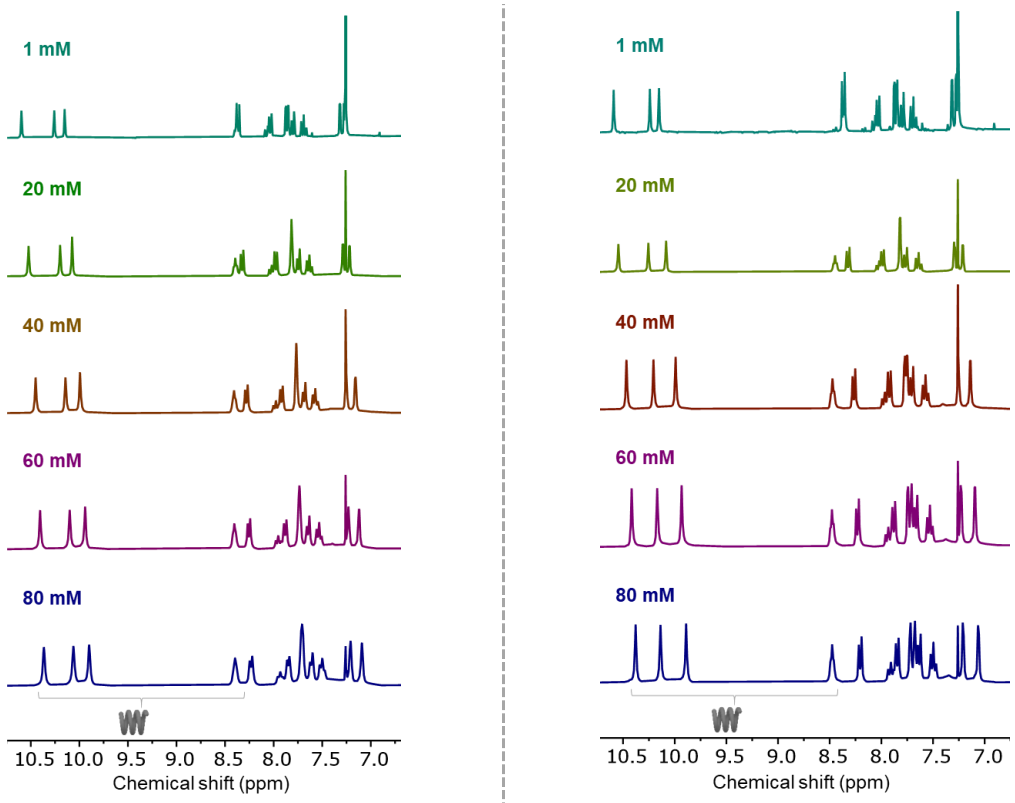


*Figure III–36. Left. First dispersion. Right. Second dispersion of foldamer **B** at 80 mM ($CDCl_3$, 298 K, 300 MHz).*

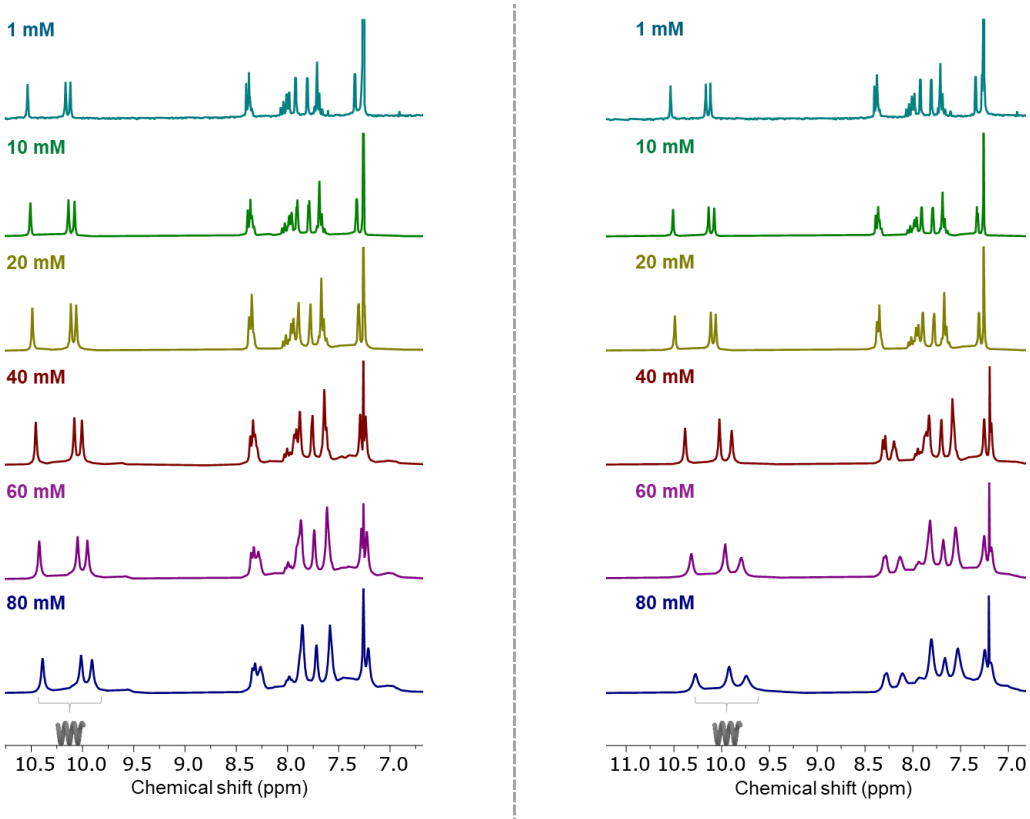


*Figure III–37. Left. First dispersion. Right. Second dispersion of foldamer **I** at 80 mM ($CDCl_3$, 298 K, 300 MHz).*

### B.3.c.iii.2) Foldamer H

The dynamics of foldamer **H** in solution was studied following the same methodology. The first dilution, conducted in $CDCl_3$, showed the presence of two sets of signals at high concentration (76.6 mM): the most intense one clearly corresponds to the single helical state, while a very broad signal at *ca* 10.2 ppm, which could be assigned to double helices, is observed but cannot be accurately integrated (Figure III–38).

Noteworthily, the $^1H$ NMR spectra recorded at high concentrations along a second dilution experiment (led with the same batch after evaporation under vacuum and dispersion in $CDCl_3$) showed the presence of two sets of signals, which correspond to single and double helices. Diluting these samples led to the disappearance of the second set of signals, which indicates that double helices get dissociated. Thereby, these experiments show that foldamer **H** did not reach the thermodynamic equilibrium in these conditions and thus, highlight the important role of triazole into the observed kinetically–trapped state.

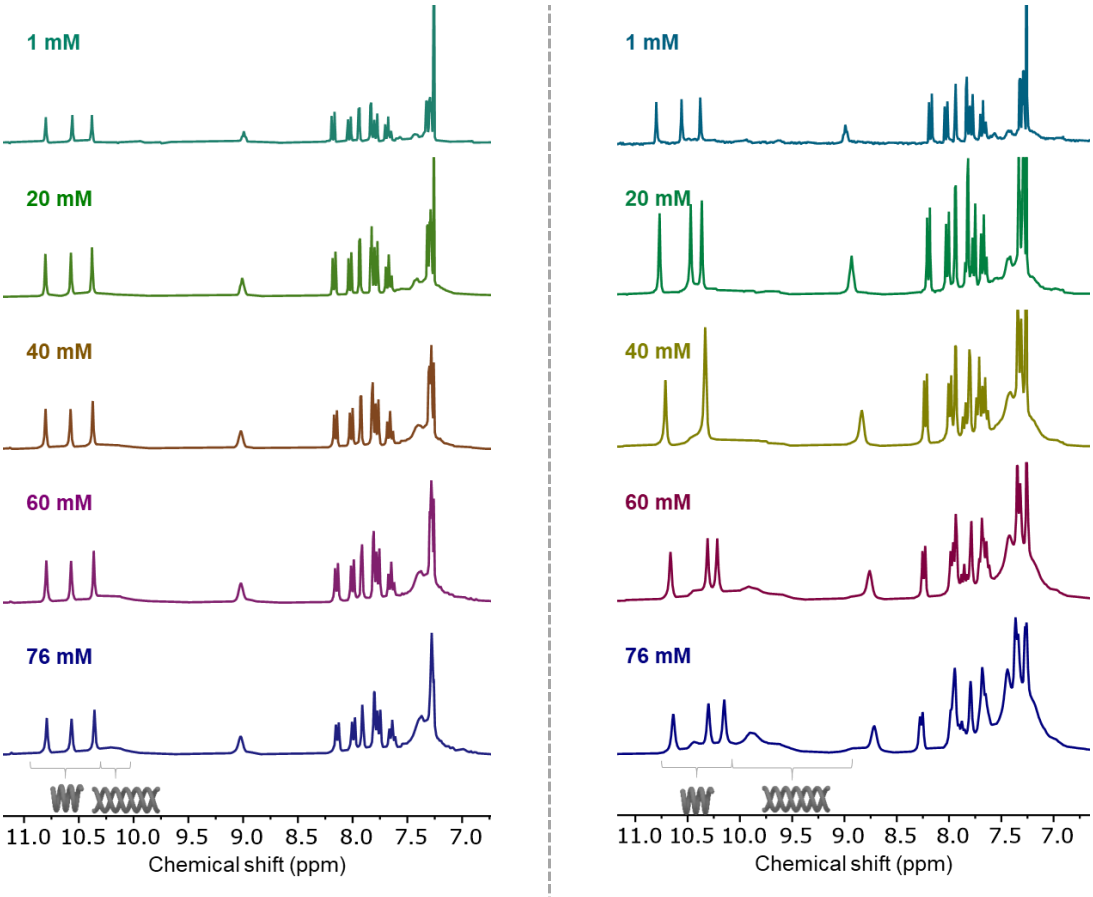


*Figure III–38. Left. First dispersion. Right. Second dispersion of foldamer **H** at 76 mM ($CDCl_3$, 298 K, 300 MHz).*

### B.3.c.iii.3) *Foldamer J and K*

• *Variable–concentration $^1$H NMR spectroscopy*

The behaviors of foldamers **J** and **K** in solution were first studied through variable–concentration $^1$H NMR experiments (80 mM, $CDCl_3$), by analogy to the previously *clicked* foldamers. Regarding foldamer **J**, no additional set of signals was observed between the first and the second dispersion experiment. Surprisingly, this foldamer did not exhibit any hybridization in either the first or the second experiment (Figure III–39). $^1$H NMR DOSY experiment shows a hydrodynamic radius (13.5 Å) comparable to that obtain for the previous foldamers as single helices. On the contrary, foldamer **K** hybridizes in both the first and the second one, with higher percentage for the double helices during the first dispersion.

These experiments led us to consider three hypotheses for foldamer **J**: 1) foldamer **J** reaches the thermodynamic equilibrium , there is no kinetically–trapped state for this foldamer and **J** displays a very weak dimerization constant; 2) foldamer **J** is kinetically–trapped in a state because of a particularly high energetical barrier, which would require high temperatures to escape from this state; 3) the hybridization equilibrium of foldamer **J** is fast at the NMR timescale, which prevents the observation of two distinct sets for single and double helices.

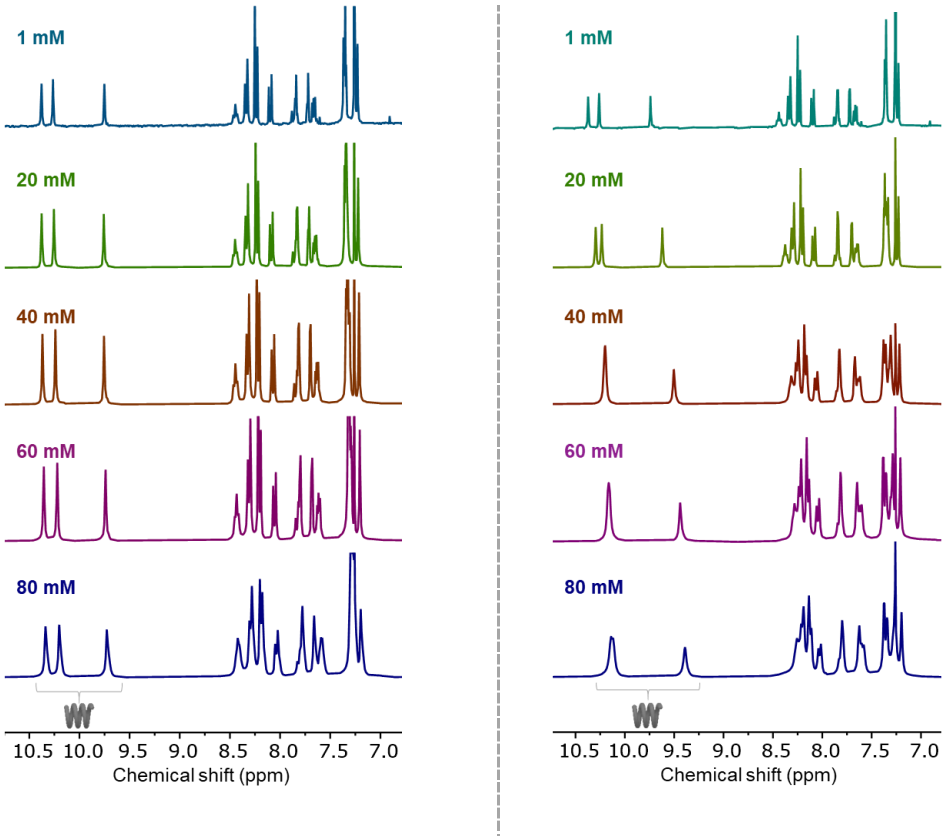


*Figure III–39. Left. First dispersion. Right. Second dispersion of foldamer **J** at 80 mM ($CDCl_3$, 298 K, 300 MHz).*

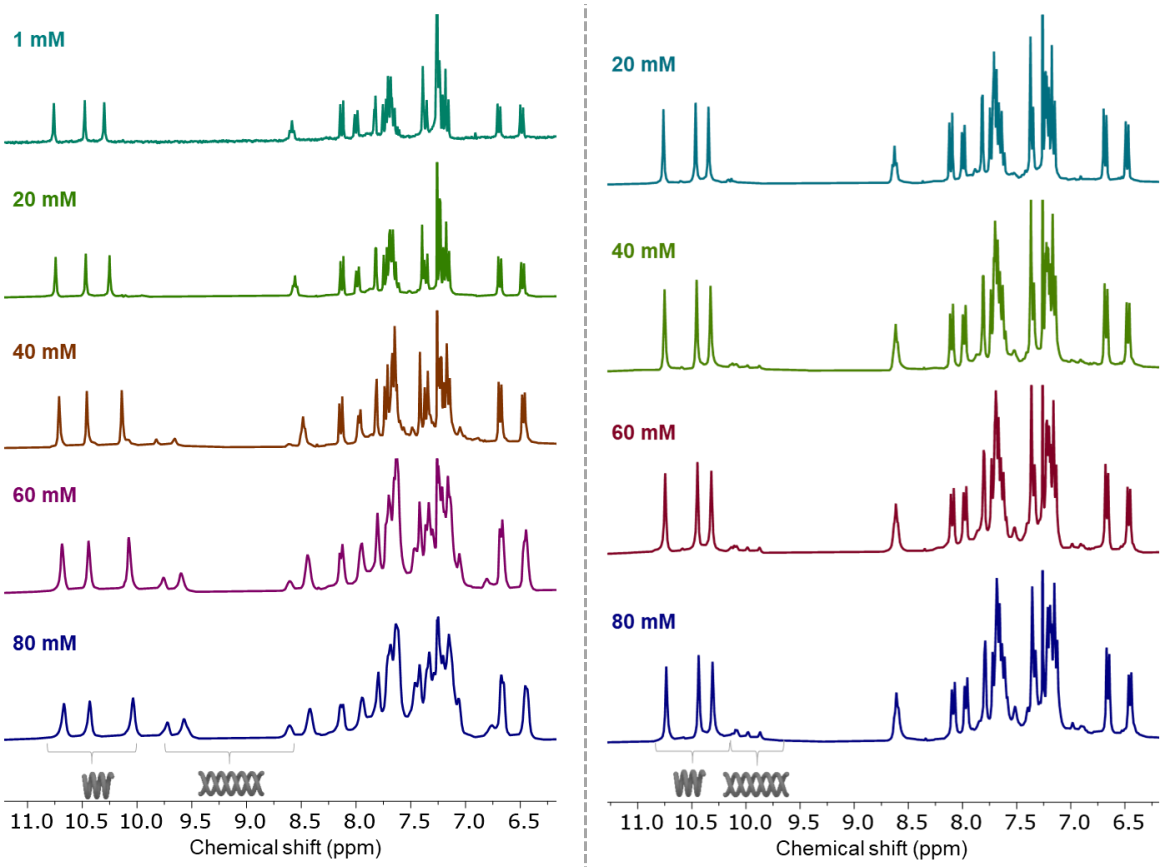


*Figure III–40. Left. First dispersion. Right. Second dispersion of foldamer **K** at 80 mM ($CDCl_3$, 298 K, 300 MHz).*

- *Impact of thermal energy*

The previous analyses were conducted using a 300 MHz NMR spectrometer. Due to the possibility of fast exchange at the NMR timescale for foldamer **J**, further studies were performed using a spectrometer displaying a higher frequency (500 MHz).

Hypothesizing that foldamer **J** could also be trapped in a kinetically–trapped state, a solution of **J** (80 mM, $CDCl_3$) was heated at 45°C for few hours and $^1$H NMR spectra were periodically recorded (Figure III–41). No significant variation was observed and specifically, no second set of signals appeared, which indicates that this foldamer did not undergo hybridization, even upon heating for hours. It is noteworthy that one amide proton (δ = 9.66 ppm) undergoes broadening upon heating. However, no variation in integration was detected. This indicates that heating to 45°C does not influence the behavior of foldamer **J** and therefore, that analyses at higher temperature may be of interest.

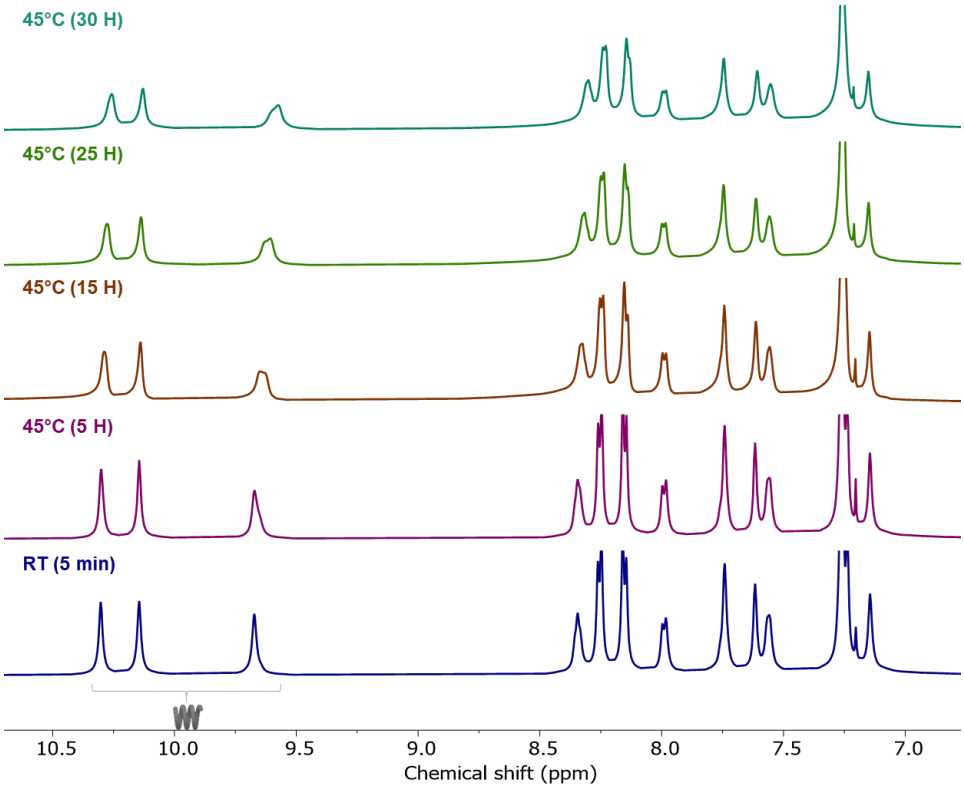


*Figure III–41. Evolution of the $^{1}H$ NMR spectra of foldamer **J** (80 mM) at 45°C as function of time ($CDCl_3$, 318 K, 500 MHz).*

In order to reach higher temperature, a solution of foldamer **J** was prepared in deuterated 1,1,2,2–tetrachloroethane at 75 mM. At 20°C, one set of signals is also observed for the amide protons. Upon heating up to 120°C, progressive variations of chemical shift (*i.e.* fast exchange) were observed, resulting either from intermolecular contacts between helical structures or between the foldamer host and water molecules. On the other hand, new signals were not observed in the 9.7–8.5 ppm range, which indicates that hybridization does not take place, even upon heating. On the contrary, new signals did appear in this range of chemical shifts at very low temperature (–20°C – Figure III–42). This suggests that double helices may be formed at low temperatures and thus, that the dimerization constant was particularly low for foldamer **J** in TCE, and/or that the single–to–double helix equilibrium is fast at the NMR timescale at room temperature. Additionally, one could consider also that this foldamer may be kinetically trapped with a very high–energy barrier, and so that, heating at 120°C in TCE is not sufficient to make the system dynamic.

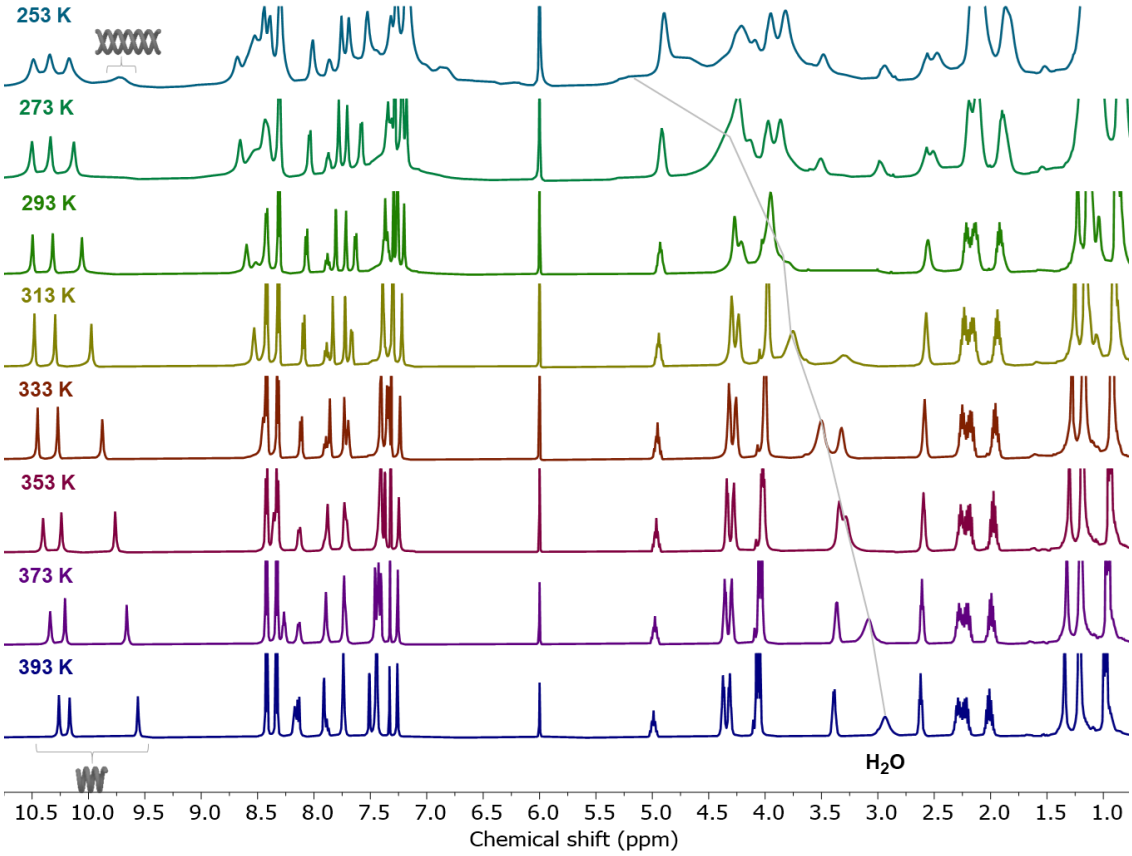


*Figure III–42. Evolution of the $^{1}H$ NMR spectra of foldamer **J** (75 mM) at different temperatures ($C_2D_2Cl_4$, 500 MHz).*

The analysis of the reference foldamers brings out significant insights, which helps understanding the behavior of these *clickable* foldamers in solution. The precursor foldamers **B** and **I** that lack both triazole and electroactive units, exhibited reproducible dilutions and the corresponding solutions were not affected by the sample preparation protocols. On the contrary, foldamer **H** is under kinetic control and its behavior depends from the sample preparation protocols.

The study of foldamers **J** and **K** demonstrates the important effect of incorporating one carbon atom to the foldamer skeleton on the behavior of this foldamer in solution. Hence, comparing foldamer **J** with one additional carbon atom to its analogous foldamer **G**, which contains the methylene linker instead of the ethylene one, highlighted the impact of the seven–membered pseudo cycle formed for foldamer **G**. This suggests that the most plausible explanation is that the triazole linker is at the origin of the kinetic trapping phenomenon. On the other hand, foldamer **J** does not exhibit any hybridization ability, which remains a puzzling observation. This might indicate that we have possibly understood the contribution of the triazole ring. Nevertheless, introducing a more flexible linker may have rendered this system

kinetically trapped through intramolecular interactions between NDI units and foldamer skeleton.

As a consequence, the formation of a seven–membered pseudo–cycle by intramolecular hydrogen bonds renders foldamers inactive as single helices, which explains the formation of a supramolecular polymer during the first dilution. Then, the heating effect breaks these intramolecular hydrogen bonds, making foldamers active and allowing the hybridization phenomenon.

# IV. Pyrene and NDI: a new pair of D–A functionalized foldamers

As explained in the introduction of Chapter 3 (§I.D.2), another donor–acceptor pair, the 'pyrene–naphthalene diimide' one, held our attention along the PhD time. This work was led in parallel to the complex physico–chemical study led with the DAN– and NDI–containing foldamers. Though much remains to be done, it appeared relevant to present the corresponding preliminary results that we consider original and exciting for the future. In our opinion, this is especially true with regard to the luminescent properties of these foldamers, which will be studied in a near future.

## A. Synthesis of pyrene–functionalized foldamer L

Azidomethylpyrene **III–28** was obtained quantitatively after nucleophilic substitution between sodium azide and the commercially available 1–(bromomethyl)pyrene in DMF. Then, copper–catalyzed azide–alkyne cycloaddition was performed between bis(alkyne) **B** and **III–28** to afford foldamer **L** with a yield of 88 % (Scheme III–21).

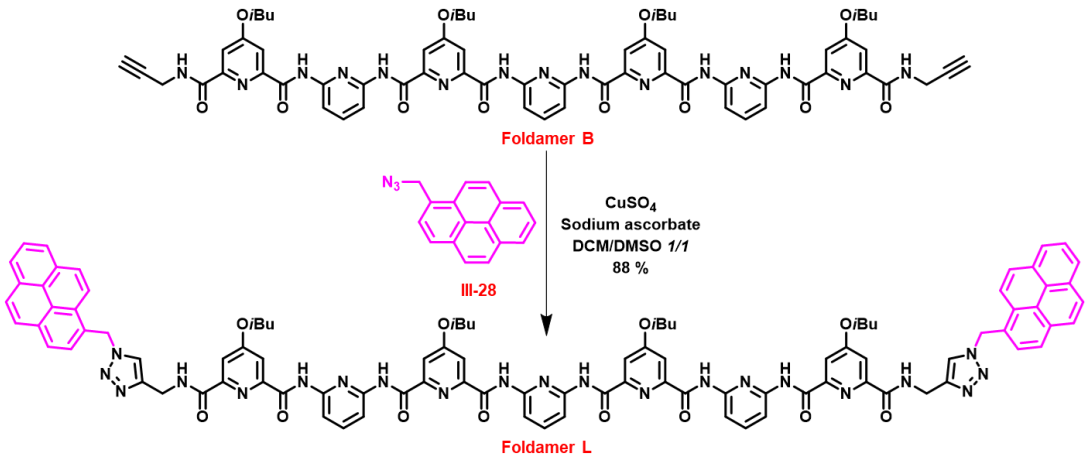


*Scheme III–21. Synthesis of foldamer **L**.*

## B. Analysis of foldamer L in solution by $^1$H NMR spectroscopy

By analogy to the analysis conducted with the above–mentioned foldamers, the first dilution of foldamer **L** shows two equilibrium at the NMR timescale: 1) a fast one indicating the formation of a supramolecular polymer through interactions between single helical structures and, 2) a slow equilibrium with the appearance of a second weak set of signals at high concentrations revealing the presence of double helices. At this stage, one will note that the concentration of double helices marginally increased along the second dilution experiment, with a percentage of double helix increasing from 31 % to 40 % (Figure III–43).

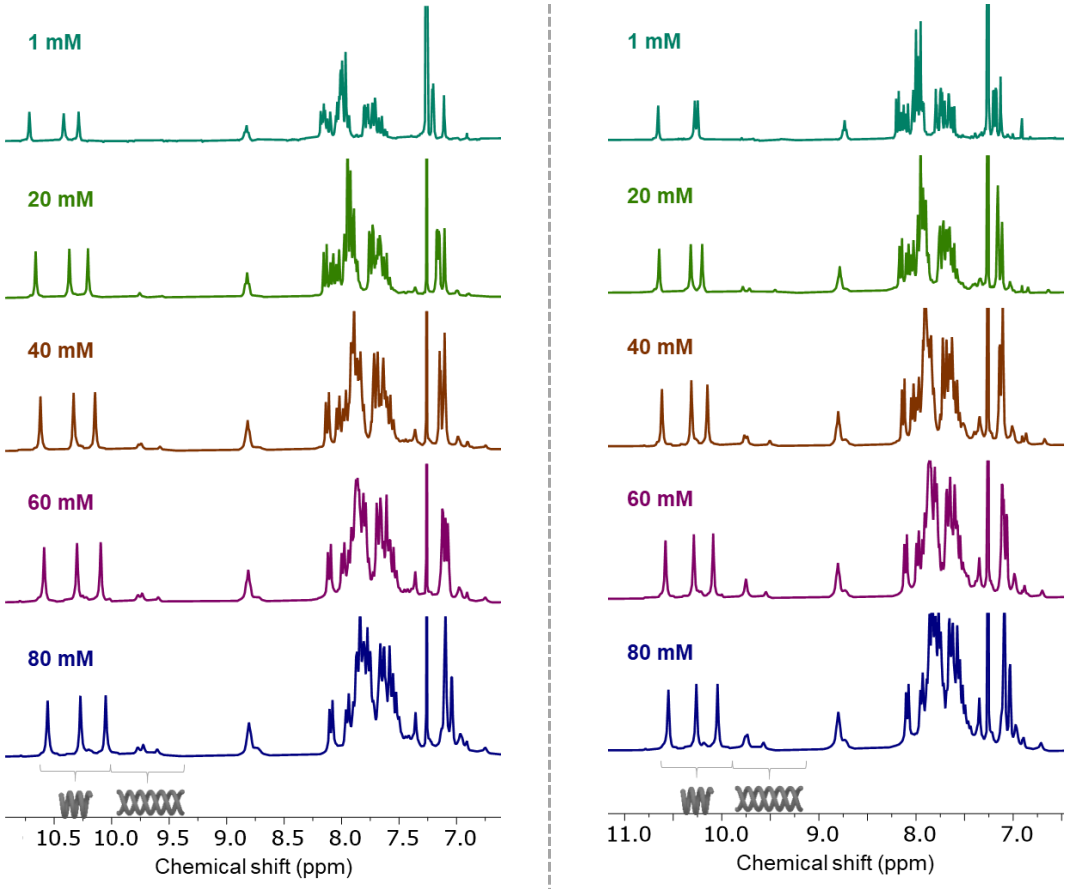


*Figure III–43. Left. First dispersion. Right. Second dispersion of foldamer **L** at 80 mM ($CDCl_3$, 298 K, 300 MHz).*

## C. Cross–hybridization between foldamers G and L

### C.1. $^1$H NMR spectroscopy

A solution of foldamers **G** (80 mM) and **L** (80 mM) was prepared in $CDCl_3$. The first dilution shows one set of signals for the amide protons, which are in a fast equilibrium at the NMR timescale. These amide signals integrate for 16 protons that correspond to the amide protons of both foldamers. These observations indicate the presence of single helices of

foldamers **G** and **L** in solution, which interact in a supramolecular polymer fashion (Figure III–44).

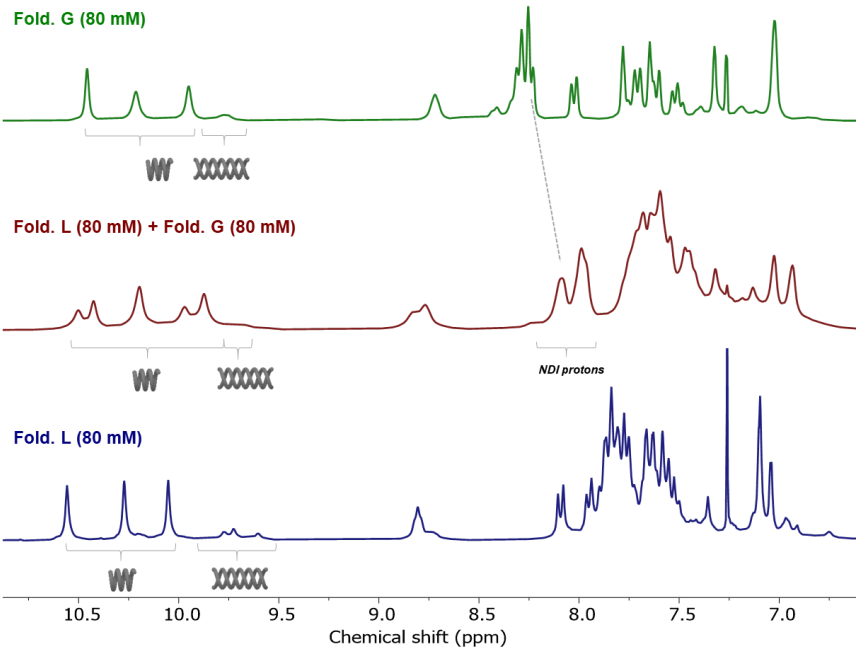


*Figure III–44. Comparison between foldamers **G** (80 mM), **L** (80 mM) and their mixture at 80 mM (1st dispersion, $CDCl_3$, 298 K, 300 MHz).*

However, the second dilution of the same sample showed important differences as expected for this set of kinetically trapped *clicked* foldamers. Indeed, a second set of signals appeared, which corresponds to the formation of double helical structures (from 6 % of double helices in the first dilution to 67 % in the second one). These signals disappeared upon dilution, which aligns with the fact that the double helices are formed generally at high concentration and dissociate into single helices at low concentrations (Figure III–45).

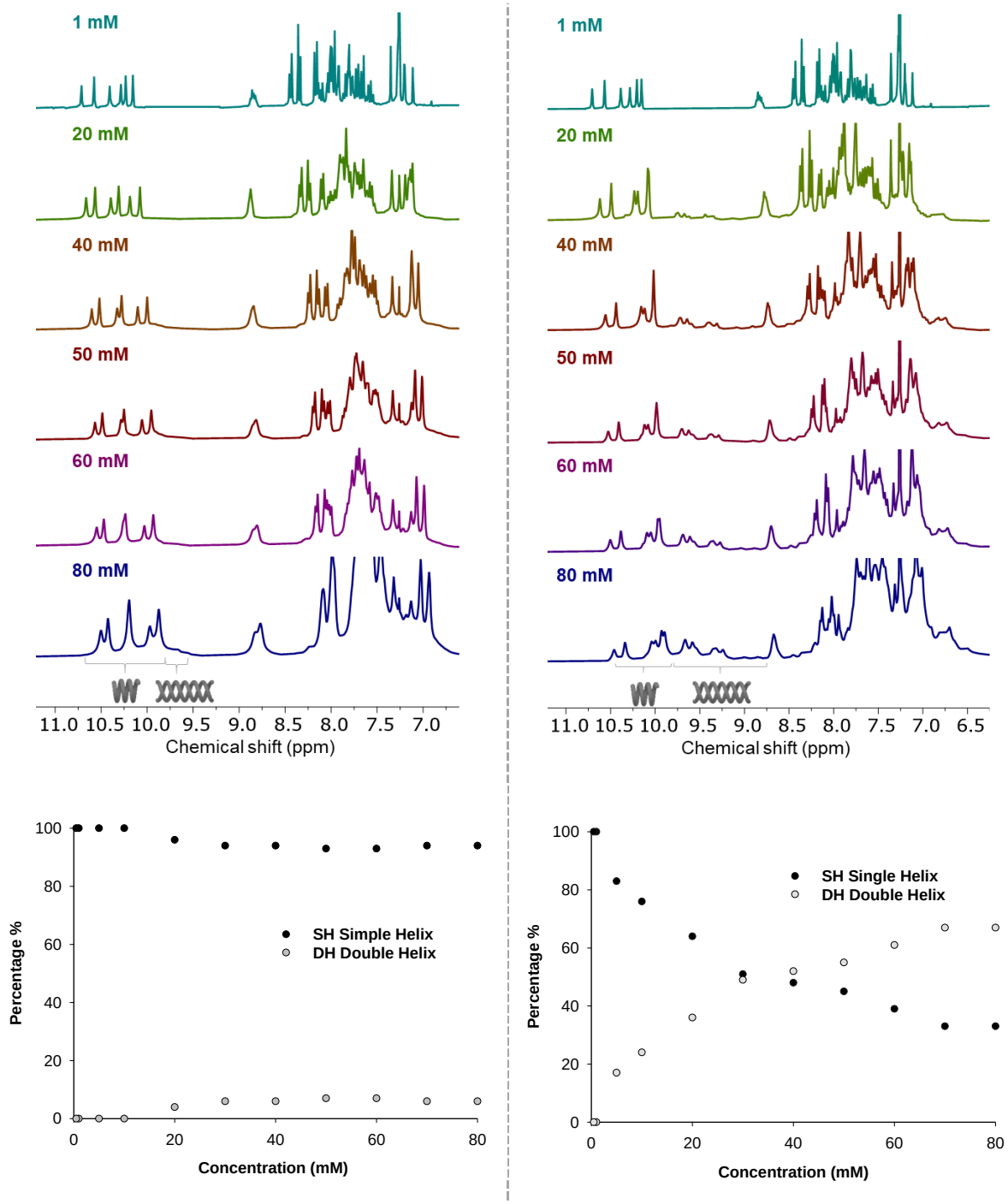


*Figure III–45. First and second dispersion of the mixture of foldamers **G** (80 mM) and **L** (80 mM) in $CDCl_3$ (298 K, 300 MHz) and comparison of the evolution of the percentage of SH vs DH as function of the concentration between the first and the second dilution.*

The comparison between the mixture and each foldamer alone demonstrated the formation of new signals (Figure III–46), which do not correspond to homoduplexes. This indicates the formation of heteroduplexes, which were also detected by ESI MS.

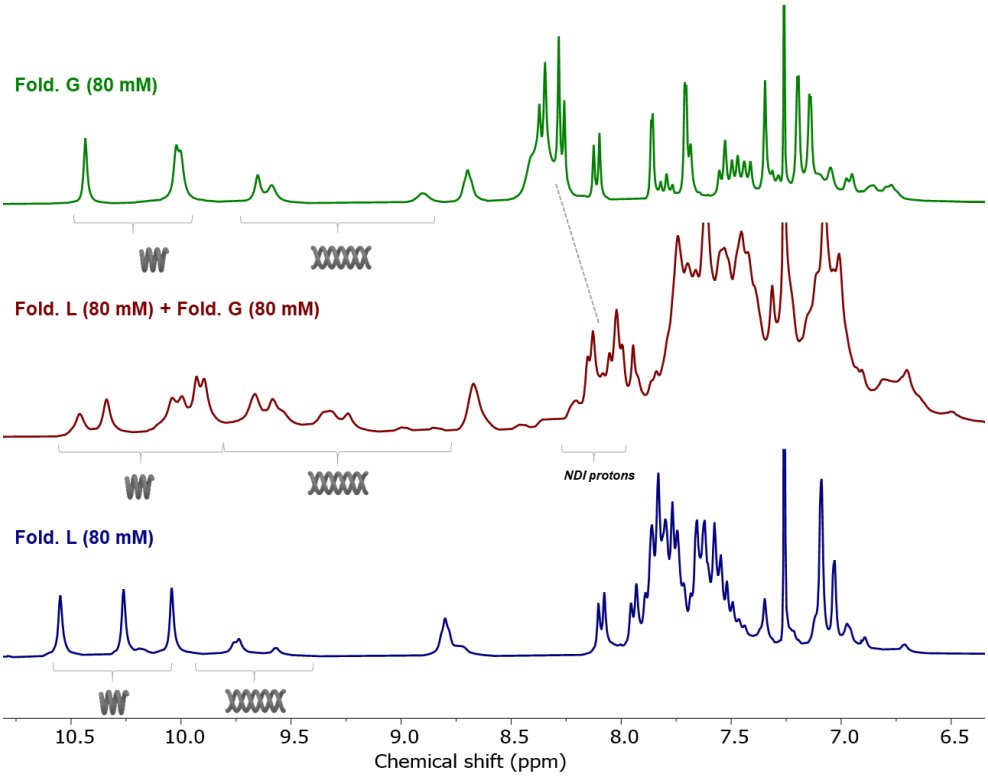


*Figure III–46. Comparison between foldamers **G**, **L** and their mixture at 80 mM ($2^{nd}$ dispersion, $CDCl_3$, 298 K, 300 MHz).*

## C.2. UV–visible absorption spectroscopy

When mixing foldamers **G** and **L**, the solution turns red, which is distinct from the individual solution color of foldamers: brown for foldamer **L** and yellow for foldamer **G** (–*Right*). The red solution demonstrates the formation of a charge transfer complex between the donor and acceptor moieties at high concentrations (60 mM) in chloroform. UV–visible absorption analyses further confirmed the presence of a new absorption band at around 520–525 nm[161] for the mixture, which was not observed for each foldamer individually (Figure III–47). This is consistent with previous reports NDI–Py CT complexes.[25,30,162–166] This absorption band confirms the formation of a charge transfer complex between the donor pyrene and the acceptor NDI along the first dispersion in chloroform. Given the conclusion drawn from $^{1}$H NMR spectroscopy measurements, this color change most likely results from a supramolecular polymerization process. Further studies will focus on the impact of time and temperature over the spectroscopic properties of these mixtures, be they containing supramolecular polymers and/or heteroduplexes.

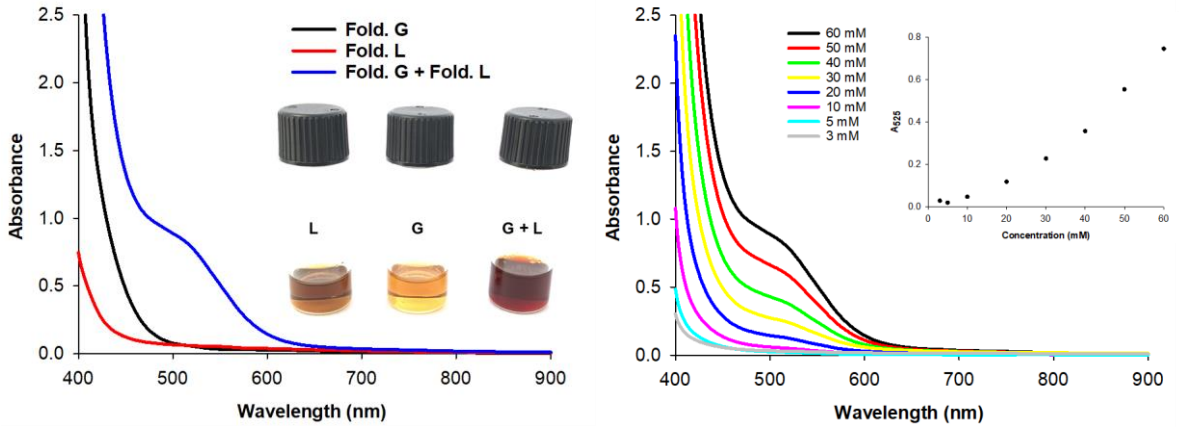


*Figure III–47. Left. UV–vis absorption spectra of foldamers **G** (60 mM), **L** (60 mM) and their mixture in $CHCl_3$ at RT; Foldamer **L** (brown color); Center. Foldamer **G** (yellow color); and the mixture of foldamer **L** and **G** (red color). Right. Evolution of the CT band upon dilution.*

# V. Conclusions

The objective of this work was to synthesize and characterize a novel generation of π–functional foldamers functionalized with electron–deficient and electron–donating chromophores in order to elaborate heteroduplexes in a selective manner. This goal was partially achieved through the preparation of a series of functionalized foldamers through copper–catalyzed azide–alkyne cycloaddition between bisalkyne **B** and azide derivatives with good yields. Noticeably, the preparation of foldamer **B** was optimized and scaled up to 1 gram (11 steps). This notably allowed for the preparation of six electroactive foldamers along this PhD work, for which three X–ray crystal structures were obtained.

Comparing TTF–containing foldamers **A** (Chapter 2) and **B** (Chapter 3), which include different linkers (amide for foldamer **A** and $–CH_2–$triazole$–CH_2–$ for foldamer **C**), showed that, in the neutral state, foldamer **A** does not hybridize and that **C** does. Thereby, this comparison highlights that the nature of the linker may greatly influence the behavior of these foldamers in solution.

This assessment was further confirmed by studying DAN– and NDI–containing foldamers **F** and **G**. Understanding their behavior proved to be particularly challenging. Indeed, their supramolecular arrangements in solution involve both supramolecular polymerization processes and hybridization into duplexes. The analyses conducted by $^1$H NMR spectroscopy revealed that they are actually under kinetic control at room temperature, which was not expected. A collection of $^1$H NMR experiments was recorded on foldamer **G** in order to determine the origin of this kinetic trapping phenomenon. These experiments showed the

critical role of temperature on the behavior of foldamers at high concentrations. To identify the non–covalent interactions responsible for these unexpected results, crystallographic structures of the obtained foldamers were thoroughly analysed and revealed the presence of an intramolecular hydrogen bond leading to the formation of a seven–membered pseudo cycle. The analysis of the reference foldamers **B** and **H** proved to be particularly valuable since it showed that the triazole linker contributes to the obtaining of a kinetically–trapped state.

Additional reference foldamers were synthesized in order to bring more insights regarding this particular issue. In this context, an ethylene spacer was installed between the triazole and the π–functional unit in foldamer **I**, in order to break the seven–membered pseudo–cycle formed by intramolecular hydrogen bonding. At the moment, we do not fully understand its behavior and further physico–chemical characterizations appear necessary.

Altogether, these results suggest that the triazole linker is responsible for the kinetic trapping. At room temperature, when mixing both foldamers, the intramolecular hydrogen bond renders the foldamers inactive as single helix, and thus favors the formation of a supramolecular polymer. However, when heating to 45°C, the intramolecular hydrogen bonds are weakened and the single helices become active, which allows the hybridization of single helices into duplexes and notably, heteroduplexes. The formation of the latter was confirmed through $^{1}$H NMR spectroscopy (observation of signals, which did not correspond to single helices or the corresponding homoduplexes), as well as by ESI mass spectrometry in the case of associations **F–G** and **G–L**.

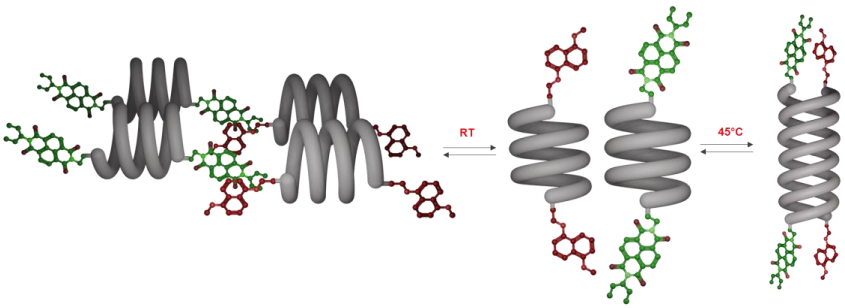


As a conclusion, we have experienced quite a chaotic path on this project. However, dedicating efforts to the understanding of this singular supramolecular behavior allowed for identifying the limitations of our design and strategy. Though we currently lack information about the selectivity, heteroduplexes were definitely obtained, which constitutes an achievement. We are now considering other grafting strategies and π–functional units to

promote the selective formation of heteroduplexes. These tracks are presented in the Conclusion and Perspectives.

(1) Qi, S.; Zhang, C.; Yan, T.; Yang, F.; Zhang, J.; Mao, S.; Dong, Z. Hybrid Helical Polymer Nanochannels Constructed by Combining Aromatic Amide and Pyridine-Oxadiazole Structural Sequences. *Macromolecular Rapid Communications* **2020**, *41* (24), 2000099.

(2) Chen, F.; Shen, J.; Li, N.; Roy, A.; Ye, R.; Ren, C.; Zeng, H. Pyridine/Oxadiazole-based Helical Foldamer Ion Channels with Exceptionally High K+/Na+ Selectivity. *Angewandte Chemie International Edition* **2020**, *59* (4), 1440–1444.

(3) Ferrand, Y.; Huc, I. Designing Helical Molecular Capsules Based on Folded Aromatic Amide Oligomers. *Accounts of Chemical Research* **2018**, *51* (4), 970–977.

(4) Girvin, Z. C.; Andrews, M. K.; Liu, X.; Gellman, S. H. Foldamer–Templated Catalysis of Macrocycle Formation. *Science* **2019**, *366* (6472), 1528–1531.

(5) Legrand, B.; Aguesseau–Kondrotas, J.; Simon, M.; Maillard, L. Catalytic Foldamers: When the Structure Guides the Function. *Catalysts* **2020**, *10* (6), 700.

(6) Das, A.; Ghosh, S. Supramolecular Assemblies by Charge-transfer Interactions between Donor and Acceptor Chromophores. *Angewandte Chemie International Edition* **2014**, *53* (8), 2038–2054.

(7) Cubberley, M. S.; Iverson, B. L. 1H NMR Investigation of Solvent Effects in Aromatic Stacking Interactions. *Journal of the American Chemical Society* **2001**, *123* (31), 7560–7563.

(8) Zych, A. J.; Iverson, B. L. Synthesis and Conformational Characterization of Tethered, Self–Complexing 1,5–Dialkoxynaphthalene/1,4,5,8–Naphthalenetetracarboxylic Diimide Systems. *Journal of the American Chemical Society* **2000**, *122* (37), 8898–8909.

(9) Martinez, C. R.; Iverson, B. L. Rethinking the Term "Pi–Stacking." *Chem. Sci.* **2012**, *3* (7), 2191–2201.

(10) Ji, X.; Ahmed, M.; Long, L.; Khashab, N. M.; Huang, F.; Sessler, J. L. Adhesive Supramolecular Polymeric Materials Constructed from Macrocycle–Based Host–Guest Interactions. *Chemical Society Reviews* **2019**, *48* (10), 2682–2697.

(11) Deepthi, K.; Amal, R. R.; Rajeev, V. R.; Unni, K. N.; Gowd, E. B. Directed Assembly of Hierarchical Supramolecular Block Copolymers: A Strategy to Create Donor–Acceptor Charge–Transfer Stacks. *Macromolecules* **2019**, *52* (7), 2889–2899.

(12) Lehn, J.–M. Towards Complex Matter: Supramolecular Chemistry and Self–Organization. *European Review* **2009**, *17* (2), 263–280.

(13) De Greef, T. F.; Smulders, M. M.; Wolffs, M.; Schenning, A. P.; Sijbesma, R. P.; Meijer, E. W. Supramolecular Polymerization. *Chemical Reviews* **2009**, *109* (11), 5687–5754.

(14) Nakanishi, T. Supramolecular Soft and Hard Materials Based on Self–Assembly Algorithms of Alkyl–Conjugated Fullerenes. *Chemical Communications* **2010**, *46* (20), 3425–3436.

(15) Tovar, J. D. Supramolecular Construction of Optoelectronic Biomaterials. *Accounts of chemical research* **2013**, *46* (7), 1527–1537.

(16) Rest, C.; Kandanelli, R.; Fernández, G. Strategies to Create Hierarchical Self–Assembled Structures via Cooperative Non–Covalent Interactions. *Chemical Society Reviews* **2015**, *44* (8), 2543–2572.

(17) Yan, X.; Wang, F.; Zheng, B.; Huang, F. Stimuli–Responsive Supramolecular Polymeric Materials. *Chemical Society Reviews* **2012**, *41* (18), 6042–6065.

(18) Chen, Z.; Lohr, A.; Saha–Möller, C. R.; Würthner, F. Self–Assembled π–Stacks of Functional Dyes in Solution: Structural and Thermodynamic Features. *Chemical Society Reviews* **2009**, *38* (2), 564–584.

(19) Würthner, F. Perylene Bisimide Dyes as Versatile Building Blocks for Functional Supramolecular Architectures. *Chemical Communications* **2004**, 14, 1564–1579.

(20) Maggini, L.; Bonifazi, D. Hierarchised Luminescent Organic Architectures: Design, Synthesis, Self–Assembly, Self–Organisation and Functions. *Chemical Society Reviews* **2012**, *41* (1), 211–241.

(21) Babu, S. S.; Praveen, V. K.; Ajayaghosh, A. Functional π–Gelators and Their Applications. *Chemical Reviews* **2014**, *114* (4), 1973–2129.

(22) Aida, T.; Meijer, E. W.; Stupp, S. I. Functional Supramolecular Polymers. *Science* **2012**, *335* (6070), 813–817.

(23) Mishra, A.; Ma, C.–Q.; Bauerle, P. Functional Oligothiophenes: Molecular Design for Multidimensional Nanoarchitectures and Their Applications. *Chemical Reviews* **2009**, *109* (3), 1141–1276.

(24) Peng, X.; Wang, L.; Chen, S. Donor–Acceptor Charge Transfer Assemblies Based on Naphthalene Diimides (NDIs). *Journal of Inclusion Phenomena and Macrocyclic Chemistry* **2021**, *99*, 131–154.

(25) Das, A.; Ghosh, S. H–Bonding Directed Programmed Supramolecular Assembly of Naphthalene–Diimide (NDI) Derivatives. *Chemical Communications* **2016**, *52* (42), 6860–6872.

(26) Amabilino, D. B.; Stoddart, J. F. Interlocked and Intertwined Structures and Superstructures. *Chemical reviews* **1995**, *95* (8), 2725–2828.

(27) Dietrich–Buchecker, C. O.; Sauvage, J. P. Interlocking of Molecular Threads: From the Statistical Approach to the Templated Synthesis of Catenands. *Chemical Reviews* **1987**, *87* (4), 795–810.

(28) Balzani, V.; Gómez–López, M.; Stoddart, J. F. Molecular Machines. *Accounts of Chemical Research* **1998**, *31* (7), 405–414.

(29) Ko, Y. H.; Kim, E.; Hwang, I.; Kim, K. Supramolecular Assemblies Built with Host–Stabilized Charge–Transfer Interactions. *Chemical Communications* **2007**, 13, 1305–1315.

(30) Das, A.; Ghosh, S. Supramolecular Assemblies by Charge-transfer Interactions between Donor and Acceptor Chromophores. *Angewandte Chemie International Edition* **2014**, *53* (8), 2038–2054.

(31) Safont–Sempere, M. M.; Fernández, G.; Würthner, F. Self–Sorting Phenomena in Complex Supramolecular Systems. *Chemical Reviews* **2011**, *111* (9), 5784–5814.

(32) Kandanelli, R.; Maitra, U. Charge–Transfer Interaction Mediated Organogels from Bile Acid Appended Anthracenes: Rheological and Microscopic Studies. *Photochemical & Photobiological Sciences* **2012**, *11* (11), 1724–1729.

(33) Peigneguy, F.; Oliveras–González, C.; Voltz, M.; Ibrahim, N.; Sallé, M.; Avarvari, N.; Canevet, D. Donor–Acceptor Organogels and Xerogels from C 3–Symmetric Pyrene and Naphthalene–Diimide Components. *Journal of Materials Chemistry C* **2022**, *10* (37), 13989–13999.

(34) Bag, B. G.; Maity, G. C.; Dinda, S. K. Donor− Acceptor Interaction Promoted Gelation: Visual Observation of Color Change. *Organic letters* **2006**, *8* (24), 5457–5460.

(35) Rizkov, D.; Gun, J.; Lev, O.; Sicsic, R.; Melman, A. Donor− Acceptor–Promoted Gelation of Polyaromatic Compounds. *Langmuir* **2005**, *21* (26), 12130–12138.

(36) Mei, X.; Ouyang, J. Electronically and Ionically Conductive Gels of Ionic Liquids and Charge–Transfer Tetrathiafulvalene–Tetracyanoquinodimethane. *Langmuir* **2011**, *27* (17), 10953–10961.

(37) áVijay Kumar, P.; D'Souza, L. First Donor–Acceptor Interaction Promoted Gelation of Organic Fluids. *Chemical Communications* **1999**, 7, 595–596.

(38) Das, A.; Molla, M. R.; Banerjee, A.; Paul, A.; Ghosh, S. Hydrogen-Bonding Directed Assembly and Gelation of Donor–Acceptor Chromophores: Supramolecular Reorganization from a Charge-Transfer State to a Self-Sorted State. *Chemistry–A European Journal* **2011**, *17* (22), 6061–6066.

(39) Das, A.; Molla, M. R.; Maity, B.; Koley, D.; Ghosh, S. Hydrogen-Bonding Induced Alternate Stacking of Donor (D) and Acceptor (A) Chromophores and Their Supramolecular Switching to Segregated States. *Chemistry–A European Journal* **2012**, *18* (32), 9849–9859.

(40) Moffat, J. R.; Smith, D. K. Metastable Two–Component Gel—Exploring the Gel–Crystal Interface. *Chemical Communications* **2008**, 19, 2248–2250.

(41) Babu, P.; Sangeetha, N. M.; Vijaykumar, P.; Maitra, U.; Rissanen, K.; Raju, A. R. Pyrene-Derived Novel One-and Two-Component Organogelators. *Chemistry–A European Journal* **2003**, *9* (9), 1922–1932.

(42) Das, R. K.; Banerjee, S.; Raffy, G.; Del Guerzo, A.; Desvergne, J.–P.; Maitra, U. Spectroscopic, Microscopic and First Rheological Investigations in Charge–Transfer Interaction Induced Organogels. *Journal of Materials Chemistry* **2010**, *20* (34), 7227–7235.

(43) Liu, Y.; Zheng, N.; Li, H.; Yin, B. Supramolecular Gels Based on Monopyrrolotetrathiafulvalene and Its TCNQ Charge–Transfer Complex. *Soft Matter* **2013**, *9* (21), 5261–5269.

(44) Gainar, A.; Lai, T.; Oliveras-González, C.; Pop, F.; Raynal, M.; Isare, B.; Bouteiller, L.; Linares, M.; Canevet, D.; Avarvari, N. Tuning the Organogelating and Spectroscopic Properties of a C3-Symmetric Pyrene-Based Gelator through Charge Transfer. *Chemistry–A European Journal* **2021**, *27* (7), 2410–2420.

(45) Rao, K. V.; Jayaramulu, K.; Maji, T. K.; George, S. J. Supramolecular Hydrogels and High-aspect-ratio Nanofibers through Charge-transfer-induced Alternate Coassembly. *Angewandte Chemie* **2010**, *122* (25), 4314–4318.

(46) Wang, C.; Wang, Z.; Zhang, X. Amphiphilic Building Blocks for Self–Assembly: From Amphiphiles to Supra–Amphiphiles. *Accounts of Chemical Research* **2012**, *45* (4), 608–618.

(47) Molla, M. R.; Ghosh, S. Aqueous Self–Assembly of Chromophore–Conjugated Amphiphiles. *Physical Chemistry Chemical Physics* **2014**, *16* (48), 26672–26683.

(48) Molla, M. R.; Ghosh, S. Hydrogen-Bonding-Mediated Vesicular Assembly of Functionalized Naphthalene–Diimide-Based Bolaamphiphile and Guest-Induced Gelation in Water. *Chemistry–A European Journal* **2012**, *18* (32), 9860–9869.

(49) Chakraborty, S.; Ray, D.; Aswal, V. K.; Ghosh, S. Multi-Stimuli-Responsive Directional Assembly of an Amphiphilic Donor–Acceptor Alternating Supramolecular Copolymer. *Chemistry–A European Journal* **2018**, *24* (61), 16379–16387.

(50) Liu, K.; Yao, Y.; Liu, Y.; Wang, C.; Li, Z.; Zhang, X. Self–Assembly of Supra–Amphiphiles Based on Dual Charge–Transfer Interactions: From Nanosheets to Nanofibers. *Langmuir* **2012**, *28* (29), 10697–10702.

(51) Molla, M. R.; Das, A.; Ghosh, S. Self-Sorted Assembly in a Mixture of Donor and Acceptor Chromophores. *Chemistry–A European Journal* **2010**, *16* (33), 10084–10093.

(52) Wang, C.; Guo, Y.; Wang, Z.; Zhang, X. Superamphiphiles Based on Charge Transfer Complex: Controllable Hierarchical Self–Assembly of Nanoribbons. *Langmuir* **2010**, *26* (18), 14509–14511.

(53) Liu, K.; Wang, C.; Li, Z.; Zhang, X. Superamphiphiles Based on Directional Charge-transfer Interactions: From Supramolecular Engineering to Well-defined Nanostructures. *Angewandte Chemie International Edition* **2011**, *50* (21), 4952–4956.

(54) Rao, K. V.; George, S. J. Supramolecular Alternate Co-Assembly through a Non-Covalent Amphiphilic Design: Conducting Nanotubes with a Mixed D–A Structure. *Chemistry–A European Journal* **2012**, *18* (45), 14286–14291.

(55) Zhang, X.; Wang, C. Supramolecular Amphiphiles. *Chemical Society Reviews* **2011**, *40* (1), 94–101.

(56) Wang, C.; Guo, Y.; Wang, Y.; Xu, H.; Wang, R.; Zhang, X. Supramolecular Amphiphiles Based on a Water-Soluble Charge-Transfer Complex: Fabrication of Ultralong Nanofibers with Tunable Straightness. *Angewandte Chemie International Edition* **2009**, *48* (47), 8962–8965.

(57) Evans, D. F.; Wennerström, H. The Colloidal Domain: Where Physics, Chemistry, Biology, and Technology Meet. **1999**.

(58) Burattini, S.; Greenland, B. W.; Merino, D. H.; Weng, W.; Seppala, J.; Colquhoun, H. M.; Hayes, W.; Mackay, M. E.; Hamley, I. W.; Rowan, S. J. A Healable Supramolecular Polymer Blend Based on Aromatic Π− π Stacking and Hydrogen–Bonding Interactions. *Journal of the American Chemical Society* **2010**, *132* (34), 12051–12058.

(59) Burattini, S.; Colquhoun, H. M.; Fox, J. D.; Friedmann, D.; Greenland, B. W.; Harris, P. J.; Hayes, W.; Mackay, M. E.; Rowan, S. J. A Self–Repairing, Supramolecular Polymer System: Healability as a Consequence of Donor–Acceptor π–π Stacking Interactions. *Chemical Communications* **2009**, 44, 6717–6719.

(60) Burattini, S.; Greenland, B. W.; Hayes, W.; Mackay, M. E.; Rowan, S. J.; Colquhoun, H. M. A Supramolecular Polymer Based on Tweezer–Type Π− π Stacking Interactions: Molecular Design for Healability and Enhanced Toughness. *Chemistry of Materials* **2011**, *23* (1), 6–8.

(61) Fox, J.; Wie, J. J.; Greenland, B. W.; Burattini, S.; Hayes, W.; Colquhoun, H. M.; Mackay, M. E.; Rowan, S. J. High–Strength, Healable, Supramolecular Polymer Nanocomposites. *Journal of the American Chemical Society* **2012**, *134* (11), 5362–5368.

(62) Narasimha, K. Macromolecular Effect Stabilized Color–Tunable and Room Temperature Charge–Transfer Complexes Based on Donor–Acceptor Assemblies. *ACS Applied Polymer Materials* **2020**, *2* (3), 1145–1159.

(63) Jalani, K.; Kumar, M.; George, S. J. Mixed Donor–Acceptor Charge–Transfer Stacks Formed via Hierarchical Self–Assembly of a Non–Covalent Amphiphilic Foldamer. *Chemical Communications* **2013**, *49* (45), 5174–5176.

(64) Hart, L. R.; Hunter, J. H.; Nguyen, N. A.; Harries, J. L.; Greenland, B. W.; Mackay, M. E.; Colquhoun, H. M.; Hayes, W. Multivalency in Healable Supramolecular Polymers: The Effect of Supramolecular Cross–Link Density on the Mechanical Properties and Healing of Non–Covalent Polymer Networks. *Polymer Chemistry* **2014**, *5* (11), 3680–3688.

(65) Greenland, B. W.; Bird, M. B.; Burattini, S.; Cramer, R.; O'Reilly, R. K.; Patterson, J. P.; Hayes, W.; Cardin, C. J.; Colquhoun, H. M. Mutual Binding of Polymer End–Groups by Complementary π–π–Stacking: A Molecular "Roman Handshake." *Chemical Communications* **2013**, *49* (5), 454–456.

(66) Parker, M. P.; Murray, C. A.; Hart, L. R.; Greenland, B. W.; Hayes, W.; Cardin, C. J.; Colquhoun, H. M. Mutual Complexation between π–π Stacked Molecular Tweezers. *Crystal Growth & Design* **2018**, *18* (1), 386–392.

(67) Bradford, V. J.; Iverson, B. L. Amyloid–like Behavior in Abiotic, Amphiphilic Foldamers. *Journal of the American Chemical Society* **2008**, *130* (4), 1517–1524.

(68) Gabriel, G. J.; Iverson, B. L. Aromatic Oligomers That Form Hetero Duplexes in Aqueous Solution. *Journal of the American Chemical Society* **2002**, *124* (51), 15174–15175.

(69) Gabriel, G. J.; Sorey, S.; Iverson, B. L. Altering the Folding Patterns of Naphthyl Trimers. *Journal of the American Chemical Society* **2005**, *127* (8), 2637–2640.

(70) Scott Lokey, R.; Iverson, B. L. Synthetic Molecules That Fold into a Pleated Secondary Structure in Solution. *Nature* **1995**, *375* (6529), 303–305.

(71) Wang, X.; Wicher, B.; Ferrand, Y.; Huc, I. Orchestrating Directional Molecular Motions: Kinetically Controlled Supramolecular Pathways of a Helical Host on Rodlike Guests. *Journal of the American Chemical Society* **2017**, *139* (27), 9350–9358.

(72) Hua, Y.; Liu, Y.; Chen, C.–H.; Flood, A. H. Hydrophobic Collapse of Foldamer Capsules Drives Picomolar–Level Chloride Binding in Aqueous Acetonitrile Solutions. *Journal of the American Chemical Society* **2013**, *135* (38), 14401–14412.

(73) Hasegawa, T.; Furusho, Y.; Katagiri, H.; Yashima, E. Enantioselective Synthesis of Complementary Double-helical Molecules That Catalyze Asymmetric Reactions. *Angewandte Chemie International Edition* **2007**, *46* (31), 5885–5888.

(74) Guichard, G.; Huc, I. Synthetic Foldamers. *Chem. Commun.* **2011**, *47* (21), 5933–5941.

(75) Huisgen, R. 1, 3-dipolar Cycloadditions. Past and Future. *Angewandte Chemie International Edition in English* **1963**, *2* (10), 565–598.

(76) Rostovtsev, V. V.; Green, L. G.; Fokin, V. V.; Sharpless, K. B. A Stepwise Huisgen Cycloaddition Process: Copper (I)-catalyzed Regioselective "Ligation" of Azides and Terminal Alkynes. *Angewandte Chemie* **2002**, *114* (14), 2708–2711.

(77) Tornøe, C. W.; Christensen, C.; Meldal, M. Peptidotriazoles on Solid Phase:[1, 2, 3]–Triazoles by Regiospecific Copper (I)–Catalyzed 1, 3–Dipolar Cycloadditions of Terminal Alkynes to Azides. *The Journal of Organic Chemistry* **2002**, *67* (9), 3057–3064.

(78) Berionni, G.; Goncalves, A.–M.; Mathieu, C.; Devic, T.; Etchéberry, A.; Goumont, R. Electrochemical and Spectrophotometrical Investigation of the Electron–Accepting Strength of Organic Superelectrophiles: X–Ray Structure of Their Charge Transfer Complexes with Tetrathiafulvalene. *Physical Chemistry Chemical Physics* **2011**, *13* (7), 2857–2869.

(79) Reinheimer, E. W.; Galán–Mascarós, J. R.; Dunbar, K. R. Synthesis and Structure of Charge Transfer Salts of Tetrathiafulvalene (TTF) and Tetramethyl–TTF with 2, 4, 7–Trinitro and 2, 4, 5, 7–Tetranitro–9–Fluorenone. *Synthetic Metals* **2009**, *159* (1–2), 45–51.

(80) Salmerón–Valverde, A.; Bernès, S. Crystal Growth and Characterization of Solvated Organic Charge–Transfer Complexes Built on TTF and 9–Dicyanomethylenefluorene Derivatives. *CrystEngComm* **2015**, *17* (32), 6227–6235.

(81) Das, A.; Molla, M. R.; Maity, B.; Koley, D.; Ghosh, S. Hydrogen–Bonding Induced Alternate Stacking of Donor (D) and Acceptor (A) Chromophores and Their Supramolecular Switching to Segregated States. *Chemistry – A European Journal* **2012**, *18* (32), 9849–9859.

(82) Al Kobaisi, M.; Bhosale, S. V.; Latham, K.; Raynor, A. M.; Bhosale, S. V. Functional Naphthalene Diimides: Synthesis, Properties, and Applications. *Chemical Reviews* **2016**, *116* (19), 11685–11796.

(83) Das, A.; Ghosh, S. H–Bonding Directed Programmed Supramolecular Assembly of Naphthalene–Diimide (NDI) Derivatives. *Chemical Communications* **2016**, *52* (42), 6860–6872.

(84) Welford, A.; Maniam, S.; Gann, E.; Jiao, X.; Thomsen, L.; Langford, S. J.; McNeill, C. R. Influence of Alkyl Side–Chain Type and Length on the Thin Film Microstructure and OFET Performance of Naphthalene Diimide–Based Organic Semiconductors. *Organic Electronics* **2019**, *75*, 105378.

(85) Sikder, A.; Ray, D.; Aswal, V. K.; Ghosh, S. Supramolecular Assembly of a Molecularly Engineered Protein and Polymer. *Chemistry–A European Journal* **2019**, *25* (44), 10464–10471.

(86) Reczek, J. J.; Villazor, K. R.; Lynch, V.; Swager, T. M.; Iverson, B. L. Tunable Columnar Mesophases Utilizing C2 Symmetric Aromatic Donor−Acceptor Complexes. *Journal of the American Chemical Society* **2006**, *128* (24), 7995–8002. https://doi.org/10.1021/ja061649s.

(87) Berl, V.; Huc, I.; Khoury, R. G.; Lehn, J.–M. Helical Molecular Programming: Folding of Oligopyridine-dicarboxamides into Molecular Single Helices. *Chemistry–A European Journal* **2001**, *7* (13), 2798–2809.

(88) Berl, V.; Huc, I.; Khoury, R. G.; Lehn, J.–M. Helical Molecular Programming: Supramolecular Double Helices by Dimerization of Helical Oligopyridine-dicarboxamide Strands. *Chemistry–A European Journal* **2001**, *7* (13), 2810–2820.

(89) Baptiste, B.; Zhu, J.; Haldar, D.; Kauffmann, B.; Léger, J.–M.; Huc, I. Hybridization of Long Pyridine-Dicarboxamide Oligomers into Multi-Turn Double Helices: Slow Strand Association and Dissociation, Solvent Dependence, and Solid State Structures. *Chemistry–An Asian Journal* **2010**, *5* (6), 1364–1375.

(90) Ikkanda, B. A.; Iverson, B. L. Exploiting the Interactions of Aromatic Units for Folding and Assembly in Aqueous Environments. *Chem. Commun.* **2016**, *52* (50), 7752–7759. https://doi.org/10.1039/C6CC01861K.

(91) Haldar, D.; Jiang, H.; Léger, J.–M.; Huc, I. Double versus Single Helical Structures of Oligopyridine–Dicarboxamide Strands. Part 2: The Role of Side Chains. *Tetrahedron* **2007**, *63* (27), 6322–6330.

(92) Haldar, D.; Jiang, H.; Léger, J.–M.; Huc, I. Interstrand Interactions between Side Chains in a Double-Helical Foldamer. *Angewandte Chemie* **2006**, *118* (33), 5609–5612.

(93) Kulikov, O. V.; Thompson, S.; Xu, H.; Incarvito, C. D.; Scott, R. T.; Saraogi, I.; Nevola, L.; Hamilton, A. D. Design and Synthesis of Oligoamide-based Double A-helix Mimetics. *European Journal of Organic Chemistry* **2013**, *2013* (17), 3433–3445.

(94) Montalbetti, C. A.; Falque, V. Amide Bond Formation and Peptide Coupling. *Tetrahedron* **2005**, *61* (46), 10827–10852.

(95) Berl, V.; Huc, I.; Khoury, R. G.; Lehn, J.–M. Helical Molecular Programming: Supramolecular Double Helices by Dimerization of Helical Oligopyridine-dicarboxamide Strands. *Chemistry–A European Journal* **2001**, *7* (13), 2810–2820.

(96) Faour, L. Architectures Stimulables à Base de Foldamères Photo–et Électroactifs, Université d'Angers, 2018.

(97) Garin, J.; Orduna, J.; Uriel, S.; Moore, A. J.; Bryce, M. R.; Wegener, S.; Yufit, D. S.; Howard, J. A. Improved Syntheses of Carboxytetrathiafulvalene, Formyltetrathiafulvalene and (Hydroxymethyl) Tetrathiafulvalene: Versatile Building Blocks for New Functionalised Tetrathiafulvalene Derivatives. *Synthesis* **1994**, *1994* (05), 489–493.

(98) Kaminska, I.; Barras, A.; Coffinier, Y.; Lisowski, W.; Roy, S.; Niedziolka–Jonsson, J.; Woisel, P.; Lyskawa, J.; Opallo, M.; Siriwardena, A. Preparation of a Responsive Carbohydrate–Coated Biointerface Based on Graphene/Azido–Terminated Tetrathiafulvalene Nanohybrid Material. *ACS applied materials & interfaces* **2012**, *4* (10), 5386–5393.

(99) Percec, V.; Imam, M. R.; Peterca, M.; Wilson, D. A.; Graf, R.; Spiess, H. W.; Balagurusamy, V. S.; Heiney, P. A. Self–Assembly of Dendronized Triphenylenes into Helical Pyramidal Columns and Chiral Spheres. *Journal of the American Chemical Society* **2009**, *131* (22), 7662–7677.

(100) Sanders, A. M.; Magnanelli, T. J.; Bragg, A. E.; Tovar, J. D. Photoinduced Electron Transfer within Supramolecular Donor–Acceptor Peptide Nanostructures under Aqueous Conditions. *Journal of the American Chemical Society* **2016**, *138* (10), 3362–3370.

(101) Hunter, C. A.; Sanders, J. K. The Nature of. Pi.–. Pi. Interactions. *Journal of the American Chemical Society* **1990**, *112* (14), 5525–5534.

(102) Berl, V.; Huc, I.; Khoury, R. G.; Lehn, J.–M. Helical Molecular Programming: Folding of Oligopyridine-dicarboxamides into Molecular Single Helices. *Chemistry–A European Journal* **2001**, *7* (13), 2798–2809.

(103) Das, A.; Molla, M. R.; Banerjee, A.; Paul, A.; Ghosh, S. Hydrogen-Bonding Directed Assembly and Gelation of Donor–Acceptor Chromophores: Supramolecular Reorganization from a Charge-Transfer State to a Self-Sorted State. *Chemistry–A European Journal* **2011**, *17* (22), 6061–6066.

(104) Das, A.; Ghosh, S. Supramolecular Assemblies by Charge-transfer Interactions between Donor and Acceptor Chromophores. *Angewandte Chemie International Edition* **2014**, *53* (8), 2038–2054.

(105) Reczek, J. J.; Villazor, K. R.; Lynch, V.; Swager, T. M.; Iverson, B. L. Tunable Columnar Mesophases Utilizing C2 Symmetric Aromatic Donor− Acceptor Complexes. *Journal of the American Chemical Society* **2006**, *128* (24), 7995–8002.
(106) Ikkanda, B. A.; Iverson, B. L. Exploiting the Interactions of Aromatic Units for Folding and Assembly in Aqueous Environments. *Chemical Communications* **2016**, *52* (50), 7752–7759.
(107) Das, A.; Molla, M. R.; Maity, B.; Koley, D.; Ghosh, S. Hydrogen-Bonding Induced Alternate Stacking of Donor (D) and Acceptor (A) Chromophores and Their Supramolecular Switching to Segregated States. *Chemistry–A European Journal* **2012**, *18* (32), 9849–9859.
(108) Berl, V.; Huc, I.; Khoury, R. G.; Krische, M. J.; Lehn, J.–M. Interconversion of Single and Double Helices Formed from Synthetic Molecular Strands. *Nature* **2000**, *407* (6805), 720–723.
(109) Sorrenti, A.; Leira–Iglesias, J.; Markvoort, A. J.; de Greef, T. F.; Hermans, T. M. Non–Equilibrium Supramolecular Polymerization. *Chemical Society Reviews* **2017**, *46* (18), 5476–5490.
(110) Chen, H.; Huang, Z.; Wu, H.; Xu, J.–F.; Zhang, X. Supramolecular Polymerization Controlled through Kinetic Trapping. *Angewandte Chemie International Edition* **2017**, *56* (52), 16575–16578.
(111) Wehner, M.; Würthner, F. Supramolecular Polymerization through Kinetic Pathway Control and Living Chain Growth. *Nature Reviews Chemistry* **2020**, *4* (1), 38–53.
(112) Coste, M.; Suárez–Picado, E.; Ulrich, S. Hierarchical Self–Assembly of Aromatic Peptide Conjugates into Supramolecular Polymers: It Takes Two to Tango. *Chemical Science* **2022**, *13* (4), 909–933.
(113) Korevaar, P. A.; George, S. J.; Markvoort, A. J.; Smulders, M. M.; Hilbers, P. A.; Schenning, A. P.; De Greef, T. F.; Meijer, E. W. Pathway Complexity in Supramolecular Polymerization. *Nature* **2012**, *481* (7382), 492–496.
(114) Haedler, A. T.; Meskers, S. C.; Zha, R. H.; Kivala, M.; Schmidt, H.–W.; Meijer, E. W. Pathway Complexity in the Enantioselective Self–Assembly of Functional Carbonyl–Bridged Triarylamine Trisamides. *Journal of the American Chemical Society* **2016**, *138* (33), 10539–10545.
(115) Korevaar, P. A.; de Greef, T. F.; Meijer, E. W. Pathway Complexity in π–Conjugated Materials. *Chemistry of Materials* **2014**, *26* (1), 576–586.
(116) Matern, J.; Dorca, Y.; Sánchez, L.; Fernández, G. Revising Complex Supramolecular Polymerization under Kinetic and Thermodynamic Control. *Angewandte Chemie International Edition* **2019**, *58* (47), 16730–16740.
(117) Pezzato, C.; Cheng, C.; Stoddart, J. F.; Astumian, R. D. Mastering the Non–Equilibrium Assembly and Operation of Molecular Machines. *Chemical Society Reviews* **2017**, *46* (18), 5491–5507.
(118) Lehn, J.–M. From Supramolecular Chemistry towards Constitutional Dynamic Chemistry and Adaptive Chemistry. *Chemical Society Reviews* **2007**, *36* (2), 151–160.
(119) Lehn, J.–M. Perspectives in Chemistry—Steps towards Complex Matter. *Angewandte Chemie International Edition* **2013**, *52* (10), 2836–2850.
(120) Lehn, J.–M. Supramolecular Chemistry—Scope and Perspectives Molecules, Supermolecules, and Molecular Devices (Nobel Lecture). *Angewandte Chemie International Edition in English* **1988**, *27* (1), 89–112.
(121) Lehn, J.–M. Toward Self–Organization and Complex Matter. *Science* **2002**, *295* (5564), 2400–2403.
(122) Lehn, J.–M. Towards Complex Matter: Supramolecular Chemistry and Self–Organization. *European Review* **2009**, *17* (2), 263–280.
(123) Krieg, E.; Weissman, H.; Shimoni, E.; Bar On, A.; Rybtchinski, B. Understanding the Effect of Fluorocarbons in Aqueous Supramolecular Polymerization: Ultrastrong Noncovalent Binding and Cooperativity. *Journal of the American Chemical Society* **2014**, *136* (26), 9443–9452.
(124) Kim, J.–K.; Lee, E.; Kim, M.–C.; Sim, E.; Lee, M. Reversible Transformation of Helical Coils and Straight Rods in Cylindrical Assembly of Elliptical Macrocycles. *Journal of the American Chemical Society* **2009**, *131* (49), 17768–17770.
(125) Tidhar, Y.; Weissman, H.; Wolf, S. G.; Gulino, A.; Rybtchinski, B. Pathway-dependent Self-assembly of Perylene Diimide/Peptide Conjugates in Aqueous Medium. *Chemistry–A European Journal* **2011**, *17* (22), 6068–6075.
(126) Bae, J.; Choi, J.–H.; Yoo, Y.–S.; Oh, N.–K.; Kim, B.–S.; Lee, M. Helical Nanofibers from Aqueous Self–Assembly of an Oligo (p–Phenylene)–Based Molecular Dumbbell. *Journal of the American Chemical Society* **2005**, *127* (27), 9668–9669.
(127) Cohen, E.; Weissman, H.; Pinkas, I.; Shimoni, E.; Rehak, P.; Král, P.; Rybtchinski, B. Controlled Self–Assembly of Photofunctional Supramolecular Nanotubes. *ACS nano* **2018**, *12* (1), 317–326.
(128) Fukui, T.; Kawai, S.; Fujinuma, S.; Matsushita, Y.; Yasuda, T.; Sakurai, T.; Seki, S.; Takeuchi, M.; Sugiyasu, K. Control over Differentiation of a Metastable Supramolecular Assembly in One and Two Dimensions. *Nature chemistry* **2017**, *9* (5), 493–499.
(129) Helmers, I.; Shen, B.; Kartha, K. K.; Albuquerque, R. Q.; Lee, M.; Fernández, G. Impact of Positional Isomerism on Pathway Complexity in Aqueous Media. *Angewandte Chemie International Edition* **2020**, *59* (14), 5675–5682.
(130) Ogi, S.; Fukui, T.; Jue, M. L.; Takeuchi, M.; Sugiyasu, K. Kinetic Control over Pathway Complexity in Supramolecular Polymerization through Modulating the Energy Landscape by Rational Molecular Design. *Angewandte Chemie* **2014**, *126* (52), 14591–14595.
(131) Ogi, S.; Grzeszkiewicz, C.; Würthner, F. Pathway Complexity in the Self–Assembly of a Zinc Chlorin Model System of Natural Bacteriochlorophyll J–Aggregates. *Chemical Science* **2018**, *9* (10), 2768–2773.
(132) Singh, A.; Joseph, J. P.; Gupta, D.; Sarkar, I.; Pal, A. Pathway Driven Self–Assembly and Living Supramolecular Polymerization in an Amyloid–Inspired Peptide Amphiphile. *Chemical Communications* **2018**, *54* (76), 10730–10733.
(133) Matsumoto, N. M.; Lafleur, R. P.; Lou, X.; Shih, K.–C.; Wijnands, S. P.; Guibert, C.; van Rosendaal, J. W.; Voets, I. K.; Palmans, A. R.; Lin, Y. Polymorphism in Benzene–1, 3, 5–Tricarboxamide Supramolecular Assemblies in Water: A Subtle Trade–off between Structure and Dynamics. *Journal of the American Chemical Society* **2018**, *140* (41), 13308–13316.
(134) Helmers, I.; Niehues, M.; Kartha, K. K.; Ravoo, B. J.; Fernández, G. Synergistic Repulsive Interactions Trigger Pathway Complexity. *Chemical Communications* **2020**, *56* (63), 8944–8947.
(135) Cohen, E.; Weissman, H.; Pinkas, I.; Shimoni, E.; Rehak, P.; Král, P.; Rybtchinski, B. Controlled Self–Assembly of Photofunctional Supramolecular Nanotubes. *ACS Nano* **2018**, *12* (1), 317–326.
(136) Bae, J.; Choi, J.–H.; Yoo, Y.–S.; Oh, N.–K.; Kim, B.–S.; Lee, M. Helical Nanofibers from Aqueous Self–Assembly of an Oligo (p–Phenylene)–Based Molecular Dumbbell. *Journal of the American Chemical Society* **2005**, *127* (27), 9668–9669.
(137) Ogi, S.; Stepanenko, V.; Thein, J.; Würthner, F. Impact of Alkyl Spacer Length on Aggregation Pathways in Kinetically Controlled Supramolecular Polymerization. *Journal of the American Chemical Society* **2016**, *138* (2), 670–678.
(138) Valera, J. S.; Gómez, R.; Sánchez, L. Kinetic Traps to Activate Stereomutation in Supramolecular Polymers. *Angewandte Chemie* **2019**, *131* (2), 520–524.
(139) Ogi, S.; Stepanenko, V.; Sugiyasu, K.; Takeuchi, M.; Würthner, F. Mechanism of Self–Assembly Process and Seeded Supramolecular Polymerization of Perylene Bisimide Organogelator. *Journal of the American Chemical Society* **2015**, *137* (9), 3300–3307.

(140) Ogi, S.; Grzeszkiewicz, C.; Würthner, F. Pathway Complexity in the Self–Assembly of a Zinc Chlorin Model System of Natural Bacteriochlorophyll J–Aggregates. *Chemical Science* **2018**, *9* (10), 2768–2773.

(141) Greciano, E. E.; Matarranz, B.; Sánchez, L. Pathway Complexity Versus Hierarchical Self-Assembly in N-Annulated Perylenes: Structural Effects in Seeded Supramolecular Polymerization. *Angewandte Chemie International Edition* **2018**, *57* (17), 4697–4701.

(142) Greciano, E. E.; Sánchez, L. Seeded Supramolecular Polymerization in a Three-Domain Self-Assembly of an N-Annulated Perylenetetracarboxamide. *Chemistry–A European Journal* **2016**, *22* (38), 13724–13730.

(143) Helmers, I.; Niehues, M.; Kartha, K. K.; Ravoo, B. J.; Fernández, G. Synergistic Repulsive Interactions Trigger Pathway Complexity. *Chemical Communications* **2020**, *56* (63), 8944–8947.

(144) Valera, J. S.; Gómez, R.; Sánchez, L. Tunable Energy Landscapes to Control Pathway Complexity in Self-Assembled N-Heterotriangulenes: Living and Seeded Supramolecular Polymerization. *Small* **2018**, *14* (3), 1702437.

(145) Helmers, I.; Ghosh, G.; Albuquerque, R. Q.; Fernandez, G. Pathway and Length Control of Supramolecular Polymers in Aqueous Media via a Hydrogen Bonding Lock. *Angewandte Chemie International Edition* **2021**, *60* (8), 4368–4376.

(146) Ogi, S.; Fukui, T.; Jue, M. L.; Takeuchi, M.; Sugiyasu, K. Kinetic Control over Pathway Complexity in Supramolecular Polymerization through Modulating the Energy Landscape by Rational Molecular Design. *Angewandte Chemie* **2014**, *126* (52), 14591–14595.

(147) Jin, F.; Balasubramaniam, R.; Stebe, K. J. Surfactant Adsorption to Spherical Particles: The Intrinsic Length Scale Governing the Shift from Diffusion to Kinetic–Controlled Mass Transfer. *The Journal of Adhesion* **2004**, *80* (9), 773–796.

(148) Tidhar, Y.; Weissman, H.; Wolf, S. G.; Gulino, A.; Rybtchinski, B. Pathway-dependent Self-assembly of Perylene Diimide/Peptide Conjugates in Aqueous Medium. *Chemistry–A European Journal* **2011**, *17* (22), 6068–6075.

(149) Korevaar, P. A.; Newcomb, C. J.; Meijer, E. W.; Stupp, S. I. Pathway Selection in Peptide Amphiphile Assembly. *Journal of the American Chemical Society* **2014**, *136* (24), 8540–8543.

(150) Matern, J.; Fernández, Z.; Bäumer, N.; Fernández, G. Expanding the Scope of Metastable Species in Hydrogen Bonding-Directed Supramolecular Polymerization. *Angewandte Chemie International Edition* **2022**, *61* (26), e202203783.

(151) Ogi, S.; Matsumoto, K.; Yamaguchi, S. Seeded Polymerization through the Interplay of Folding and Aggregation of an Amino-acid-based Diamide. *Angewandte Chemie* **2018**, *130* (9), 2363–2367.

(152) Besenius, P. Controlling Supramolecular Polymerization through Multicomponent Self-assembly. *Journal of Polymer Science Part A: Polymer Chemistry* **2017**, *55* (1), 34–78.

(153) Hadar, M.; Kaizerman-Kane, D.; Zafrani, Y.; Cohen, Y. Temperature-Dependent and pH-Responsive Pillar [5] arene-Based Complexes and Hydrogen-Bond-Based Supramolecular Pentagonal Boxes in Water. *Chemistry–A European Journal* **2020**, *26* (49), 11250–11255.

(154) Benchimol, E.; Nguyen, B.–N. T.; Ronson, T. K.; Nitschke, J. R. Transformation Networks of Metal–Organic Cages Controlled by Chemical Stimuli. *Chemical Society Reviews* **2022**, *51* (12), 5101–5135.

(155) Rizwan, M.; Yahya, R.; Hassan, A.; Yar, M.; Azzahari, A. D.; Selvanathan, V.; Sonsudin, F.; Abouloula, C. N. pH Sensitive Hydrogels in Drug Delivery: Brief History, Properties, Swelling, and Release Mechanism, Material Selection and Applications. *Polymers* **2017**, *9* (4), 137.

(156) Ghosh, G.; Barman, R.; Mukherjee, A.; Ghosh, U.; Ghosh, S.; Fernández, G. Control over Multiple Nano-and Secondary Structures in Peptide Self-assembly. *Angewandte Chemie International Edition* **2022**, *61* (5), 202.

(157) Ávila–Rovelo, N. R.; Ruiz–Carretero, A. Recent Progress in Hydrogen–Bonded π–Conjugated Systems Displaying J–Type Aggregates. *Organic Materials* **2020**, *2* (01), 047–063.

(158) Basak, S.; Nandi, N.; Baral, A.; Banerjee, A. Tailor–Made Design of J–or H–Aggregated Naphthalenediimide–Based Gels and Remarkable Fluorescence Turn on/off Behaviour Depending on Solvents. *Chemical Communications* **2015**, *51* (4), 780–783.

(159) Rowan, A. E.; Nolte, R. J. Helical Molecular Programming. *Angewandte Chemie International Edition* **1998**, *37* (1-2), 63–68.

(160) Yan, F.; Lartey, M.; Jariwala, K.; Bowser, S.; Damodaran, K.; Albenze, E.; Luebke, D. R.; Nulwala, H. B.; Smit, B.; Haranczyk, M. Toward a Materials Genome Approach for Ionic Liquids: Synthesis Guided by Ab Initio Property Maps. *The Journal of Physical Chemistry B* **2014**, *118* (47), 13609–13620.

(161) Bartocci, S.; Berrocal, J. A.; Guarracino, P.; Grillaud, M.; Franco, L.; Mba, M. Peptide–Driven Charge–Transfer Organogels Built from Synergetic Hydrogen Bonding and Pyrene–Naphthalenediimide Donor–Acceptor Interactions. *Chemistry – A European Journal* **2018**, *24* (12), 2920–2928.

(162) Burattini, S.; Colquhoun, H. M.; Fox, J. D.; Friedmann, D.; Greenland, B. W.; Harris, P. J.; Hayes, W.; Mackay, M. E.; Rowan, S. J. A Self–Repairing, Supramolecular Polymer System: Healability as a Consequence of Donor–Acceptor π–π Stacking Interactions. *Chemical Communications* **2009**, No. 44, 6717–6719.

(163) Jiang, Q.; Zhang, H.–Y.; Han, M.; Ding, Z.–J.; Liu, Y. pH–Controlled Intramolecular Charge–Transfer Behavior in Bistable [3] Rotaxane. *Organic Letters* **2010**, *12* (8), 1728–1731.

(164) Colquhoun, H. M.; Williams, D. J.; Zhu, Z. Macrocyclic Aromatic Ether–Imide–Sulfones: Versatile Supramolecular Receptors with Extreme Thermochemical and Oxidative Stability. *Journal of the American Chemical Society* **2002**, *124* (45), 13346–13347.

(165) Jalani, K.; Kumar, M.; George, S. J. Mixed Donor–Acceptor Charge–Transfer Stacks Formed via Hierarchical Self–Assembly of a Non–Covalent Amphiphilic Foldamer. *Chemical Communications* **2013**, *49* (45), 5174–5176.

(166) Molla, M. R.; Ghosh, S. Hydrogen-Bonding-Mediated Vesicular Assembly of Functionalized Naphthalene–Diimide-Based Bolaamphiphile and Guest-Induced Gelation in Water. *Chemistry–A European Journal* **2012**, *18* (32), 9860–9869.

# Brief synthesis, general conclusions and perspectives

The aim of this thesis work consisted in synthesizing electroactive helical oligopyridine dicarboxamide foldamers in order to elaborate homoduplexes through redox stimulations and heteroduplexes based on donor–acceptor interactions. This section will briefly summarize the results obtained during this thesis and propose a series of perspectives.

- **Redox –triggered hybridization of homoduplexes**

Foldamer **A**, which is endowed with tetrathiafulvalene as redox units and amide linkers, was successfully synthesized after thirteen steps in about four months. Five crystallographic structures were obtained in different solvents, highlighting the single helical state of foldamer **A** regardless of the solvent nature. In these five crystallographic structures, TTF units definitely constitute a part of the helix. Furthermore, the organization of the single helices within the lattice varies in each solvent, with TTF units participating to intra – and/or intermolecular non –covalent interactions, such as hydrogen bond, π –π stacking and CH –π interactions.

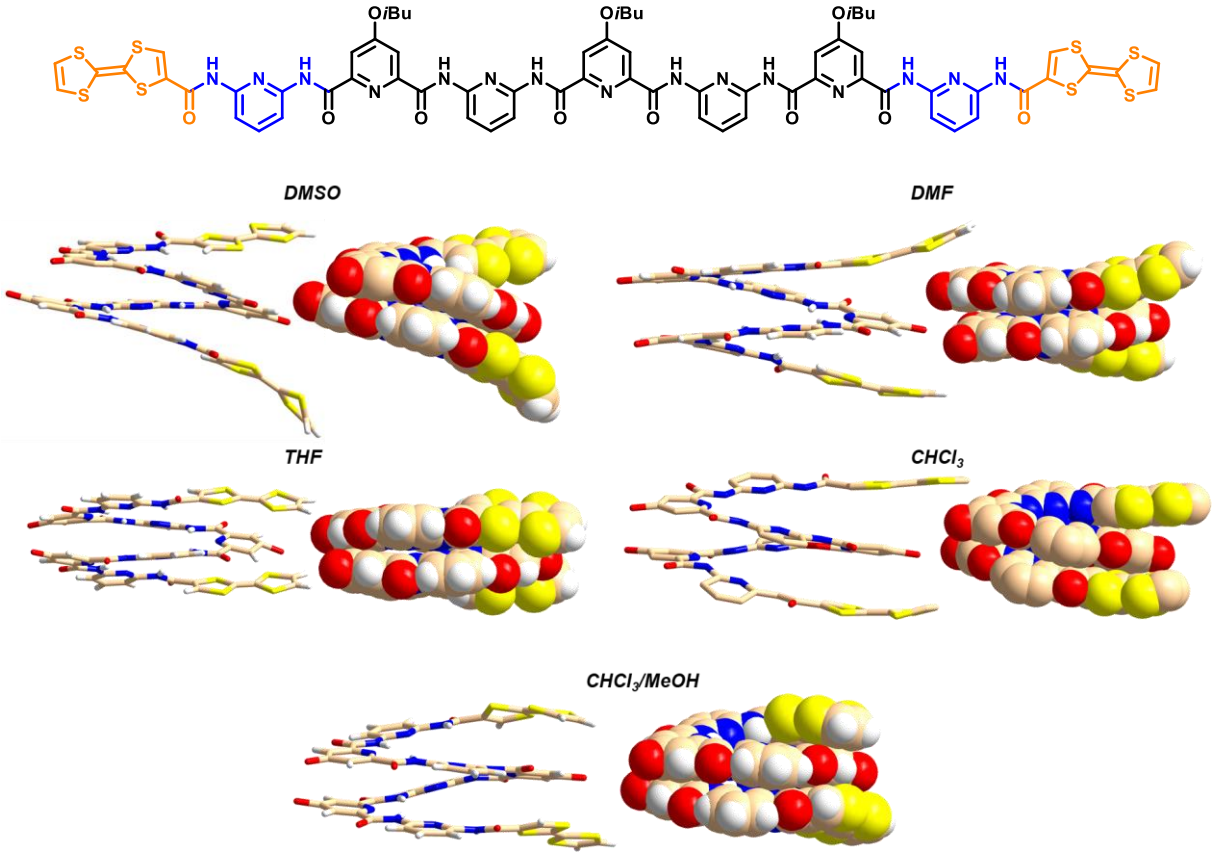


To investigate the behavior of foldamer **A** in solution and its hybridization process, several parameters were analysed, contributing to a comprehensive understanding. In the

neutral state, similar $^{1}H$ NMR spectra were recorded in the different tested solvents (4 mmol.L $^{-1}$, 298 K, in $CDCl_3$, $C_2D_2Cl_4$, pyridine–$d_5$, THF–$d_4$, DMSO–$d_6$, and DMF–$d_7$): one set of signals was systematically observed for amide protons, at chemical shifts that indicate the adoption of a single helical state. Analyses in $CDCl_3$, a solvent known for promoting the formation of hybridized species, revealed that foldamer **A** only adopts a single helical arrangement at concentrations up to 5.2 mmol.L $^{-1}$, its solubility limit at room temperature. At this stage, one will also note that varying the temperature had no influence on the behavior of this foldamer. The absence of double helices in solution was further confirmed through titration experiments with chloride anions, which is known for promoting the dissociation of double helices and leading to the formation of anion–foldamer complexes. Indeed, we solely observed progressive variations of chemical shifts and never, the appearance of a second set of signals, which would have pointed towards the formation of single helices from a solution of fully hybridized foldamers.

The previous observations highlighted that the single helical structure of foldamer **A** is particularly stable in solution, which may limit its ability to hybridize. Therefore, to take advantage of the redox properties of the TTF unit and weaken the stability of the single helical state, we considered the possibility to oxidize tetrathiafulvalene units and study the supramolecular behaviour of the corresponding species. In this context, electrochemical and spectroelectrochemical analyses were performed. These demonstrated the formation of hybridized species upon oxidation through the dimerization of $TTF^{\bullet+}$ radical cations. Considering these results, we were able to trigger the hybridization of a helical foldamer, despite the absence of double helices in the neutral state. This occurred by altering the stability of the single helical state through oxidation and setting up an additional driving force.

## ▪ Heteroduplex formation through donor –acceptor interactions

The main part of this thesis work was dedicated to the design of heteroduplexes through donor–acceptor interactions. Considering 1) the important role of the amide linker with TTF units in the stability of the single helical form of foldamer **A**, 2) the need for obtaining hybridized species in the neutral state, and 3) the long time needed to synthesize one foldamer through amide linker, we envisaged grafting the electroactive chromophores during the last step and this, via copper –catalysed azide –alkyne cycloaddition. On this basis, foldamer **B** was synthesized and constituted the central foldamer precursor, which led to the preparation of a series of donor and acceptor strands: foldamers **C**, **D**, **E**, **F**, **G** and **L** endowed with

tetrathiafulvalene TTF, trinitrofluorenone derivative TNF, naphthalene diimide NDI, dialkoxynaphthalene DAN, and pyrene units, respectively.

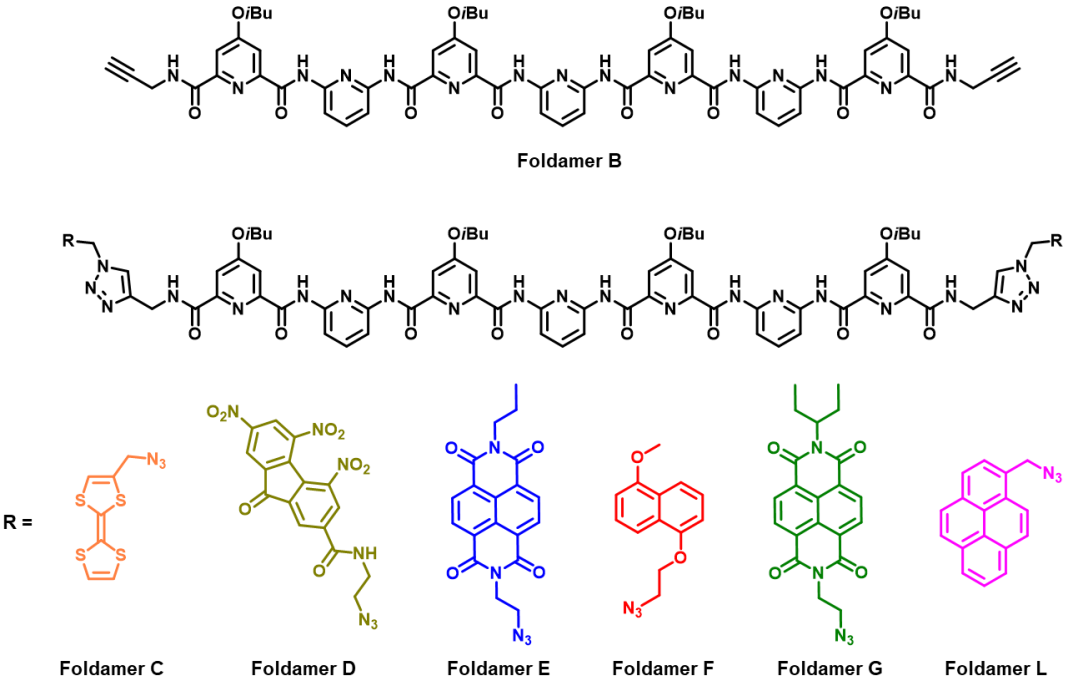


The foldamers were studied individually and in mixtures of donor and acceptor strands. Noteworthy is the fact that foldamer **C**, bearing TTF units through triazole linker, exhibited a high solubility in chloroform and hybridized into double helices in the neutral state; this appears consistent with our findings regarding foldamer **A** in Chapter 2.

Foldamer **D** displays a weak stability and undergoes degradation when exposed to oxygen in the air. On the other hand, foldamer **C** presents sensitivity to high temperatures due to the presence of TTF units. These observations hindered further characterizations of foldamers **C** and **D**. As a result, new donor (foldamer **F**) and acceptor (Foldamer **E**) strands were designed. Several attempts of hybridization were carried out between foldamers **E** and **F**, but proved unsuccessful due to the low solubility of foldamer **E**. Consequently, a branched alkyl chain was introduced to the NDI units to enhance its solubility, resulting in the formation of foldamer **G**.

The solutions ($CDCl_3$, 60 mmol.L$^{-1}$, 298 K) of foldamers **F** and **G** exhibited a red color, distinct from each foldamer alone, suggesting the formation of a charge transfer complex. This was confirmed through UV –visible absorption spectroscopy, with the clear observation of a charge transfer band. Along the "first dispersion" experiments, $^1$H NMR spectroscopy showed that a single set of signals involved into fast equilibria was observed for amide protons. This

indicates that the interactions between donor and acceptor chromophores occur between single helices, promoting the formation of a supramolecular polymer (the large diffusion coefficients determined by DOSY NMR spectroscopy corroborate this assertion).

However, an unexpected behavior was detected along the "second dispersion" experiments of the same samples: a second set of signals corresponding to the duplexes appeared. The aromatic signals of DAN and NDI units do not correspond to the signals of the duplexes **(F)**$_2$ and **(G)**$_2$, which means they can be attributed to the heteroduplexes, as confirmed by ESI MS. Thereby, this apparent lack of reproducibility actually indicated that the solutions of these foldamers did not reach their thermodynamic equilibrium, and were under kinetic control. This assessment proved to be also true for each foldamer individually.

On this ground, various $^1$H NMR experiments were conducted on foldamer **G** to understand the respective influences of kinetic parameters, such as temperature, concentration, and time. These experiments highlighted the important role of the temperature at high concentrations, and indicated that non–covalent interactions are responsible for this singular behavior. The analysis of the crystallographic structures of foldamers and reference compounds showed that π–π stacking between the electroactive units and the foldamer skeleton could be the origin of the kinetically trapped states. In addition, an intramolecular hydrogen bond was detected in the foldamers, promoting the formation of a seven–membered pseudo–cycle, which is known as the origin for many kinetically trapped systems. This suggests that the electroactive units and/or the triazole connector are accountable for this behavior.

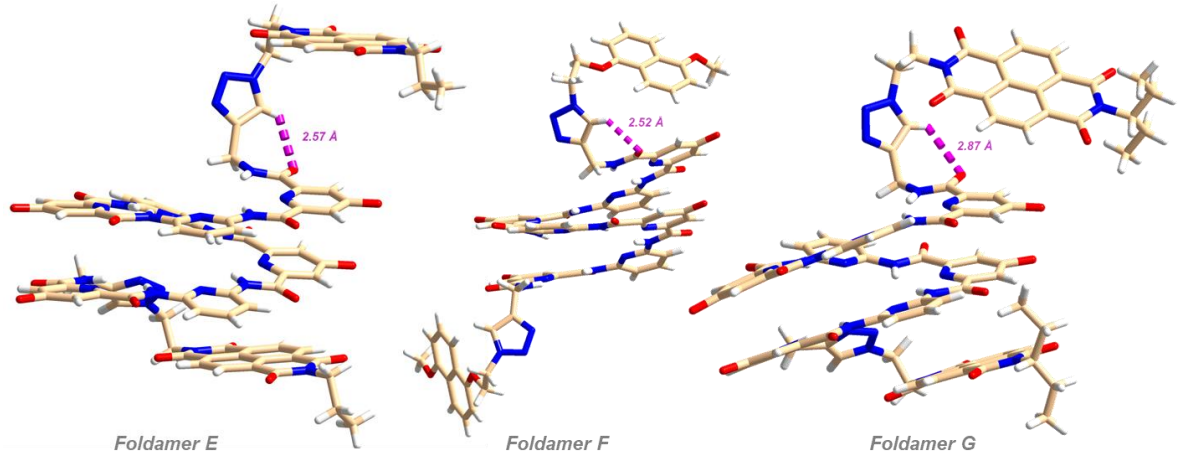


Foldamers **B** and **H** served as references. Foldamer **B**, which lacks both triazole linkers and electroactive units, is under thermodynamic control. On the contrary, foldamer **H**, which features triazole linkers but does not include electroactive moieties, was under kinetic control,

which suggests that the presence of triazole linkers and hence, the formation of a seven–membered pseudo cycle, contribute to the formation of inactive species that cannot hybridize.

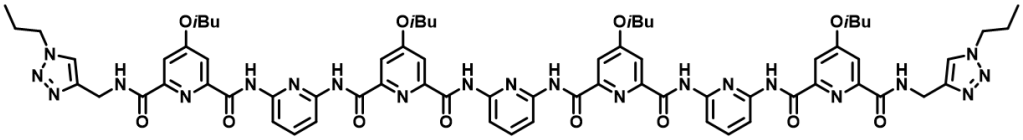


Foldamer H

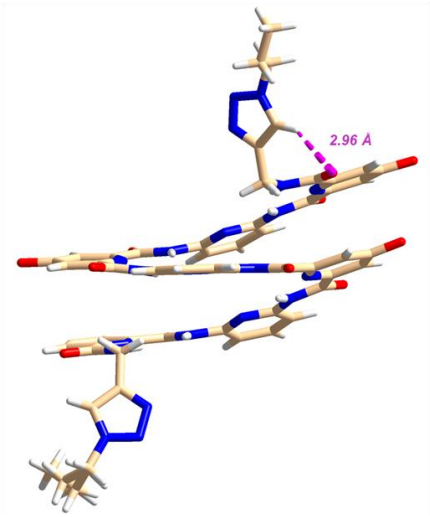


In order to weaken this intramolecular hydrogen bond, foldamer **I**, which includes an additional methylene group between amide functions and triple bonds, was designed and allowed for isolating foldamers **J** and **K**.

Foldamer **J** was unable to hybridize at room temperature, which could point towards another kinetically–trapped state. However, heating up to 120°C in 1,1,2,2–tetrachloroethane did not allow for observing the formation of double helices. Alternatively, a second set of signals appeared at low temperatures (–20°C), which suggests that double helices could be formed at low temperature. Consequently, two hypothesis are currently under consideration: 1) foldamer **J** displays a particularly weak hybridization propensity and hence, it only dimerized at low temperature, and 2) it is kinetically–trapped in a particularly deep potential well, because of strong intra– or intermolecular interactions.

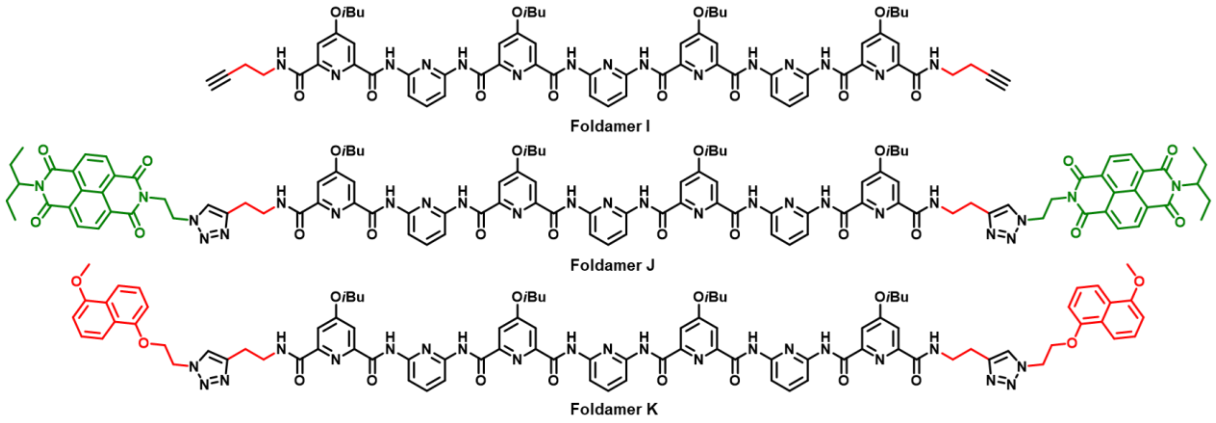


In summary, these observations suggest that the most plausible explanation is that the triazole linker is responsible for the behavior of foldamers **F** and **G** through the formation of seven–membered pseudo cycle leading to inactive single helices during the first dilution, which favors the formation of a supramolecular polymer through intermolecular interactions between chromophores. However, the heating process weakens the intramolecular hydrogen bond, which makes foldamers able to hybridize and promotes duplex formation upon heating at sufficiently high concentrations.

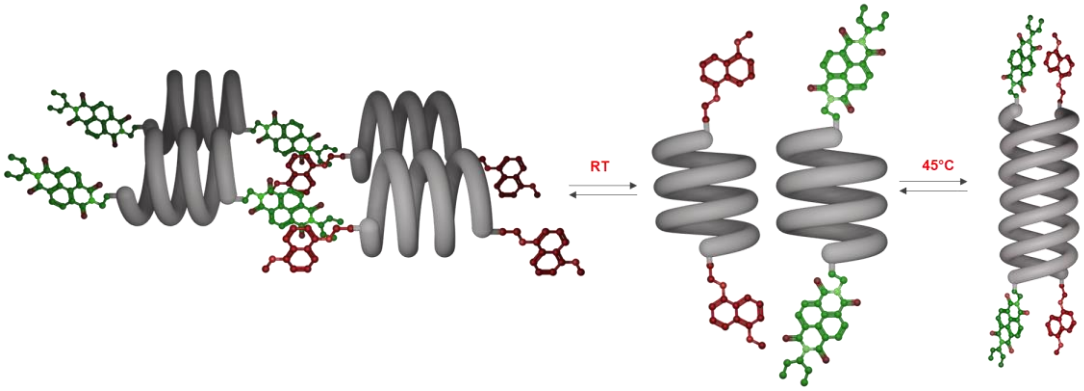


- ## Perspectives

### Towards the selective formation of heteroduplexes through concave–convex interactions

As first perspectives, a project started in collaboration with Prof. Nazario Martin and Prof. Maria Angeles Herranz at the University Complutense of Madrid, where I stayed one month, is presented. Since the selective formation of heteroduplexes was not achieved (Chapter 3) and since this may be the result of aromatic interactions between identical planar functional units, we envisaged to take advantage of an interaction between two fragments displaying complementary shapes. In this context, using concave–convex interactions between an extended tetrathiafulvalene and a fullerene appeared particularly relevant. This was all the truer

because these functional units are also electroactive (exTTF can be readily oxidized, while fullerenes undergo reduction processes).

In this context, the purpose of my one–month stay in Madrid consisted in synthesizing the necessary azide derivatives to allow for the functionalization of the foldamer. After isolating these precursors, the synthesis of the exTTF–based foldamer was achieved in twenty steps. However, several issues were encountered for the synthesis of the fullerene–containing foldamer (solubility, stability/degradation of the azide derivative). To date, a mixture of mono– and bis–functionalized foldamer was obtained but the desired compound could not be isolated.

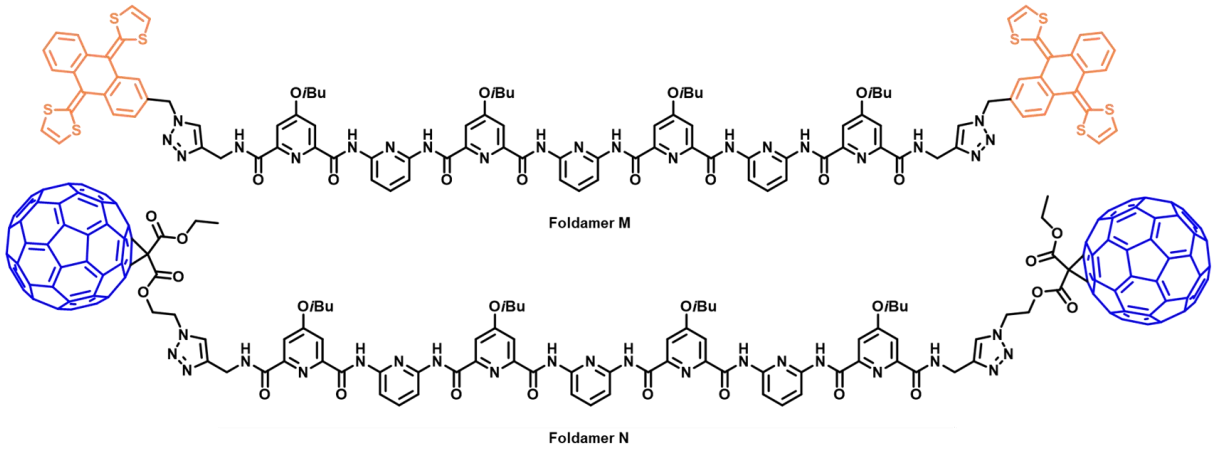


Foldamer M




Foldamer N

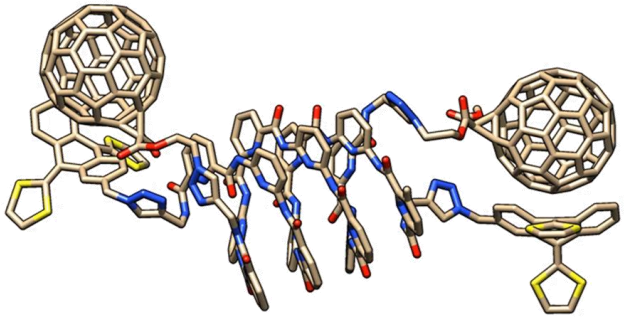

Optimized geometry by Hyperchem - Molecular Mechanics

**Modifying the linker to avoid kinetically–trapped states**

The role of the linker was found to be essential in both the second and the third chapters. In the second chapter, the TTF units were attached through a rigid and short amide linker. This spacer directs the orientation of TTF units making them part of the helix and enabling them to interact directly with the foldamer skeleton. The corresponding interactions lead to the obtaining of kinetically trapped single helices and inhibit the hybridization process in the neutral state. In the third chapter, the functionalization of foldamer skeleton was tackled through triazole connector, which is a flexible linker. The latter permits the hybridization in the neutral state, but affects the arrangement of these foldamers by switching from supramolecular polymer

to heteroduplexes through kinetically trapped foldamers due to the formation of a seven membered pseudo cycle involving the linker. As a consequence, a track that could be followed for future developments could rely on the replacement of this linker to avoid kinetically–trapped states and permit hybridization. As illustrative examples, an acetylenic linker could be envisaged. In this manner, foldamer **B** would represent a valuable building block and simple Sonogashira coupling could lead to the isolation of π–functional foldamers.

**Increasing the number of functional units to increase the cross–hybridization**

In order to improve the selectivity of the cross–hybridization process, a rather straightforward strategy could consist in grafting additional functional units on the foldamer skeleton to promote aromatic interactions between electron rich and poor moieties. To do so, a new design would be necessary. Instead of grafting π–functional units at the extremities of the skeleton, electron–rich or poor fragments would be grafted on the helical backbone for this second generation of electroactive foldamers, as illustrated below. In this manner, the alternate –D–A–D–A stack would drive the equilibrium towards heteroduplex with an ever–better selectivity.

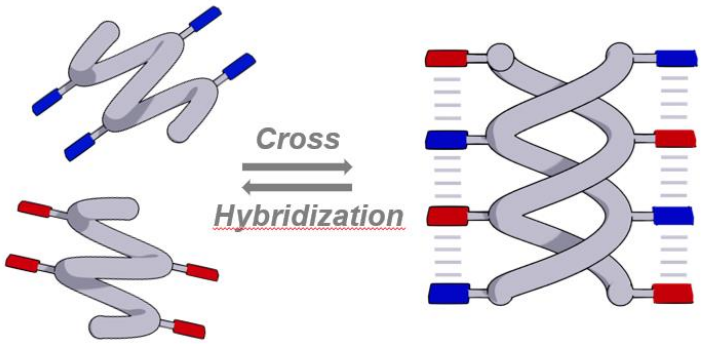


*Cartoon representing the cross hybridization of two 2nd generation strands*

# *General procedures*

The starting materials were purchased and used without further purification. All solvents and reagents were dried according to standard procedures (Sodium/benzophenone for tetrahydrofuran and diethyl ether, $CaH_2$ for dichloromethane, acetonitrile, triethylamine and *N*,*N*–diisopropylethylamine, $P_2O_5$ for chloroform). All air–sensitive reactions were carried out under argon atmosphere using standard Schlenk flask techniques. Thin–layer chromatography (TLC) was performed on aluminium plates coated with MerckSilica gel 60 F254. Developed plates were air–dried and scrutinized under a UV lamp. Silica gel SIGMA Aldrich Chemistry ($SiO_2$, pore size 60 Å, 40–63 μm technical grades) was used for preparative silica gel chromatography.

**Recycling high performance liquid chromatography**

Crude compounds were solubilized in HPLC grade chloroform (stabilized with ethanol, 5 mL). Prior to injection, the solution was filtered through a 0.45 μm PTFE filter (VWR 25mm syringe filter w/ 0.45 μm membrane). Purification was performed on a LC–9160NEXT system from the Japan Analytical Industry Co., Ltd. (JAI) equipped with coupled UV–vis 4Ch NEXT and RI–700 II detectors at room temperature through a set of two JAIGEL–2H and 2.5H columns at an elution rate of 10 $mL.min^{-1}$.
Compounds were detected by UV irradiation (Bioblock Scientific) or staining with iodine, unless otherwise stated.

**$^1$H and $^{13}$C Nuclear Magnetic Resonance (NMR)** spectra were recorded using deuterated solvent as internal reference on a BRUKER Advance DRX 300 ($^1$H, 300 MHz; $^{13}$C, 75 MHz) or 500 ($^1$H, 500 MHz; $^{13}$C, 125 MHz) spectrometer. Coupling constants (J) are denoted in Hz and chemical shifts (δ) in parts per million (ppm) relative to TMS. Multiplicities are denoted as follows: s = singlet, d = doublet, dd = doublet of doublet t = triplet, q = quartet m = multiplet, br = broad.

**Mass spectra** were recorded by Dr Ingrid Freuze on a Jeol JMS 700 (high–resolution mass spectra (HRMS) or a Bruker Biflex III spectrometer (MALDI–TOF).

**X–Ray single–crystal diffraction** data were collected by Dr Magali Allain (MOLTECH–Anjou) on an Agilent SuperNova diffractometer equipped with an Atlas CCD detector and micro–focus Cu–Kα radiation (λ = 1.54184 Å). The structure was solved by direct methods, expanded and refined on F2 by full matrix least–squares techniques using SHELX97 programs (G.M. Sheldrick, 1998).

**UV–Visible absorption** spectra were recorded on a JASCO V–730 spectrophotometer.

**Cyclic voltammetry** experiments were carried out on a potentiostat Bio–Logic SP–300. Tetrabutylammonium hexafluorophosphate (0.1 M) was used as supporting electrolyte. The cell was equipped with three electrodes: a platinum working electrode (Ø = 2 mm), a platinum wire as auxiliary electrode and a silver/silver nitrate (0.01 M, $CH_3CN$, $TBAPF_6$) reference electrode. The potentials are given with respect to the ferrocene/ferrocenium redox couple.

**Spectroelectrochemistry** measurements were performed by Dr Christelle Gautier (MOLTECH–Anjou) and were carried out in direct reflecting mode on the working electrode (*e.g.* Pt) with a homemade bench, developed by Dr Eric Levillain and Dr Olivier Alévêque,

composed of different Princeton Instruments modules (light sources, fibers, monochromators, spectroscopy camera, and software). The connection between the light source, the cell and the spectrophotometer is ensured through a "Y–shaped" optical fiber bundle: 18 fibers guide the light to the cell, and 19 fibers collect the reflected light from the cell to visible (320-1080 nm/maximum acquisition frequency 2 MHz) and IR (900-1700 nm / maximum acquisition frequency 8 MHz) CCD detectors. The sensitivity of the spectroscopic measurement (< 3 e− at 100 kHz and < 13 e− at 2 MHz between 320 and 1080 nm; 400 e− (high gain) and 5000 electrons (low gain) between 900 nm and 1700 nm) allows performing a spectroelectrochemistry experiment under the usual conditions of electrochemistry.

**The DataFit program** was run to assess equilibrium constants by fitting theoretical models to experimental data. This home-made program was developed in the MATLAB environment by members of the MOLTECH-Anjou laboratory, namely Olivier Alévêque, Yohann Morille and Eric Levillain. The convergence between the experimental dataset and the theoretical equations can be reached according to various algorithms (Levenberg–Marquardt, quadratic or Nielsen). This program has differents strengths: the parameters to be fitted can be selected before any fitting calculation; after fitting a dataset, residuals are calculated for each point and plotted; it allows for plotting together experimental points and simulations to get a deep insight on the impact of the different fitted values; eventually, it affords statistical feedbacks that may help avoiding misinterpretations.

# *Experimental procedures and compounds characterizations*

***General procedures for preparing the solutions of foldamers and reference compounds:*** Foldamers and reference compounds were directly weighed into the NMR tube/vial in both cases, whether considering each foldamer/reference compound alone or in mixture.

## Chapter II

### Compound II–7[1]

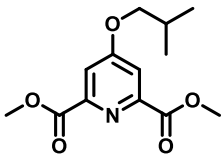

**Chemical Formula:** $C_{13}H_{17}NO_5$
**Molecular Weight:** 267.1107

Dimethyl 4–hydroxypyridine–2,6–dicarboxylate (5 g, 23 mmol), and $K_2CO_3$ (13 g, 94 mmol, 4 eq.) were dissolved in dry DMF (50 mL) and the mixture was heated to 80°C under argon atmosphere for 90 min. The solution was cooled to 70°C and 1–iodo–2–methylpropane (5.4 mL, 47 mmol, 2 eq.) was added. The mixture was stirred for 3 hours and the solvent was removed under reduced pressure. The resulting solid was dissolved in 50 mL of toluene and washed with water (3 × 50 mL). The organic phase was dried over anhydrous $MgSO_4$ and the solvent was evaporated to afford compound **II–7** as a brown oil that crystallises upon standing at room temperature (5.4 g, 60 %).

$^1$H NMR (300 MHz, $CDCl_3$) δ 7.80 (s, 2H), 4.01 (s, 6H), 3.90 (d, J = 6.5 Hz, 2H), 2.24 – 2.05 (m, 1H), 1.05 (d, J = 6.7 Hz, 6H).

$^{13}$C NMR (75 MHz, $CDCl_3$) δ 167.3, 165.3, 149.7, 114.7, 75.3, 53.4, 28.1, 19.1.

### Compound II–8[1]

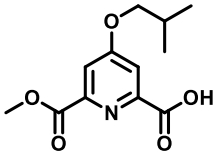

**Chemical Formula:** $C_{12}H_{15}NO_5$
**Molecular Weight:** 253.0950

Diester **II–7** (510 mg, 1.9 mmol, 1 eq.) was dissolved in methanol (6 mL) and the mixture was cooled in an ice bath. A solution of sodium hydroxide (77 mg, 2 mmol, 1 eq.) in methanol (6 mL) was added slowly. The mixture was left to stir overnight, allowing the ice bath to melt. The solvent was evaporated under reduced pressure, and water (50 mL) was added. The precipitate was dissolved ultrasonically and the starting material was extracted with DCM (3 × 50 mL). The water phase was acidified with a 1M HCl solution and then re–extracted with

3 × 50mL of DCM. The organic layer was dried on magnesium sulfate, filtred and evaporated to afford compound **II–8** as a white solid (360 mg, 75 %).

$^{1}$H NMR (300 MHz, $CDCl_3$) δ 7.80 (s, 2H), 4.01 (s, 6H), 3.90 (d, J=6.5 Hz, 2H).

$^{13}$C NMR (125 MHz, $CDCl_3$) δ 168.4, 164.5, 164, 148.3, 148.1, 116.2, 112.3, 75.8, 53.3, 3.1, 19.1.

## Compound II–9[1]

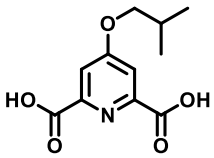


**Chemical Formula:** $C_{11}H_{13}NO_5$
**Molecular Weight:** 239.0794

Potassium hydroxide (800 mg, 14 mmol) was dissolved in methanol (20 mL) and was added to a solution of compound **II–7** (0.9 g, 2 mmol) in methanol (20 mL). The mixture was stirred at room temperature overnight. A white precipitate appeared, was filtered and washed with 10 mL of methanol. The solid was subsequently suspended in water, protonated with hydrochloric acid 3M, washed with water, and dried under vacuum to afford **II–9** as a white solid (833 mg, quantitative yield).

$^{1}$H NMR (300 MHz, DMSO–$d_6$) δ 7.68 (s, 2H), 3.98 (d, J = 6.5 Hz, 2H), 2.05 (m, 1H), 0.98 (d, J = 6.7 Hz, 6H).

$^{13}$C NMR (75 MHz, DMSO–$d_6$) δ 166.9, 165.3, 149.7, 74.5, 27.4, 18.7.

## Compound II–10[2]

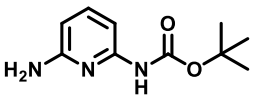


**Chemical Formula:** $C_{10}H_{15}N_3O_2$
**Molecular Weight:** 209.1164

2,6–Diaminopyridine (5 g, 45 mmol, 1 eq.) and di–*tert*–butyl dicarbonate (10 g, 45 mmol, 1 eq.) were dissolved in 60 mL of THF. The mixture was heated to reflux overnight. The solvent was removed under reduced pressure and the crude was purified by silica gel chromatography (eluent $Et_2O$/PE 1/1) to afford **II–10** as white powder (5.7 g, 61 %).

$^{1}$H NMR (300 MHz, $CDCl_3$) δ 8.54 (s, 1H), 7.36 (t, *J* = 8.0 Hz, 1H), 7.17 (d, *J* = 8.0 Hz, 1H), 6.11 (dd, *J* = 7.9, 0.8 Hz, 1H), 4.65 (s, 2H), 1.48 (s, 9H).

$^{13}$C NMR (75 MHz, $CDCl_3$) δ 157.61, 152.80, 150.85, 139.85, 103.04, 101.89, 80.85, 28.30.

## Compound II–11[1]

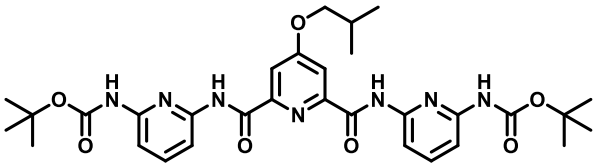

**Chemical Formula:** $C_{31}H_{39}N_7O_7$
**Molecular Weight:** 621.2911

Under argon atmosphere, dry diacid **II–9** (1 g, 4 mmol) was mixed with dry dichloromethane (10 mL). Oxalyl chloride (1.7 mL, 20 mmol, 5 eq.) was added, as well as a drop of dry dimethylformamide. Gas release was observed and the mixture was stirred for two hours under argon atmosphere. Dichloromethane and oxalyl chloride were evaporated under vacuum using a liquid nitrogen trap and the resulting solid was dried under vacuum for three hours. Dry dichloromethane (8 mL) was subsequently added. In another Schlenk, dry **II–10** (1.9 g, 9 mmol) was dissolved in 10 mL of dry dichloromethane and dry DIPEA (2.7 g, 20 mmol) was added. The resulting mixture was added dropwise to the solution of acid chloride and stirred for 16 hours under argon atmosphere. The solvent was removed under reduced pressure and the crude was purified by silica gel chromatography (eluent DCM/EtOAc 99/1) to afford **II–11** as a white powder (1.8 g, 71 %).

$^1$H NMR (300 MHz, $CDCl_3$) δ 10.18 (s, 2H), 8.08 (dd, *J* = 7.8, 1.0 Hz, 2H), 7.96 (s, 2H), 7.76 (t, *J* = 8.0 Hz, 2H), 7.69 (dd, *J* = 8.2, 1.1 Hz, 2H), 7.24 (s, 2H), 3.96 (d, *J* = 6.5 Hz, 2H), 2.17 (dq, *J* = 13.6, 6.8 Hz, 1H), 1.54 (s, 18H), 1.07 (d, *J* = 6.7 Hz, 6H).

$^{13}$C NMR (75 MHz, $CDCl_3$) δ 168.4, 161.8, 152.2, 150.7, 150.5, 149.3, 140.9, 112.3, 109.0, 108.6, 81.4, 28.4, 28.1, 19.1.

## Compound II–12

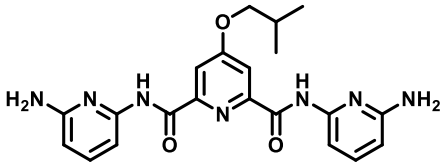

**Chemical Formula:** $C_{21}H_{23}N_7O_3$
**Molecular Weight:** 421.1862

**II–11** (970 mg, 1.5 mmol) was dissolved in 8 mL of dichloromethane and trifluoroacetic acid (1.2 g, 11 mmol) was added slowly. The mixture was stirred for four hours at room temperature. Then, 20 mL of a saturated solution of sodium bicarbonate and chloroform were added. After extraction, the organic phase was washed three times with water and dried over magnesium sulfate. The solvent was removed under reduced pressure to afford **II–12** as white powder (650 mg, quantitative).

$^1$H NMR (300 MHz, $CDCl_3$) δ 10.02 (s, 2H), 7.95 (s, 2H), 7.76 (d, J = 7.9 Hz, 2H), 7.53 (t, J = 7.9 Hz, 2H), 6.30 (d, J = 8.0 Hz, 2H), 4.73 (br, 4H), 3.95 (d, J = 6.5 Hz, 2H), 2.17 (m, 1H), 1.06 (d, J = 6.7 Hz, 6H).

$^{13}$C NMR (75 MHz, $CDCl_3$) δ 168.5, 161.6, 157.7, 150.7, 149.4, 140.5, 112.0, 105.1, 103.8, 75.5, 28.2, 19.2.

## Compound II–13

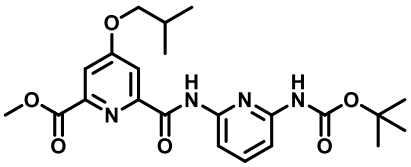

**Chemical Formula:** $C_{22}H_{28}N_4O_6$
**Molecular Weight:** 444.2009

Dry carboxylic acid **II–8** (1.2 g, 4.9 mmol, 1 eq.) was dissolved in 10 mL of dry dichloromethane under inert conditions. Oxalyl chloride (830 µL, 9 mmol, 2 eq.) and a drop of dry dimethylformamide were added. A gas release was observed and the mixture was stirred for 2 hours under argon atmosphere. The excess of oxalyl and dichloromethane was removed by distillation and the solid was left under vacuum for 3 h. The resulting acid chloride was dissolved in dry THF (10 mL). Then, a solution of **II–10** (1.2 g, 5.8 mmol, 1.2 eq.) and DIPEA (4.2 mL, 24 mmol, 5 eq.) in THF (10 mL) was added to the solution of acid chloride. The mixture was then stirred at room temperature for 12 h. The solvent was removed under reduced pressure and the residue was purified by silica gel chromatography using dichloromethane to afford compound **II–13** as a white solid (1.9 g, 90 %).

$^1$H NMR (300 MHz, $CDCl_3$) δ 10.24 (s, 1H), 8.02 (dd, *J* = 7.4, 1.3 Hz, 1H), 7.93 (d, *J* = 2.5 Hz, 1H), 7.76 (d, *J* = 2.5 Hz, 1H), 7.75 – 7.67 (m, 2H), 7.12 (s, 1H), 4.03 (s, 3H), 3.92 (d, *J* = 6.5 Hz, 2H), 2.15 (m, 1H), 1.53 (s, 9H), 1.06 (d, *J* = 6.7 Hz, 6H).

$^{13}$C NMR (75MHz, $CDCl_3$) δ 167.9, 165.1, 161.9, 152.3, 151.5, 150.6, 149.2, 148.4, 140.7, 115.1, 111.2, 108.5, 108.2, 81.2, 75.4, 53.1, 28.4, 28.2, 19.2.

HRMS (MALDI–TOF) calcd for $C_{22}H_{28}N_4O_6$, 467.1906 $[M + Na]^+$; found, 467.1900.

## Compound II–14

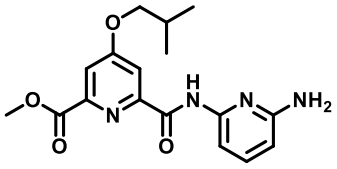

**Chemical Formula:** $C_{17}H_{20}N_4O_5$
**Molecular Weight:** 344.1485

Protected **II–13** (1.1 g, 2.5 mmol, 1 eq.) was dissolved in 8 mL of dichloromethane and trifluoroacetic acid (7.3 mL, 40 eq.) was added. The mixture was stirred for 4 hours at room temperature. The reaction mixture was washed with saturated $NaHCO_3$ solution, extracted with chloroform (150 mL) and washed with water (3 × 50 mL). The organic phases were combined, dried over magnesium sulfate and concentrated under reduced pressure to afford compound **II–14** as a white solid (836 mg, 99 %).

$^{1}$H NMR (300 MHz, $CDCl_3$) δ 10.19 (s, 1H), 7.93 (d, J = 2.5 Hz, 1H), 7.75 (d, J = 2.5 Hz, 1H), 7.71 (d, J = 7.9 Hz, 1H), 7.52 (t, J = 7.9 Hz, 1H), 6.34 (d, J = 7.9 Hz, 1H), 4.72 (s, 2H), 4.04 (s, 3H), 3.92 (d, J = 6.5 Hz, 2H), 2.23 – 2.09 (m, 1H), 1.06 (d, J = 6.7 Hz, 6H).

$^{13}$C NMR (75 MHz, $CDCl_3$) δ 167.7, 165.1, 161.6, 157.7, 151.7, 149.4, 148.2, 134, 114.9, 111, 104.8, 103.4, 75.3, 53, 29.7, 28, 19.1.

HRMS (MALDI–TOF) calcd for $C_{17}H_{20}N_4O_4$, 344.1485 $[M + H]^+$; found, 345.1553.

## Compound II–15[3]

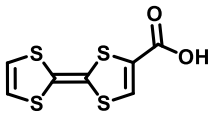

**Chemical Formula:** $C_7H_4O_2S_4$
**Molecular Weight:** 247.9094

Into a stirred solution of TTF (2 g, 9.8 mmol) in anhydrous diethyl ether (120 mL) at –78°C under argon atmosphere, a solution of LDA 1M in THF/hexane (11 mmol) was added dropwise. A thick yellow suspension appeared and the stirring was continued for 45 min at –78°C. $CO_2$ gas was bubbled through the stirred suspension for 1h at –78°C to give an orange suspension and the mixture was then slowly allowed to warm to room temperature over 16 H. The mixture was filtered and the solid was washed thoroughly with diethyl ether, affording the lithium salt of TTF–carboxylate as an orange solid. To a stirred solution of the latter salt in $H_2O$, 10 mL of a solution of hydrochloric acid 1M were added slowly and a deep red solid precipitated immediately. The red solid was collected by filtration, washed thoroughly with water and dried under vacuum to give **II–15** (2.2 g, 88 %).

$^{1}$H NMR (300 MHz, Acetone–$d_6$) δ 7.63 (s, 1H), 6.66 (s, 2H).

## Compound II–16

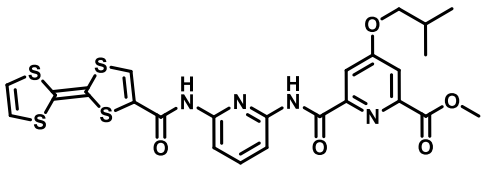

**Chemical Formula:** $C_{24}H_{22}N_4O_5S_4$
**Molecular Weight:** 574.0473

To a solution of TTF–COOH **II–15** (530 mg, 2.1 mmol) in 15 mL dry dichloromethane under argon atmosphere at 0°C, 4–dimethylaminopyridine (111 mg, 0.9 mmol) was added. The mixture was stirred at 0°C for 10 minutes and then, *N,N'*–dicyclohexylcarbodiimide (314 mg, 1.5 mmol) was added. The mixture was stirred for 40 minutes at 0°C. In another Schlenk, **II–14** (524 mg, 1.5 mmol) was dissolved in 15 mL of dry dichloromethane and the resulting solution was added dropwise to the solution of activated acid at 0°C. The mixture was stirred overnight at room temperature under argon atmosphere. The resulting suspension was filtered

and the filtrate was purified by silica gel chromatography (eluent DCM/EtOAc/$Et_3N$ 95/4/1) to afford compound **II–16** as a red solid (440 mg, 53 %).

$^1$H NMR (500 MHz, DMSO–$d_6$) δ 11.11 (s, 1H), 10.23 (s, 1H), 8.12 (s, 1H), 8.05 (d, *J* = 8.0 Hz, 1H), 7.94 (t, *J* = 8.1 Hz, 1H), 7.89 (d, *J* = 2.4 Hz, 1H), 7.84 (d, *J* = 8.2 Hz, 1H), 7.79 (d, *J* = 2.4 Hz, 1H), 6.76 (s, 2H), 4.06 (d, *J* = 6.5 Hz, 2H), 3.95 (s, 3H), 2.08 (s, 1H), 1.02 (d, *J* = 6.7 Hz, 6H).

$^{13}$C NMR (125 MHz, DMSO–$d_6$) δ 167.5, 164.0, 161.0, 150.4, 148.8, 141.0, 133.2, 128.5, 120.3, 120.0, 114.7, 113.0, 111.1, 110.4, 105.2, 74.8, 52.9, 30.6, 27.4, 18.7.

HRMS (MALDI–TOF) calcd. for $C_{67}H_{59}N_{15}O_{11}S_8$ $[M]^+$; 574.0461; found, 574.0467.

## Compound II–17

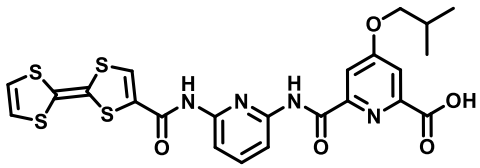

**Chemical Formula:** $C_{23}H_{20}N_4O_5S_4$
**Molecular Weight:** 560.0317

Solid lithium hydroxide (45 mg, 1.9 mmol) was dissolved in a minimal amount of water and was added dropwise to a solution of **II–16** (440 mg, 0.7 mmol) in 20 mL of tetrahydrofuran. The mixture was stirred at room temperature for three hours. Then, acetic acid was added dropwise to a neutral pH (monitored by litmus paper). The solvent was evaporated under reduced pressure and the resulting solid was washed by water and filtrated to afford compound **II–17** as a red powder (430 mg, quantitative).

$^1$H NMR (500 MHz, DMSO–$d_6$) δ 11.11 (s, 1H), 10.23 (s, 1H), 8.12 (s, 1H), 8.05 (d, *J* = 8.0 Hz, 1H), 7.94 (t, *J* = 8.1 Hz, 1H), 7.89 (d, *J* = 2.4 Hz, 1H), 7.84 (d, *J* = 8.2 Hz, 1H), 7.79 (d, *J* = 2.4 Hz, 1H), 6.76 (s, 2H), 4.06 (d, *J* = 6.5 Hz, 2H), 3.95 (s, 3H), 2.08 (s, 1H), 1.02 (d, *J* = 6.7 Hz, 6H).

$^{13}$C NMR (125 MHz, DMSO–$d_6$) δ 166.7, 166.7, 161.9, 157.8, 150.2, 149.3, 149.1, 140.9, 133.4, 128.3, 120.2, 120.0, 112.9, 109.8, 108.9, 108.6, 105.2, 74.2, 45.3, 27.4, 18.8, 9.0.

HRMS (MALDI–TOF) calcd. for $C_{23}H_{20}N_4O_5S_4$ $[M]^+$; 560.0317; found, 560.0322.

## Foldamer A

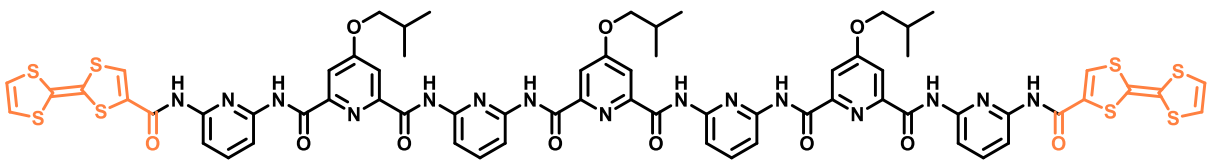

**Chemical Formula:** $C_{67}H_{59}N_{15}O_{11}S_8$
**Molecular Weight:** 1505.2284

Dry **II–17** (98 mg, 0.2 mmol, 2.3 equivalents) was dissolved in dry dichloromethane (5 mL) under argon atmosphere and 1–chloro–N,N,2–trimethyl–1–propenylamine (Ghosez's reagent,

61 mg, 0.45 mmol, 6 equivalents) was added. The mixture was stirred for 4 hours under argon atmosphere. The latter was evaporated under vacuum using a liquid nitrogen trap. The resulting solid was dried for 3 hours under vacuum and 6 mL of dry tetrahydrofuran was added. In another Schlenk, dry **II–12** (32 mg, 0.7 mmol) was dissolved in 4 mL of dry tetrahydrofuran and dry DIPEA (52 mg, 0.6 mmol) was added. The latter mixture was added dropwise to the solution of acyl chloride and was stirred for 20 hours at room temperature. The solvent was removed under reduced pressure and the crude was purified by silica gel chromatography (eluent DCM/EtOAc/$Et_3N$ 79/20/1) and HPLC to afford foldamer **A** as an orange–red solid (42 mg, 37 %).

$^1$H NMR (500 MHz, DMSO–$d_6$) δ 10.47 (s, 2H), 10.43 (s, 2H), 10.35 (s, 2H), 10.26 (s, 2H), 7.96 (d, *J* = 7.9 Hz, 2H), 7.82 (d, *J* = 2.5 Hz, 2H), 7.80 (s, 2H), 7.79 – 7.77 (m, 2H), 7.73 (d, *J* = 4.2 Hz, 2H), 7.72 – 7.69 (m, 4H), 7.65 (t, *J* = 8.0 Hz, 2H), 7.43 (d, *J* = 7.9 Hz, 2H), 7.29 (d, *J* = 2.4 Hz, 2H), 6.74 (q, *J* = 6.3 Hz, 4H), 4.09 (d, *J* = 6.5 Hz, 4H), 3.94 (d, *J* = 6.8 Hz, 2H), 2.20 (m, 2H), 2.14 – 2.10 (m, 1H), 1.13 (d, *J* = 6.7 Hz, 12H), 1.03 (d, *J* = 6.7 Hz, 6H).

$^{13}$C NMR (125 MHz, DMSO–$d_6$) δ 168.8, 168.5, 161.6, 161.3, 160.7, 157.6, 150.8, 150.7, 150.4, 149.6, 149.5, 149.1, 141.9, 141.3, 134.3, 128.7, 121.3, 120.8, 112.6, 112.3, 112.0, 111.7, 110.3, 109.9, 109.7, 109.64, 106.40, 80.1, 75.8, 31.6, 28.5, 28.4, 19.8, 19.7.

HRMS (MALDI–TOF) calcd. for $C_{67}H_{59}N_{15}O_{11}S_8$ $[M + Na]^+$; 1528.2160; found, 1528.2176.

## Compound II–18

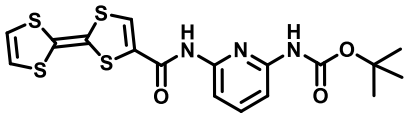

**Chemical Formula:** $C_{17}H_{17}N_3O_3S_4$
**Molecular Weight:** 439.0153

To a solution of **II–15** (132 mg, 535 µmol, 1.4 eq.) in 15 mL dry dichloromethane under argon atmosphere at 0°C, 4–dimethylaminopyridine (65 mg, 321 µmol, 0.6 eq.) was added. The mixture was stirred at 0°C for 10 minutes and then, *N,N'*–dicyclohexylcarbodiimide (110 mg, 535 µmol, 1 eq.) was added. The mixture was stirred for 40 minutes at 0°C. In another Schlenk, **II–10** (80 mg, 382 µmol) was dissolved in 15 mL of dry dichloromethane and the resulting solution was added dropwise to the solution of activated acid at 0°C. The mixture was stirred overnight at room temperature under argon atmosphere. The resulting suspension was filtrated and the filtrate was purified by silica gel chromatography (eluent DCM/EtOAc/$Et_3N$ 95/4/1) to afford compound **II–18** as a red solid (89 mg, 53 %).

$^1$H NMR (300 MHz, DMSO–$d_6$) δ 10.54 (s, 1H), 9.43 (s, 1H), 8.03 (s, 1H), 7.73 (t, *J* = 8.1 Hz, 1H), 7.51 (ddd, *J* = 14.9, 8.1, 0.8 Hz, 2H), 6.74 (d, *J* = 6.6 Hz, 2H), 1.47 (s, 9H).

$^{13}$C NMR (75 MHz, DMSO–$d_6$) δ 157.8, 149.5, 139.9, 133.3, 128.1, 120.3, 120.0, 112.7, 108.9, 105.4, 79.8, 28.0.

HRMS (MALDI–TOF) calcd. for $C_{17}H_{17}N_3O_3S_4$ $[M]^+$; 439.0153; found, 439.0147.

# Chapter III

## Compound III–1

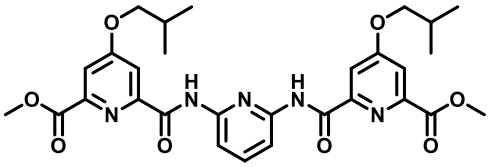

**Chemical Formula:** $C_{29}H_{33}N_5O_8$
**Molecular Weight:** 579.2329

Dry carboxylic acid **II–8** (1 g, 4 mmol, 2.3 eq.) was dissolved in 10 mL of dry dichloromethane under inert conditions. Oxalyl chloride (830 µL, 9 mmol, 2 eq.) and a drop of dry dimethylformamide were added. A Gas release was observed and the mixture was stirred for 2 hours under argon atmosphere. The excess of oxalyl and dichloromethane were removed under vacuum using a liquid nitrogen trap and the solid was left under vacuum for 3 h. The resulting acid chloride was dissolved in dry THF (10 mL). Then, a solution of 2,6–diaminopyridine (200 mg, 1.9 mmol, 1eq.) and DIPEA (3.6 mL, 20 mmol, 5 eq.) in THF (10 mL) was added to the solution of acid chloride. The mixture was then stirred at room temperature for 12 H. The solvent was removed under reduced pressure and the residue was purified by silica gel chromatography using DCM/EtOAc 90/10 to afford compound **III–1** as a white solid (795 mg, 75 %).

$^{1}$H NMR (300 MHz, $CDCl_3$) δ 10.4 (s, 2H), 8.2 (s, 1H), 8.18 (s, 1H), 7.96 (d, J = 2.5Hz, 2H), 7.86 (t, J = 8.1Hz, 1H), 7.79 (d, J = 6.5Hz, 4H), 4.07 (s, 6H), 3.94 (d, J = 6.5Hz, 4H), 2.17 (m, 2H), 1.07 (d, J = 6.7Hz, 12H).

$^{13}$C NMR (75 MHz, $CDCl_3$) δ 167.9, 165.2, 162.1, 151.5, 149.5, 148.5, 140.8, 115.1, 111.4, 110.3, 75.4, 53.1, 28.2, 19.2.

HRMS (MALDI–TOF) calcd for $C_{29}H_{33}N_5O_8$, 602.2235 $[M + Na]^+$; found, 602.2221.

## Compound III–2

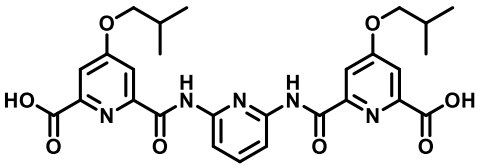

**Chemical Formula:** $C_{27}H_{29}N_5O_8$
**Molecular Weight:** 551.2016

Sodium hydroxide (78 mg, 2 mmol, 3 eq.) was dissolved in water (3 mL) and was added at 0 °C to a solution of compound **7** (376 mg, 65 µmol, 1 eq.) in THF (15 mL). The mixture was stirred at room temperature overnight. Acetic acid was added to the solution (pH = 7). After evaporation of the solvent under reduced pressure, the residue was dissolved in water (30 mL) and extracted with dichloromethane (3 × 30 mL). The organic phases were combined, dried over magnesium sulfate and concentrated under reduced pressure to afford compound **III–2** as a white solid (360 mg, quantitative).

$^{1}$H NMR (300 MHz, DMSO–$d_6$) δ 11.15 (s, 2H), 8.16–7.77 (m, 7H), 4,06 (d, J = 6.5Hz, 2H, 4H), 2.09 (m, 2H), 1.02(d, J = 6.7Hz, 12H).

$^{13}$C NMR (75 MHz, DMSO–$d_6$) δ 167.3, 165.2, 161.62, 150.3, 149.7, 149.7, 140.7, 113.3, 111.1, 109.6, 74.6, 27.5, 18.7.

HRMS (MALDI–TOF) calcd for $C_{27}H_{29}N_5O_8$, 574.1908 $[M + Na]^+$; found, 574.1908.

## Compound III–3

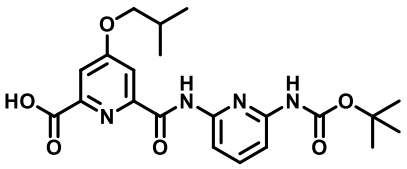

**Chemical Formula:** $C_{21}H_{26}N_4O_6$
**Molecular Weight:** 430.1852

Sodium hydroxide (162 mg, 4 mmol) was dissolved in water (6 mL) and was added at 0 °C to a solution of compound **II–13** (600 mg, 1.4 mmol) in THF (30 mL). The mixture was stirred at room temperature overnight. Acetic acid was added to the solution (pH = 7). After evaporation of the solvent under reduced pressure, the residue was dissolved in water (30 mL) and extracted with dichloromethane (3 × 30 mL). The organic phases were combined, dried over magnesium sulfate and concentrated under reduced pressure to afford compound **III–3** as a white solid (575 mg, quantitative).

$^{1}$H NMR (300 MHz, $CDCl_3$) δ 10.33 (s, 1H), 8.07 (dd, *J* = 7.7, 1.0 Hz, 1H), 8.01 (d, *J* = 2.5 Hz, 1H), 7.91 (d, *J* = 2.5 Hz, 1H), 7.78 (t, *J* = 8.0 Hz, 1H), 7.72 (d, *J* = 7.2 Hz, 1H), 7.35 (s, 1H), 3.96 (d, *J* = 6.5 Hz, 2H), 2.24 – 2.11 (m, 1H), 1.55 (s, 10H), 1.07 (d, *J* = 6.7 Hz, 6H).

$^{13}$C NMR (75 MHz, $CDCl_3$) δ 168.1, 166.7, 162.1, 152.3, 151.1, 150.4, 149, 148.3, 141.4, 114.6, 112.4, 109, 108.7, 81.5, 75.4, 28.4, 28.2, 19.2.

HRMS (MALDI–TOF) calcd for $C_{21}H_{26}N_4O_6$, 453.1749 $[M + Na]^+$; found, 453.1750.

## Compound III–4

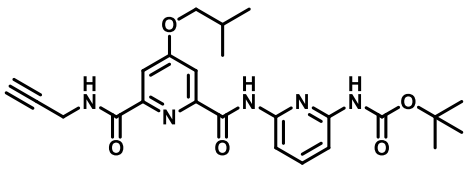

**Chemical Formula:** $C_{24}H_{29}N_5O_5$
**Molecular Weight:** 467.2169

The dry carboxylic acid **III–3** (400 mg, 929 µmol, 1 eq.) was dissolved in 5 mL of dry dichloromethane under argon atmosphere and 1–chloro–*N*,*N*,2–trimethyl–1–propenylamine (Ghosez's reagent, 0.75 mL, 5.6 mmol, 6 eq.) was added. The mixture was stirred overnight at room temperature. The latter was evaporated under vacuum using a liquid nitrogen trap and the

solid is dried under vacuum for 3 hours. The latter was dissolved in 10 mL of anhydrous THF and added dropwise to a mixture of propragylamine (178 µL, 2.8 mmol, 3 eq.) and DIPEA (810 µL, 4.6 mmol, 5 eq.) in 5 mL of dry THF. The mixture was stirred overnight at room temperature. The solvent was then removed under reduced pressure and the crude was purified by silica gel chromatography (eluent DCM/EtOAc 95/5) to afford compound **III–4** as a white solid (390 mg, 94 %).

$^{1}$H NMR (300 MHz, $CDCl_3$) δ 9.88 (s, 1H), 8.07–7.69 (m, 6H), 7.05 (s, 1H), 4.36 (dd, J = 5.8Hz, 2.5Hz, 2H), 3.93 (d, J = 6.5Hz, 2H), 2.33 (t, J = 2.5Hz, 1H), 2.15 (m, 1H), 1.54 (s, 9H), 1.05 (d, J = 6.7Hz, 6H).

$^{13}$C NMR (125 MHz, $CDCl_3$) δ 168.4, 163.3, 161.7, 152.2, 150.6, 150.4, 112.2, 112.1, 108.6, 108.5, 81.6, 79.6, 75.5, 71.8, 29.4, 28.4, 28.1, 19.2.

HRMS (MALDI–TOF) calcd for $C_{21}H_{26}N_4O_6$, 490.2073 $[M + Na]^+$; found, 490.2060.

## Compound III–5

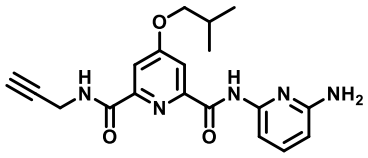

**Chemical Formula:** $C_{19}H_{21}N_5O_3$
**Molecular Weight:** 367.1644

Protected **III–4** (1.1 g, 2.4 mmol, 1 eq.) was dissolved in 8 mL of dichloromethane and trifluoroacetic acid (7 mL, 40 eq.) was added. The mixture was stirred for 4 hours at room temperature. The reaction mixture was washed with saturated $NaHCO_3$ solution, extracted with chloroform (150 mL) and washed with water (3 × 50 mL). The organic phases were combined, dried over magnesium sulfate and concentrated under reduced pressure to afford compound **III–5** as a white solid (875 mg, quantitative).

$^{1}$H NMR (300 MHz, $CDCl_3$) δ 10.19 (s, 1H), 7.93 (s, 1H), 7.73 (dd, 2H), 7.52 (t, 1H), 6.33 (dd, J = 8.0, 0.7 Hz, 1H), 4.62 (s, 2H), 4.03 (s, 3H), 3.96 (d, 2H), 2.03 (m, 1H) 1.04 (d, 6H).

$^{13}$C NMR (75 MHz, $CDCl_3$) δ 168.3, 163.4, 161.63, 157.2, 150.5, 150.4, 149.3, 140.7, 112, 111.8, 105.1, 103.8, 79.8, 75.4, 71.5, 53.6, 29.8, 29.3, 28.1, 19.2.

HRMS (MALDI–TOF) calcd for $C_{21}H_{26}N_4O_6$, 390.1543 $[M + Na]^+$; found, 390.1536.

## Foldamer B

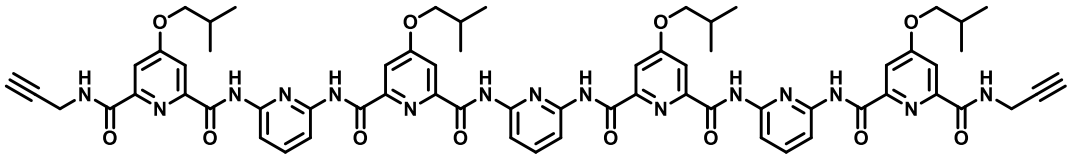

**Chemical Formula:** $C_{65}H_{67}N_{15}O_{12}$
**Molecular Weight:** 1249.5094

Dry diacid **III–2** (220 mg, 400 µmol, 1 eq.) was dissolved in 10 mL of dry dichloromethane under argon atmosphere and Ghosez's reagent (0.42 mL, 3 mmol, 8 eq.) was added. The mixture was stirred overnight at room temperature. The latter was evaporated under vacuum using a liquid nitrogen trap and the solid is dried under vacuum for 3 hours. In another schlenk, amine **III–4 (**440 mg, 1.2 mmol, 2.5 eq.) was dissolved in 10 mL of dry THF and DIPEA (0.3 mL, 2 mmol, 5 eq.) was added. Then, this mixture was added dropwise to a solution of the resulting acid chloride in 7 mL of dry THF. The mixture was stirred overnight at room temperature. The solvent was removed under reduced pressure and the crude was purified by silica gel chromatography (eluent DCM) to afford foldamer **B** as a white solid (416 mg, 84 %).

$^{1}$H NMR (500 MHz, DMSO–$d_6$) δ 10.84 (s, 2H), 10.65 (s, 2H), 10.27 (s, 2H), 9.78 (t, *J* = 6.0 Hz, 2H), 8.23 (dd, *J* = 8.9, 6.9 Hz, 1H), 8.16 (d, *J* = 8.5 Hz, 2H), 7.87 (d, *J* = 8.1 Hz, 2H), 7.81 – 7.74 (m, 4H), 7.68 (t, *J* = 8.0 Hz, 2H), 7.64 (t, *J* = 3.4 Hz, 2H), 7.34 (d, *J* = 2.6 Hz, 2H), 7.13 (d, *J* = 2.5 Hz, 2H), 4.02 (dd, *J* = 27.4, 6.5 Hz, 8H), 3.71 – 3.67 (m, 4H), 2.97 (t, *J* = 2.5 Hz, 2H), 2.22 – 2.08 (m, 4H), 1.10 (dd, *J* = 6.6, 1.3 Hz, 24H).

$^{13}$C NMR (125 MHz, DMSO–$d_6$) δ 167.0, 166.2, 161.1, 161.3, 160.5, 159.5, 150.0, 149.3, 149.0, 148.9, 148.2, 147.9, 142.3, 139.7, 111.2, 110.8, 110.4, 110.1, 108.8, 108.5, 80.4, 74.4, 74.1, 72.5, 27.1, 18.4.

HRMS (MALDI–TOF) calcd for $C_{65}H_{67}N_{15}O_{18}$, 1272.4994 $[M + Na]^+$; found, 1272.4985.

## Compound III–6[4]

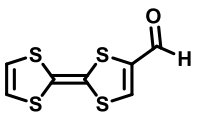


**Chemical Formula:** $C_7H_4OS_4$
**Molecular Weight:** 231.9145

Dry TTF (1.5 g, 7 mmol, 1 eq.) was dissolved in anhydrous diethyl ether (150 mL) under argon atmosphere. The solution was cooled down to –78°C and a solution of LDA 1 M in THF/hexane (7 mmol) was added dropwise. A thick yellow suspension appeared and the medium was stirred for 30 min at –78°C. Then, *N*–methyl–*N*–phenylformamide (3 g, 24 mmol, 3 eq.) was added dropwise and the mixture was stirred for 45 min at –78°C and the allowed to warm up to room temperature overnight. Diethyl ether (70 mL) and hydrochloric acid 3 M (70 mL) were added, producing a deep red solution. The organic layer was separated and washed with hydrochloric acid (3 × 50 mL) and water (3 × 50 mL). The solvent was removed under reduced pressure and the crude was purified by silica gel chromatography (eluent DCM/PE/$Et_3N$ 79/20/1) to afford compound **III–6** as a red solid (1.3 g, 76 %).

$^{1}$H NMR (300 MHz, $CDCl_3$) δ 9.45 (s, 1H), 7.43 (s, 1H), 6.41 – 6.26 (m, 2H).

$^{13}$C NMR (75 MHz, $CDCl_3$) δ 179.8, 141.5, 140.1, 119.5, 118.9, 116.0, 105.6.

## Compound III–7[4]

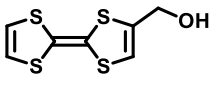


**Chemical Formula:** $C_7H_6OS_4$
**Molecular Weight:** 233.9301

Sodium borohydride (173 mg, 4.3 mmol, 2 eq.) was added to a solution of 4–formyltetrathiafulvalene **III–6** (500 mg, 2 mmol) in absolute ethanol (45 mL). The solution quickly turned yellow and the mixture was stirred for 1 hour at room temperature. Dichloromethane (100 mL) was added and the organic layer was washed with a saturated solution of sodium chloride (3 × 50 mL) and water (3 × 50 mL), dried over magnesium sulfate and evaporated under vacuum. The crude was purified by silica gel chromatography (eluent DCM/PE/$Et_3N$ 60/39/1) to afford compound **III–7** as a yellow oil that solidifies on standing at RT (351 mg, 70 %).

$^1$H NMR (300 MHz, Acetone–$d_6$) δ 6.61 (s, 2H), 6.44 (t, J = 1.3 Hz, 1H), 4.36 (br, 2H).

$^{13}$C NMR (75 MHz, Acetone–$d_6$) δ 139.3, 120.3, 120.2, 114.7, 110.6, 110.2, 60.3.

## Compound III–8[5]

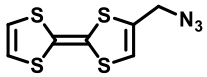

**Chemical Formula:** $C_7H_5N_3S_4$
**Molecular Weight:** 258.9366

4–(Hydroxymethyl)tetrathiafulvalene **III–7** (350 mg, 1 mmol) was dissolved in dry DMF (35 mL), then diphenyl phosphoryl azide (DPPA) (2 g, 7 mmol, 5 eq.) was added. The mixture was cooled in an ice bath and 1,8–diazabicyclo[5.4.0]undec–7–ene (DBU) (255 mg, 1.6 mmol, 1.1 eq.) was added. After stirring for 4 hours under argon atmosphere at room temperature, sodium azide (491 mg, 7.5 mmol, 5 eq.) was added and the mixture was stirred overnight. DMF was partially evaporated and dichloromethane (80 mL) was added. The organic layer was washed with water (3 x 100 mL), dried over magnesium sulfate and the solvent was partially evaporated under reduced pressure. The desired product was purified by silica gel chromatography (DCM/PE/$Et_3N$ 39/60/1, solid deposit in DCM/$Et_3N$) to afford **III–8** as a yellow oil that solidifies on standing at RT (349 mg, 90 %).

$^1$H NMR (300 MHz, Acetonitrile–$d_3$) δ 6.49 (t, J = 1.1 Hz, 1H), 6.47 (s, 2H), 4.15 (br, 2H).

## Foldamer C

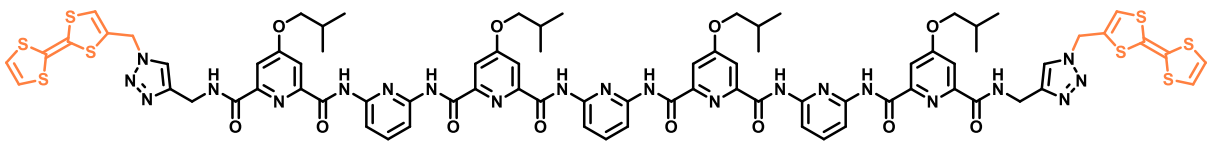

**Chemical Formula:** $C_{79}H_{77}N_{21}O_{12}S_8$
**Molecular Weight:** 1767.3826

Foldamer **B** (100 mg, 80 µmol, 1 eq.) and azide **III–8** (83 mg, 320 µmol, 4 eq.) were dissolved in a mixture of DMSO and dry DCM (1/1, 4 mL) and the solution was purged with argon for 10 minutes. Then, copper sulfate (1.3 mg, 8 µmol, 0.1 eq.) and sodium ascorbate (1.6 mg, 8 µmol, 0.1 eq.) were added. The mixture was stirred overnight at room temperature. The solution was diluted with dichloromethane (20 mL) and washed with water (3 × 30 mL). The organic layer was evaporated and the crude was purified first by silica gel chromatography (eluent DCM

and then DCM/MeOH/$Et_3N$ 96/3/1) and then via recycling size exclusion chromatography (sec) to afford foldamer **C** as a yellow solid (119 mg, 85 %).

$^1$H NMR (500 MHz, DMSO–$d_6$) δ 10.85 (s, 2H), 10.67 (s, 2H), 10.24 (s, 2H), 9.98 (t, *J* = 6.3 Hz, 2H), 8.24 (q, *J* = 5.4 Hz, 3H), 7.90 – 7.82 (m, 4H), 7.81 – 7.75 (m, 4H), 7.72 – 7.62 (m, 4H), 7.32 (d, *J* = 2.6 Hz, 2H), 7.08 (d, *J* = 2.4 Hz, 2H), 6.76 (s, 2H), 6.62 – 6.54 (m, 4H), 5.28 (s, 4H), 4.16 (s, 4H), 4.03 (dd, *J* = 12.6, 6.5 Hz, 8H), 2.17 (dtd, *J* = 13.3, 6.6, 1.9 Hz, 3H), 1.11 (t, *J* = 6.8 Hz, 24H).

$^{13}$C NMR (125 MHz, DMSO–$d_6$) δ 167.4, 166.5, 162.4, 161.7, 160.9, 159.8, 150.3, 149.8, 149.4, 149.3, 148.4, 148.2, 145.2, 140.0, 130.0, 123.0, 120.5, 119.8, 111.7, 111.5, 110.7, 110.4, 109.0, 108.6, 107.3, 74.8, 74.5, 47.8, 40.4, 27.5, 18.8.

HRMS (MALDI–TOF) calcd for $C_{79}H_{77}N_{12}O_{12}S_8$, 1790.3735 $[M + Na]^+$; found, 1790.3718.

## Compound III–9[6]

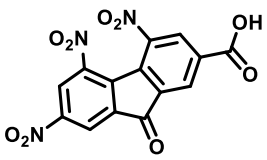


**Chemical Formula:** $C_{14}H_5N_3O_9$
**Molecular Weight:** 359.0026

9–Fluorenone–2–carboxylic acid (940 mg, 4 mmol, 1 eq.) was added slowly to a solution of sulphuric acid (18 mL) and nitric acid (18 mL, 99 %) at 0°C. The solution was stirred for 5 minutes at 0°C, and then, allowed to reflux for 3 hours. The reaction was cooled to room temperature and the mixture was poured into 400 mL of crushed ice. A yellow precipitate was collected by filtration and washed three times with cold water. The precipitate was dried under vacuum to afford compound **III–9** as yellow solid (1 g, 69 %).

$^1$H NMR (300 MHz, DMSO–$d_6$) δ 8.93 (d, *J* = 2.2 Hz, 1H), 8.70 (d, *J* = 2.1 Hz, 1H), 8.63 (s, 1H), 8.46 (s, 1H).

HRMS (MALDI–TOF) calcd for $C_{14}H_5N_3O_9$, 359.0020 $[M]^+$; found, 359.0031.

## Compound III–10

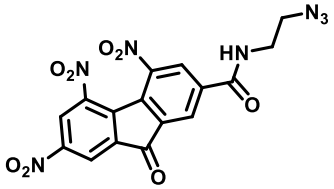


**Chemical Formula:** $C_{16}H_9N_7O_8$
**Molecular Weight:** 427.0513

Dry compound **III–9** (480 mg, 1 mmol, 1 eq.) was dissolved in 5 mL of dry dichloromethane under inert conditions. Oxalyl chloride (573 µL, 6.7 mmol, 5 eq.) and a drop of dry dimethylformamide were added. A gas release was observed and the mixture was stirred for 2 hours under argon atmosphere. Excess oxalyl chloride and dichloromethane were removed

under vacuum using a liquid nitrogen trap and the solid was left under vacuum for 3 H. The resulting acid chloride was dissolved in dry THF (10 mL). Then, a solution of 2–azidoethanamine (1.5 g, 13.36 mmol, 10 eq.) and DIPEA (1.2 mL, 6.7 mmol, 5 eq.) in THF (10 mL) was added to the solution of acid chloride. The mixture was then stirred at room temperature for 12 h. The solvent was removed under reduced pressure and the residue was purified by silica gel chromatography using DCM/EtOAc (90/10) to afford compound **III–10** as a white solid (380 mg, 54 %).

$^{1}$H NMR (300 MHz, $CDCl_3$) δ 8.95 (d, *J* = 2.1 Hz, 1H), 8.82 (d, *J* = 2.1 Hz, 1H), 8.62 (d, *J* = 1.7 Hz, 1H), 8.54 (d, *J* = 1.6 Hz, 1H), 7.20 (t, *J* = 5.6 Hz, 1H), 3.76 – 3.67 (m, 2H), 3.67 – 3.60 (m, 2H).

$^{13}$C NMR (75 MHz, $CDCl_3$) δ 185.1, 163.2, 149.6, 146.9, 139.3, 138.6, 138.5, 137.9, 129.7, 126.9, 125.5, 122.8, 50.6, 40.0.

HRMS (MALDI–TOF) calcd for $C_{16}H_9N_7O_8$, 427.0524 $[M]^+$; found, 427.0518.

## Foldamer D

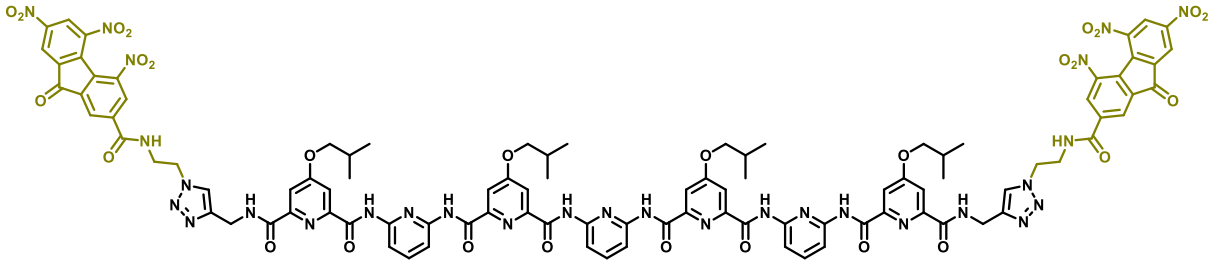

**Chemical Formula:** $C_{97}H_{85}N_{29}O_{28}$
**Molecular Weight:** 2103.6119

Foldamer **B** (150 mg, 120 µmol, 1 eq.) and azide **III–10** (230 mg, 480 µmol, 4 eq.) were dissolved in a mixture of DMSO and dry DCM (1/1, 5 mL) and the solution was purged with argon for 10 minutes. Then, copper sulfate (2 mg, 12 µmol, 0.1 eq.) and sodium ascorbate (2.6 mg, 12 µmol, 0.1 eq.) were added. The mixture was stirred overnight at room temperature. The solution was diluted with dichloromethane (20 mL) and washed with water (3 × 30 mL). The organic layer was evaporated and the crude was purified first by silica gel chromatography (eluent DCM and then DCM/MeOH 98/2) and then via recycling size exclusion chromatography (sec) to afford foldamer **D** as a brown solid (184 mg, 70 %).

$^{1}$H NMR (300 MHz, DMSO–$d_6$) δ 10.73 (s, 2H), 10.64 (s, 2H), 10.18 (s, 2H), 9.90 (t, *J* = 6.2 Hz, 2H), 9.06 (t, *J* = 5.7 Hz, 2H), 8.91 (d, *J* = 2.1 Hz, 2H), 8.60 (d, *J* = 2.1 Hz, 2H), 8.48 (d, *J* = 1.6 Hz, 2H), 8.32 (d, *J* = 1.6 Hz, 2H), 8.22 – 8.14 (m, 3H), 7.85 – 7.68 (m, 6H), 7.68 – 7.55 (m, 6H), 7.25 (d, *J* = 2.6 Hz, 2H), 7.03 (d, *J* = 2.5 Hz, 2H), 4.45 (t, *J* = 3.8 Hz, 4H), 4.09 (m, 4H), 4.00 (m, 8H), 3.64 (m, 4H), 2.17 (td, *J* = 6.6, 2.9 Hz, 4H), 1.11 (dd, *J* = 6.7, 1.3 Hz, 24H).

HRMS (MALDI–TOF) calcd for $C_{97}H_{85}N_{29}O_{28}$, 2104.62300 $[M + H]^+$; found, 2104.6191.

## Compound III–12

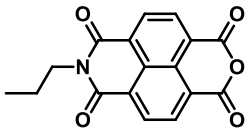

**Chemical Formula:** $C_{17}H_{11}NO_5$
**Molecular Weight:** 309.0637

A mixture of propylamine (1.35 mL, 11 mmol, 1 eq.) and dry DIPEA (4.78 mL, 27 mmol, 2.5 eq.) in 3 mL of dry DMF was added dropwise to a solution of 1, 4, 5, 8–naphthalenetetracarboxylic acid dianhydride (3 g, 11 mmol, 1 eq.) in 30 mL of dry DMF heated to reflux. The mixture was stirred overnight at 140°C under argon conditions and then allowed to warm up to room temperature. The solvent was removed under reduced pressure and the crude was purified by silica gel chromatography using dichloromethane as eluent to afford compound **III–12** as a white powder (560 mg, 15 %).

$^1$H NMR (300 MHz, $CDCl_3$) δ 8.82 (s, 4H), 4.21–4.15 (t, J = 7.6 Hz, 2H), 1.78 (m, 2H), 1.03 (t, J = 7.4 Hz, 3H).

$^{13}$C NMR (75 MHz, $CDCl_3$) δ 162.4, 159.0, 133.3, 131.4, 129.0, 128.1, 122.9, 42.8, 21.5, 11.6.

## Compound III–13

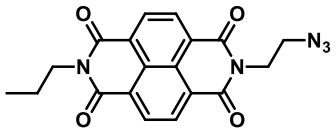

**Chemical Formula:** $C_{19}H_{15}N_5O_4$
**Molecular Weight:** 377.1124

A mixture of 2–azidoethanamine (696 mg, 8 mmol, 5 eq.) and dry DIPEA (0.85 mL, 4 mmol, 2.5 eq.) in 5 mL of dry DMF, was added dropwise to a solution of **III–12** (0.5 g, 1.6 mmol, 1eq.) in 30 mL of dry DMF at room temperature under argon atmosphere. The mixture was heated to reflux overnight. The solvent was evaporated and the crude was dissolved in dichloromethane, washed with water (3 × 30 mL), dried over magnesium sulfate and concentrated under reduced pressure to afford compound **III–13** as a pale orange powder (987 mg, 82 %).

$^1$H NMR (300 MHz, $CDCl_3$) δ 8.73 (d, *J* = 1.2 Hz, 4H), 4.44 (t, *J* = 6.2 Hz, 2H), 4.14 (dd, *J* = 8.6, 6.7 Hz, 2H), 3.67 (t, *J* = 6.1 Hz, 2H), 1.74 (ddd, *J* = 13.3, 8.3, 6.7 Hz, 2H), 1.01 (t, *J* = 7.4 Hz, 3H).

$^{13}$C NMR (75 MHz, $CDCl_3$) δ 162.9, 162.7, 131.3, 131.0, 126.9, 126.8, 126.2, 48.8, 42.5, 39.3, 21.4, 11.5.

HRMS (MALDI–TOF) calcd for $C_{19}H_{15}N_5O_4$, 377.1131 $[M]^+$; found, 377.1129.

## Foldamer E

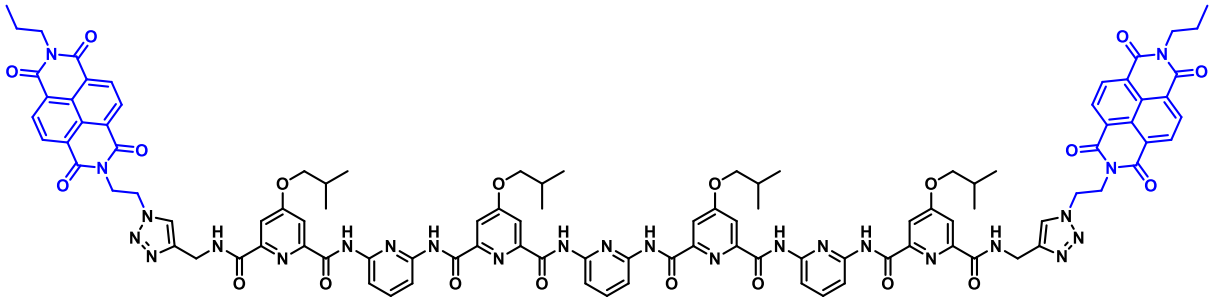

**Chemical Formula:** $C_{103}H_{97}N_{26}O_{20}$
**Molecular Weight:** 2003.7342

Foldamer **B** (100 mg, 80 µmol, 1 eq.) and azide **III–13** (105 mg, 280 µmol, 3.5 eq.) were dissolved in a mixture of DMSO and dry DCM (1/1, 4 mL) and the solution was purged with argon for 10 minutes. Then, copper sulfate (1.3 mg, 8 µmol, 0.1 eq.) and sodium ascorbate (1.6 mg, 8 µmol, 0.1 eq.) were added. The mixture was stirred overnight at room temperature. The solution was diluted with dichloromethane (20 mL) and washed with water (3 × 30 mL). The organic layer was evaporated and the crude was purified by silica gel chromatography (eluent DCM and then DCM/MeOH 97/3) to afford foldamer **E** as a yellow solid (104 mg, 65 >w%).

$^{1}$H NMR (500 MHz, DMSO–$d_6$) δ 10.84 (s, 2H), 10.57 (s, 2H), 10.24 (s, 2H), 9.88 (t, *J* = 6.2 Hz, 2H), 8.48 – 8.38 (m, 8H), 8.19 – 8.08 (m, 4H), 7.88 (d, *J* = 8.0 Hz, 2H), 7.79 (d, *J* = 8.3 Hz, 4H), 7.75 – 7.68 (m, 4H), 7.55 (d, *J* = 2.4 Hz, 2H), 7.21 (d, *J* = 2.5 Hz, 2H), 7.08 (d, *J* = 2.4 Hz, 2H), 4.58 (t, *J* = 5.7 Hz, 4H), 4.31 (t, *J* = 5.9 Hz, 4H), 4.06 (s, 4H), 3.96 (dd, *J* = 11.0, 6.3 Hz, 12H), 2.15 (m, 4H), 1.65 (m, *J* = 7.4 Hz, 4H), 1.09 (d, *J* = 6.7 Hz, 24H), 0.94 (t, *J* = 7.4 Hz, 6H).

$^{13}$C NMR (125 MHz, DMSO–$d_6$) δ 167.2, 166.5, 162.3, 161.7, 160.9, 150.2, 149.9, 149.7, 149.4, 149.2, 148.6, 148.3, 144.7, 140.0, 130.3, 130.1, 126.1, 125.8, 123.6, 111.0, 110.7, 109.3, 74.7, 74.4, 46.89, 41.65, 40.43, 34.0, 27.53, 20.7, 18.8, 11.3.

HRMS (MALDI–TOF) calcd. for $C_{103}H_{97}N_{25}O_{20}$, 2042.6974 $[M + K]^+$; found, 2042.6973.

## Compound III–14

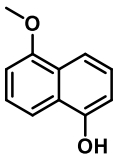

**Chemical Formula:** $C_{11}H_{10}O_2$
**Molecular Weight:** 174.0681

1,5–Dihydroxynaphthalene (5 g, 31 mmol, 1 eq.) and potassium carbonate $K_2CO_3$ (4.75 g, 34 mmol, 1.10 eq.) were dissolved in ACN (100 mL) under argon atmosphere. Then, 1.93 mL (4.43 g, 1 eq.) of iodomethane was added. The mixture was stirred overnight at 80°C. The solvent was evaporated, the solid was dissolved in 300 mL of DCM and filtered over celite. The organic layer was washed with $NaHCO_3$ (3 × 100 mL) and $H_2O$ (3 × 100 mL), dried over magnesium sulfate and the solvent was evaporated under reduced pressure. The desired product

was purified by silica gel chromatography (eluent DCM) to afford **III–14** as a beige powder (1.9 g, 35 %).

$^{1}$H NMR (300 MHz, DMSO–$d_6$) δ 10.07 (s, 1H), 7.69 (ddt, $J$ = 38.7, 8.4, 0.9 Hz, 2H), 7.32 (ddd, $J$ = 16.0, 8.5, 7.6 Hz, 2H), 6.98 – 6.86 (m, 2H), 3.93 (s, 3H).

$^{13}$C NMR (75 MHz, DMSO–$d_6$) δ 154.7, 153.1, 126.3, 125.6, 124.6, 114.2, 112.0, 108.7, 104.5, 55.4.

## Compound III–15

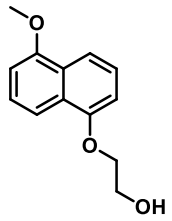


**Chemical Formula:** $C_{13}H_{14}O_3$
**Molecular Weight:** 218.0943

5–Methoxynaphthalen–1–ol **III–14** (812 mg, 4 mmol, 1 eq.) and potassium carbonate $K_2CO_3$ (3.2 g, 23 mmol, 5 eq.) were dissolved in dry DMF (40 mL) under argon atmosphere. The solution was heated to 90°C and then, 992 µL (13 mmol, 3 eq.) was added. The mixture was stirred overnight at 90°C. DMF was evaporated, and the solid was dissolved in 100 mL of DCM and filtrated over celite. The organic layer was washed with $NaHCO_3$ (3 × 100 mL) and $H_2O$ (3 × 100 mL), dried over magnesium sulfate and the solvent was evaporated under reduced pressure. The desired product was purified by silica gel chromatography (eluent DCM) to afford **III–15** as a brown powder (1 g, quantitative).

$^{1}$H NMR (300 MHz, DMSO–$d_6$) δ 7.76 (ddt, $J$ = 36.2, 8.5, 0.9 Hz, 2H), 7.39 (ddd, $J$ = 8.5, 7.7, 6.6 Hz, 2H), 6.98 (ddd, $J$ = 7.7, 2.1, 1.0 Hz, 2H), 4.96 (t, $J$ = 5.7 Hz, 1H), 4.48 (s, 2H), 4.14 (dd, $J$ = 5.4, 4.5 Hz, 2H), 3.95 (s, 3H), 3.91 – 3.80 (m, 2H).

$^{13}$C NMR (75 MHz, $CDCl_3$) δ 155.4, 154.2, 126.7, 125.4, 125.2, 114.8, 114.0, 105.9, 104.7, 69.7, 64.6, 61.7, 55.6.

HRMS (MALDI–TOF) calcd for $C_{13}H_{14}O_3$, 218.0943 $[M]^+$; found, 218.0945.

## Compound III–16

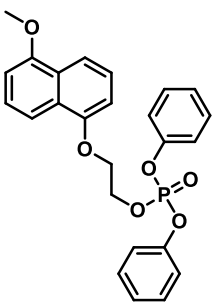


**Chemical Formula:** $C_{25}H_{23}O_6P$
**Molecular Weight:** 450.1232

To a solution of **III–15** (160 mg, 733 µmol, 1 eq.) in 8 mL of dry DMF under argon atmosphere, 0.8 mL (3 mmol, 5 eq.) diphenyl phosphoryl azide (DPPA) was added. The mixture was cooled in an ice bath and 1,8–diazabicyclo[5.4.0]undec–7–ene (DBU) (0.12 mL, 806 µmol, 1.1 eq.) was added. After stirring for 4 hours under argon atmosphere at room temperature, the reaction was stopped. DMF was evaporate and the corresponding oil was dissolved in DCM (50 mL) and washed with water (3 × 50 mL), dried over magnesium sulfate and the solvent was evaporated under reduced pressure. The desired product was purified by silica gel chromatography (eluent DCM) to afford **III–16** as a brown oil (252 mg, 79 %).

$^{1}$H NMR (300 MHz, $CDCl_3$) δ 7.95 – 7.84 (m, 2H), 7.40 – 7.23 (m, 10H), 7.21 – 7.05 (m, 2H), 6.86 – 6.67 (m, 2H), 4.73 – 4.61 (m, 2H), 4.25 (td, *J* = 4.4, 1.6 Hz, 2H), 3.95 (s, 3H).

$^{13}$C NMR (75 MHz, $CDCl_3$) δ 155.0, 153.7, 150.4, 129.7, 126.5, 125.3, 124.9, 120.0, 114.8, 114.3, 105.5, 67.2, 66.7, 55.4.

HRMS (MALDI–TOF) calcd for $C_{25}H_{23}O_9P$, 450.1225 $[M]^+$; found, 450.1226.

## Compound III–17

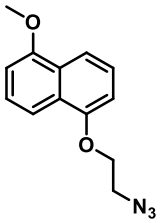


**Chemical Formula:** $C_{13}H_{13}N_3O_2$
**Molecular Weight:** 2243.1008

To a solution of **III–16** (252 mg, 580 µmol, 1 eq.) in 7 mL of dry DMF, 188 mg of sodium azide $NaN_3$ and 1 mL of $H_2O$ were added. The mixture was heated to 80°C overnight. The solution was diluted with 30 mL of DCM, washed with $H_2O$ (3 × 50 mL), dried over magnesium sulfate and the solvent was evaporated under reduced pressure. The crude was purified by silica gel chromatography (eluent DCM) to afford **III–17** as a white powder (87 mg, 61 %).

$^{1}$H NMR (300 MHz, $CDCl_3$) δ 7.93 – 7.82 (m, 2H), 7.39 (ddd, *J* = 12.8, 8.6, 7.7 Hz, 2H), 6.91 – 6.79 (m, 2H), 4.36 – 4.27 (m, 2H), 4.00 (s, 3H), 3.72 (t, *J* = 4.9 Hz, 2H).

$^{13}$C NMR (75 MHz, $CDCl_3$) δ 155.3, 154.0, 126.8, 126.6, 125.6, 125.0, 115.1, 114.3, 105.5, 104.8, 67.3, 55.6, 50.6, 29.8.

HRMS (MALDI–TOF) calcd for $C_{45}H_{48}N_{10}O_9$, 243.1005 $[M]^+$; found, 243.1002.

## Foldamer F

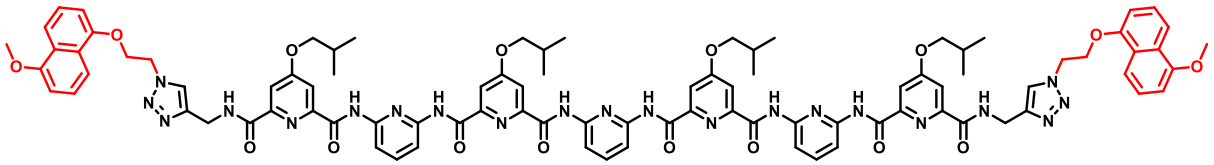

**Chemical Formula:** $C_{91}H_{93}N_{21}O_{16}$
**Molecular Weight:** 1735.7109

Foldamer **B** (100 mg, 80 µmol, 1 eq.) and azide **III–17** (78 mg, 320 µmol, 4 eq.) were dissolved in a mixture of DMSO and dry DCM (1/1, 4 mL) and the solution was purged with argon for 10 minutes. Then, copper sulfate (1.3 mg, 8 µmol, 0.1 eq.) and sodium ascorbate (1.6 mg, 8 µmol, 0.1 eq.) were added. The mixture was stirred overnight at 35°C. The solution was diluted with dichloromethane (20 mL) and washed with water (3 × 30 mL). The organic layer was evaporated and the crude was purified first by silica gel chromatography (eluent DCM and then DCM/MeOH 97/3) and then via recycling size exclusion chromatography (sec) to afford foldamer **F** as a yellow solid (89 mg, 65 %).

$^1$H NMR (500 MHz, DMSO–$d_6$) δ 10.81 (s, 2H), 10.65 (s, 2H), 10.19 (s, 2H), 9.97 (t, *J* = 6.2 Hz, 2H), 8.24 – 8.17 (m, 3H), 7.96 (s, 2H), 7.88 (d, *J* = 8.1 Hz, 2H), 7.80 – 7.74 (m, 4H), 7.68 (d, *J* = 2.5 Hz, 2H), 7.65 (t, *J* = 8.0 Hz, 2H), 7.57 (d, *J* = 8.4 Hz, 2H), 7.34 (d, *J* = 8.4 Hz, 2H), 7.31 (d, *J* = 2.6 Hz, 2H), 7.25 (t, *J* = 8.1 Hz, 2H), 7.07 (d, *J* = 2.5 Hz, 2H), 7.03 (t, *J* = 8.1 Hz, 2H), 6.87 (d, *J* = 7.6 Hz, 2H), 6.74 (d, *J* = 7.7 Hz, 2H), 4.76 (t, *J* = 5.0 Hz, 4H), 4.39 (t, *J* = 5.1 Hz, 4H), 4.14 (s, 4H), 4.03 (dd, *J* = 17.2, 6.5 Hz, 8H), 3.84 (s, 6H), 2.23 – 2.13 (m, *J* = 6.8 Hz, 4H), 1.11 (dd, *J* = 6.7, 3.5 Hz, 24H).

$^{13}$C NMR (125 MHz, DMSO–$d_6$) δ 167.3, 166.5, 162.3, 161.7, 160.8, 159.7, 154.4, 153.0, 150.3, 149.9, 149.7, 149.4, 149.2, 148.4, 148.1, 144.8, 125.6, 125.1, 123.5, 113.9, 113.2, 106.0, 104.6, 74.6, 66.4, 55.3, 48.8, 27.5, 18.8.

HRMS (MALDI–TOF) calcd for $C_{91}H_{93}N_{21}O_{16}$, 1758.7032 $[M + Na]^+$; found, 1758.7001.

## Compound III–18

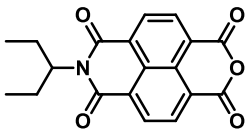

**Chemical Formula:** $C_{19}H_{15}NO_9$
**Molecular Weight:** 337.0950

A mixture of pentan–3–amine (1.69 mL, 11 mmol, 1 eq.) and dry DIPEA (4.8 mL, 28 mmol, 2.5 eq.) in 3 mL of dry DMF was added dropwise to a solution of 1, 4, 5, 8–naphthalenetetracarboxylic acid dianhydride (3 g, 11 mmol, 1 eq.) in 30 mL of dry DMF heated to reflux. The mixture was stirred overnight at 140°C under argon conditions and then allowed to warm up to room temperature. The solvent was removed under reduced pressure and the crude was purified by silica gel chromatography using dichloromethane as eluent to afford compound **III–18** as a white powder (1.2 g, 32 %).

$^{1}$H NMR (500 MHz, $CDCl_3$) δ 8.83 – 8.76 (m, 4H), 5.02 (m, 1H), 2.27 – 2.14 (m, 2H), 1.93 (m, 2H), 0.89 (td, *J* = 7.5, 1.6 Hz, 6H).

$^{13}$C NMR (125 MHz, $CDCl_3$) δ 163.0, 159.0, 133.2, 131.3, 128.9, 128.2, 127.1, 122.7, 58.6, 25.0, 11.4.

HRMS (MALDI–TOF) calcd for $C_{19}H_{15}NO_5$, 338.1023 $[M + H]^+$; found, 338.1023.

## Compound III–19

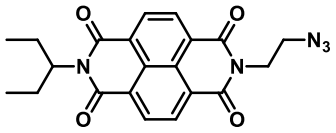

**Chemical Formula:** $C_{21}H_{19}N_5O_4$
**Molecular Weight:** 405.1437

A mixture of 2–azidoethanamine (1.3 g, 15 mmol, 5 eq.) and dry DIPEA (1.7 mL, 9 mmol, 2.5 eq.) in 5 mL of dry DMF, was added dropwise to a solution of **III–18** (1 g, 3 mmol, 1eq.) in 30 mL of dry DMF at room temperature under argon atmosphere. The mixture was heated to reflux overnight. The solvent was evaporated and the crude was dissolved in dichloromethane, washed with water (3 × 30mL), dried over magnesium sulfate and concentrated under reduced pressure to afford compound **III–19** as a pale orange powder (987 mg, 82 %).

$^{1}$H NMR (300 MHz, $CDCl_3$) δ 8.82 – 8.70 (m, 4H), 5.03 (tt, *J* = 9.5, 5.9 Hz, 1H), 4.47 (t, *J* = 6.1 Hz, 2H), 3.69 (t, *J* = 6.1 Hz, 2H), 2.22 (tt, *J* = 14.8, 7.5 Hz, 2H), 1.93 (tt, *J* = 13.4, 7.4 Hz, 2H), 0.90 (t, *J* = 7.5 Hz, 6H).

$^{13}$C NMR (75 MHz, $CDCl_3$) δ 163.1, 131.4, 127.0, 126.8, 126.0, 58.3, 48.8, 25.0, 11.4.

HRMS (MALDI–TOF) calcd for $C_{21}H_{19}N_5O_4$, 405.1447 $[M]^+$; found, 405.1442.

## Compound III–20

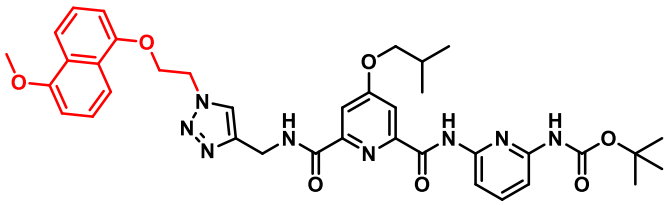

**Chemical Formula:** $C_{37}H_{42}N_8O_7$
**Molecular Weight:** 710.3176

**III–4** (100 mg, 213 µmol, 1 eq.) and azide **III–17** (62 mg, 256 µmol, 1.2 eq.) were dissolved in a mixture of DMSO and dry DCM (*1/1*) and the solution was purged with argon. Then, copper sulfate (3.4 mg, 21 µmol, 0.1 eq.) and sodium ascorbate (4.2 mg, 21 µmol, 0.1 eq.) were added. The mixture was stirred overnight at room temperature. The solution was diluted with dichloromethane (20 mL) and washed with water (3 × 50 mL). The organic layer was evaporated and the crude was purified by silica gel chromatography (eluent DCM/EtOAc 9/1) to afford **III–20** as a white solid (129 mg, 84 %).

$^{1}$H NMR (500 MHz, $CDCl_3$) δ 10.15 (s, 1H), 8.94 (t, , *J* = 7.5 Hz 1H), 8.01 (dd, *J* = 7.6, 1.2 Hz, 1H), 7.92 – 7.86 (m, 2H), 7.83 (dd, *J* = 9.5, 1.8 Hz, 2H), 7.74 (t, *J* = 7.9 Hz, 1H), 7.70 (d, *J* = 8.0 Hz, 1H), 7.66 (dt, *J* = 8.5, 0.9 Hz, 1H), 7.37 (s, 1H), 7.34 – 7.26 (m, 2H), 6.78 (t, *J* = 7.2 Hz, 2H), 4.94 (t, *J* = 5.0 Hz, 2H), 4.80 (d, *J* = 5.8 Hz, 2H), 4.54 (t, *J* = 5.0 Hz, 2H), 3.95 (s, 3H), 3.92 (d, *J* = 6.5 Hz, 2H), 2.15 (dq, *J* = 13.2, 6.8 Hz, 1H), 1.56 (s, 9H), 1.05 (d, *J* = 6.7 Hz, 6H).

$^{13}$C NMR (125 MHz, $CDCl_3$) δ 168.2, 163.5, 161.5, 155.2, 153.2, 152.3, 150.5, 150.1, 149.0, 144.9, 140.7, 126.7, 126.3, 125.7, 124.8, 123.3, 115.5, 113.6, 111.6, 111.3, 108.3, 105.7, 104.7, 81.2, 75.3, 66.5, 55.5, 49.9, 34.9, 19.1.

HRMS (MALDI–TOF) calcd for $C_{37}H_{42}N_8O_7$, 733.3049 $[M + Na]^+$; found, 733.3068.

## Compound III–21

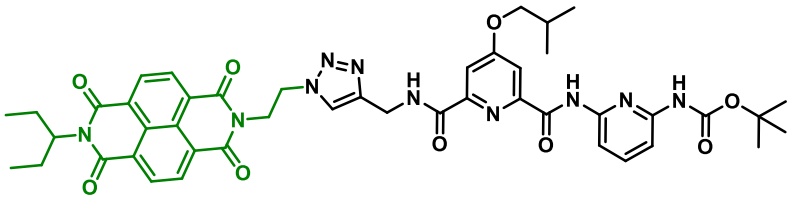

**Chemical Formula:** $C_{45}H_{48}N_{10}O_9$
**Molecular Weight:** 872.3606

**III–4** (100 mg, 213 µmol, 1 eq.) and azide **III–19** (104 mg, 256 µmol, 1.2 eq.) were dissolved in a mixture of DMSO and dry DCM (*1/1*) and the solution was purged with argon. Then, copper sulfate (3.4 mg, 21 µmol, 0.1 eq.) and sodium ascorbate (4.2 mg, 21 µmol, 0.1 eq.) were added. The mixture was stirred overnight at room temperature. The solution was diluted with dichloromethane (20 mL) and washed with water (3 × 50 mL). The organic layer was evaporated and the crude was purified by silica gel chromatography (eluent $CHCl_3$/EtOAc 9/1) to afford **III–21** as a yellow solid (180 mg, 96 %).

$^{1}$H NMR (300 MHz, $CDCl_3$) δ 9.92 (s, 1H), 8.91 (t, *J* = 5.1 Hz, 1H), 8.46 (s, 4H), 7.88 (t, *J* = 1.6 Hz, 1H), 7.86 – 7.78 (m, 3H), 7.66 (d, *J* = 7.9 Hz, 1H), 7.45 (t, *J* = 8.0 Hz, 1H), 7.30 (s, 1H), 5.06 – 4.94 (m, 1H), 4.88 (t, *J* = 5.5 Hz, 2H), 4.75 (d, *J* = 5.2 Hz, 2H), 4.67 (t, *J* = 5.5 Hz, 2H), 3.96 (d, *J* = 6.5 Hz, 2H), 2.17 (m, 3H), 1.95 (m, 2H), 1.56 (s, 9H), 1.08 (d, *J* = 6.7 Hz, 6H), 0.93 (t, *J* = 7.4 Hz, 6H).

$^{13}$C NMR (75 MHz, $CDCl_3$) δ 168.6, 162.9, 162.6, 160.6, 152.0, 150.3, 149.6, 148.3, 144.7, 139.9, 130.7, 126.4, 125.3, 122.6, 110.9, 107.7, 106.9, 81.0, 58.1, 48.2, 40.0, 35.2, 28.1, 24.8, 19.0, 11.3.

HRMS (MALDI–TOF) calcd for $C_{45}H_{48}N_{10}O_9$, 911.3236 $[M + K]^+$; found, 911.3237.

## Compound III–22

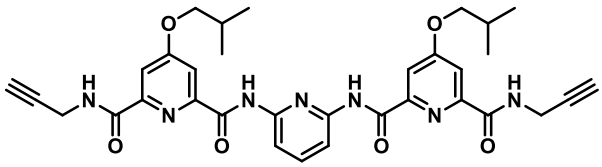

**Chemical Formula:** $C_{33}H_{35}N_7O_6$
**Molecular Weight:** 625.2649

The dry carboxylic acid **III–2** (137 mg, 248 µmol, 1 eq.) was dissolved in 5 mL of dry dichloromethane under argon atmosphere and 1–chloro–*N*,*N*,2–trimethyl–1–propenylamine (Ghosez's reagent, 0.26 mL, 2 mmol, 8 eq.) was added. The mixture was stirred overnight at room temperature. The latter was evaporated under vacuum using a liquid nitrogen trap and the solid is dried under vacuum for 3 hours. The latter was dissolved in 10 mL of anhydrous THF and added dropwise to a mixture of propragylamine (73 µL, 993 µmol, 4 eq.) and DIPEA (210 µL, 1 mmol, 5 eq.) in 5 mL of dry THF. The mixture was stirred overnight at room temperature. The solvent was then removed under reduced pressure and the crude was purified by silica gel chromatography (eluent DCM/EtOAc 95/5) to afford compound **III–22** as a white solid (135 mg, 87 %).

$^{1}$H NMR (300 MHz, $CDCl_3$) δ 10.24 (s, 2H), 8.77 – 8.67 (m, 2H), 8.15 (d, *J* = 8.1 Hz, 2H), 7.96 – 7.88 (m, 4H), 7.82 (t, *J* = 8.1 Hz, 1H), 4.36 (dd, *J* = 5.8, 2.5 Hz, 4H), 3.85 (d, *J* = 6.5 Hz, 4H), 2.23 (t, *J* = 2.5 Hz, 2H), 2.11 (dt, *J* = 13.3, 6.7 Hz, 2H), 1.01 (d, *J* = 6.7 Hz, 12H).

$^{13}$C NMR (75 MHz, $CDCl_3$) δ 168.4, 163.6, 162.1, 151.0, 150.4, 149.3, 141.3, 112.2, 110.6, 79.8, 75.4, 71.6, 29.3, 28.0, 19.1.

HRMS (MALDI–TOF) calcd for $C_{33}H_{35}N_7O_6$, 626.2711 $[M + H]^+$; found, 626.2721.

## Compound III–23

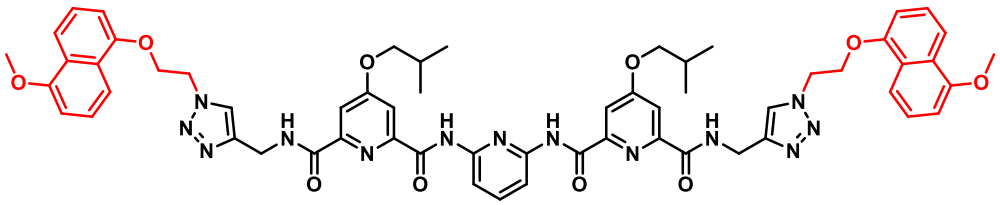

**Chemical Formula:** $C_{59}H_{61}N_{13}O_{10}$
**Molecular Weight:** 1111.4664

Dialkyne **III–22** (70 mg, 112 µmol, 1 eq.) and azide **III–17** (95 mg, 392 µmol, 3.5 eq.) were dissolved in a mixture of DMSO and dry DCM (*1/1*) and the solution was purged with argon for 10 minutes. Then, copper sulfate (178 µg, 1 µmol, 0.1 eq.) and sodium ascorbate (221 µg, 1 µmol, 0.1 eq.) were added. The mixture was stirred overnight at 35°C. The solution was diluted with dichloromethane (20 mL) and washed with water (3 × 30 mL). The organic layer was evaporated and the crude was purified by silica gel chromatography (eluent DCM) to afford **III–23** as a yellow solid (96 mg, 78 %).

$^{1}$H NMR (300 MHz, $CDCl_3$) δ 10.20 (s, 2H), 9.14 (s, 2H), 8.12 (d, *J* = 8.0 Hz, 2H), 7.85 (d, *J* = 2.5 Hz, 2H), 7.83 – 7.76 (m, 5H), 7.73 (dd, *J* = 8.5, 0.9 Hz, 2H), 7.59 (dd, *J* = 8.6, 0.9 Hz, 2H), 7.19 (t, *J* = 8.1 Hz, 4H), 6.64 (ddd, *J* = 15.1, 7.7, 0.9 Hz, 4H), 4.67 (t, *J* = 5.0 Hz, 4H), 4.63 (d, *J* = 6.2 Hz, 4H), 4.30 (t, *J* = 5.0 Hz, 4H), 3.90 (s, 6H), 3.87 (d, *J* = 6.5 Hz, 4H), 2.14 (m, *J* = 6.6 Hz, 2H), 1.04 (d, *J* = 6.7 Hz, 12H).

$^{13}$C NMR (75 MHz, $CDCl_3$) δ 168.2, 163.7, 161.8, 155.2, 153.3, 150.8, 149.9, 149.3, 145.4, 141.0, 126.6, 126.3, 125.7, 124.9, 123.5, 115.3, 113.7, 111.7, 110.4, 105.7, 104.6, 75.3, 66.5, 55.5, 49.8, 34.8, 28.1, 19.1.

HRMS (MALDI–TOF) calcd for $C_{59}H_{61}N_{13}O_{10}$, 1134.4565 $[M + Na]^+$; found, 1134.4556.

## Compound III–24

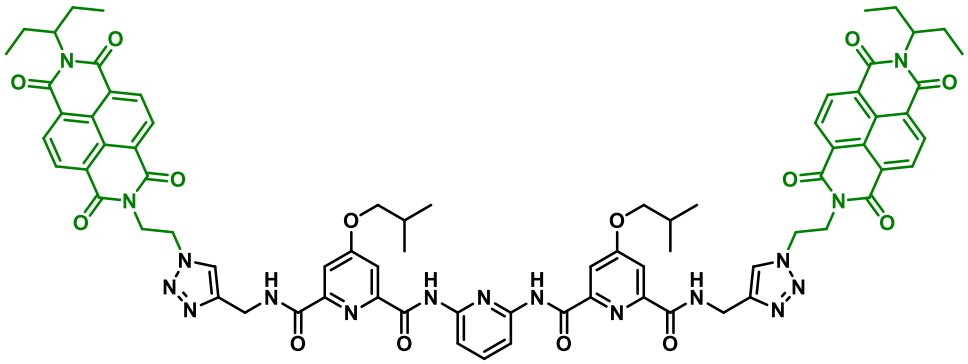

**Chemical Formula:** $C_{75}H_{73}N_{17}O_{14}$
**Molecular Weight:** 1435.5523

Dialkyne **III–22** (70 mg, 112 µmol, 1 eq.) and azide **III–19** (113 mg, 280 µmol, 2.5 eq.) were dissolved in a mixture of DMSO and dry DCM (*1/1*) and the solution was purged with argon for 10 minutes. Then, copper sulfate (178 µg, 1 µmol, 0.1 eq.) and sodium ascorbate (221 µg, 1 µmol, 0.1 eq.) were added. The mixture was stirred overnight at room temperature. The solution was diluted with dichloromethane (20 mL) and washed with water (3 × 30 mL). The organic layer was evaporated and the crude was purified by silica gel chromatography (eluent DCM) to afford **III–24** as a yellow solid (144 mg, 90 %).

$^{1}$H NMR (300 MHz, $CDCl_3$) δ 10.11 (s, 2H), 8.94 (s, 2H), 8.61 – 8.49 (m, 8H), 7.93 – 7.85 (m, 4H), 7.85 – 7.76 (m, 4H), 7.61 (d, *J* = 8.3 Hz, 2H), 4.99 (tt, *J* = 9.4, 5.9 Hz, 2H), 4.61 (dt, *J* = 18.1, 6.2 Hz, 12H), 3.95 (d, *J* = 6.5 Hz, 4H), 2.18 (dqd, *J* = 14.7, 7.4, 2.7 Hz, 6H), 1.92 (ddd, *J* = 13.6, 7.5, 6.1 Hz, 4H), 1.07 (d, *J* = 6.7 Hz, 12H), 0.89 (t, *J* = 7.4 Hz, 12H).

$^{13}$C NMR (75 MHz, $CDCl_3$) δ 168.3, 163.5, 162.8, 161.6, 150.8, 145.3, 131.0, 126.8, 126.6, 125.5, 123.5, 111.7, 110.0, 75.4, 58.3, 40.2, 34.9, 28.1, 25.0, 19.2, 11.4.

HRMS (MALDI–TOF) calcd for $C_{75}H_{73}N_{17}O_{14}$, 1458.5397 $[M + Na]^+$; found, 1458.5415.

## Foldamer G

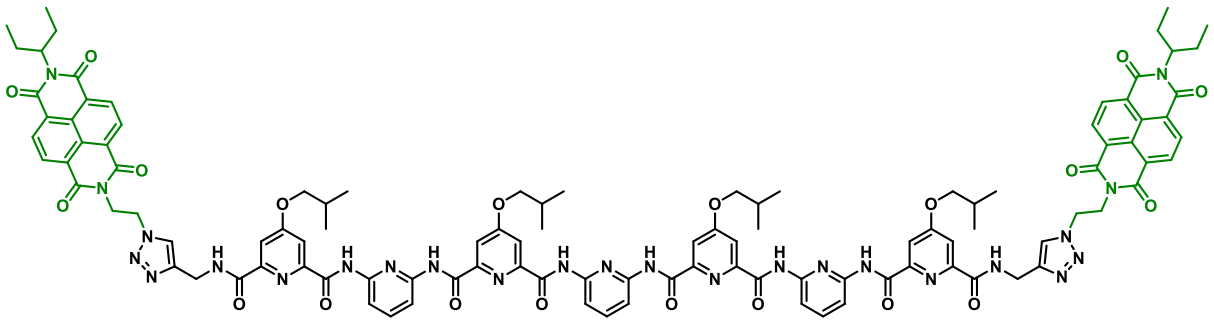

**Chemical Formula:** $C_{107}H_{105}N_{25}O_{20}$
**Molecular Weight:** 2059.7968

Foldamer **B** (100 mg, 80 µmol, 1 eq.) and azide **III–19** (105 mg, 280 µmol, 3.5 eq.) were dissolved in a mixture of DMSO and dry DCM (*1/1*, 4 mL) and the solution was purged with argon for 10 minutes. Then, copper sulfate (1.3 mg, 8 µmol, 0.1 eq.) and sodium ascorbate (1.6 mg, 8 µmol, 0.1 eq.) were added. The mixture was stirred overnight at room temperature. The solution was diluted with dichloromethane (20 mL) and washed with water (3 × 30 mL). The organic layer was evaporated and the crude was purified first by silica gel chromatography (eluent DCM and then DCM/MeOH 97/3) and then via recycling size exclusion chromatography (sec) to afford foldamer **G** as a yellow solid (86 mg, 85 %).

$^{1}$H NMR (500 MHz, DMSO–$d_6$) δ 10.85 (s, 2H), 10.64 (s, 2H), 10.23 (s, 2H), 9.93 (t, *J* = 6.3 Hz, 2H), 8.47 (dd, *J* = 46.5, 7.6 Hz, 8H), 8.21 – 8.13 (m, 3H), 7.92 – 7.85 (m, 4H), 7.80 – 7.75 (m, 3H), 7.67 (t, *J* = 8.0 Hz, 3H), 7.64 (d, *J* = 2.5 Hz, 2H), 7.28 (d, *J* = 2.6 Hz, 2H), 7.06 (d, *J* = 2.5 Hz, 2H), 4.85 (qd, *J* = 9.7, 5.7 Hz, 2H), 4.57 (d, *J* = 6.0 Hz, 4H), 4.35 (d, *J* = 6.0 Hz, 4H), 4.01 (dd, *J* = 25.6, 6.5 Hz, 12H), 2.17 (m, 4H), 2.13 – 2.03 (m, 4H), 1.84 (m, 4H), 1.11 (dd, *J* = 6.7, 3.8 Hz, 24H), 0.79 (t, *J* = 7.4 Hz, 12H).

$^{13}$C NMR (125 MHz, DMSO–$d_6$) δ 167.3, 166.5, 162.3, 161.7, 160.9, 159.8, 150.3, 149.9, 149.7, 149.4, 149.2, 148.4, 148.2, 144.6, 130.4, 126.1, 125.9, 125.7, 123.6, 111.2, 110.4, 109.0, 108.5, 74.76, 74.51, 57.18, 46.87, 27.5, 24.3, 18.8, 11.1.

HRMS (MALDI–TOF) calcd for $C_{107}H_{106}N_{25}O_{20}$, 2059.7979 $[M]^+$; found, 2059.7973.

## Foldamer H

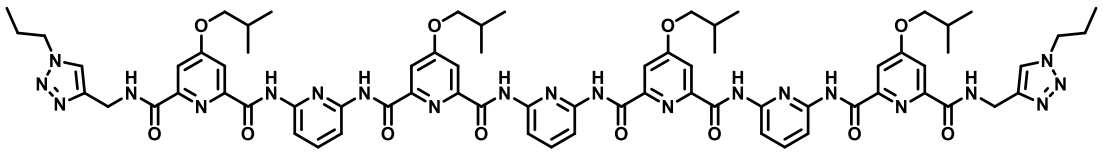

**Chemical Formula:** $C_{71}H_{81}N_{21}O_{12}$
**Molecular Weight:** 1419.6374

Foldamer **B** (60 mg, 48 µmol, 1 eq.) and 1–azidopropane **III–25** (58 mg, 240 µmol, 5 eq.) were dissolved in a mixture of DMSO and dry DCM (*1/1*, 4 mL) and the solution was purged with argon for 10 minutes. Then, copper sulfate (0.77 mg, 4.8 µmol, 0.1 eq.) and sodium ascorbate (0.95 mg, 4.8 µmol, 0.1 eq.) were added. The mixture was stirred overnight at room temperature. The solution was diluted with dichloromethane (20 mL) and washed with water (3 × 30 mL). The organic layer was evaporated and the crude was purified first by silica gel chromatography (eluent DCM and then DCM/MeOH 97/3) and then via recycling size exclusion chromatography (sec) to afford foldamer **H** as a white solid (41 mg, 60 %).

$^{1}$H NMR (500 MHz, DMSO–$d_6$) δ 10.88 (s, 2H), 10.69 (s, 2H), 10.25 (s, 2H), 9.99 (t, *J* = 6.3 Hz, 2H), 8.27 – 8.19 (m, 3H), 7.88 (d, *J* = 8.1 Hz, 2H), 7.79 (dd, *J* = 10.7, 2.8 Hz, 6H), 7.71 – 7.63 (m, 4H), 7.32 (d, *J* = 2.6 Hz, 2H), 7.08 (d, *J* = 2.4 Hz, 2H), 4.15 (t, *J* = 6.9 Hz, 8H), 4.03 (dd, *J* = 14.3, 6.4 Hz, 8H), 2.21 – 2.15 (m, 4H), 1.69 (h, *J* = 7.3 Hz, 4H), 1.11 (t, *J* = 7.1 Hz, 24H), 0.71 (t, *J* = 7.4 Hz, 6H).

$^{13}$C NMR (125 MHz, DMSO–$d_6$) δ 167.3, 166.5, 162.3, 161.8, 160.9, 159.8, 150.3, 149.3, 149.80, 149.4, 149.3, 148.4, 148.2, 122.8, 110.4, 74.4, 50.6, 28.2, 23.0, 22.0, 18.8, 13.9, 10.71.

HRMS (MALDI–TOF) calcd for $C_{71}H_{681}N_{21}O_{12}$, 1442.6282 $[M + Na]^+$; found, 1442.6265.

## Compound III–26

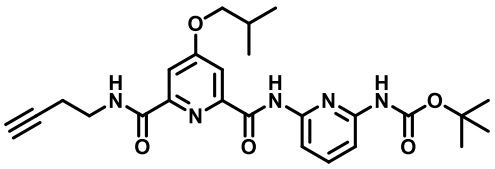

**Chemical Formula:** $C_{25}H_{31}N_5O_5$
**Molecular Weight:** 481.2325

The dry carboxylic acid **II–8** (540 mg, 1 mmol, 1 eq.) was dissolved in 8 mL of dry dichloromethane under argon atmosphere and 1–chloro–*N*,*N*,2–trimethyl–1–propenylamine (Ghosez's reagent, 1.3 mL, 10 mmol, 8 eq.) was added. The mixture was stirred overnight at room temperature. The latter was evaporated under vacuum using a liquid nitrogen trap and the solid was dried under vacuum for 3 hours. The latter was dissolved in 10 mL of anhydrous THF and added dropwise to a mixture of but–3–yne–1–amine (205 µL, 2.5 mmol, 2 eq.) and DIPEA (806 µL, 6 mmol, 5 eq.) in 5 mL of dry THF. The mixture was stirred overnight at room temperature. The solvent was then removed under reduced pressure and the crude was purified by silica gel chromatography (eluent DCM/EtOAc 95/5) to afford compound **III–26** as a transparent oil (507 mg, 84 %).

$^1$H NMR (300 MHz, $CDCl_3$) δ 9.95 (s, 1H), 8.37 (t, *J* = 6.5 Hz, 1H), 8.03 (dd, *J* = 7.6, 1.3 Hz, 1H), 7.91 – 7.83 (m, 2H), 7.78 – 7.66 (m, 2H), 7.15 (s, 1H), 3.91 (d, *J* = 6.5 Hz, 2H), 3.68 (q, *J* = 6.5 Hz, 2H), 2.58 (td, *J* = 6.7, 2.6 Hz, 2H), 2.24 (t, *J* = 2.6 Hz, 1H), 2.13 (m, 1H), 1.52 (s, 9H), 1.04 (d, *J* = 6.7 Hz, 6H).

$^{13}$C NMR (75 MHz, $CDCl_3$) δ 168.4, 163.5, 161.7, 152.1, 150.8, 150.5, 150.1, 149.1, 140.96 111.8, 108.5, 81.5, 75.4, 70.9, 38.0, 28.3, 28.1, 19.6, 19.1.

HRMS (MALDTI–TOF) calcd for $C_{75}H_{73}N_{17}O_{14}$, 504.2205 $[M + Na]^+$; found, 504.2217.

## Compound III–27

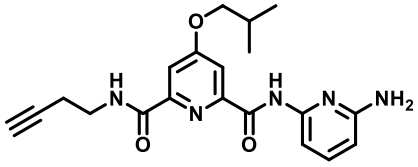

**Chemical Formula:** $C_{20}H_{23}N_5O_3$
**Molecular Weight:** 381.1801

Protected **III–26** (507 g, 1 mmol) was dissolved in 8 mL of dichloromethane and trifluoroacetic acid (TFA, 3.7 mL, 40 eq.) was added. The mixture was stirred for 4 hours at room temperature. The reaction mixture was washed with saturated $NaHCO_3$ solution, extracted with chloroform (100 mL) and washed with water (3 × 50 mL). The organic phases were combined, dried over magnesium sulfate and concentrated under reduced pressure to afford compound **III–27** as a white solid (400 mg, quantitative).

$^1$H NMR (500 MHz, $CDCl_3$) δ 9.96 (s, 1H), 8.49 (t, *J* = 6.6 Hz, 1H), 7.86 (dt, *J* = 15.4, 1.9 Hz, 2H), 7.72 (dd, *J* = 7.9, 1.1 Hz, 1H), 7.51 (td, *J* = 7.9, 1.4 Hz, 1H), 6.31 (d, *J* = 8.0 Hz, 1H), 4.49 (s, 2H), 3.90 (dd,

*J* = 6.6, 1.3 Hz, 2H), 3.66 (qd, *J* = 6.6, 1.5 Hz, 2H), 2.56 (td, *J* = 6.7, 2.6 Hz, 2H), 2.35 (m, *J* = 2.7 Hz, 1H), 2.12 (m, 1H), 1.03 (d, *J* = 6.7 Hz, 6H).

$^{13}$C NMR (125 MHz, $CDCl_3$) δ 168.3, 163.5, 161.6, 157.3, 150.8, 150.3, 149.3, 140.4, 111.8, 104.9, 103.7, 81.5, 75.3, 71.2, 37.9, 28.1, 19.5, 19.1.

HRMS (MALDI–TOF) calcd for $C_{75}H_{73}N_{17}O_{14}$, 404.1701 $[M + Na]^+$; found, 404.1693.

## Foldamer I

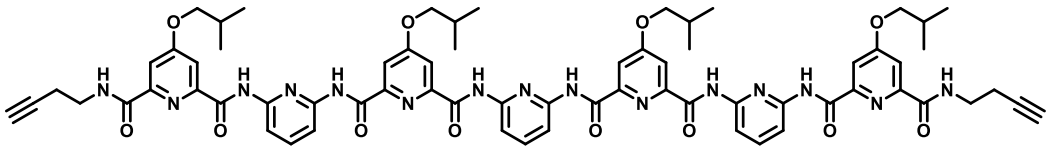

**Chemical Formula:** $C_{67}H_{71}N_{15}O_{12}$
**Molecular Weight:** 1277.5407

Dry diacid **III–2** (120 mg, 217 µmol, 1 eq.) was dissolved in 6 mL of dry dichloromethane under argon atmosphere and Ghosez's reagent (0.25 mL, 1.8 mmol, 8 eq.) was added. The mixture was stirred overnight at room temperature. The latter was evaporated under vacuum using a liquid nitrogen trap and the solid is dried under vacuum for 3 hours. In another schlenk, amine **III–22** (250 mg, 652 µmol, 3 eq.) was dissolved in 10 mL of dry THF and DIPEA (0.15 mL, 1 mmol, 5 eq.) was added. Then, this mixture was added dropwise to a solution of the resulting acid chloride in 7 mL of dry THF. The mixture was stirred overnight at room temperature. The solvent was removed under reduced pressure and the crude was purified by silica gel chromatography (eluent DCM/MeOH 99/1) to afford foldamer **I** as a white solid (180 mg, 64 %).

$^1$H NMR (500 MHz, DMSO–$d_6$) δ 10.79 (s, 2H), 10.57 (s, 2H), 10.22 (s, 2H), 9.55 (t, *J* = 6.0 Hz, 2H), 8.25 – 8.15 (m, 3H), 7.87 (d, *J* = 8.1 Hz, 2H), 7.80 – 7.75 (m, 4H), 7.69 – 7.63 (m, 4H), 7.30 (d, *J* = 2.6 Hz, 2H), 7.07 (d, *J* = 2.4 Hz, 2H), 4.03 (dd, *J* = 19.6, 6.6 Hz, 8H), 3.03 (d, *J* = 8.6 Hz, 4H), 2.75 (t, *J* = 2.6 Hz, 2H), 2.23 (td, *J* = 7.2, 2.5 Hz, 4H), 2.17 (dt, *J* = 13.1, 6.6 Hz, 4H), 1.11 (dd, *J* = 6.6, 3.1 Hz, 24H).

$^{13}$C NMR (125 MHz, DMSO–$d_6$) δ 167.3, 166.5, 162.3, 161.7, 160.8, 159.7, 150.2, 149.9, 149.7, 149.3, 149.2, 148.3, 148.1, 142.6, 140.0, 111.1, 110.7, 110.4, 109.0, 108.5, 81.8, 74.8, 74.4, 72.2, 27.5, 18.8, 18.3.

HRMS (MALDI–TOF) calcd for $C_{67}H_{71}N_{15}O_{12}$, 1300.5274 $[M + Na]^+$; found, 1300.5298.

## Foldamer J

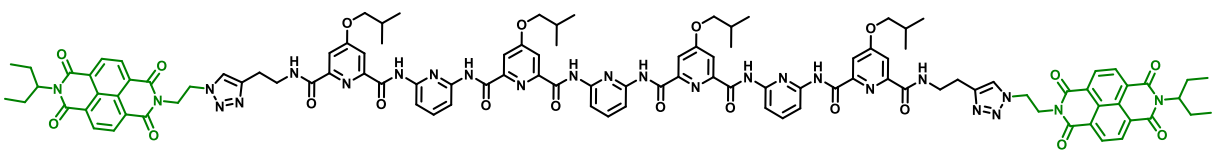

**Chemical Formula:** $C_{109}H_{109}N_{25}O_{20}$
**Molecular Weight:** 2087.8281

Foldamer **I** (80 mg, 62 µmol, 1 eq.) and azide **III–19** (101 mg, 250 µmol, 4 eq.) were dissolved in a mixture of DMSO and dry DCM (*1/1*) and the solution was purged with argon for 10 minutes. Then, copper sulfate (1 mg, 6 µmol, 0.1 eq.) and sodium ascorbate (1.2 mg, 6 µmol, 0.1 eq.) were added. The mixture was stirred overnight at room temperature. The solution was diluted with dichloromethane (20 mL) and washed with water (3 × 30 mL). The organic layer was evaporated and the crude was purified by silica gel chromatography (eluent DCM and then DCM/MeOH 97/3) to afford foldamer **J** as a yellow solid (106 mg, 81 %).

$^{1}$H NMR (500 MHz, $CDCl_3$) δ 10.42 (s, 2H), 10.27 (s, 2H), 9.85 (s, 2H), 8.50 (t, *J* = 6.0 Hz, 2H), 8.36 (d, *J* = 7.5 Hz, 4H), 8.25 (d, *J* = 7.5 Hz, 4H), 8.09 (d, *J* = 8.1 Hz, 2H), 7.88 – 7.81 (m, 3H), 7.73 (d, *J* = 2.5 Hz, 2H), 7.66 (dd, *J* = 7.0, 1.7 Hz, 2H), 7.39 – 7.35 (m, 4H), 7.34 (d, *J* = 2.6 Hz, 2H), 7.31 (d, *J* = 2.5 Hz, 2H), 7.22 (s, 2H), 4.96 (tt, *J* = 9.2, 6.1 Hz, 2H), 4.26 (t, *J* = 5.7 Hz, 4H), 4.19 (d, *J* = 5.7 Hz, 4H), 4.00 (dd, *J* = 6.6, 4.1 Hz, 8H), 3.34 (m, 4H), 2.59 (q, *J* = 8.4, 6.2 Hz, 4H), 2.26 (m, 4H), 2.18 (m, 4H), 1.93 (m, 4H), 1.17 (dd, *J* = 6.8, 5.3 Hz, 24H), 0.90 (t, *J* = 7.4 Hz, 12H).

$^{13}$C NMR (125 MHz, $CDCl_3$) δ 168.1, 167.7, 162.6, 162.4, 161.5, 161.1, 160.5, 149.9, 149.8, 149.2, 149.0, 148.6, 148.4, 146.2, 140.6, 130.8, 126.5, 126.2, 125.2, 122.2, 112.7, 112.4, 111.2, 110.8, 109.8, 109.4, 75.6, 75.4, 58.3, 47.6, 40.0, 38.5, 29.8, 28.2, 25.1, 24.9, 19.2, 11.4.

HRMS (MALDI–TOF) calcd for $C_{109}H_{109}N_{25}O_{20}$, 2110.8236 $[M + Na]^+$; found, 2110.8172.

## Foldamer K

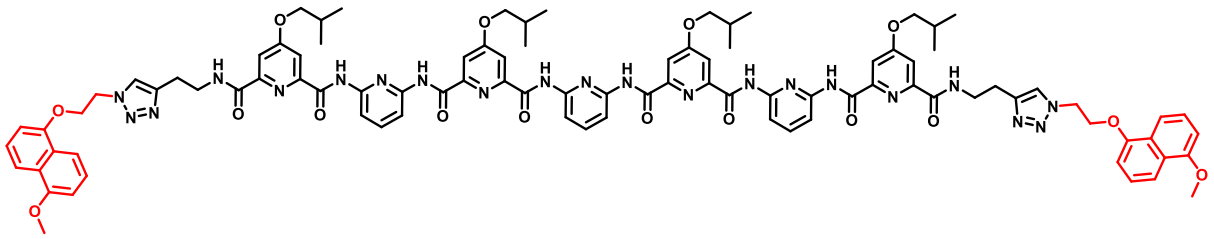

**Chemical Formula:** $C_{93}H_{97}N_{21}O_{16}$
**Molecular Weight:** 1763.7422

Foldamer **I** (100 mg, 80 µmol, 1 eq.) and azide **III–17** (101 mg, 313 µmol, 4 eq.) were dissolved in a mixture of DMSO and dry DCM (*1/1*) and the solution was purged with argon for 10 minutes. Then, copper sulfate (1.2 mg, 8 µmol, 0.1 eq.) and sodium ascorbate (1.5 mg, 8 µmol, 0.1 eq.) were added. The mixture was stirred overnight at room temperature. The solution was diluted with dichloromethane (20 mL) and washed with water (3 × 30 mL). The organic layer was evaporated and the crude was purified by silica gel chromatography (eluent DCM and then DCM/MeOH 96/4) to afford foldamer **K** as a white solid (106 mg, 81 %).

$^{1}$H NMR (500 MHz, DMSO–$d_6$) δ 10.71 (s, 2H), 10.54 (s, 2H), 10.24 (s, 2H), 9.42 (t, *J* = 6.2 Hz, 2H), 7.97 (d, *J* = 7.9 Hz, 2H), 7.84 – 7.78 (m, 4H), 7.76 (d, *J* = 8.1 Hz, 2H), 7.71 (d, *J* = 2.6 Hz, 2H), 7.69 – 7.62 (m, 6H), 7.50 (d, *J* = 8.4 Hz, 2H), 7.31 (m, 3H), 7.27 (m, 4H), 7.11 (d, *J* = 2.4 Hz, 2H), 6.90 (dd, *J* = 20.3, 7.8 Hz, 4H), 4.79 (t, *J* = 5.1 Hz, 4H), 4.42 (t, *J* = 5.1 Hz, 4H), 4.03 (t, 8H), 3.89 (s, 6H), 3.16 (4H), 2.66 (t, *J* = 8.1 Hz, 4H), 2.21 – 2.14 (m, 4H), 1.11 (d, *J* = 6.5 Hz, 24H).

$^{13}$C NMR (125 MHz, DMSO–$d_6$) δ 167.3, 166.5, 162.3, 161.6, 160.8, 159.8, 154.5, 153.2, 150.1, 149.6, 149.4, 149.1, 148.2, 143.9, 143.0, 125.7, 125.5, 125.3, 122.7, 114.1, 113.4, 111.3, 110.5, 106.0, 104.9, 74.8, 74.4, 66.6, 55.5, 48.9, 27.6, 18.9.

HRMS (MALDI–TOF) calcd for $C_{93}H_{97}N_{21}O_{16}$, 1786.7325 $[M + Na]^+$; found, 1786.7314.

## Compound III–28[7]

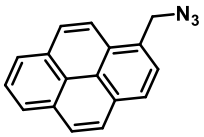

**Chemical Formula:** $C_{17}H_{11}N_3$
**Molecular Weight:** 257.0953

To a solution of 1–bromomethylpyrene (1.2 g, 4. mmol, 1 eq.) in 40 mL of DMF, sodium azide (1.3 g, 20 mmol, 5 eq.) was added. The mixture was stirred overnight at room temperature. DMF was partially evaporated. The crude was diluted in ethyl acetate (50 mL) and washed with brine and then with water (3 × 50 mL). The organic phase was dried over magnesium sulfate and the solvent was evaporated under reduced pressure. The desired product was isolated by silica gel chromatography (eluent EtOAc/PE 90/10) to afford **III–28** as a brown solid (997 mg, 95 %).

$^1$H NMR (300 MHz, $CDCl_3$) δ 7.98 – 8.25 (m, 9H), 5.04 (s, 2H).

## Foldamer L

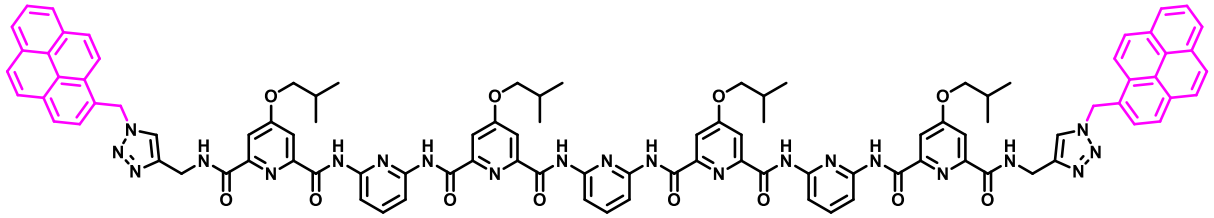

**Chemical Formula:** $C_{99}H_{89}N_{21}O_{12}$
**Molecular Weight:** 1763.7000

Foldamer **B** (100 mg, 80 µmol, 1 eq.) and azide **III–28** (82 mg, 320 µmol, 4 eq.) were dissolved in a mixture of DMSO and dry DCM (1/1, 4 mL) and the solution was purged with argon for 10 minutes. Then, copper sulfate (1.3 mg, 8 µmol, 0.1 eq.) and sodium ascorbate (1.6 mg, 8 µmol, 0.1 eq.) were added. The mixture was stirred overnight at 35°C. The solution was diluted with dichloromethane (20 mL) and washed with water (3 × 30 mL). The organic layer was evaporated and the crude was purified first by silica gel chromatography (eluent DCM and then DCM/MeOH 97/3) and then via recycling size exclusion chromatography (sec) to afford foldamer **L** as a yellow solid (124 mg, 88 %).

$^1$H NMR (500 MHz, DMSO–$d_6$) δ 10.78 (s, 2H), 10.62 (s, 2H), 10.20 (s, 2H), 9.90 (t, $J$ = 6.1 Hz, 2H), 8.42 (d, $J$ = 9.3 Hz, 2H), 8.25 (t, $J$ = 7.5 Hz, 4H), 8.19 (dd, $J$ = 8.6, 6.3 Hz, 3H), 8.14 (d, $J$ = 9.3 Hz, 4H), 8.08 (d, $J$ = 8.9 Hz, 2H), 8.03 (t, $J$ = 7.6 Hz, 3H), 7.93 – 7.87 (m, 4H), 7.81 (s, 2H), 7.77 – 7.70 (m, 4H), 7.67 – 7.59 (m, 4H), 7.25 (d, $J$ = 2.5 Hz, 2H), 7.05 (d, $J$ = 2.4 Hz, 2H), 6.21 (m, 4H), 4.11 – 4.07 (m, 4H), 3.98 (dd, $J$ = 17.2, 6.5 Hz, 8H), 2.14 (m, 6.8 Hz, 4H), 1.08 (d, $J$ = 6.7 Hz, 24H).

$^{13}$C NMR (125 MHz, DMSO–$d_6$) δ 167.8, 166.9, 162.8, 162.1, 161.3, 160.2, 150.7, 150.2, 149.8, 149.7, 148.8, 148.6, 145.4, 131.3, 131.1, 130.5, 129.5, 128.7, 128.6, 128.2, 128.0, 127.6, 126.9, 126.1, 125.9, 125.4, 124.3, 124.0, 123.6, 123.1, 111.9, 111.1, 109.2, 75.2, 74.9, 51.1, 28.0, 19.3.

HRMS (MALDI–TOF) calcd for $C_{99}H_{89}N_{21}O_{12}$, 1786.6876 $[M + Na]^+$; found, 1786.6891.

(1) Baptiste, B.; Zhu, J.; Haldar, D.; Kauffmann, B.; Léger, J.–M.; Huc, I. Hybridization of Long Pyridine-Dicarboxamide Oligomers into Multi-Turn Double Helices: Slow Strand Association and Dissociation, Solvent Dependence, and Solid State Structures. *Chemistry–An Asian Journal* **2010**, *5* (6), 1364–1375.
(2) Caldwell, S. T.; Cooke, G.; Hewage, S. G.; Mabruk, S.; Rabani, G.; Rotello, V.; Smith, B. O.; Subramani, C.; Woisel, P. Model Systems for Flavoenzyme Activity: Intramolecular Self–Assembly of a Flavin Derivative via Hydrogen Bonding and Aromatic Interactions. *Chemical communications* **2008**, No. 35, 4126–4128.
(3) Garin, J.; Orduna, J.; Uriel, S.; Moore, A. J.; Bryce, M. R.; Wegener, S.; Yufit, D. S.; Howard, J. A. Improved Syntheses of Carboxytetrathiafulvalene, Formyltetrathiafulvalene and (Hydroxymethyl) Tetrathiafulvalene: Versatile Building Blocks for New Functionalised Tetrathiafulvalene Derivatives. *Synthesis* **1994**, *1994* (05), 489–493.
(4) Garin, J.; Orduna, J.; Uriel, S.; Moore, A. J.; Bryce, M. R.; Wegener, S.; Yufit, D. S.; Howard, J. A. Improved Syntheses of Carboxytetrathiafulvalene, Formyltetrathiafulvalene and (Hydroxymethyl) Tetrathiafulvalene: Versatile Building Blocks for New Functionalised Tetrathiafulvalene Derivatives. *Synthesis* **1994**, *1994* (05), 489–493.
(5) Kaminska, I.; Barras, A.; Coffinier, Y.; Lisowski, W.; Roy, S.; Niedziolka–Jonsson, J.; Woisel, P.; Lyskawa, J.; Opallo, M.; Siriwardena, A. Preparation of a Responsive Carbohydrate–Coated Biointerface Based on Graphene/Azido–Terminated Tetrathiafulvalene Nanohybrid Material. *ACS applied materials & interfaces* **2012**, *4* (10), 5386–5393.
(6) Percec, V.; Imam, M. R.; Peterca, M.; Wilson, D. A.; Graf, R.; Spiess, H. W.; Balagurusamy, V. S.; Heiney, P. A. Self–Assembly of Dendronized Triphenylenes into Helical Pyramidal Columns and Chiral Spheres. *Journal of the American Chemical Society* **2009**, *131* (22), 7662–7677.
(7) Diesendruck, C. E.; Zhu, L.; Moore, J. S. Alkyne Mechanochemistry: Putative Activation by Transoidal Bending. *Chemical Communications* **2014**, *50* (87), 13235–13238.

# Appendix 1

## Electrocrystallization technique

Electrocrystallization is a crystallization method that requires electroactive species, whose electro–oxidation (or reduction) leads to a stable radical. If soluble, the generated radical species may diffuse into solution, but under suitable conditions of concentration, solvent, temperature, current density, and supporting electrolyte, they will precipitate (crystallize) on the electrode as radical cation salts.

An illustration of a standard electrocrystallization cell is given below.

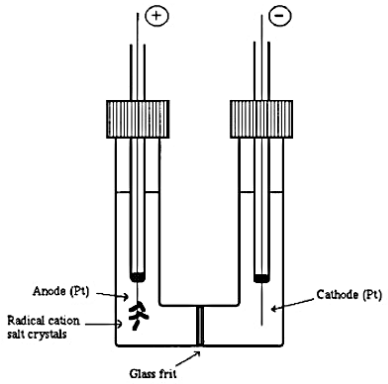


## Electrocrystallization of foldamer A

| | *Solvent* | *Counter ions* | *Current* | *temperature* | *Results* |
|---|---|---|---|---|---|
| ***Cell 1*** | THF | $TBAPF_6$ (13 eq.) | 0.4 µA | 20°C | Precipitate |
| ***Cell 2*** | $CHCl_3$ | $TBAPF_6$ (10 eq.) | 0.2 µA | 20°C | Precipitate |
| ***Cell 3*** | $CHCl_3$/ACN 1:1 | $TBAPF_6$ (10 eq.) | 0.2 µA | 20°C | Precipitate |
| ***Cell 4*** | DCM | $TBAPF_6$ (10 eq.) | 0.2 µA | 20°C | Amorphous Solid |
| ***Cell 5*** | DCM | $TBA_2Mo_6O_{19}$ (10 eq.) | 0.2 µA | 20°C | Precipitate |
| ***Cell 6*** | DCM | $TBAClO_4$ (10 eq.) | 0.2 µA | 20°C | Precipitate |
| ***Cell 7*** | DCM | Fumarate org. anion (10 eq.) | 0.2 µA Then 0.5 µA | 20°C | Precipitate |
| ***Cell 8*** | DCM | $TBAI_3$ (10 eq.) | 0.2 µA Then 1 µA | 20°C Then 4°C | Soluble no variations |
| ***Cell 9*** | DCM | $TEAFeCl_4$ (10 eq.) | 0.2 µA Then 1 µA | 20°C Then 4°C | Precipitate |
| ***Cell 10*** | DCM/ACN 1:1 | $TBAPF_6$ (10 eq.) | 0.5 µA Then 1 µA | 4°C | Precipitate |
| ***Cell 11*** | DCM/MeOH 1:1 | $TBAPF_6$ (10 eq.) | 0.5 µA Then 1 µA | 4°C | Precipitate |

# Appendix 2

**Cross–hybridization tests of foldamers E and F in different solvents and the corresponding observations.**

| ***Solvents*** | ***Results*** |
|---|---|
| *$CHCl_3$ / DCM / TCE* | *Pink suspension* |
| *THF* | *Pink suspension* |
| *Toluene* | *Pink suspension* |
| *DMSO* | *Orange solution* |
| *THF / Heptane* | *Pink precipitate* |
| *THF + Toluene / Cyclohexane* | *Pink precipitate* |
| *THF / $Et_2O$* | *Pink suspension* |
| *THF / MeOH* | *Pink precipitate* |
| *Toluene / MeOH* | *Orange precipitate* |
| *DMF / Acetone* | *Yellow solution* |
| *$CH_3NO_2$* | *Brown precipitate* |
| *Benzene* | *Pink solution* |
| *Pyridine / Acetone* | *Pink suspension* |
| *Pyridine / Acetonitrile* | *Orange suspension* |
| *Pyridine + DCM* | *Pink precipitate* |
| *Nitrobenzene* | *Pink solution* |
| *DMF* | *Pink solution* |

# Appendix 3

## $^{1}$H NMR 1$^{st}$ dispersion foldamers F and G ($CDCl_3$)

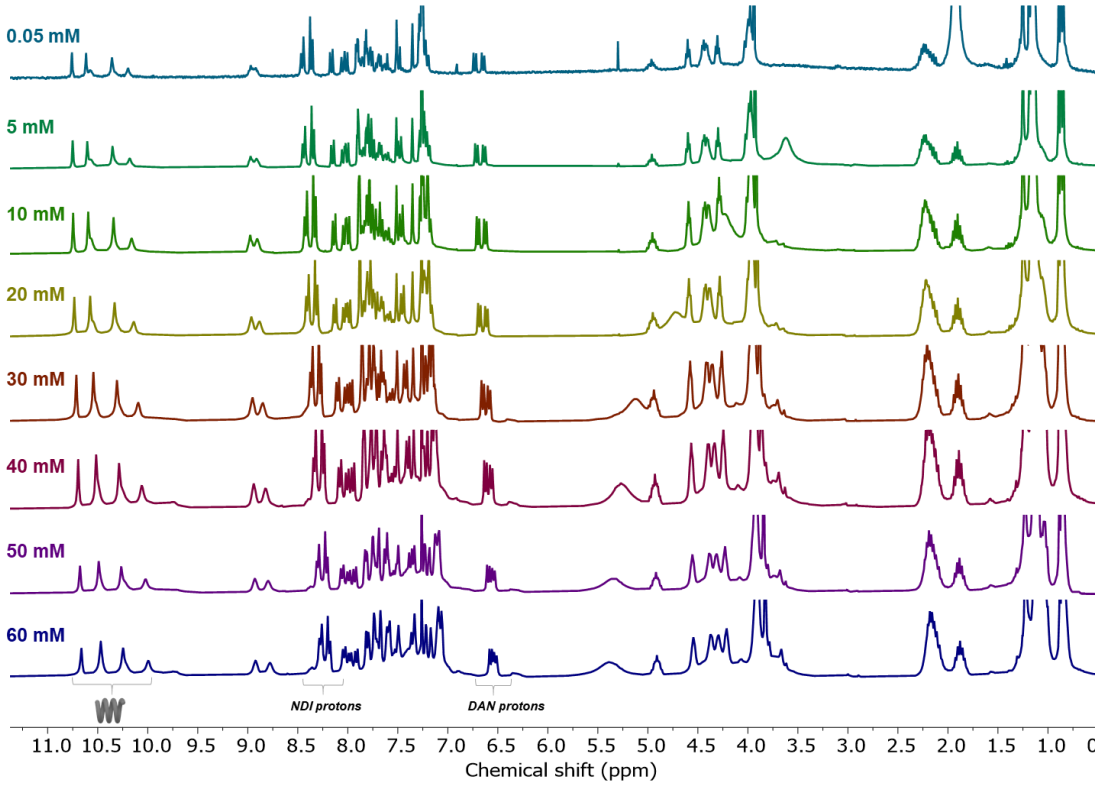


## $^{1}$H NMR 2$^{nd}$ dispersion foldamers F and G ($CDCl_3$)

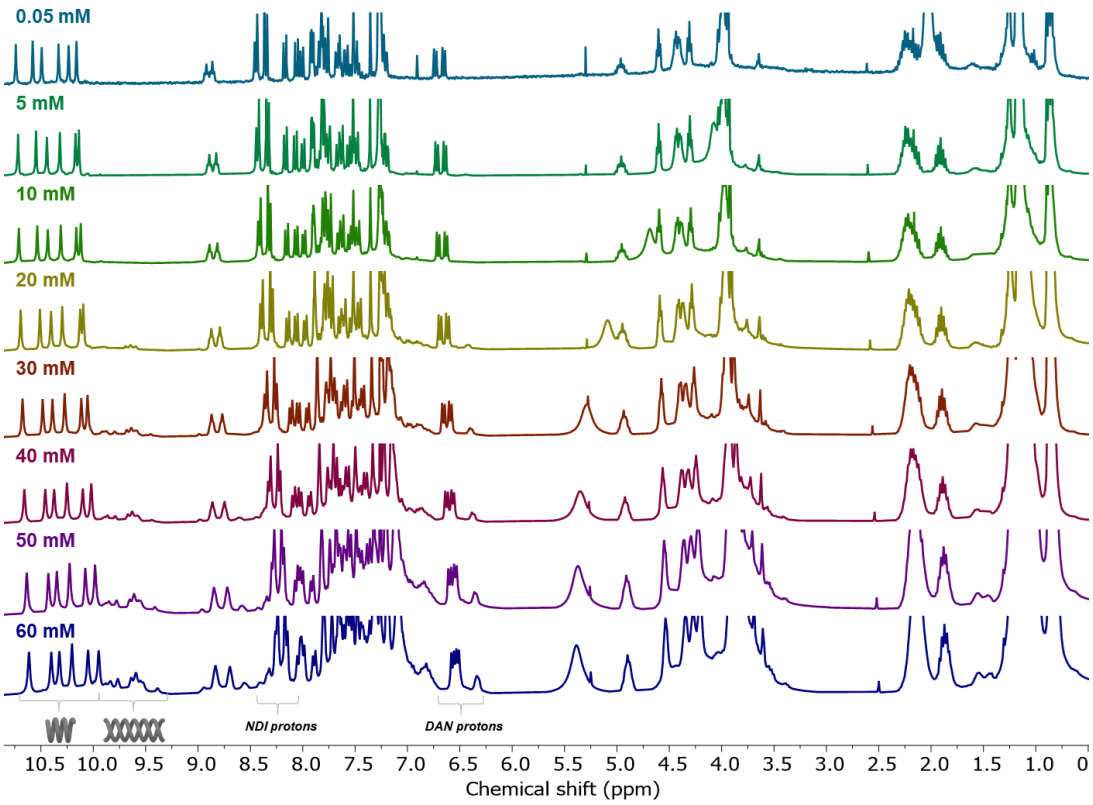

## $^{1}$H NMR 1$^{st}$ dispersion foldamer F ($CDCl_3$)

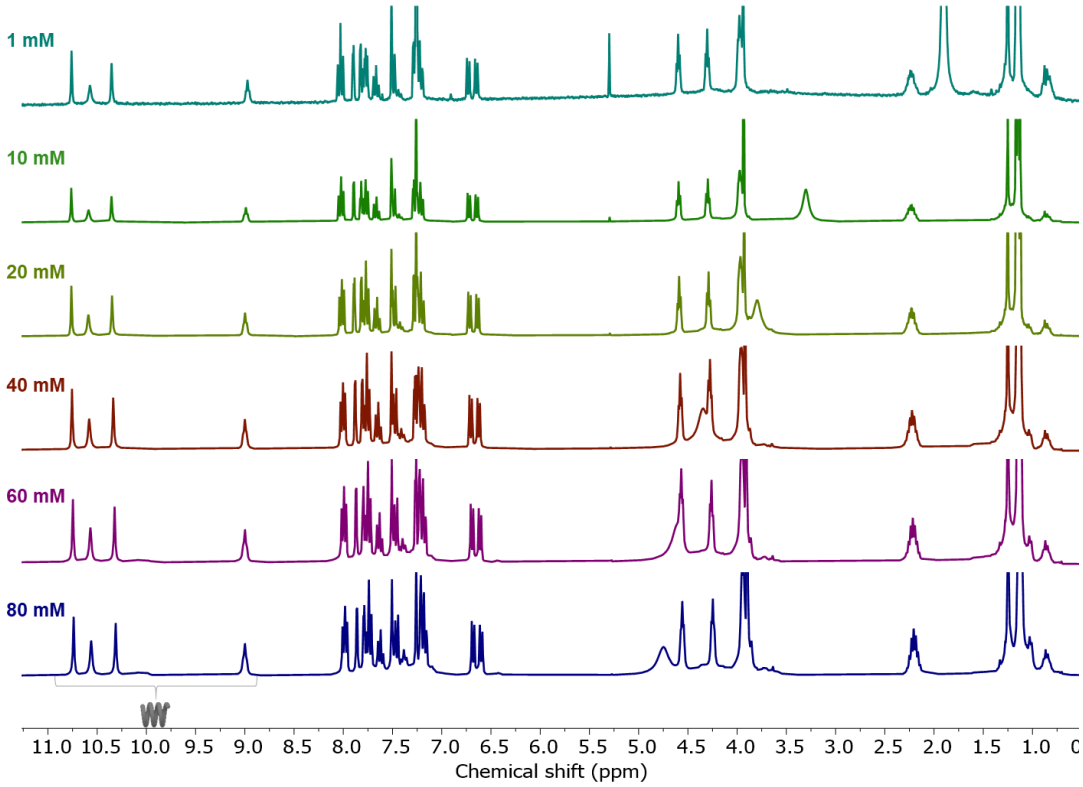


## $^{1}$H DOSY ($CDCl_3$)

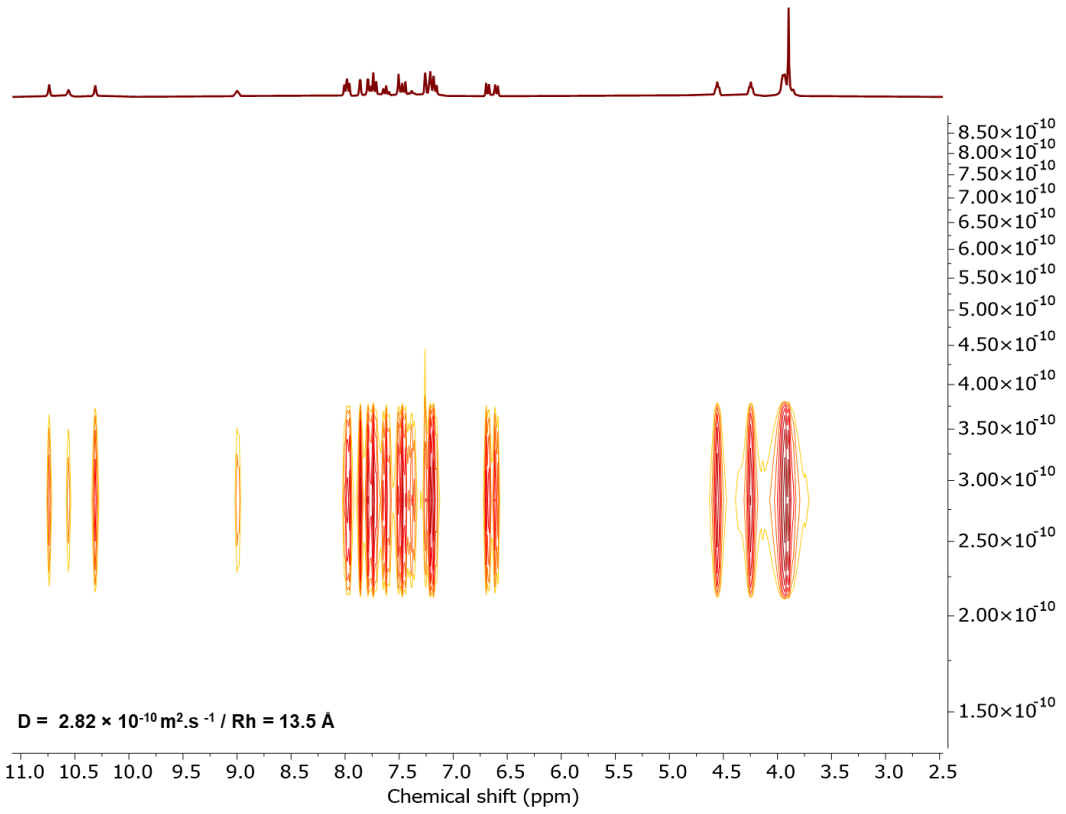

## $^{1}$H NMR 2$^{nd}$ dispersion foldamer F ($CDCl_3$)

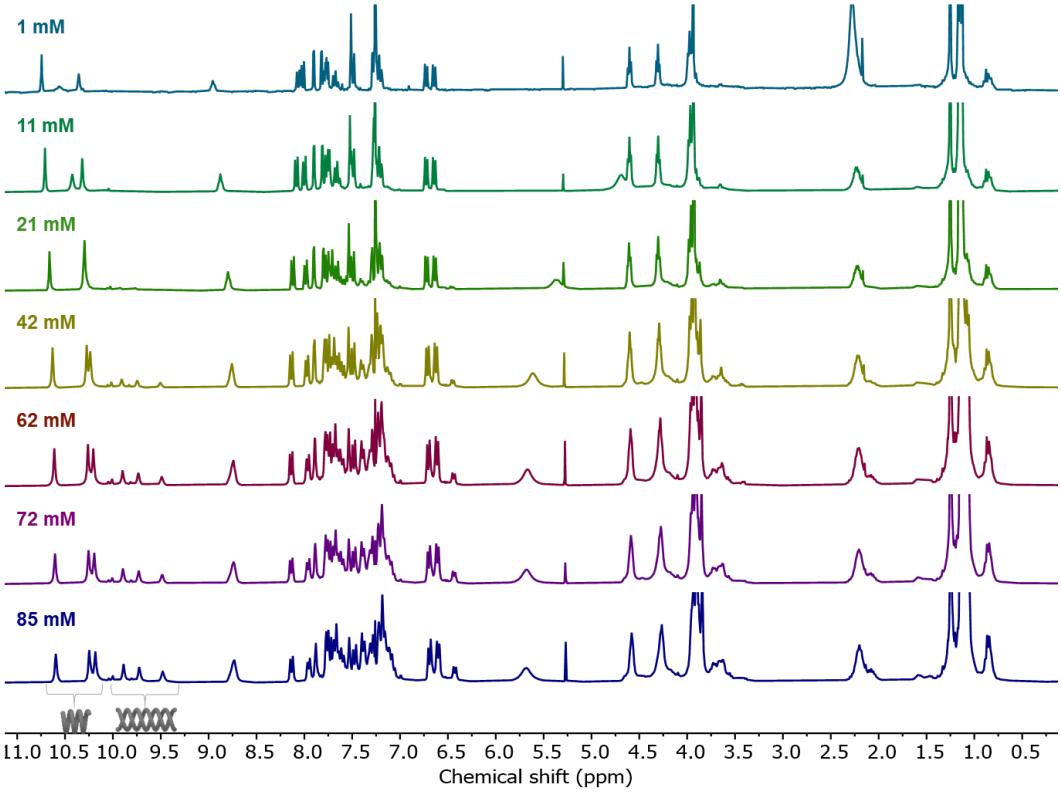


## $^{1}$H DOSY ($CDCl_3$)

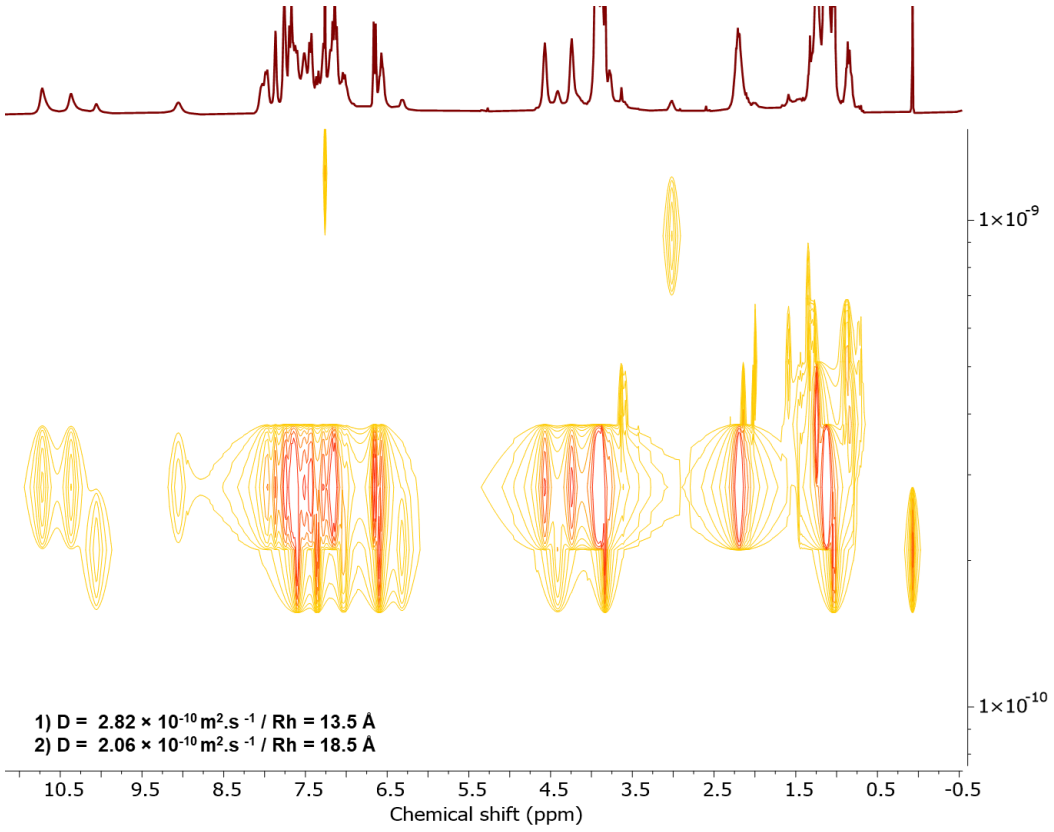

**$^{1}$H NMR 1$^{st}$ dispersion foldamer G ($CDCl_3$)**

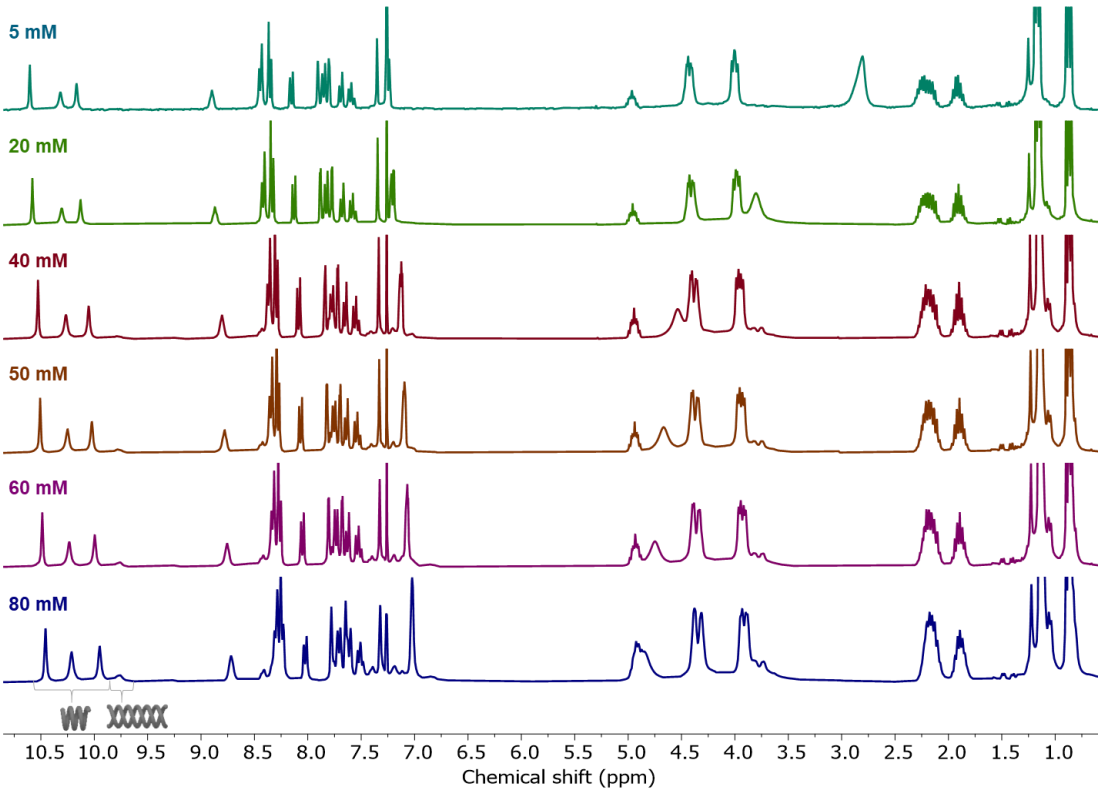


**$^{1}$H DOSY ($CDCl_3$)**

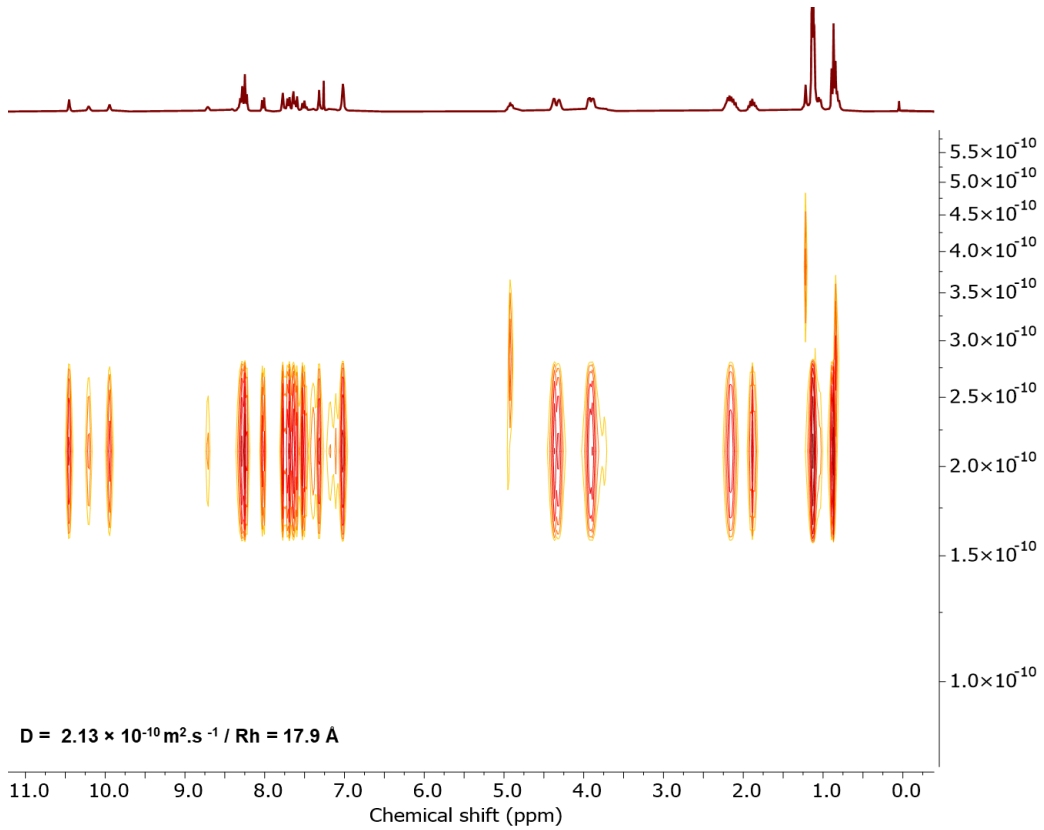

**$^{1}$H NMR 2$^{nd}$ dispersion foldamer G ($CDCl_3$)**

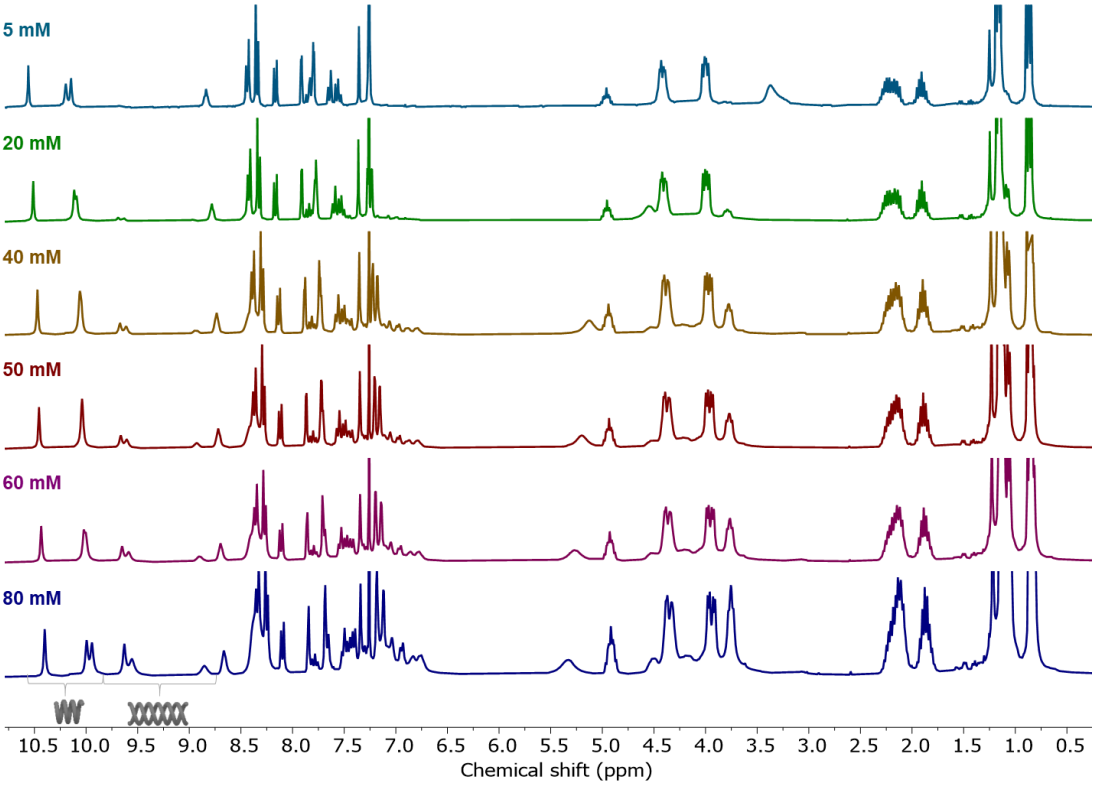


**$^{1}$H DOSY ($CDCl_3$)**

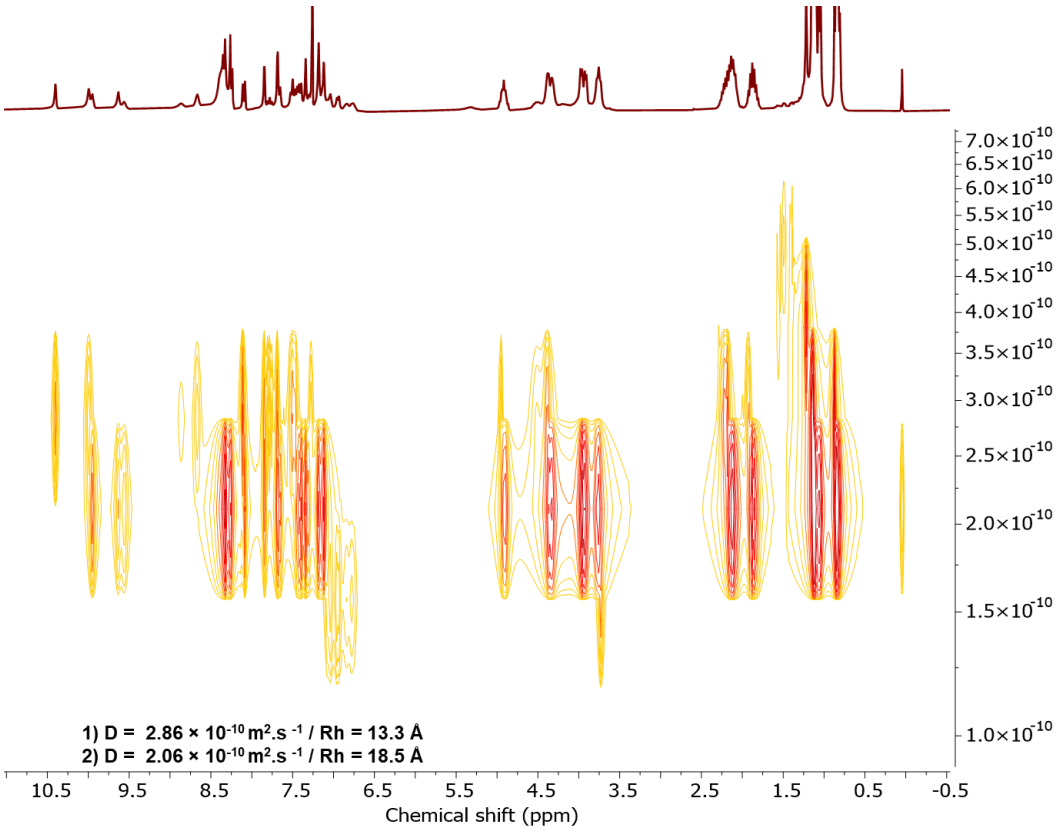

## $^{1}$H NMR 1$^{st}$ dispersion foldamer B ($CDCl_3$)

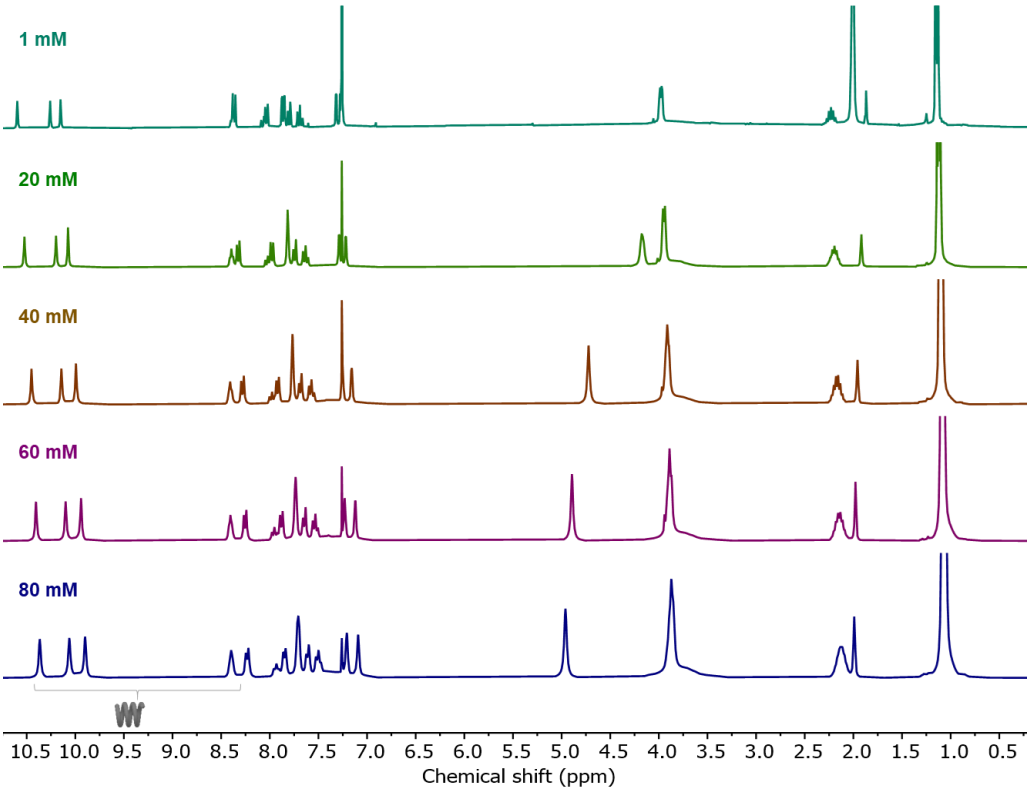


## $^{1}$H DOSY ($CDCl_3$)

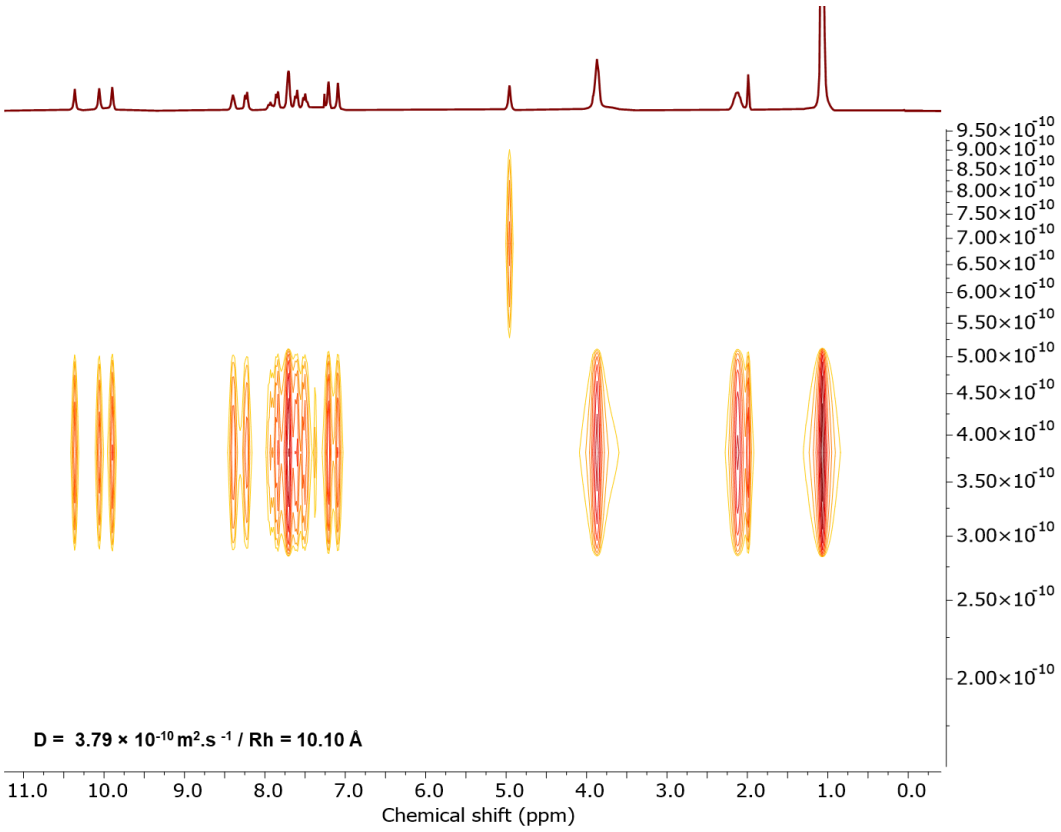

## $^{1}$H NMR 2$^{nd}$ dispersion foldamer B ($CDCl_3$)

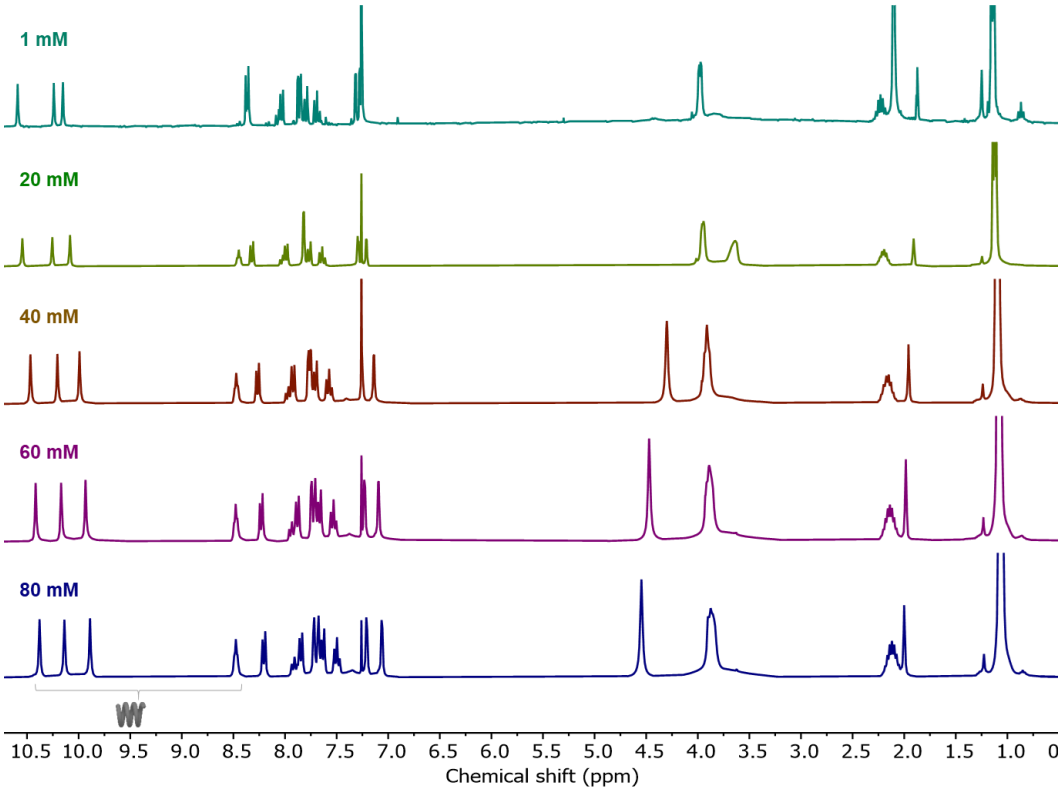


## $^{1}$H DOSY ($CDCl_3$)

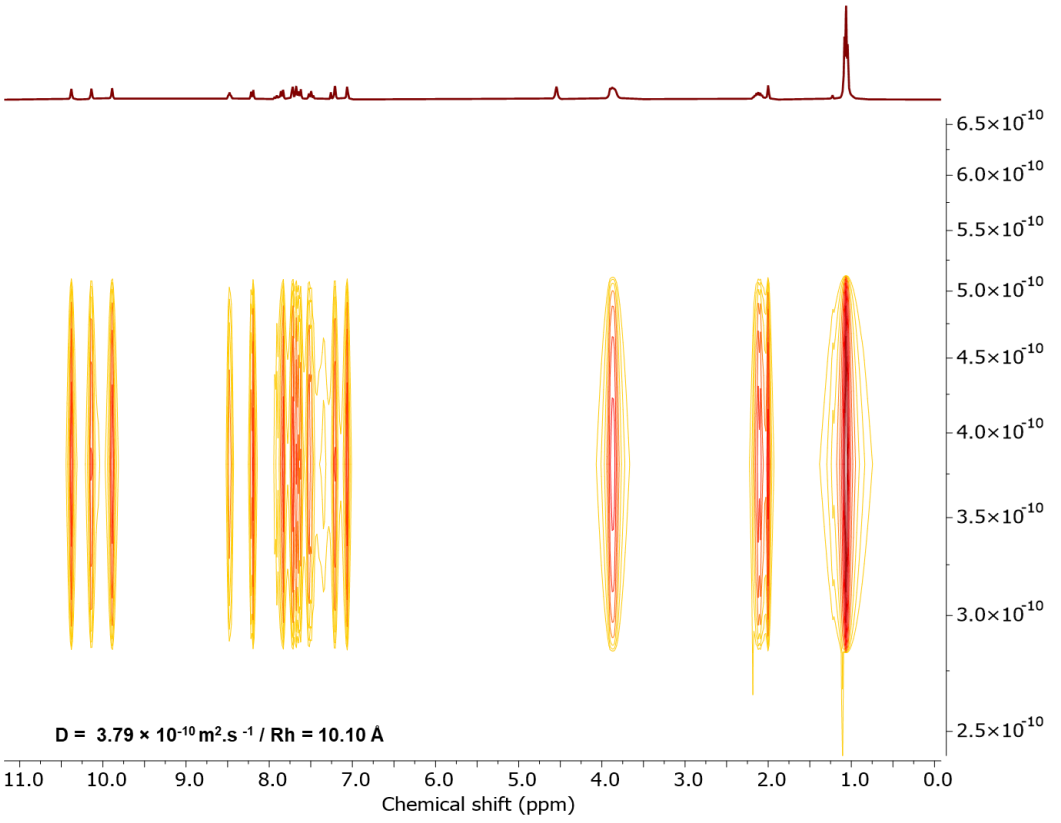

**$^{1}$H NMR 1$^{st}$ dispersion foldamer H ($CDCl_3$)**

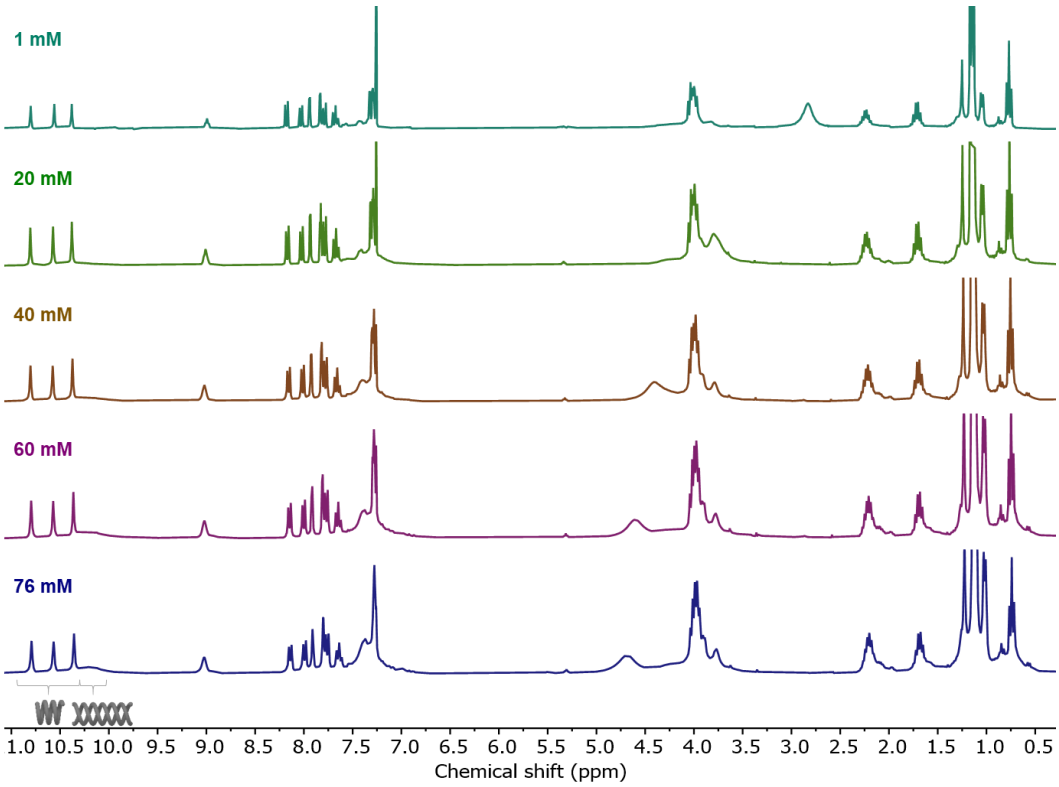


**$^{1}$H NMR 2$^{nd}$ dispersion foldamer H ($CDCl_3$)**

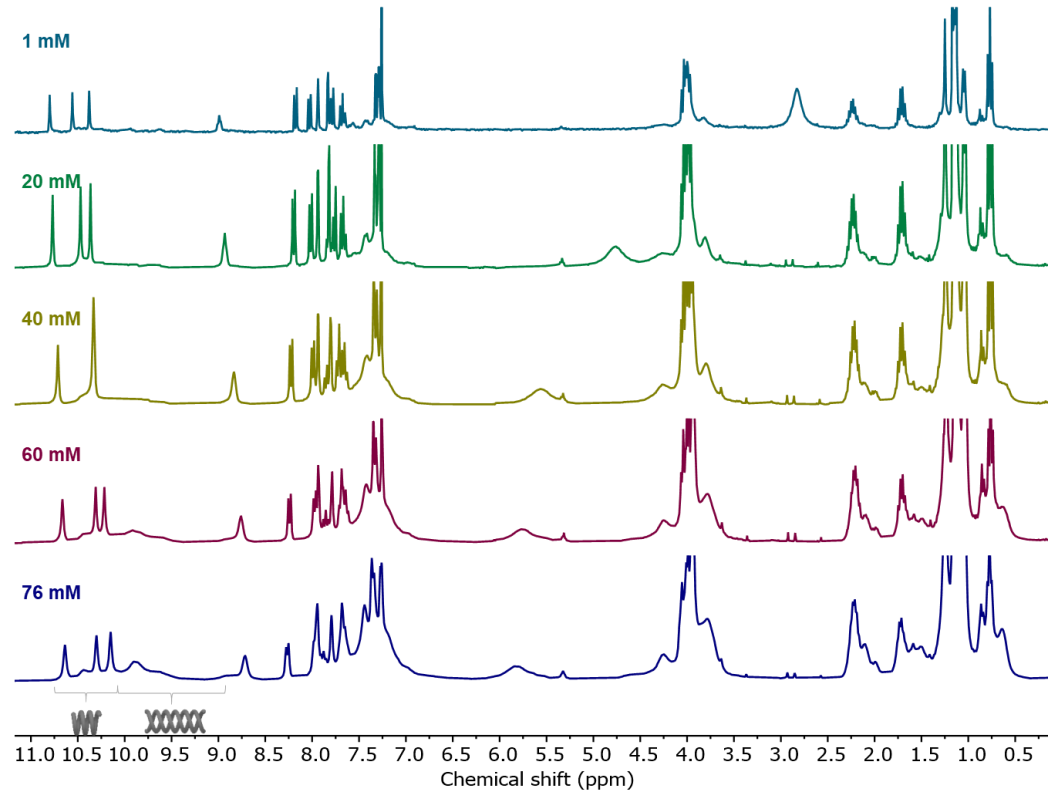

**$^{1}$H NMR 1$^{st}$ dispersion foldamer I ($CDCl_3$)**

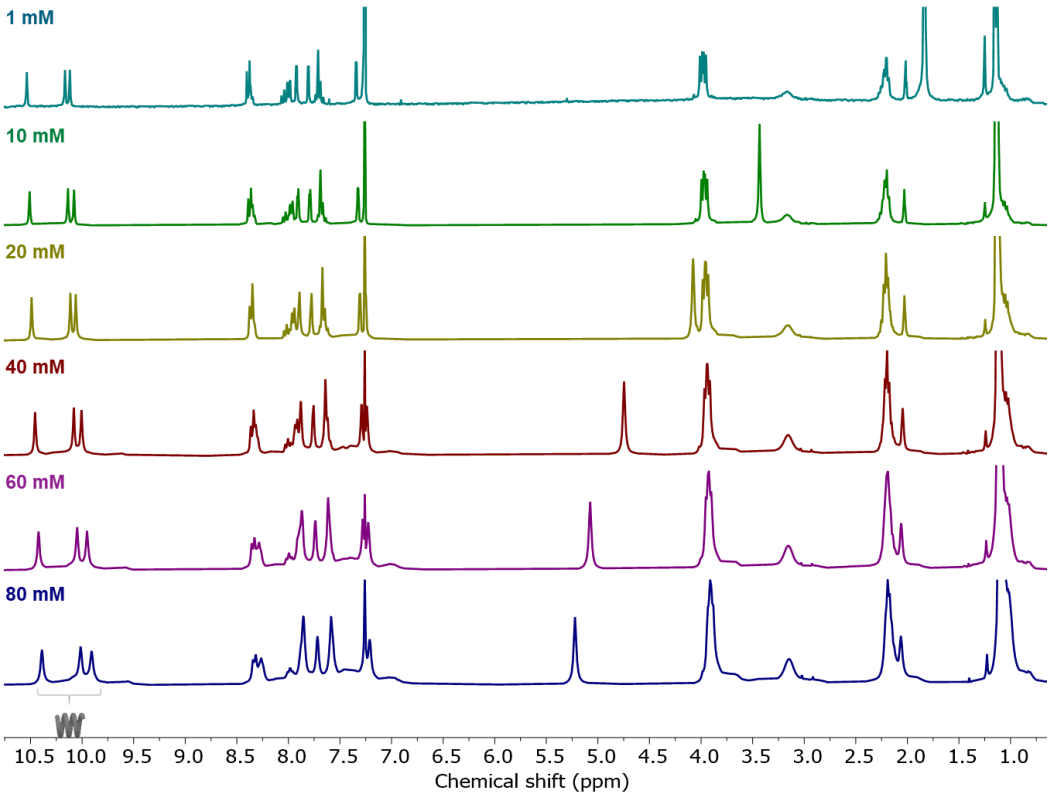


**$^{1}$H NMR 2$^{nd}$ dispersion foldamer I ($CDCl_3$)**

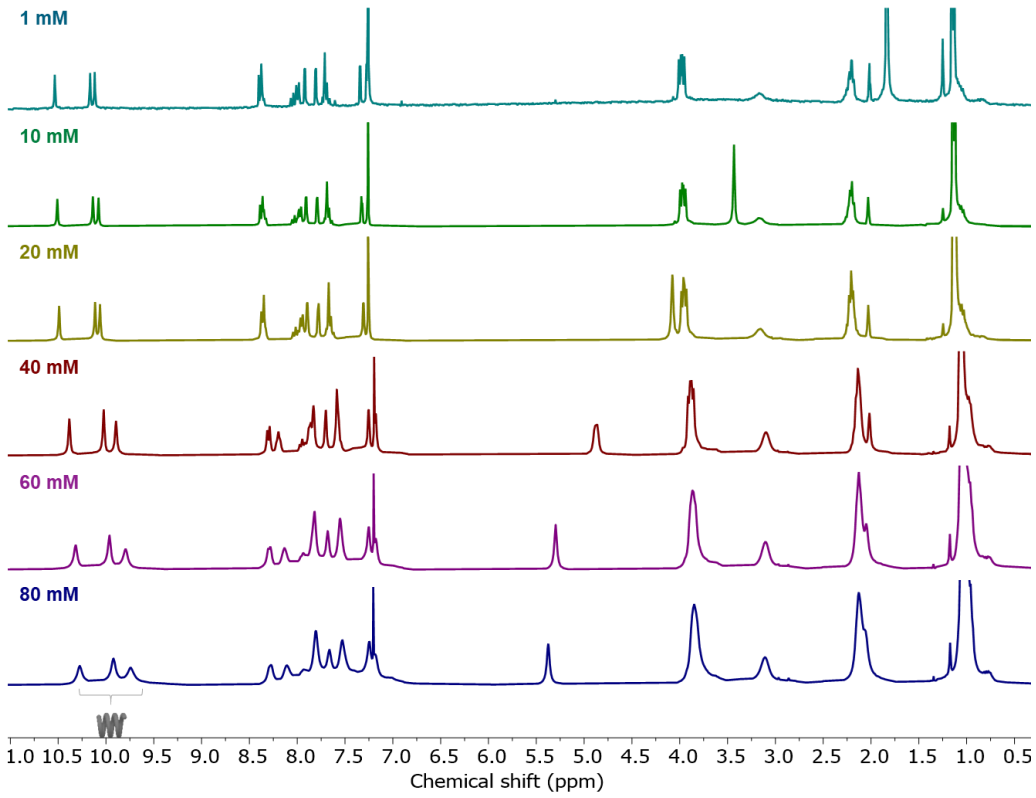

## $^{1}$H NMR 1$^{st}$ dispersion foldamer J ($CDCl_3$)

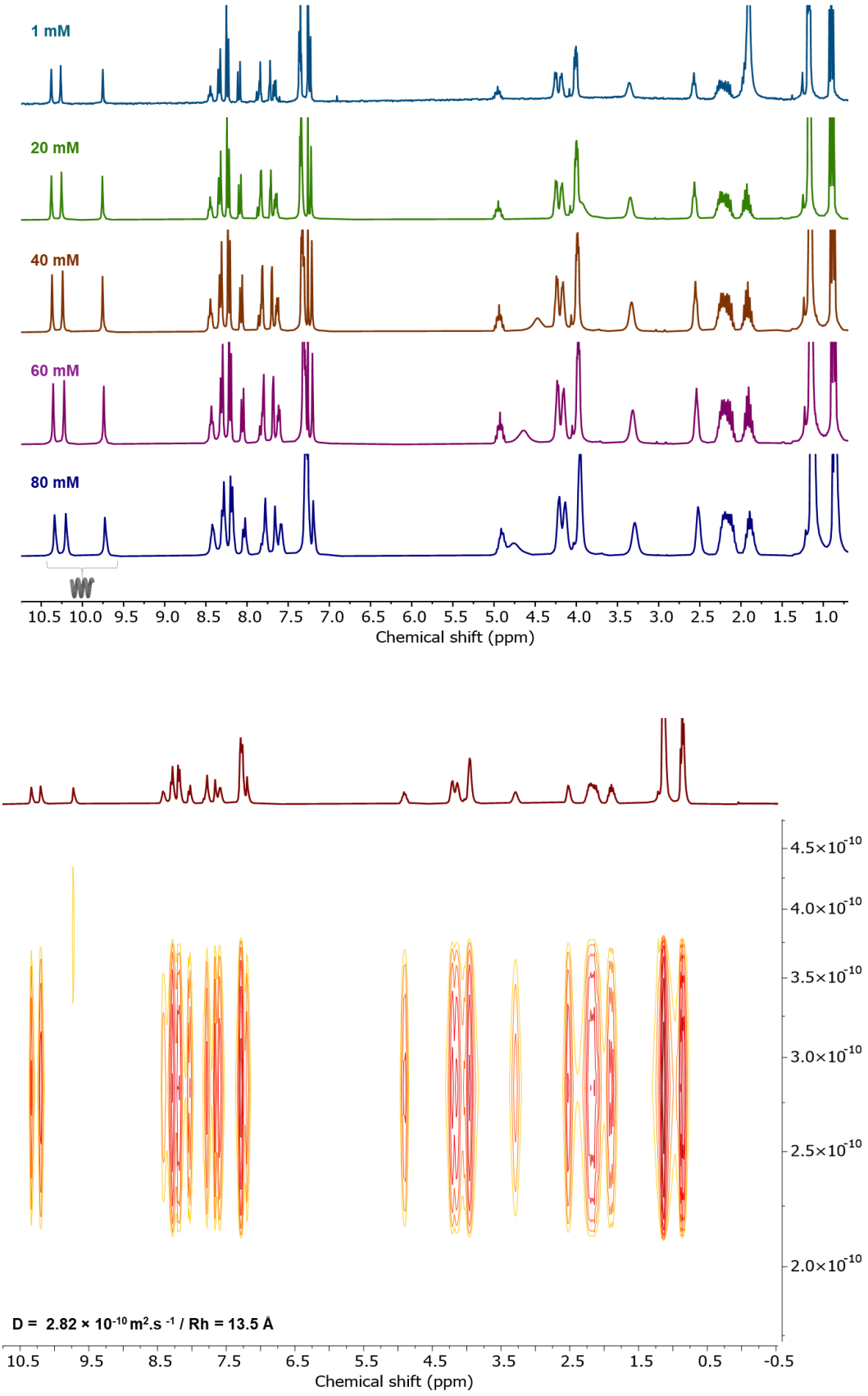

**$^{1}$H NMR 2$^{nd}$ dispersion foldamer J ($CDCl_3$)**

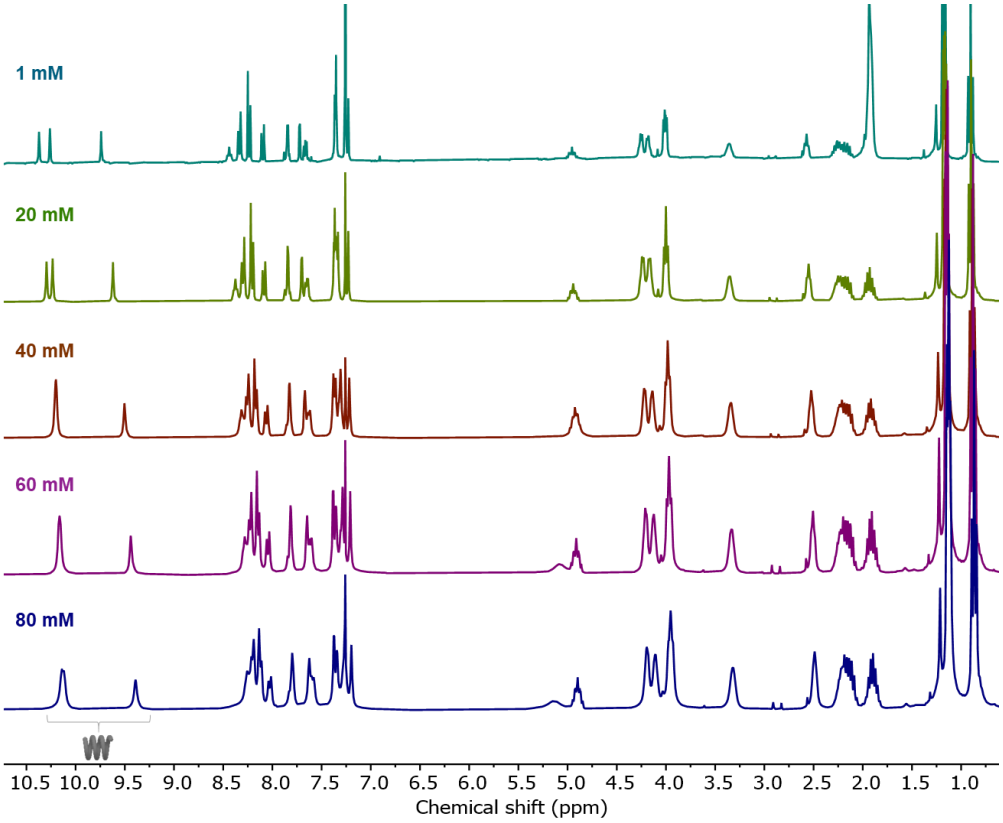


**$^{1}$H NMR 1$^{st}$ dispersion foldamer K ($CDCl_3$)**

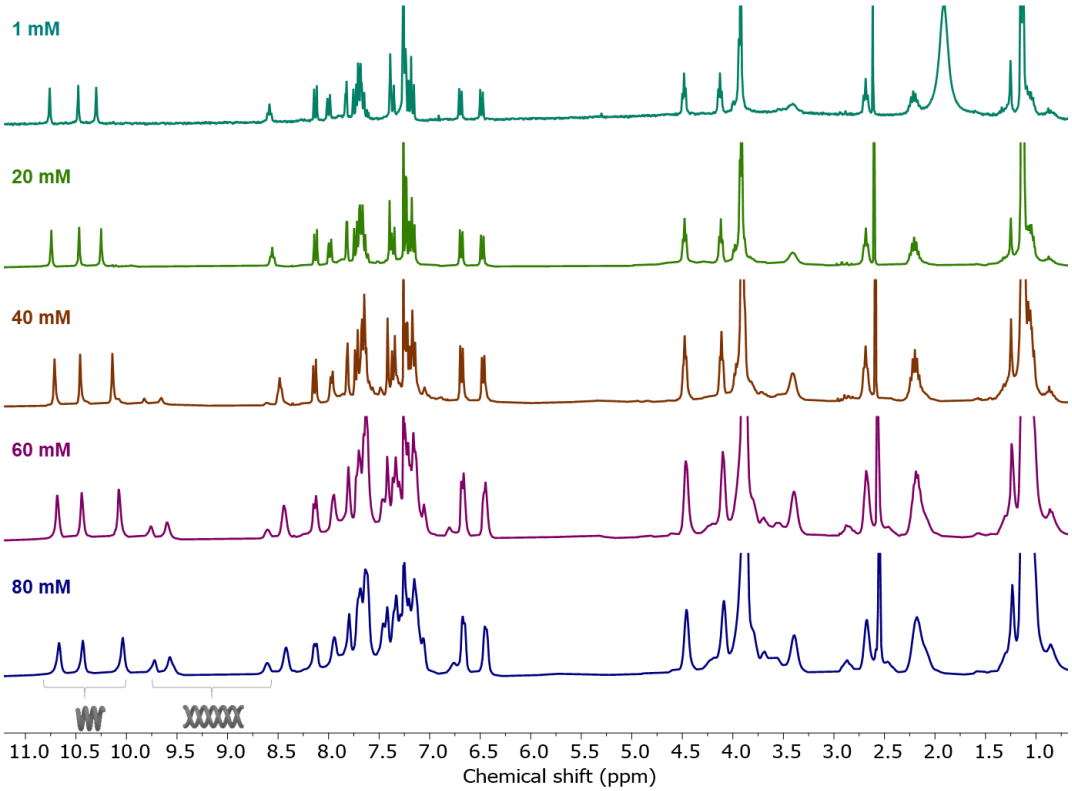

**$^{1}$H NMR 2$^{nd}$ dispersion foldamer K ($CDCl_3$)**

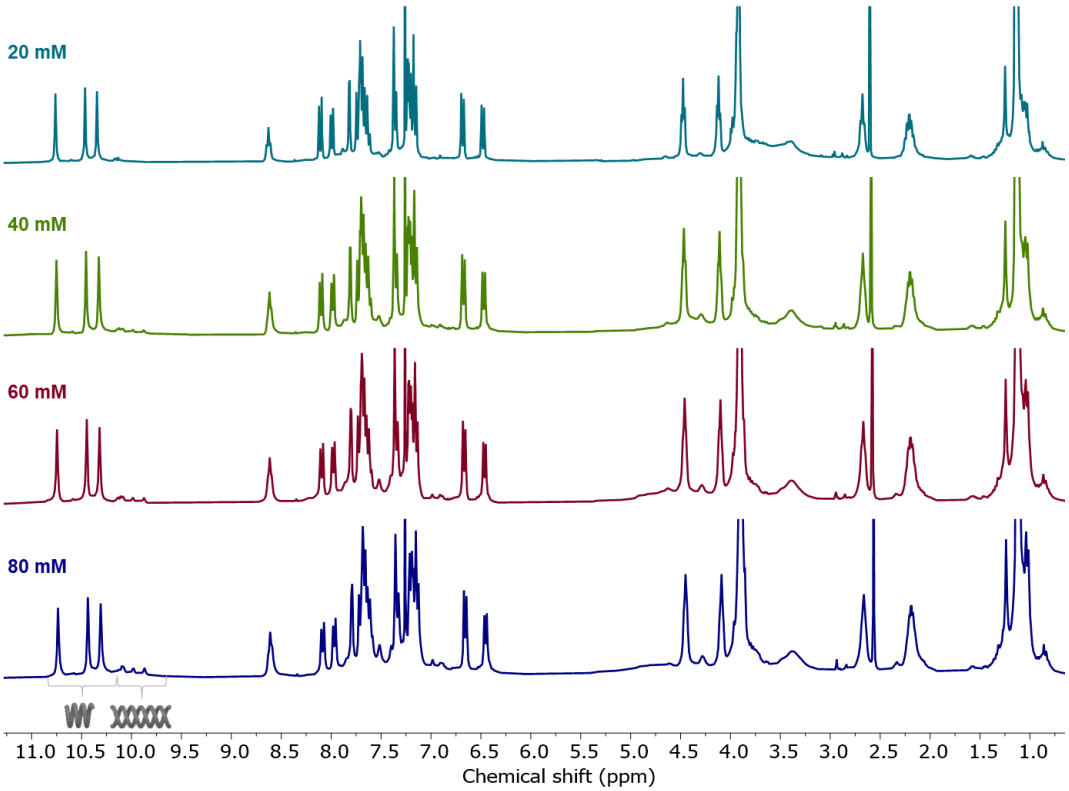


**$^{1}$H NMR 1$^{st}$ dispersion foldamer L ($CDCl_3$)**

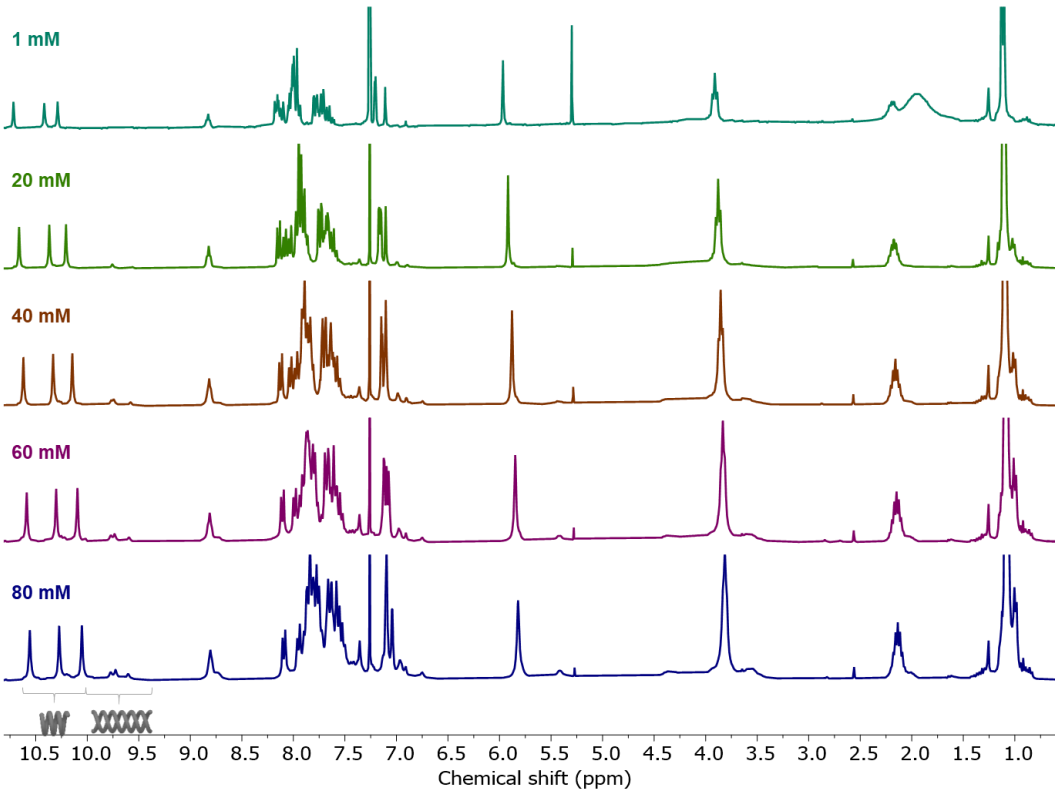

**$^{1}$H NMR 2$^{nd}$ dispersion foldamer L ($CDCl_3$)**

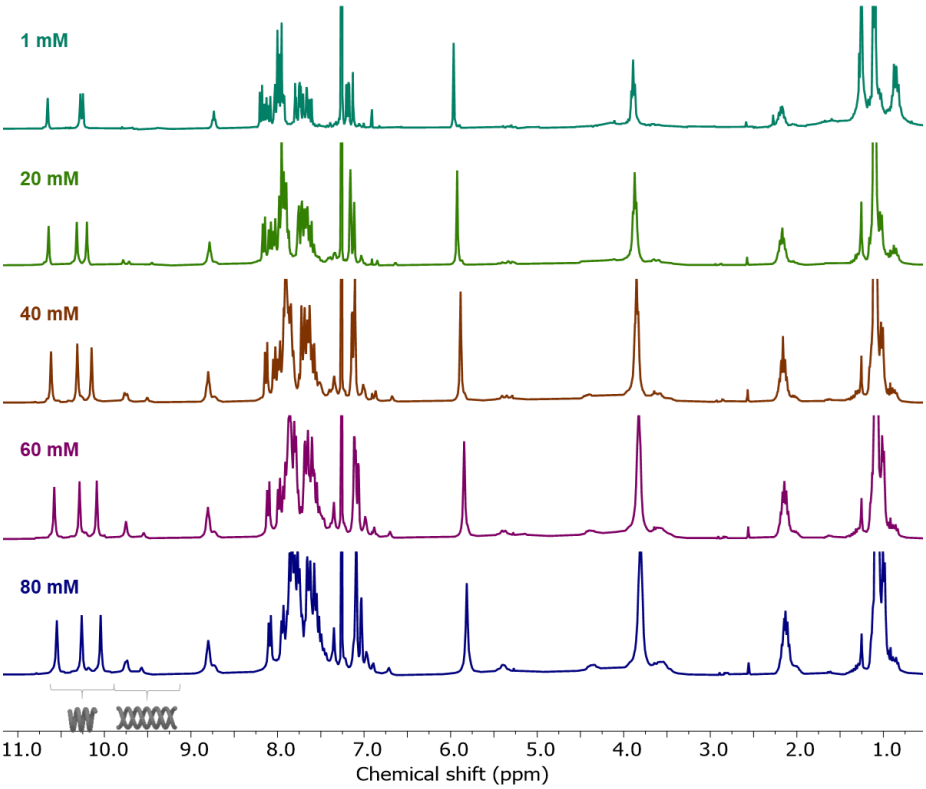


**$^{1}$H NMR 1$^{st}$ dispersion foldamers G and L ($CDCl_3$)**

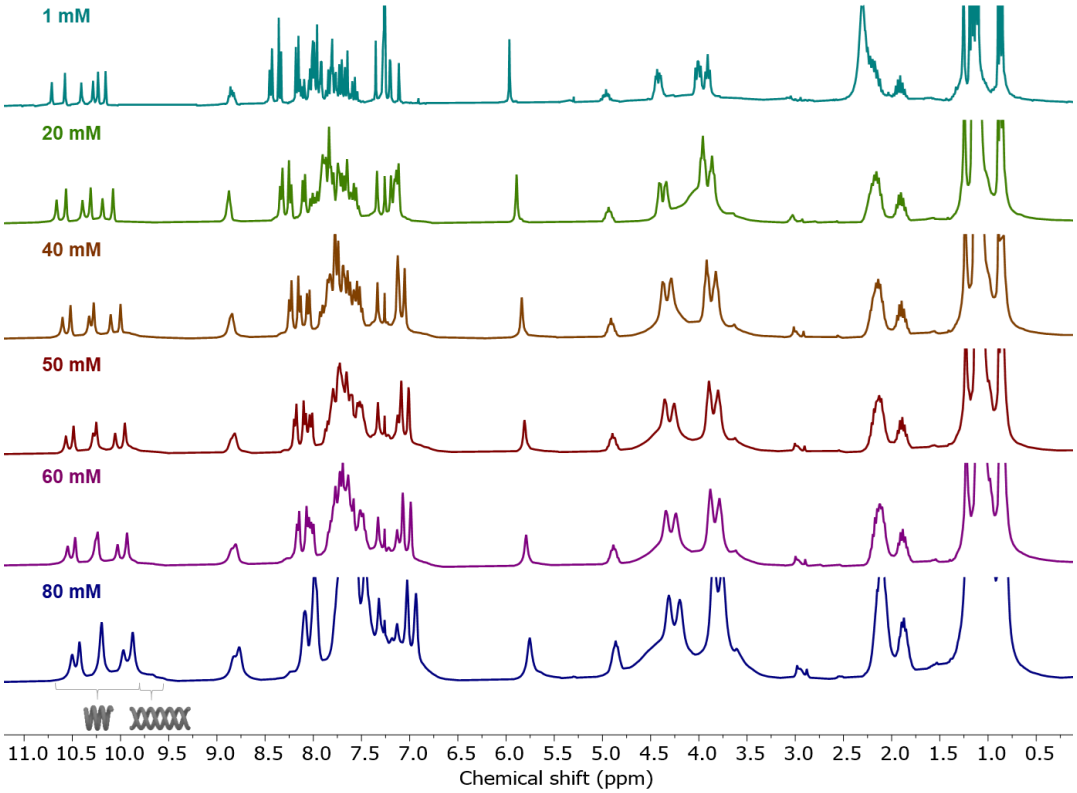

**$^{1}$H NMR 2$^{nd}$ dispersion foldamers G and L ($CDCl_3$)**

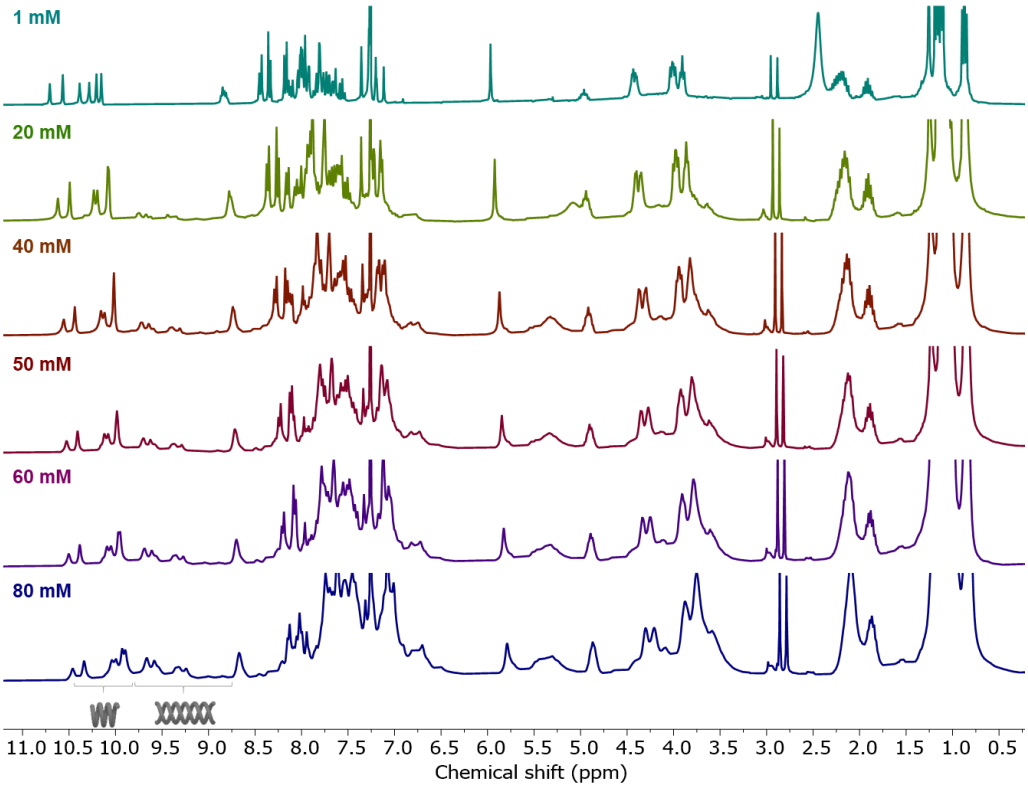

# Appendix 5

## Crystallographic data and structures

## Foldamer A (prepared by crystallization from DMF)

| | | |
|---|---|---|
| Identification code | | SA53DMF |
| Empirical formula | | C85 H103 N21 O18 S8 |
| | or | C67 H59 N15 O11 S8, 6(C3 H7 N O), H2 |
| Formula weight | | 1963.36 |
| Temperature | | 150.0 (1) K |
| Wavelength | | 1.54184 A |
| Crystal system, space group | | Triclinic, P -1 |
| Unit cell dimensions | | a = 13.5568(5) A alpha = 75.382(3) deg. |
| | | b = 19.2138(8) A beta = 70.996(3) deg. |
| | | c = 20.3931(7) A gamma = 73.192(4) deg. |
| Volume | | 4733.8 (3) A^3 |
| Z, Calculated density | | 2, 1.377 Mg/m^3 |
| Absorption coefficient | | 2.390 mm^-1 |
| F(000) | | 2064 |
| Crystal size | | 0.129 x 0.092 x 0.025 mm |
| Theta range for data collection | | 2.440 to 72.201 deg. |
| Limiting indices | | -16<=h<=16, -23<=k<=23, -25<=l<=24 |
| Reflections collected / unique | | 41263 / 17977 [R(int) = 0.0467] |
| Completeness to theta = 69.000 | | 98.1 % |
| Absorption correction | | Semi-empirical from equivalents |
| Max. and min. transmission | | 1.00000 and 0.92259 |
| Refinement method | | Full-matrix least-squares on F^2 |
| Data / restraints / parameters | | 17977 / 4 / 1283 |
| Goodness-of-fit on F^2 | | 1.023 |
| Final R indices [I>2sigma(I)] | | R1 = 0.0553, wR2 = 0.1324 [12888 Fo] |
| R indices (all data) | | R1 = 0.0821, wR2 = 0.1501 |
| Largest diff. peak and hole | | 1.283 and -0.487 e.A^-3 |

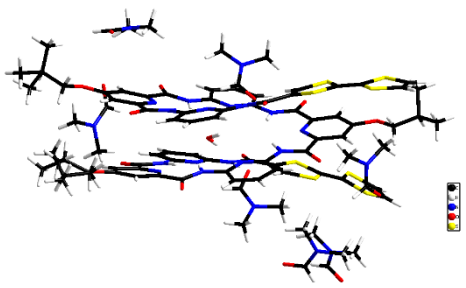

## Foldamer A (prepared by slow evaporation from THF)

| | | |
|---|---|---|
| Identification code | | SA53THF |
| Empirical formula | | C71 H71 N15 O14 S8 |
| | or | C67 H59 N15 O15 S8, C4 H8 O, 2 (H2 O) |
| Formula weight | | 1614.90 |
| Temperature | | 200.0 (1) K |
| Wavelength | | 1.54184 A |
| Crystal system, space group | | Monoclinic, C c |
| Unit cell dimensions | | a = 14.6614(5) A alpha = 90 deg. |
| | | b = 34.5009(10) A beta = 107.033(3) deg. |
| | | c = 15.6881(5) A gamma = 90 deg. |
| Volume | | 7587.5 (4) A^3 |
| Z, Calculated density | | 4, 1.414 Mg/m^3 |
| Absorption coefficient | | 2.796 mm^-1 |
| F(000) | | 3368 |
| Crystal size | | 0.128 x 0.161 x 0.099 mm |
| Theta range for data collection | | 3.403 to 76.220 deg. |
| Limiting indices | | -17<=h<=18, -41<=k<=43, -19<=l<=18 |
| Reflections collected / unique | | 17167 / 10604 [R(int) = 0.0260] |
| Completeness to theta = 69.000 | | 98.0 % |
| Absorption correction | | Semi-empirical from equivalents |
| Max. and min. transmission | | 1.00000 and 0.92 |
| Refinement method | | Full-matrix least-squares on F^2 |
| Data / restraints / parameters | | 10604 / 46 / 1011 |
| Goodness-of-fit on F^2 | | 1.032 |
| Final R indices [I>2sigma(I)] | | R1 = 0.0561, wR2 = 0.1527 [8115 Fo] |
| R indices (all data) | | R1 = 0.0742, wR2 = 0.1741 |
| Largest diff. peak and hole | | 0.455 and -0.459 e.A^-3 |

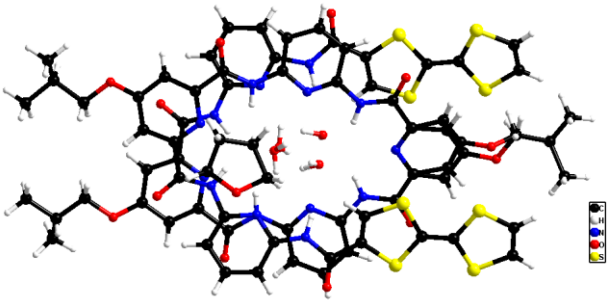

## Foldamer A (prepared by slow evaporation from $CHCl_3$/MeOH mixture)

| | | |
|---|---|---|
| Identification code | | SA53 |
| Empirical formula | | C70 H68 C13 N15 O13 S8 |
| | or | C67 H59 N15 O11 S8, C H C13, 2 (C H4 O) |
| Formula weight | | 1690.22 |
| Temperature | | 150.0 (1) K |
| Wavelength | | 1.54184 A |
| Crystal system, space group | | Triclinic, P -1 |
| Unit cell dimensions | | a = 14.6163(8) A alpha = 72.163(5) deg. |
| | | b = 15.2164(10) A beta = 75.972(5) deg. |
| | | c = 19.6458(10) A gamma = 69.475(5) deg. |
| Volume | | 3850.4(4) A^3 |
| Z, Calculated density | | 2, 1.458 Mg/m^3 |
| Absorption coefficient | | 3.707 mm^-1 |
| F(000) | | 1752 |
| Crystal size | | 0.300 x 0.131 x 0.027 mm -yellow plate |
| Theta range for data collection | | 3.198 to 77.208 deg. |
| Limiting indices | | -14<=h<=17, -18<=k<=19, -24<=l<=24 |
| Reflections collected / unique | | 33208 / 15285 [R(int) = 0.0751] |
| Completeness to theta = 69.000 | | 97.9 % |
| Absorption correction | | Gaussian |
| Max. and min. transmission | | 1.000 and 0.507 |
| Refinement method | | Full-matrix least-squares on F^2 |
| Data / restraints / parameters | | 15285 / 6 / 1012 |
| Goodness-of-fit on F^2 | | 1.030 |
| Final R indices [I>2sigma(I)] | | R1 = 0.0787, wR2 = 0.2061 [9220 Fo] |
| R indices (all data) | | R1 = 0.1249, wR2 = 0.2331 |
| Largest diff. peak and hole | | 0.773 and -0.816 e.A^-3 |

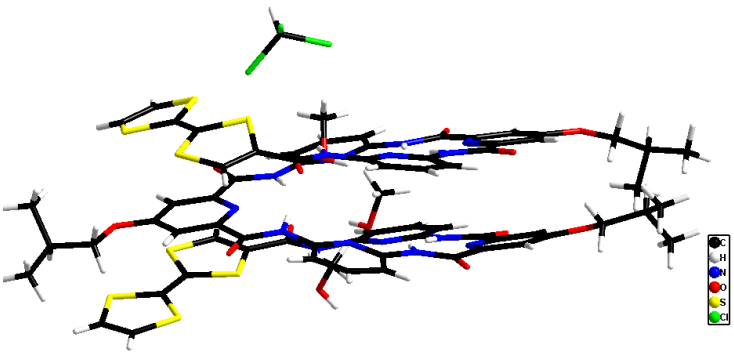

## Compound II–18 (prepared by crystallization from DMSO)

| | | |
|---|---|---|
| Identification code | | SA77 |
| Empirical formula | | C26 H28 N4 O6 S5 |
| | or | C24 H22 N4 O5 S4, C2 H6 O S |
| Formula weight | | 652.82 |
| Temperature | | 150.0(1) K |
| Wavelength | | 1.54184 A |
| Crystal system, space group | | Triclinic, P -1 |
| Unit cell dimensions | | a = 9.7580(7) A alpha = 78.781(6) deg. |
| | | b = 10.9173(9) A beta = 87.277(5) deg. |
| | | c = 14.8296(8) A gamma = 74.927(7) deg. |
| Volume | | 1496.30(19) A^3 |
| Z, Calculated density | | 2, 1.449 Mg/m^3 |
| Absorption coefficient | | 3.973 mm^-1 |
| F(000) | | 680 |
| Crystal size | | 0.107 x 0.074 x 0.028 mm - orange needle |
| Theta range for data collection | | 3.038 to 76.185 deg. |
| Limiting indices | | -12<=h<=11, -13<=k<=13, -18<=l<=18 |
| Reflections collected / unique | | 12240 / 5962 [R(int) = 0.0449] |
| Completeness to theta = 69.000 | | 98.1 % |
| Absorption correction | | Semi-empirical from equivalents |
| Max. and min. transmission | | 1.00000 and 0.91338 |
| Refinement method | | Full-matrix least-squares on F^2 |
| Data / restraints / parameters | | 5962 / 0 / 395 |
| Goodness-of-fit on F^2 | | 1.019 |
| Final R indices [I>2sigma(I)] | | R1 = 0.0572, wR2 = 0.1405 [3875 Fo] |
| R indices (all data) | | R1 = 0.0917, wR2 = 0.1588 |
| Largest diff. peak and hole | | 0.745 and -0.424 e.A^-3 |

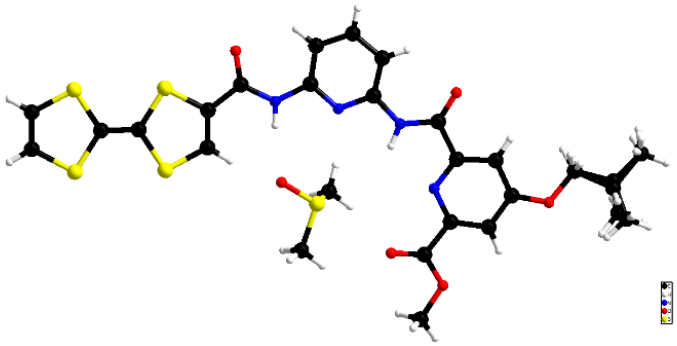

## Foldamer B (prepared by crystallization from DMF)

| | | |
|---|---|---|
| Identification code | | SA131DMF |
| Empirical formula | | C71 H83 N17 O15 |
| | or | C65 H67 N15 O12, 2(C3 H7 N O), H2 O |
| Formula weight | | 1414.54 |
| Temperature | | 220.0(1) K |
| Wavelength | | 1.54184 A |
| Crystal system, space group | | Triclinic, P -1 |
| Unit cell dimensions | | a = 11.1275(3) A alpha = 92.251(2) deg. |
| | | b = 16.6438(5) A beta = 102.283(2) deg. |
| | | c = 20.2552(6) A gamma = 102.087(2) deg. |
| Volume | | 3570.39(18) A^3 |
| Z, Calculated density | | 2, 1.316 Mg/m^3 |
| Absorption coefficient | | 0.781 mm^-1 |
| F(000) | | 1496 |
| Crystal size | | 0.371 x 0.310 x 0.073 mm |
| Theta range for data collection | | 2.726 to 75.305 deg. |
| Limiting indices | | -12<=h<=13, -20<=k<=20, -25<=l<=25 |
| Reflections collected / unique | | 30444 / 14133 [R(int) = 0.0365] |
| Completeness to theta = 69.000 | | 98.0 % |
| Absorption correction | | Semi-empirical from equivalents |
| Max. and min. transmission | | 1.00000 and 0.48250 |
| Refinement method | | Full-matrix least-squares on F^2 |
| Data / restraints / parameters | | 14133 / 25 / 958 |
| Goodness-of-fit on F^2 | | 1.013 |
| Final R indices [I>2sigma(I)] | | R1 = 0.0652, wR2 = 0.1846 [10855 Fo] |
| R indices (all data) | | R1 = 0.0814, wR2 = 0.2036 |
| Largest diff. peak and hole | | 0.538 and -0.295 e.A^-3 |

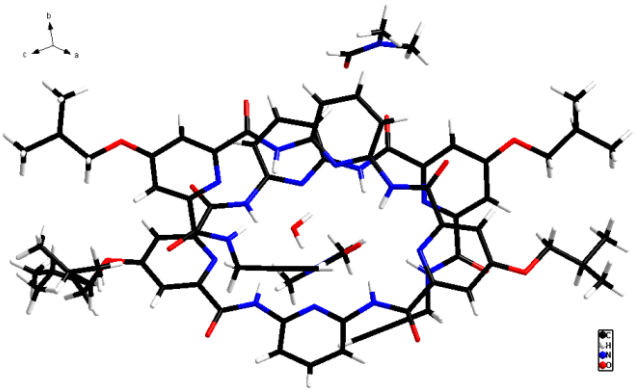

## Foldamer E (prepared by slow evaporation from DMF)

| | | |
|---|---|---|
| Identification code | | SA107DMF-200K |
| Empirical formula | | C115 H130.50 N29 O26.75 |
| | or | C103 H97 N25 O20, 4(C3 H7 N O), 2.75(H2O) |
| Formula weight | | 2346.98 |
| Temperature | | 200.0(1) K |
| Wavelength | | 1.54184 A |
| Crystal system, space group | | Triclinic, P -1 |
| Unit cell dimensions | | a = 16.3782(4) A alpha = 96.308(2) deg. |
| | | b = 19.1983(7) A beta = 93.107(2) deg. |
| | | c = 20.0125(5) A gamma = 110.673(3) deg. |
| Volume | | 5822.4(3) A^3 |
| Z, Calculated density | | 2, 1.339 Mg/m^3 |
| Absorption coefficient | | 0.810 mm^-1 |
| F(000) | | 2475 |
| Crystal size | | 0.226 x 0.196 x 0.046 mm |
| Theta range for data collection | | 2.484 to 76.408 deg. |
| Limiting indices | | -20<=h<=20, -23<=k<=24, -20<=l<=25 |
| Reflections collected / unique | | 65005 / 23396 [R(int) = 0.0351] |
| Completeness to theta = 69.000 | | 98.5 % |
| Absorption correction | | Semi-empirical from equivalents |
| Max. and min. transmission | | 1.00000 and 0.65717 |
| Refinement method | | Full-matrix least-squares on F^2 |
| Data / restraints / parameters | | 23396 / 1 / 1581 |
| Goodness-of-fit on F^2 | | 1.081 |
| Final R indices [I>2sigma(I)] | | R1 = 0.1170, wR2 = 0.3394 [19475 Fo] |
| R indices (all data) | | R1 = 0.1277, wR2 = 0.3480 |
| Largest diff. peak and hole | | 00.770 and -0.532 e.A^-3 |

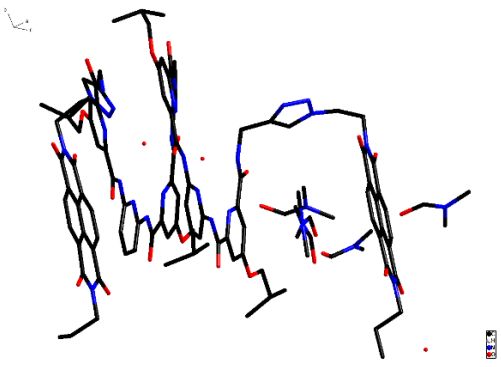

## Foldamer F (prepared by slow evaporation from DMSO)

| | |
|---|---|
| Identification code | SA169 |
| Empirical formula | C101 H125 N21 O22 S5 |
| | or (C91 H93 N21 O16), 5(C2 H6 O S), H2 O |
| Formula weight | 2145.51 |
| Temperature | 200.0(1) K |
| Wavelength | 1.54184 A |
| Crystal system, space group | Monoclinic, P 21/c |
| Unit cell dimensions | a = 16.9946(11) A alpha = 90 deg. |
| | b = 39.559(3) A beta = 96.821(6) deg. |
| | c = 16.4159(12) A gamma = 90 deg. |
| Volume | 10958.3(13) A^3 |
| Z, Calculated density | 4, 1.300 Mg/m^3 |
| Absorption coefficient | 1.618 mm^-1 |
| F(000) | 4536 |
| Crystal size | 0.394 x 0.192 x 0.038 mm-colorless plate |
| Theta range for data collection | 2.619 to 72.376 deg. |
| Limiting indices | -20<=h<=20, -41<=k<=48, -19<=l<=15 |
| Reflections collected / unique | 53480 / 20811 [R(int) = 0.0942] |
| Completeness to theta = 69.000 | 98.0 % |
| Absorption correction | Semi-empirical from equivalents |
| Max. and min. transmission | 1.00000 and 0.49596 |
| Refinement method | Full-matrix least-squares on F^2 |
| Data / restraints / parameters | 20811 / 95 / 1381 |
| Goodness-of-fit on F^2 | 1.014 |
| Final R indices [I>2sigma(I)] | R1 = 0.1191, wR2 = 0.3084 [8378 Fo] |
| R indices (all data) | R1 = 0.1997, wR2 = 0.3766 |
| Largest diff. peak and hole | 0.627 and -0.566 e.A^-3 |

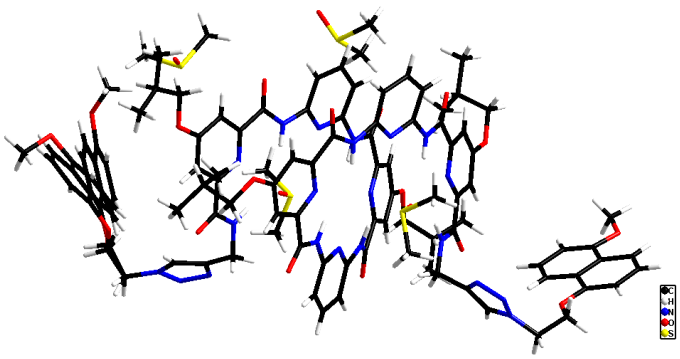

## Foldamer H (prepared by slow evaporation from DMSO)

| | | |
|---|---|---|
| Identification code | | SA0176 |
| Empirical formula | | C77 H99 N21 O15 S3 |
| | or | C71 H81 N21 O12, 3(C2 H6 O S) |
| Formula weight | | 1654.95 |
| Temperature | | 230.0(1) K |
| Wavelength | | 1.54184 A |
| Crystal system, space group | | Triclinic, P -1 |
| Unit cell dimensions | | a = 13.0219(3) A alpha = 83.211(2) deg. |
| | | b = 16.0741(5) A beta = 82.576(2) deg. |
| | | c = 22.4832(6) A gamma = 69.386(2) deg. |
| Volume | | 4354.4(2) A^3 |
| Z, Calculated density | | 2, 1.262 Mg/m^3 |
| Absorption coefficient | | 1.382 mm^-1 |
| F(000) | | 1752 |
| Crystal size | | 0.306 x 0.113 x 0.028 mm - colorless needle |
| Theta range for data collection | | 2.946 to 74.096 deg. |
| Limiting indices | | -15<=h<=16, -18<=k<=20, -25<=l<=28 |
| Reflections collected / unique | | 40249 / 16947 [R(int) = 0.0372] |
| Completeness to theta = 69.000 | | 98.1 % |
| Absorption correction | | Semi-empirical from equivalents |
| Max. and min. transmission | | 1.00000 and 0.57374 |
| Refinement method | | Full-matrix least-squares on F^2 |
| Data / restraints / parameters | | 16947 / 27 / 1074 |
| Goodness-of-fit on F^2 | | 1.025 |
| Final R indices [I>2sigma(I)] | | R1 = 0.0677, wR2 = 0.1895 [13028 Fo] |
| R indices (all data) | | R1 = 0.0836, wR2 = 0.2093 |
| Largest diff. peak and hole | | 0.659 and -0.542 e.A^-3 |

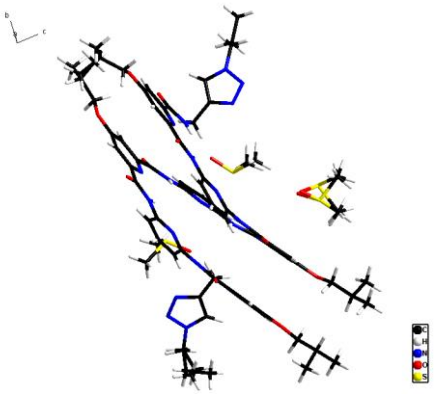

## Compound III–21 (prepared by crystallization from DMSO)

| | | |
|---|---|---|
| Identification code | | SA079 |
| Empirical formula | | C47 H50 Cl4 N10 O9 |
| | or | C45 H48 N10 O9, C2 H2 Cl4 |
| Formula weight | | 1040.77 |
| Temperature | | 200.0(1) K |
| Wavelength | | 1.54184 A |
| Crystal system, space group | | Triclinic, P -1 |
| Unit cell dimensions | | a = 6.9216(4) A alpha = 90.087(5) deg. |
| | | b = 16.8646(13) A beta = 93.789(4) deg. |
| | | c = 21.1261(11) A gamma = 95.043(5) deg. |
| Volume | | 2451.1(3) A^3 |
| Z, Calculated density | | 2, 1.410 Mg/m^3 |
| Absorption coefficient | | 2.749 mm^-1 |
| F(000) | | 1084 |
| Crystal size | | 0.421 x 0.078 x 0.023 mm - yellow needle |
| Theta range for data collection | | 3.376 to 72.483 deg. |
| Limiting indices | | -8<=h<=7, -20<=k<=20, -25<=l<=25 |
| Reflections collected / unique | | 13892 / 13892 [R(int) = ?] |
| Completeness to theta = 69.000 | | 98.0 % |
| Absorption correction | | Semi-empirical from equivalents |
| Max. and min. transmission | | 1.00000 and 0.72249 |
| Refinement method | | Full-matrix least-squares on F^2 |
| Data / restraints / parameters | | 13892 / 0 / 639 |
| Goodness-of-fit on F^2 | | 1.049 |
| Final R indices [I>2sigma(I)] | | R1 = 0.0823, wR2 = 0.2560 [7782 Fo] |
| R indices (all data) | | R1 = 0.1252, wR2 = 0.2737 |
| Largest diff. peak and hole | | 0.457 and -0.463 e.A^-3 |

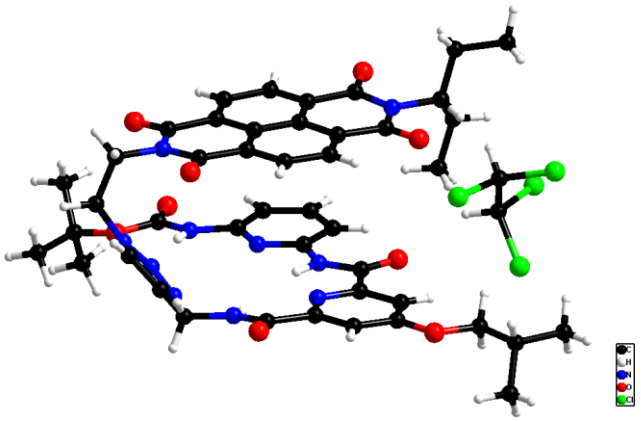

COLLEGE DOCTORAL PAYS DE LA LOIRE
ED MATIERE, MOLECULES MATERIAUX ET GEOSCIENCES

université angers

Titre : **Hybridation contrôlée de foldamères hélicoïdaux électroactifs pour la conception d'homo – et d'hétéroduplexes**

**Mots clés :** Foldamères, Structures hélicoïdales, Electroactivité, π –Dimérisation, Interactions aromatiques, Homoduplexes, Hétéroduplexes, Polymère supramoléculaire, Systèmes hors –équilibre

**Résumé :** Les foldamères de type oligoarylamide constituent une famille d'oligomères capables de se replier en structures hélicoïdales et de s'hybrider pour former des hélices doubles. L'objectif central de ce travail de thèse a consisté à pourvoir de telles espèces d'unités redox, afin de contrôler leur hybridation en homo – et en hétéroduplexes de manière sélective. Dans une première partie, un oligoarylamide fonctionnalisé par deux unités tétrathiafulvalène (TTF) via un espaceur amide rigide et court a été synthétisé. Cinq structures cristallographiques différentes de ce foldamère sous sa forme 'hélice simple' ont été obtenues. L'apparente stabilité de cet arrangement à l'état neutre a pu être confirmée par diverses études spectroscopiques en solution. De manière originale, il a été montré que l'oxydation des unités TTF déclenche l'hybridation de ce foldamère, *i.e.* la formation d'hélices doubles, via la formation de dimères de radicaux –cations. Dans une seconde partie, une série de foldamères dotés de groupements donneurs ou accepteurs de densité électronique a été synthétisée. Ces oligomères se sont avérés piégés cinétiquement dans leur forme 'hélice simple' du fait d'interactions intramoléculaires. Ainsi, la présence du connecteur triazole explique, au moins en partie, l'obtention d'un système hors équilibre, bien que la contribution d'interactions aromatiques intramoléculaires ne puisse être exclue. Ainsi, les foldamères de cette famille tendent à former des polymères supramoléculaires lors de leur première dispersion. A travers une étude relativement détaillée, il a été montré que le système était piégé cinétiquement à température ambiante et que la composition du milieu n'évoluait pas avec le temps. En revanche, un simple chauffage à 45°C (dans le chloroforme) permet l'obtention d'un système métastable, qui permet progressivement le déplacement de l'équilibre vers la forme hybridée.

Title: **Controlled hybridization of helical electroactive foldamers for the design of homo – and heteroduplexes**

**Keywords :** Oligoarylamide foldamers, Helical structures, Electroactive units, π –dimerization, Charge –transfer complexes, Homoduplexes, Heteroduplexes, Supramolecular polymer, Out –of –equilibrium

**Abstract:** Oligoarylamide foldamers represent a family of oligomers that are capable of folding into helical structures and hybridizing to form double helices through non –covalent interactions. The central objective of this thesis work consisted in designing electroactive helical foldamers to control their hybridization into homo – or heteroduplexes in a selective manner. In this context, a strand functionalized with two tetrathiafulvalene (TTF) units via a rigid and short amide spacer was synthesized. Five different crystallographic structures of this foldamer in its 'single helix' form were obtained. The apparent stability of this arrangement in the neutral state was confirmed through various spectroscopic studies in solution. Interestingly, the oxidation of the TTF units triggered the hybridization of this foldamer, through the formation of radical cation dimers. In a second part, foldamers endowed with electron –donating groups or electron –withdrawing acceptors was synthesized. These oligomers were found to be kinetically trapped in their 'single helix' form due to intramolecular interactions. Thus, the presence of the triazole motif explains, at least in part, why an out –of –equilibrium system is obtained. As a result, these foldamers tend to form supramolecular polymers along their initial dispersion. Through a relatively detailed study, it was shown that at room temperature, the system was kinetically trapped, and the composition of the medium did not evolve over time. However, a simple heating to 45°C (in chloroform) allowed for reaching a metastable system, which gradually towards the hybridized form.